STELLINGEN

behorende bij het proefschrift

Modelling of hydraulics and morphology in mountain rivers.

Jan Sieben

12 mei 1997

1. Ontkoppelde berekeningen van veranderingen in waterbeweging en morfologie hebben voor bergrivieren nauwelijks een efficienter computer model tot gevolg.

2. Zonder zijdelingse toe- of afvoer van water en/of sediment, kan een watersprong in een waterloop met een beweeglijke bodem niet stilstaan.

3. Voor het voorspellen van veranderingen in rivieren met een beweeglijke bodem is niet alleen het benodigde aantal randvoorwaarden maar ook de verdeling ervan over de randen gelijk voor alle stromingsregimes.

4. Uit de wiskundige analyse van de beweging van water en sediment blijkt dat de beweeglijkheid van de rivierbodem moet resulteren in een transkritisch overgangsgebied tussen subkritische en superkritische stroming.

5. De stabiliteitsvoorwaarden van wiskundige modellen voor veranderingen in rivierbeddingen met gegradeerd sediment zijn met name beperkend voor bergrivieren.

6. Een *mixing-layer* ter bepaling van een representatieve korrelverdeling van het rivierbed kan niet puur fysisch worden geinterpreteerd. Er kan daarom beter van een *reference-layer* worden gesproken.

7. Door het gebruik van een *transfer function* volgens Toro-Escobar *et al.* (1996) voor de longitudinale verandering in bodemsamenstelling in een rivier wordt het aantal wiskundige oplossingen te drastisch gereduceerd.
   Toro-Escobar, C.M., G. Parker and C. Paola (1996), *Transfer function for the deposition of poorly sorted gravel in response to streambed aggradation*, J. of Hydr. Res., IAHR, Vol.34, No.1, pp.35-54.

8. De betrouwbaarheid van geomorfologische voorspellingen moet altijd op de korrel genomen worden.

9. Het onderkennen van Acts-of-God getuigt van realiteitszin.

10. Het vernoemen van wiskundige modellen naar goden is de goden verzoeken.

11. Ook de toepassing van het minderhedenbeleid faalt voor individuen.

12. Onder asielzoekers in Nederland schuilen uitzonderlijke capaciteiten.

13. Versnellingen op fietsen hebben vaak vertraging tot gevolg.

Modelling of hydraulics and morphology

in

mountain rivers

door Jan SIEBEN
civiel ingenieur
geboren te Klazienaveen

Cover:

Bergstroom tussen rotsblokken, chalk drawing (1838) by Barend Cornelis Koekoek (1803-1862) from the collection of Museum Boijmans Van Beuningen Rotterdam.

Modellering van waterbeweging en morfologie in bergrivieren

Samenvatting.

De hydraulische en morfologische kenmerken van bergrivieren verschillen met die van rivieren in laagland. In het algemeen wordt de beperking van overstromingen in bergachtige gebieden vaak gecompliceerd door een grillig afvoerverloop en grote morfologische veranderingen. In combinatie met een variërende geometrie, gegradeerd sediment en veranderingen in stromingsregime, stelt dit een hoge eis aan modellen die ingrepen in rivieren ondersteunen. In deze studie zijn de invloeden van condities in bergrivieren op één-dimensionale, wiskundige modellen geanalyseerd.

Deze analyse omvat de toepasbaarheid van vereenvoudigde modellen, de stabiliteit van het wiskundig model in geval van gegradeerd sediment en het gedrag van discontinue stroming. Het numeriek model dat hiertoe is ontwikkeld is gebaseerd op de *Godunov*-methode, met een gelijktijdige oplossing van veranderingen in de hydraulische en morfologische variabelen. Dit model is toegepast op hypothetische gevallen en gootexperimenten.

Voor testgevallen met niet-stationaire en niet-uniforme stroming en waarden van het *Froude*-getal dicht bij één, blijkt de aanname van quasi-stationaire stroming mogelijk maar niet efficiënt, terwijl de aanname van quasi-uniforme stroming efficiënt maar fout blijkt. Voor gevallen met *Froude*-getallen dichtbij één, vermindert de fout in de laatste aanname echter snel voor meer uniforme stroming.

In het geval van gegradeerd sediment en hogere waarden van het *Froude*-getal vermindert de stabiliteit van het wiskundig model voor bepaalde condities. Enkele methoden voor stabilisatie zijn geanalyseerd.

Het gedrag van discontinue stroming zoals watersprongen op een beweegbare bodem is onderzocht met behulp van schokrelaties en entropievoorwaarde. Als aan de laatste wordt voldaan, ontstaat geen conflict in informatieoverdracht en kan de discontinue oplossing, binnen de beperkingen van het model als fysisch realistisch worden beschouwd.

Modelling of hydraulics and morphology in mountain rivers

Abstract.

Hydraulic and morphological features of mountain rivers differ from those of low-land rivers. In general, flooding mitigation in mountainous areas is often complicated due to an erratic character of hydrographs and large morphological changes. In combination with a non-uniform geometry, graded sediment and changes in flow regime, this puts high claims on models that support river engineering in mountains. In this study, effects of mountain-river conditions on one-dimensional mathematical models for river hydraulics and morphology are analysed.

This analysis includes the applicability of simplified models, the mathematical stability in case of graded sediment and the behaviour of discontinuous flows at mobile beds. The numerical model that is developed hereto is based on the *Godunov* method with simultaneous solution of changes in hydraulic and morphological variables. This model is applied on hypothetical cases and flume experiments.

For test cases with strongly unsteady and non-uniform conditions of flow and values of the *Froude* number near unity, the quasi-steady flow assumption appears to be possible but not efficient, whereas the quasi-uniform flow assumption is found to be efficient but erroneous. However, this latter assumption appears to be appropriate for cases with *Froude* numbers near unity and flows with more uniform conditions.

In case of graded sediment and for high values of the *Froude* number, the mathematical stability of the model reduces for certain conditions. Some stabilizing options have been analysed.

The behaviour of discontinuous flows such as hydraulic jumps at a mobile bed can be analysed with shock relations and entropy condition. If the latter are satisfied, no conflict of information-transfer develops and within the limitations of the model, the discontinuous solution can be considered physically realistic.

Acknowledgements.

Contents.

3. Concepts for models with sediment mixtures.

4. Some effects of sediment mixtures on morphology.

5. Concepts for numerical modelling.

6. Analysis of discontinuous solutions.

7. Description of numerical model.

8. Summary and conclusions.

Appendices.

x

Chapter one.

Introduction.

1.1. General.

Mountainous regions have been fascinating mankind throughout history. Inaccessible heights, harsh climates and threatening events with overwhelming dimensions are combined with a variability and wealth of natural sources, providing special habitat for flora and fauna. From this character of mountainous areas, many reflections and reminders in human culture and history can be found. Considering the remnants of ancient and, unfortunately, present-day constructions, it is not surprising that ancient Greeks considered the Olympus appropriate for unpredictable gods.

The increasing efforts to construct and operate means for exploration, cultivation and development of rich and accessible parts of mountainous regions, have also raised a need for developing protection measures and warning systems against hazardous fluvial impacts. These impacts are caused by the complex dynamics of supply and conveyance of water and sediment in mountainous and piedmont areas. The urgency of this need is stressed by the number of casualties and the amount of damage which often are involved (Davies, 1989).

It can be stated that with the development of mountainous regions, flood mitigation measures are needed in hazardous areas. In addition to that, higher claims are put on the performance of future river engineering with increasing concerns for conservation of ecological values and other environmental qualities.

1.2. River engineering in mountainous areas.

Fluvial hazards usually concern flooding at lower regional gradients, for example terraces, flood plains and alluvial fans. To protect flat areas from sediment deposition and subsequent flooding, flood-mitigation measures in mountain-river engineering often includes erosion-prevention in upper catchments, sediment-transport reduction at instable river reaches (e.g. side-slope erosion) or sediment transport enlargement at vulnerable flat areas (e.g. Armanini *et al.*, 1989).

1

Protection measures range from slope stabilization to river engineering works, representing a long chain of processes from sediment production and rainfall in upper parts of the catchment to alluvial transport and river discharge at the base. Effects of landuse (cultivation, forestation, etc.) on river morphology illustrate to a certain extend the manageability of erosion production (Renard and Laurson, 1975). Hence, mitigation of flooding hazards implies combining different disciplines, conventions and interests (Changnon, 1986). A review of some research activity is given in Sieben (1993).

Effects of hydraulic structures on a highly non-linear system of mountain-river morphology (e.g. Iwamoto, 1985; Willi, 1989; Basile, 1994) and vice versa (e.g. Whittaker *et al.*, 1985) can be significant. However, theoretical and experimental studies for these complex conditions are relatively scarce.

1.3. Background of the study.

1.3.1. Modelling approach.

The basis for sound engineering in conditions of mountain rivers is formed by understanding phenomena. To indicate the limited domain of present knowledge with respect to hydraulics and morphology in mountainous rivers, reference is made to a debate whether or not stable, supercritical flows can be observed in mountain streams (Jarret, 1984 and 1987; Trieste, 1992; Wahl and Miller, 1996). This discussion reflects the difficulties engaged in predicting friction losses of flows at varying discharges in an irregular geometry (e.g. Bathurst *et al.*, 1981).

In research on mountain rivers, two main approaches can be distinguished that can be described roughly as follows.

> a) construct an empirical model based on analysing data sets with statistical methods, assume consistency and continuity of represented trends and extrapolate to extreme event scenarios.

> b) formulate a mechanistic concept suitable for deterministic simulation of the processes of interest, and impose boundary conditions to the model, that correspond to an extreme event scenario.

At present (1996), both approaches alone are not sufficient to obtain a reliable assessment of flooding risks. The major obstructions for application of both methods include difficult measuring conditions, sparseness of events and up-

and downscaling problems, in both time and space domains (e.g. Crosato, 1995). A brief review is given.

statistical models.

Considering the level of complexity, present knowledge on fluvial hazards is generally limited to statistical models, constructed with rough magnitudes of past events. A typical feature of water and sediment supply to mountain rivers is the extreme variability, both in time and space (Davies, 1989), with often different frequency-populations (Jarret, 1990).

However, in practice, construction of event-frequency distributions is difficult; historic data are scarce, and collection of actual data on major events is difficult, both due to hard measuring conditions and sparsity of events. Due to the often complicated (in many cases not well understood) correlation between supply and transport of both water and sediment, synthetically generated data should be handled with great care.

deterministic models.

With respect to application of theoretical simulation models for hydraulics and morphology of mountain rivers, many difficulties consist, due to lacks of knowledge and an extensive variability inherent to natural conditions. Davies (1989) ably summarizes the complexity of boundary conditions, the importance of extreme events and the possibility of fundamental changes of behaviour. Hence, applications are generally limited to extremely simplified representations of nature or isolated, local phenomena.

combination of statistical and deterministic models.

At present (1996), trends can be observed to combine both approaches in a probabilistic manner. In FRIMAR (1995), flooding risks are determined by using statistical and deterministic models to construct frequency distributions of system responses with "independent", stochastic input parameters. However, it should be noted that in a combined approach, benefits as well as drawbacks of statistical and deterministic methods are present.

A major handicap of such a chain of models is the accepted level of correlation (are sub-model variables stochastical and independent ?), effects of sub-model accuracy and the computation costs involved to construct different scenarios.

Sensitivity analyses of parameters in such a chain of models can be useful (Tung, 1996) to determine the required level of sub-model performance, priorities of research topics, format of information and reduction of computation costs.

1.3.2. Description of boundary conditions.

In this study, a deterministic model is used to study some isolated aspects of mountain-river hydraulics and morphology. As indicated in the previous section, application of deterministic models to predict mountain-river hydraulics and morphology is remote but probable in probabilistic procedures.

Isolation of fluvial morphodynamics in a study of mountain rivers requires introduction of artificial boundaries, where river-catchment interaction must be prescribed. With the description of these interactions, hydrological and sedimentological processes are involved. With respect to limitations of deterministic descriptions due to boundary conditions, a brief review is given.

The river-catchment boundary interaction (volume, duration, frequency and sequence of supply) controls both long-term and short-term changes in morphology. An example is the occurrence of local, intense rain-burst events, that can induce flash floods and debris flows which entirely change the river (e.g. Whittaker, 1985; Naef *et al.* 1988, Turner and Schuster, 1996). Nevertheless, prediction of fluvial hazards on a longer time-scale often requires integration or neglecting of seasonal (and shorter) variations (Di Silvio and Peviani, 1991).

In analogy with discharge, "base-flow related" and "sudden-event" types of sediment supply can be distinguished (Takahashi, 1991), with subsequent small and large scales. Modelling of the first type is often accomplished by regression analyses, relating local sediment yields to rainfall, catchment area characteristics and discharge. However, with the use of rather detailed geographic information systems (GIS), also mechanistic approaches at basin scale are possible (Burton and Bathurst, 1994).

The second type of sediment supply is even more complex; for a reliable prediction of land slides (with subsequent rate and volume), extensive monitoring and data analysis is required (e.g. Peviani *et al.* 1995; Turner and Schuster, 1996). To predict space-frequencies of landslide-induced flood waves, Swanson *et al.* (1985) combines the analysis of regional geology, history of slope movements and topography of the drainage system.

4

When river reaches are relatively short, boundary conditions concerning water and sediment input almost entirely dominate the response of a river. An example is the 1987 flooding of the Mallero at Sondrio in Northern Italy (Di Silvio and Peviani, 1989), where the flooded city was located only 12 km downstream of the nearest land-slide that overloaded the river. Here, also the dynamics of a narrowing river, with subsequent development of backwater curves, should be considered when predicting the propagation of an aggradation front (Bezzola *et al.*, 1990).

Apart from the conditions described above, geological constraints on slope and width determine the river type (e.g. Galay, 1987). Another hazard concerns the deposition of debris (e.g. trees etc.), which can induce the formation of natural dams, that enlarge peak-flow discharges in case of breaking (Kellerhals, 1988; Takahashi and Nakagawa, 1994).

1.4. Scope of the study.

This study concentrates on hydraulic and morphological behaviour of rivers in typical mountain-river conditions. Objective is to contribute to the analysis of flooding due to river-morphological activity. Results concern the analysis of limited, one-dimensional formulations of fluvial morphodynamics. Numerical procedures are applied to solve a mathematical model that represents hydraulic and morphological aspects of simplified mountain-river conditions.

At present, models for river morphology have been tested and applied to low-land rivers mainly (De Vries, 1993), whereas only recently, numerical models are being applied to trans- and supercritical flows (e.g. Ghilardi and Menduni, 1989; Okabe, 1992; Sloff, 1993b; Okabe *et al.* 1994). Another trend concerns expanding analyses on effects of variable river-bed composition (e.g. Parker, 1991c), with the majority of models applicable for low-land rivers only.

Hence, for conditions prevailing in mountain rivers (trans- and supercritical flows, large gradation of sediment and flows with a strongly non-uniform character), hiates consist in knowledge on the behaviour of solutions (both continuous and discontinuous flows), type of boundary conditions, possibilities for simplification and numerical solution procedures.

Because data are difficult to obtain, calibration and verification of modelling concepts is poor.

5

1.5. Major limitations of the model.

The model used is a limited perception of processes in a non-uniform, unsteady, multi-dimensional environment of fluid and sediment. The mathematical, and numerical model studied, concerns a one-dimensional flow, with a hydrostatic pressure-distribution over the depth. This formulation does certainly not correspond to many mountain streams at low-flow conditions, with turbulent fluctuations in free surface level and where flow patterns exhibit two-dimensional patterns with complex bar systems and pool-riffle sequences.

This yields a restriction of the applicability of its results. Two major aspects are reviewed.

one-dimensional hydraulics and morphology.

Morphological responses of a mountain river concern changes in plan form, channel geometry and/or bed composition. Hence, one of the major restrictions of this study with respect to morphology, is the assumption of fixed width and a single-thread flow pattern. At zones of deposition, multiple channels in a braided river system can be found, that can exhibit significant instable behaviour. Often, the development of such plan forms is assumed to be related to macro-scale bed forms including bars (either free or forced by external conditions) that develop by instability mechanisms. For mathematical treatment and review of this topic, reference is made to Seminara (1989).

For example Ryan and Grant (1991) report distinct width-responses (widening in case of aggradation) by means of areal photographs of canopy changes (sequences of opening and revegetation). Schöberl (1994) refers to braided-river sections as important storage buffers in case of large sediment supply.

rheology of flow.

One of the effects not considered in this study concerns changes in rheology. Accurate classification (Bradley and McCutcheon, 1985) and prediction of rheological behaviour, for a wide range of sediment concentrations is difficult (e.g. Rickenmann, 1991). Changes in viscous shear stresses (in laminar flow) and turbulence dampening (in turbulent flows), induce changes in velocity profiles and sediment concentrations. As a result, changes in rheology can significantly affect the friction loss and transport capacity of a flow (Bradley and McCutcheon, 1985).

6

An extreme situation consists in case of debris flows, where a fluidized mixture of sediment sizes develops, with boulders accumulating and tumbling at the front. In case of debris flow, an unsteady, pulsating mixture of water and fine and coarse sediment can develop (Rickenmann, 1991), which can dramatically change the destructive power of a flood (Davies, 1989). Initiation mechanisms include landslides (Zimmerman, 1990), instable layers of bed material (e.g. Smart and Jaeggi, 1983) or the collapse of temporary barriers, deposited in a channel. With respect to the first mechanism, the triggering role of rainfall is mentioned (Okunishi and Suwa, 1985; Chen, 1988; Cojean, 1994; Hirano *et al.* 1994). For an extensive review on the matter, reference is made to Takahashi (1991).

Similarly, air entrainment due to turbulence at free-surface level is neglected in this study. According to Chanson (1992), air entrainment can induce a significant drag reduction, with subsequent effects on friction loss and sediment transport.

1.6. Outline of the report.

In Chapter two, the system of partial differential equations that represents a cross-sectionally integrated flow with a mobile bed is analysed. This analysis concerns the behaviour of solutions and the type and number of boundary conditions for sub-, trans- and supercritical flow regimes.

The variability of river-bed and sediment-transport composition is considered in Chapter three. Here, some aspects of mathematical formulations and numerical solution procedures are considered. For example the interaction between bed level and composition is analysed. Attention is paid to the definition of model parameters such as the commonly used "mixing layer" concept.

The theoretical analyses in Chapter three are used for application to experimental analyses in Chapter four. This chapter includes analytical solutions for armouring experiments, abrasion and longitudinal sorting, and numerical solutions for degradation downstream of a dam, the propagation and deformation of small-scale bed-level disturbances and scouring in a confined section.

In Chapter five, the applicability of simplified mathematical models is analysed. The simplifications concern the decoupled solution of changes in hydraulics and morphology, and the assumption of quasi-steady and/or quasi-uniform flow

conditions. Numerical tests are added to verify results of the theoretical analysis.

In Chapter six, the behaviour of discontinuous solutions, such as hydraulic jumps, bores and aggradations fronts is analysed. Entropy conditions are considered for a simplified situation, and predictive relations for stability and propagation rate are described. Numerical solutions are added and compared with experimental observations.

In Chapter seven, the numerical model, used for several applications throughout the report, is described. A brief review of methods is given, and the application of the *Godunov* method is motivated.

A summary and conclusions can be found in Chapter 8.

Chapter two

Analysis of mathematical model.

2.1. Introduction.

Obviously, mathematical descriptions of flows with mobile beds are similar for low-land and mountain rivers. Due to the specific conditions, however, solutions can be very much different in both river types. This bears consequences with respect of simplifications in mathematical models, its initial and boundary conditions. In this chapter, some effects of conditions prevailing in mountain and piedmont rivers are analysed.

In general, changes in flow mass due to changes in suspended load are considered to be negligible in river hydraulics. At transcritical flows, however, the order of magnitude of celerities, which indicate the dynamic behaviour of solutions, is sensitive to second-order interactions between flow and sediment-load (Sloff, 1993a; Sieben, 1996). Therefore, in the mathematical model analysed in this study, flow is considered to be a mixture of water and sediment (e.g., Holly and Rahuel, 1990a and 1990b; Correia *et al.*, 1992; Okabe, 1992; Sloff, 1993a). As a result, changes in sediment transport interact with changes in flow via density-differences. Rheological changes other than density differences, which can be observed in sediment-laden and debris flows, are not taken into account.

The mathematical model concerns a one-dimensional model with variables averaged over the cross-section. Transversal exchanges of flow and sediment are not accounted for and river widths represented by B are assumed fixed.

Sediment mixtures are described with discrete size fractions. In chapter three, some consequences of implementing a variable river-bed composition are discussed. First, in this chapter, mathematical models with a constant river-bed composition are analysed.

2.2. Mathematical formulations

2.2.1. Continuity of flow and sediment mass.

To distinguish different types of sediment transport, a suspended load layer and a bed-load layer is defined (Figure 2.1) with respective sediment concentrations ϕ_s, and ϕ_b. The corresponding velocities of water in both layers are u_s and u_b.

To determine sediment-mass fluxes, velocities should be assigned to the transported sediment in both layers.
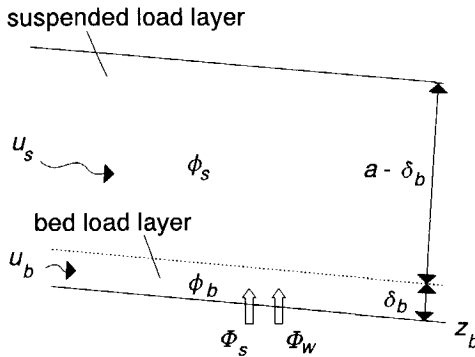
Fig.2.1 Sediment-transport layers.

Based on classical definitions of suspended load and bed load (e.g., Einstein, 1950), generally two hypotheses are applied;

- sediment particles in suspension move with the fluid (which yields a turbulence-averaged velocity and a diffusive contribution due to turbulent fluctuations in concentration and velocity)

- the concentration of sediment particles rolling and sliding in the bed -load layer adapts "instantaneously" to local conditions of flow

Out of the originally four variables (concentration and velocity in both layers) these hypotheses eliminate two. The remaining variables are sediment-concentration in suspension and a bed-load mass flux. It is noted here that in some cases, changes in bed load cannot be considered instantaneous with respect to changes in river-bed composition (see Section 3.4.3).

10

The fluxes of suspended and bed load, integrated over all size fractions, are defined as $\phi_s u_s(a-\delta_b)$ and s_b respectively. Then, the mass balance of a water-sediment mixture is

$$\frac{\partial \rho\left[a+\Delta\left(\phi_s(a-\delta_b)+\phi_b\delta_b\right)\right]B}{\partial t} + \frac{\partial \rho(1+\Delta\phi_s)u_s(a-\delta_b)B}{\partial x} +$$

$$+ \frac{\partial\left(\rho(1-\phi_b)u_b\delta_b+\rho_s s_b\right)B}{\partial x} - \rho_s\Phi_s B - \rho\Phi_w B = 0 \qquad (2.1)$$

where Φ_s and Φ_w are volumetric fluxes of sediment and water from river bed to flow. The densities of water and sediment are represented by ρ and ρ_s, the relative density of sediment is defined as $\Delta = (\rho_s-\rho)/\rho$.

The sediment-mass balance of the river bed can be written as

$$\frac{\partial z_b\rho(1+\Delta c_0)B}{\partial t} + \rho_s\Phi_s B + \rho\Phi_w B = 0 \qquad (2.2)$$

where the sediment fraction in the bed is defined as $c_0 = 1-p$ (p is porosity). The fraction of water in the total exchange with the bed is defined as

$$\Phi_w = (1-\beta_c)\left(\Phi_s + \Phi_w\right) \rightarrow \Phi_w = \frac{1-\beta_c}{\beta_c}\Phi_s \qquad (2.3)$$

With respect to density, differences can be distinguished in upward and downward fluxes. In case of erosion it can be stated $\beta_c = c_0$. In case of deposition different options exist. Deposition without infiltration implies $\beta_c = 1$.

If, however, "frozen" packages of sediment-water mixture are deposited at the bed, β_c equals the depth-averaged concentration of sediment. Then, the concentration of the mixture will not change due to fluxes between flow and bed.

Although this is arbitrary in case of sediment mixtures with wide ranges in grain size, changes in density of river bed are neglected (e.g. Schälchli, 1995). Because the density of the bed is assumed constant, it is consistent to use $\beta_c = c_0$.

If only sediment is considered, the mass balance is

$$\frac{\partial\left(\phi_s(a-\delta_b)+\phi_b\delta_b\right)B}{\partial t} + \frac{\partial\left(\phi_s u_s(a-\delta_b)+s_b\right)B}{\partial x} + c_0\frac{\partial z_b B}{\partial t} = 0 \qquad (2.4)$$

Now, combination of the mass balances for sediment (Eq.2.4) and the water-sediment mixture (Eq.2.1) yields

$$\frac{\partial aB}{\partial t} + \frac{\partial u_s(a-\delta_b)B}{\partial x} + \frac{\partial z_b B}{\partial t} + \frac{\partial\left(s_b+(1-\phi_b)\delta_b u_b\right)B}{\partial x} = 0 \qquad (2.5)$$

The thickness of the bed-load layer is of the order of a few grain sizes (e.g., Van Rijn, 1984a). In general it can be stated that $a >> \delta_b$ and $u_s >> u_b$. Therefore, Eqs 2.4 and 2.5 are simplified as

$$\frac{\partial\phi_s aB}{\partial t} + \frac{\partial\left(\phi_s ua+s_b\right)B}{\partial x} + c_0\frac{\partial z_b B}{\partial t} = 0 \qquad (2.6)$$

and

$$\frac{\partial\left(a+z_b\right)B}{\partial t} + \frac{\partial uaB}{\partial x} = 0 \qquad (2.7)$$

with $u = u_s$, representing the depth-averaged velocity of fluid and sediment in suspension. For the bed-load rate, instantaneous adaption to local conditions is assumed, conform the hypotheses mentioned in the beginning of this section.

2.2.2. Momentum equation.

In addition to the continuity equations for a water-sediment mixture, the equation of momentum can be defined. As for the continuity equations for sediment and flow, the contribution of bed load to density changes of the water-sediment mixture is neglected.

12

Then, the momentum equation is

$$\frac{\partial ua(1+\Delta\phi_s)B}{\partial t} + \frac{\partial u^2a(1+\Delta\phi_s)B}{\partial x} - \frac{g_zB}{2}\frac{\partial a^2(1+\Delta\phi_s)}{\partial x} =$$

$$= g_z(1+\Delta\phi_s)aB\frac{\partial z_b}{\partial x} + (1+\Delta\phi_s)g_xaB - \frac{\tau_bB}{\rho}$$

(2.8)

To account for steep slopes, the system of space-coordinates is rotated relative to a horizontal reference line. In Figure 2.2, the defined z- and x-axes are shown.
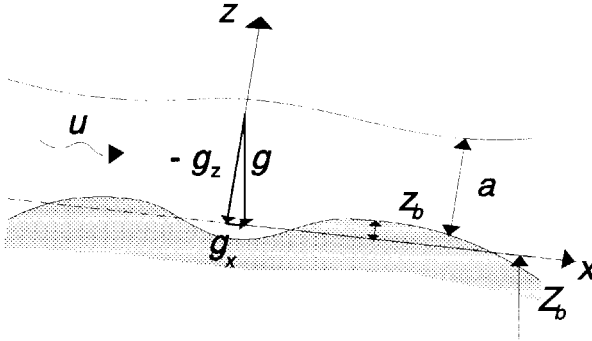
Fig.2.2 Tilted system of coordinates.

Local bed levels z_b are defined relative to Z_b. The latter represents a spatially-averaged, *constant* reference slope of the bed. The resulting components of gravity forces are

$$\begin{bmatrix} g_x \\ g_z \end{bmatrix} = -g\ \cos\theta_x \begin{bmatrix} \dfrac{\partial Z_b}{\partial x} \\ 1 \end{bmatrix} \ ; \quad \tan\theta_x = \frac{\partial Z_b}{\partial x} = -i_b$$

(2.9)

Hence, in case of river reaches with different slopes, only one average value for both reaches is used to determine the gradient in Z_b. In that case, errors are introduced with respect to the effects of gravity components in the direction of flow and perpendicular to the bed. However, in general, the effect of this correction on the solution will be minor (Appendix D).

The system of partial differential equations (PDE's) (Eqs 2.6, 2.7 and 2.8) is

13

applied in the corrector step in the numerical model as described in Chapter 7.

2.2.3. Divergent form.

The form of the mathematical model is of relevance in case of non-uniform or even discontinuous solutions (Abbot, 1974). To guarantee conservation of mass and momentum, mathematical and numerical models should be based on a system as described in Eqs 2.6, 2.7 and 2.8. For analysis of the mathematical model, however, the conservative form is not appropriate. Therefore, a divergent form is derived.

The continuity equation for the mixture can be decomposed into a balance for flow and for sediment in transport. The flow-continuity equation is

$$\frac{\partial a}{\partial t} + u\frac{\partial a}{\partial x} + a\frac{\partial u}{\partial x} + \frac{\partial z_b}{\partial t} = -\frac{ua}{B}\frac{dB}{dx} \qquad (2.10)$$

The sediment-continuity equation integrated over all size-fractions is

$$\frac{\partial s_b}{\partial x} + a\frac{\partial \phi_s}{\partial t} + ua\frac{\partial \phi_s}{\partial x} + \left(c_0 - \phi_s\right)\frac{\partial z_b}{\partial t} = -\frac{s_b}{B}\frac{dB}{dx} \qquad (2.11)$$

With the help of the separated continuity equations for flow and sediment mass, the flow-momentum equation can be written as follows

$$\frac{\partial u}{\partial t} + u\frac{\partial u}{\partial x} - g_z\frac{\partial a}{\partial x} - \frac{u}{a}\frac{\partial z_b}{\partial t} - g_z\frac{\partial z_b}{\partial x} +$$

$$+ \alpha u\frac{\partial \phi_s}{\partial t} - \alpha\frac{g_z a}{2}\left(2Fr^2+1\right)\frac{\partial \phi_s}{\partial x} = g_x - \frac{\tau_b}{\rho(1+\Delta\phi_s)a} \qquad (2.12)$$

The coefficient α is defined as

$$\alpha = \frac{\Delta}{1+\Delta\phi_s} \qquad (2.13)$$

The approximate, first-order solution of the cross-sectionally integrated balance of a concentration in suspension is

$$T_A\frac{\partial \phi_s}{\partial t} + L_A\frac{\partial \phi_s}{\partial x} + \left(\phi_s - \phi_{se}\right) = 0 \qquad (2.14)$$

14

where ϕ_{se} is the suspended-load transport-capacity, T_A and L_A are adaption period and length respectively (e.g. Galappatti 1983, Galappatti and Vreugdenhil, 1985). Armanini and Di Silvio (1988) suggested a similar PDE for separate fractions in suspension.

2.3. Characteristic equations.

2.3.1. Introduction.

The system of PDE's as described in Section 2.2 is of a hyperbolic type. This enables a transformation into an equivalent set of characteristic equations. These characteristic equations consist of celerities and ordinary differential equations (ODE's) valid along each celerity. The set of ODE's are the compatibility equations. Characteristic equations provide information on the dynamic behaviour of the mathematical model. Characteristics or celerities represent the propagation of information through the computation domain whereas compatibility equations represent the type of information carrried along the characteristics.

With respect to the application of compatibility equations, the Riemann problem can be mentioned, which concerns the behaviour of discontinuous solutions of flows (e.g., Stoker 1957, Whitham 1974; Abbott, 1974). For flows at fixed beds, an illustrative example is the construction of analytical solutions for dambreak waves by Stoker (1957).

Due to the strongly non-linear character, the application of compatibility equations to analyse mobile-bed models is not very common. Here, derivation is considered useful not only for analytical but also for numerical approaches. For example, the initial behaviour (growth or decline) of disturbances in bed level and composition can be analysed (Sieben, 1994).

2.3.2. Construction of characteristic equations.

Because the system of PDE's for a one-dimensional, depth-averaged model is hyperbolic, the original equations (with x- and t- coordinates) can be combined to a form containing ordinary differentials along characteristics, (Hirsch, 1990). Hence, differences are considered in τ-direction (Figure 2.3).

15
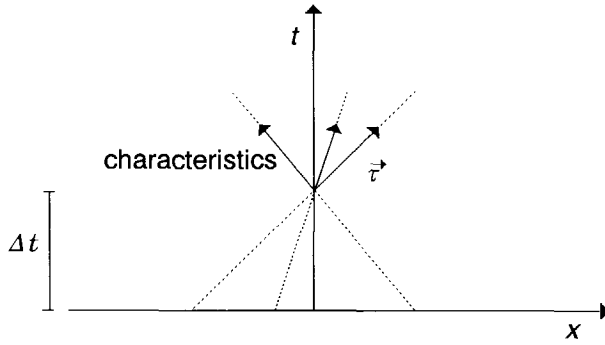
Fig.2.3 Characteristics.

To obtain the compatibility equations, a transformation must be performed. A three-step procedure as described by for example Lai (1986) or Lin and Shen (1984) can be followed.

- combine all PDE's into one PDE

- gradients in variables are stated to be along the characteristics

- solve the coefficients that are used to summon the original PDE's

This procedure is applied to the one-dimensional model of Subsection 2.2.3. If every PDE is multiplied with n_i, the sum of PDE's can be written as

$$
\begin{bmatrix} n_1 \\ un_1 - g_z n_2 \end{bmatrix} \begin{bmatrix} a_t \\ a_x \end{bmatrix}^T + \begin{bmatrix} n_2 \\ an_1 + un_2 + \psi an_3 \end{bmatrix} \begin{bmatrix} u_t \\ u_x \end{bmatrix}^T + \begin{bmatrix} n_1 - \dfrac{\ddot{u}}{a} n_2 + (c_0 - \phi_s)n_3 \\ -g_z n_2 \end{bmatrix} \begin{bmatrix} z_t \\ z_x \end{bmatrix}^T +
$$

$$
+ \begin{bmatrix} n_4 T_A + \alpha u n_2 + an_3 \\ n_4 L_A + \alpha \dfrac{-g_z a\Delta}{2}(2Fr^2 + 1)n_2 + uan_3 \end{bmatrix} \begin{bmatrix} \phi_{st} \\ \phi_{sx} \end{bmatrix}^T = O
$$

(2.15)

The source term includes contributions due to friction, gradients in width and relaxation of suspended load

$$
O = - n_1 \frac{ua}{B}\frac{dB}{dx} + n_2 \left(g_x - \frac{\tau_b}{\rho(1+\Delta\phi)a} \right) - n_3 \frac{s_b}{B}\frac{dB}{dx} + n_4 \left(\phi_{se} - \phi_s \right)
$$

(2.16)

16

Gradients in variables along a celerity are defined as

$$\frac{\mathrm{d}..}{\mathrm{d}t} = \frac{\partial ..}{\partial t} + c\,\frac{\partial ..}{\partial x} \tag{2.17}$$

where c is a celerity.

Application of this transformation to all terms at the left-hand side of Eq.2.15 requires that multiplification vectors are perpendicular to the characteristic path. For example depth is considered.

$$\begin{bmatrix} n_1 \\ un_1 - g_z n_2 \end{bmatrix} \begin{bmatrix} a_t \\ a_x \end{bmatrix}^T = \lambda \begin{bmatrix} 1 \\ c \end{bmatrix} \begin{bmatrix} a_t \\ a_x \end{bmatrix}^T \quad \cdot \quad (u-c)n_1 - g_z n_2 = 0 \tag{2.18}$$

This yields 4 conditions to solve n_i. When these values of n_i are found, a characteristic equation can be constructed for every celerity c_l.

$$n_1\frac{\mathrm{d}a}{\mathrm{d}t} + n_2\frac{\mathrm{d}u}{\mathrm{d}t} + \left(n_1 - \frac{u}{a}n_2 + (c_0-\phi)n_3\right)\frac{\mathrm{d}z_b}{\mathrm{d}t} + (n_4 T_A + \alpha u n_2 + a n_3)\frac{\mathrm{d}\phi_s}{\mathrm{d}t} = O_l \tag{2.19}$$

If explicit values for the celerities are known, Eq.2.19 can be integrated to obtain the Riemann invariants of this model. In a *linearized model*, an equivalent Riemann invariant W_l can be defined for every celerity c_l

$$W_l = n_1 a + n_2 u + \left(n_1 - \frac{u}{a}n_2 + (c_0-\phi)n_3\right) z_b + (n_4 T_A + \alpha u n_2 + a n_3)\,\phi_s \tag{2.20}$$

which enables rewriting the characteristic equations as

$$\frac{\mathrm{d}W_l}{\mathrm{d}t} = \frac{\partial W_l}{\partial t} + c_l\,\frac{\partial W_l}{\partial x} = O_l \tag{2.21}$$

17

The corresponding solution for the multiplification coefficients n_i reads

$$n_1 = g_z a(c_0 - \phi_s)c \; P \; ; \; n_2 = (c_0 - \phi_s)ca \; (u-c) \; P \; ; \; n_3 = u\left(-g_z a + c(u-c)\right) P$$

$$n_4 = a(u-c)\left(g_z au - \alpha c(c_0 - \phi_s)\left(\frac{-g_z a}{2}(2Fr^2 + 1) - uc\right) + cu(c-u)\right)$$

$$(2.22)$$

and

$$P = L_A - T_A c \qquad (2.23)$$

Hence, for every value of c, a set of n_i consists. The celerities c are roots of

$$\left(\frac{c}{u}\right)^3 - \left(2 + \frac{\psi_s}{c_0 - \phi_s}\right)\left(\frac{c}{u}\right)^2 + \left(1 + \frac{\psi}{c_0 - \phi_s} - \frac{1}{Fr^2}\right)\left(\frac{c}{u}\right) + \frac{\psi_s}{(c_0 - \phi_s)Fr^2} = 0 \qquad (2.24)$$

$$\vee \; c = \frac{L_A}{T_A}$$

2.3.3. Analysis of characteristic surfaces.

In hydraulic and morphological research, the analysis of characteristics has been applied extensively to one-dimensional models with and without mobile bed (e.g. De Vries, 1965) and 2DH-models with fixed beds (Daubert and Graffe, 1967; Katopodes and Strelkoff, 1978; Abbott, 1979) and mobile beds (Lin and Shen, 1984; Lai, 1986; De Vriend, 1987 and Sloff, 1992).

Celerities can be interpretated as propagation rates of infinitely small disturbances in model variables. By comparing fixed-bed and mobile-bed models, close correspondence of celerities can be observed for $Fr < 0.8$ and $Fr > 1.2$ and small values of s_b/q (De Vries, 1965). Hence, "instantaneous" changes in water depth and velocity can be considered decoupled from the relatively slow changes in bed level. This enables quasi-steady flow modelling as described by De Vries (1965) and Vreugdenhil and De Vries (1973).

This analysis can be applied for a two-dimensional model as well. In a 2-DH model with a hyperbolic set of PDE's, a three-dimensional space constructed by t-, x- and y-axes can be confined into a two-dimensional space constructed

18

by τ, a curve parameter along a bicharacteristic ray and s, a parameter perpendicular to the bicharacteristic ray (Figure 2.4).

To construct characteristic surfaces, it is stated that along characteristic surfaces, partial differentials are undetermined. With this condition and the Huyghens' method, characteristic surfaces can be constructed (Sieben and Sloff, 1994). For mathematical backgrounds, reference is made to Courant and Hilbert (1962), Fletcher (1988a, 1988b) or Hirsch (1988, 1990) among others.
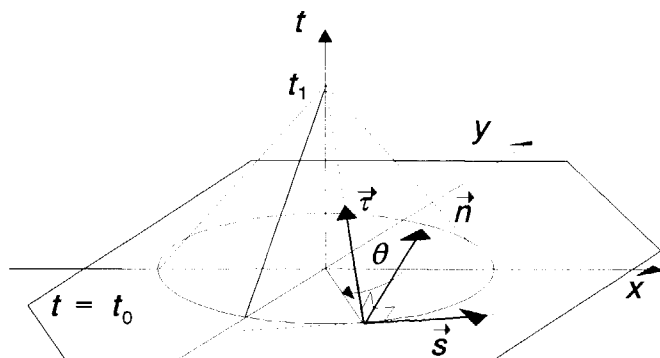
Fig.2.4 Characteristic curves.

Obviously, celerities in one-dimensional models correspond to rays along characteristic surfaces in two-dimensional models. To indicate some differences between one- and two-dimensional models, characteristics are compared. Therefore, a two-dimensional model is applied, consisting of continuity equations for flow and sediment, and momentum equations in longitudinal and transversal direction.

Flow continuity

$$\frac{\partial a}{\partial t} + \frac{\partial ua}{\partial x} + \frac{\partial va}{\partial y} = 0 \qquad (2.25)$$

Without second-order terms, the balances of x-directed and y-directed momentum in a depth-averaged flow are

$$\frac{\partial u}{\partial t} + u\frac{\partial u}{\partial x} + v\frac{\partial u}{\partial y} - g_z\frac{\partial a}{\partial x} - g_z\frac{\partial z_b}{\partial x} = g_x - \frac{\tau_{bx}}{\rho a} \qquad (2.26)$$

19

$$\frac{\partial v}{\partial t} + u\frac{\partial v}{\partial x} + v\frac{\partial v}{\partial y} - g_z\frac{\partial a}{\partial y} - g_z\frac{\partial z_b}{\partial y} = g_y - \frac{\tau_{by}}{\rho a} \qquad (2.27)$$

where u and v velocity component in x- and y-direction, and τ_{bj} bed shear-stress in j-direction. The components of bed material load are defined as

$$s_{bx} = \frac{u}{u_{tot}}s_b \quad ; \quad s_{by} = \frac{v}{u_{tot}}s_b \qquad (2.28)$$

(De Vriend, 1987). Then, the sediment mass balance is

$$\frac{\partial z_b}{\partial t} + T_1\frac{\partial u}{\partial x} + T_2\frac{\partial v}{\partial y} + T_3\left(\frac{\partial u}{\partial y} + \frac{\partial v}{\partial x}\right) = 0 \qquad (2.29)$$

with

$$T_1 = a\frac{u^2}{u_{tot}^2}\left(\psi + \frac{v^2}{u^2}\phi\right) \; ; \; T_2 = a\frac{u^2}{u_{tot}^2}\left(\frac{v^2}{u^2}\psi + \phi\right) \; ; \; T_3 = a\frac{uv}{u_{tot}^2}(\psi - \phi) \qquad (2.30)$$

$$\psi = \frac{ds_b}{du_{tot}} \; ; \; \phi = \frac{s_b}{au_{tot}}$$

For a two-dimensional model with a fixed bed, the family of characteristic surfaces consist of one characteristic plane (streamlines along which vorticity is transported, Vreugdenhil; 1989) and a circle. For a two-dimensional model with mobile bed and constant composition, one characteristic plane (vortex condition), a distorted "circle" and a small triangle can be found. The latter two curves are coupled.

If x-axes are oriented in flow direction (which implies that $v = 0$ m/s and $u = u_{tot}$), characteristic rays of the "circle" and triangle are roots of

$$\left(\frac{c}{u}\right)^3 - 2\cos\theta\left(\frac{c}{u}\right)^2 - \left[\frac{(1+\psi-Fr^2)}{Fr^2}\cos^2\theta + \frac{(1+\phi)}{Fr^2}\sin^2\theta\right]\left(\frac{c}{u}\right) +$$
$$\qquad\qquad\qquad\qquad\qquad\qquad\qquad\qquad\qquad\qquad (2.31)$$
$$+ \cos\theta\left(\frac{\psi\cos^2\theta + \phi\sin^2\theta}{Fr^2}\right) = 0$$

If the orientation θ is zero (in downstream direction), celerities of the one-

20

dimensional model are obtained.

In transversal direction, only two non-zero celerities are found (Sieben, 1994). For low values of Fr, information along these characteristic rays concerns water depth and bed level mainly (i.e. free surface level). With increasing values of Fr, information on changes in the transversal velocity component v becomes significant. At critical flow, the transfer of transversal information includes a and v, and at a slightly lower order u and z_b. Clearly, at values of Fr larger than 0.8, information on transversal changes includes all variables.

The sensitivity of characteristic surfaces to the rate of sediment transport s_b can be analysed by computing characteristic curves for different values of s_b. Both curves are combined into one graph, and differences can be noted visually. In the following analysis, sediment transport is predicted with a simple powerlaw $s_b = mu^n$ (with $m = 10^{-4}$ s^4/m^3 ; $n = 5$). Huyghens' constructions of dimensionless bicharacteristic surfaces are presented for increasing values of Fr in Figures 2.5-a to 2.5-f. Unfortunately, the scales of n and s are somewhat distorted. Flow is directed from left to right along s.

subcritical flows

For low values of Fr (Figures 2.5-a and -b), the "circle" is insensitive to the rate of sediment transport. The magnitude of the triangle is negligible. From comparison with fixed-bed models, or by analysing the compatibility equations, it can be concluded that the "circle" represents the propagation of changes in hydraulic variables. Similarly, the small triangle can be related to morphological changes.
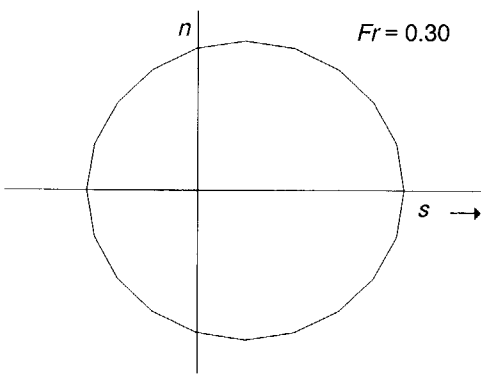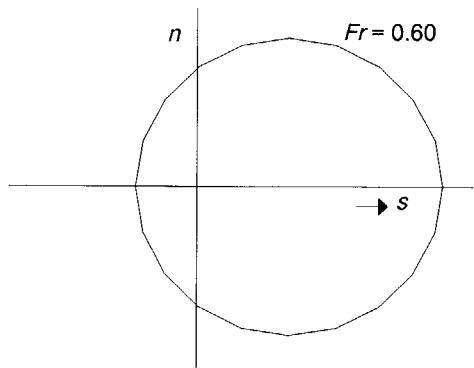
Fig. 2.5-a $Fr = 0.3$.   **Fig.2.5-b** $Fr = 0.6$.

transcritical flows

For values of Fr near unity (Figure 2.5-c), sediment-transport rates affect disturbances that propagate along the upstream-directed part of the "circle". There, the coupling between both families of curves becomes significant. This affected part expands with Fr (Figure 2.5-d).
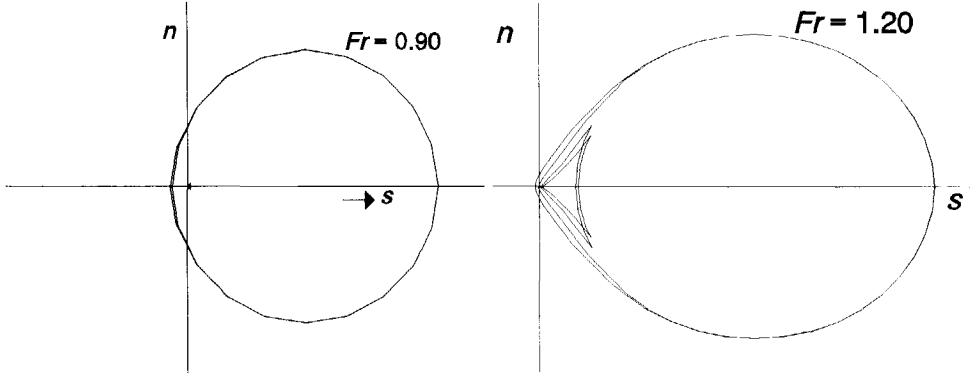
Fig.2.5-c $Fr = 0.9$.

Fig.2.5-d $Fr = 1.2$.

supercritical flows

For supercritical flows (Figures 2.5-e and-f), the effect of s_b on characteristic surfaces in transversal direction is shown. The parts of the characteristic surfaces that are sensitive to s_b are directed in upstream and downstream directions. This marks an important difference with one-dimensional models.
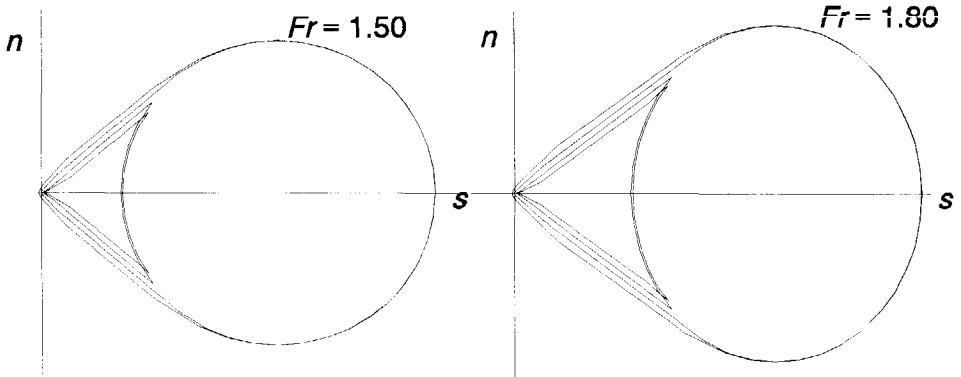
Fig.2.5-e $Fr = 1.5$.

Fig.2.5-f $Fr = 1.8$.

From analysing the compatibility equations (Sieben, 1994), it can be concluded

22

that along parts of the curve that are sensitive to transport rate, again mainly changes in bed level consist. Hence, for supercritical flow, transversal changes in bed-level can be directed in both upstream *and* downstream directions. This in contrast with one-dimensional models, where transversal propagation is omitted and changes in bed level can be related to upstream-directed characteristics mainly.

2.4. Analysis of a 1-D model.

2.4.1. Characteristic equations.

Analysis of characteristic equations provides insight into the mathematical model. This insight is inevitable in the application of numerical schemes and type and number of boundary conditions. In the following analysis, a one-dimensional model with mobile bed and constant composition is used.

$$\frac{\partial a}{\partial t} + u\frac{\partial a}{\partial x} + a\frac{\partial u}{\partial x} = 0 \tag{2.32}$$

$$\frac{\partial u}{\partial t} + u\frac{\partial u}{\partial x} - g_z\frac{\partial a}{\partial x} - g_z\frac{\partial z_b}{\partial x} = g_x - \frac{\tau_b}{\rho_m a} \tag{2.33}$$

$$\frac{\psi a}{c_0}\frac{\partial u}{\partial x} + \frac{\partial z_b}{\partial t} = 0 \quad ; \quad \psi = \frac{1}{a}\frac{ds_b}{du} \tag{2.34}$$

The corresponding compatibility equations are

$$-g_z c\frac{da}{dt} - c(u-c)\frac{du}{dt} + g_z(u-c)\frac{dz_b}{dt} = -c(u-c)\left(g_x - \frac{\tau_b}{\rho_m a}\right) \tag{2.35}$$

with

$$\left(\frac{c}{u}\right)^3 - 2\left(\frac{c}{u}\right)^2 + \left(1 - \frac{1+\psi/c_0}{Fr^2}\right)\frac{c}{u} + \frac{\psi/c_0}{Fr^2} - 0 \tag{2.36}$$

23

The change in for example U along a characteristic c_i is defined as

$$\frac{dU}{dt} = \frac{U^{n+1} - U_i^n}{\Delta t} \qquad (2.37)$$

Hence U_i^n, which represents variables at three different locations, is required to solve the characteristic equations (Figure 2.6).
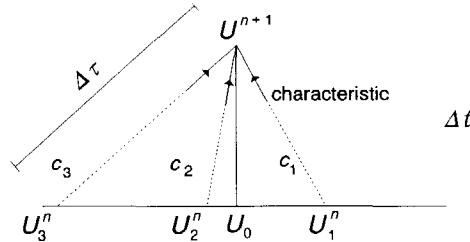
Fig.2.6 Integration along characteristics.

With the variables at the three locations, the new variables can be written as

$$U^{n+1} = \begin{bmatrix} a \\ u \\ z_b \end{bmatrix} = R \begin{bmatrix} a_1 \\ u_1 \\ z_1 \end{bmatrix} + S \begin{bmatrix} a_2 \\ u_2 \\ z_2 \end{bmatrix} + T \begin{bmatrix} a_3 \\ u_3 \\ z_3 \end{bmatrix} + \Delta t \begin{bmatrix} 0 \\ g_x - \dfrac{\tau_b}{\rho_m a} \\ 0 \end{bmatrix} \qquad (2.38)$$

with R, S and T matrices that can be constructed by solving the characteristic equations. The variables after a time step Δt can be interpretated as "weighted-averages" of the initial variables at locations $i = 1, 2$ and 3. To analyse these "weights", variables are made dimensionless by applying

$$a = a_0 a' \quad ; \quad u = u_0 u' \quad ; \quad z_b = a_0 z_b' \qquad (2.39)$$

The matrix R corresponds to the *up*stream-directed celerity c_1, the matrices S and T correspond to the small and large, *down*stream-directed celerities c_2 and c_3. In other words, the contribution of downstream information is represented by R, the contribution of upstream information by S and T. The dimensionless coefficients of R, S and T are represented in the Figures 2.7, 2.8 and 2.9.

24
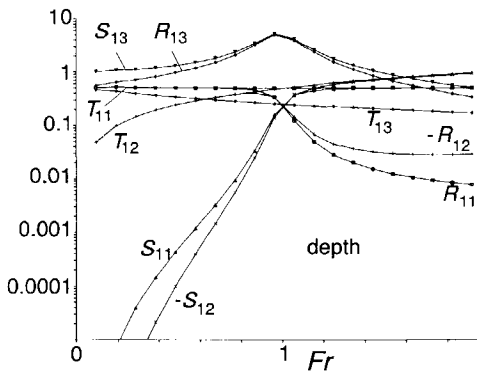
Fig.2.7 Solution of depth.
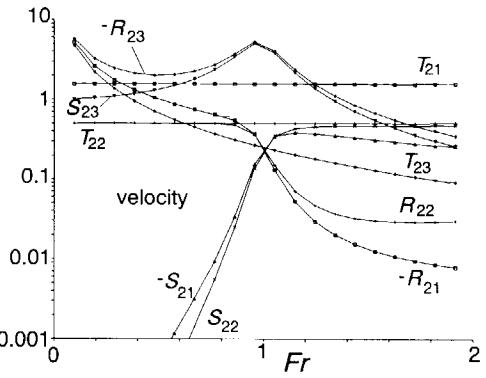
Fig.2.8 Solution of velocity.
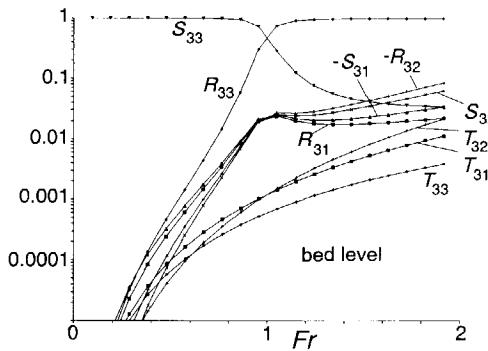
Fig.2.9 Solution of bed level.

The relative values of the coefficients in the matrices indicate the contribution of a variable (located either up- or downstream) to the solution. Based on the Figures 2.7, 2.8 and 2.9, three zones can be distinguished; subcritical flow (Fr < 0.8), transcritical flow ($0.8 < Fr < 1.2$) and supercritical flow ($Fr > 1.2$).

Subcritical flow ($Fr < 0.8$).

With respect to velocity and depth, information along c_2 (matrix S) does not

25

contribute to the solution for $Fr < 0.8$. With respect to bed level, however, the solution is mainly determined by information along c_2. Both aspects can be combined when decoupling hydraulics from morphology. This corresponds with the quasi-steady flow approach for analytical and numerical models for morphology (De Vries, 1966).

Transcritical flow $(0.8 < Fr < 1.2)$.

In transcritical flow $(0.8 < Fr < 1.2)$, the solution is merely determined by information along the up- and downstream directed c_1 and c_2 (matrices R and T), which are now an order of magnitude smaller than c_3. Velocity and depth are significantly influenced by spatial gradients in bed level; the contribution of both velocity and depth reduces. This favors the application of quasi-uniform flow models, where convective terms are neglected.

Since changes in bed levels are determined more or less symmetrically by contributions of up- and downstream bed levels, morphological changes will have a diffusive character. This has been found as well in numerical experiments (Chapter five). This corresponds with the application of parabolic models for morphology in transcritical flows (e.g. Di Silvio, 1991).

The strong diffusion in up- and downstream directions in transcritical flow, relative to one dominant direction of propagation in either sub- or supercritical flow corresponds with the observed washout of bed forms ("plane bed", Simons and Richardson, 1960 and 1961) in transitional flow regimes (e.g. Van Rijn, 1984c; Raudkivi, 1990). It is noted here that the connection between Fr and bed form type is of relevance only in case of significant coupling of bed level and water surface profiles (such as standing waves or antidunes, Taylor and Brooks, 1961). For low values of Fr, when this coupling is negligible (ripples, dunes), transport parameters are better indicators (Van Rijn, 1989).

Supercritical flows $(Fr > 1.2)$.

In supercritical flows, the effect of information along the upstream-directed celerity c_1 on the solution of velocity and depth diminishes. The effect of upstream and downstream bed levels on the solution of depth and velocity is comparable to subcritical flows. Bed levels, however, are mainly determined by information on bed levels along c_1. For morphology, this would resemble a simple-wave model promoting again a quasi-steady flow approach.

26

2.4.2. Harmonic solution.

Because the system of PDE's has a hyperbolic character; solutions concern disturbances or waves in variables, propagating in up- or downstream direction through the computation domain until a steady state is obtained. Corresponding to the type of solution, simplifications in the system of PDE's for shallow-water can be made (e.g. Jansen *et al.*, 1979 or Hager and Droux, 1986). When linearized models are used, harmonic solutions are convenient for theoretical analysis (e.g, Vreugdenhil, 1994).

To study simplifications, solutions of the complete and simplified models must be compared. First, a reference solution of the complete model is constructed. In the following analysis, river-bed compositions are again assumed to be constant. Hence, the mathematical model considered in this subsection is equal to that in Subsection 2.4.1. Conform procedures described in for example Vreugdenhil (1972, 1989), all zero-order terms in Eqs.2.32, 2.33 and 2.34 are assumed to be zero, which results in zero-order, uniform and steady flow. The derivatives of first-order terms can be made dimensionless by introducing the following transformations

$$a' = \frac{a}{a_0} \; ; \; u' = \frac{u}{u_0} \; ; \; z_b' = \frac{z_b}{a_0} \; ; \; x' = \frac{x}{u_0 T} \; ; \; t' = \frac{t}{T} \qquad (2.40)$$

The time period T represents a representative period of the solution. For shorthand writing, primes are left out.

The resulting system of three first-order PDE's, with three variables a, u and z_b can be combined into one third-order PDE with variable z_b (e.g. Barneveld, 1988)

$$\frac{\partial^3 z_b}{\partial t^3} + 2 \frac{\partial^3 z_b}{\partial x \partial t^2} + \frac{Fr^2 - 1 - \psi}{Fr^2} \frac{\partial^3 z_b}{\partial x^2 \partial t} - \frac{\psi}{Fr^2} \frac{\partial^3 z_b}{\partial x^3} +$$
$$+ E \left(\frac{\partial^2 z_b}{\partial t^2} + \frac{3}{2} \frac{\partial^2 z_b}{\partial x \partial t} \right) = 0 \qquad (2.41)$$

where

$$E = 2 \frac{-g_z}{C^2} \frac{L}{a} \qquad (2.42)$$

The length-scale L can be based on hydraulic features by $L = uT$, with T a characteristic period of a hydrograph, or on geometrical features, representing a characteristic length of bed-level fluctuations.

For constant values of Fr and ψ, different types of wave solutions can be found, identified by different values of E (relative contributions of inertia and friction) (Vreugdenhil, 1972; Grijsen and Ogink, 1973; Grijsen and Vreugdenhil, 1976; Ponce and Simons, 1977; Ponce et al., 1978). Examples of increasing E (decreasing inertia and increasing friction contribution) are surges, tidal waves and river-flood waves.

If a sinusoidal solution is used to represent a flood hydrograph, three non-trivial wave-type solutions can be found. With increasing propagation rate, these waves are identified as I (upstream), II and III (downstream). For $E = 0$, propagation rates of the three waves equal the celerities. With increasing value of E, propagation rates decrease.

These harmonic solutions can be characterized by propagation rates and damping lengths (Figures 2.10 and 2.11).
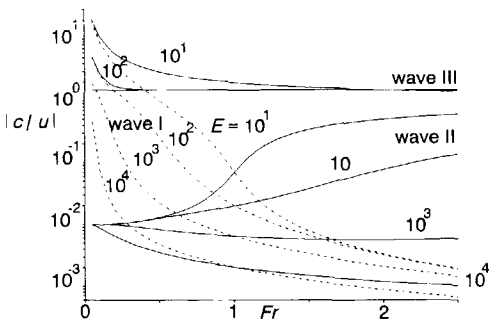
Fig.2.10 Wave propagation rates.   Fig.2.11 Wave attenuation-length.
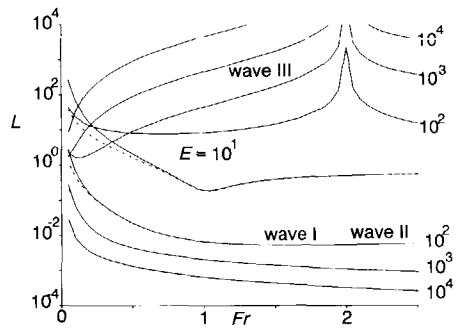
For higher values of Fr and larger values of E, wave III approaches a kinematic wave with propagation rate $3u/2$ (e.g. Jansen et al., 1979). This is in correspondence with Bren and Turner (1978), who successfully described wave

28

propagation in a rough stream (with subsequent high values of E) with a kinematic wave approximation.

The dimensionless attenuation length for wave III increases for longer waves and higher values of Fr (less damping). This reduction of damping enables development of instable wave-type solutions at $Fr \geq 2$, which corresponds with the existence of roll waves (Mayer, 1959; Ishihara, 1960; Taylor and Kennedy, 1960; Escoffier and Boyd, 1962; Dracos and Glenne, 1967; Berlamont, 1976; Berlamont and Vanderstappen, 1981; Kranenburg, 1990; Rosso, 1990).

Attenuation lengths of waves I and II are small compared to wave III. For waves I and II, a decrease in attenuation length is found with increasing value of Fr (more damping). For $Fr < 0.8$, E has small effects on downstream-propagating waves II, for $Fr > 1.2$, this is the case for upstream-propagating waves I.

To indicate the contribution of bed mobility, relative amplitudes (and phase shifts) in bed level can be constructed for each wave. The bed-level response for the different wave-type solutions is represented in Figure 2.12. Arrows indicate the effect of increasing E on the response. In a linearized model, changes in bed level due to wave III are negligible. For $E = 0$, changes in bed level exist along wave II for subcritical flows, and along wave I for supercritical flows. For $E > 10^3$, changes along waves I and II are similar. This is in correspondence with the conclusions drawn in Subsection 2.4.2.
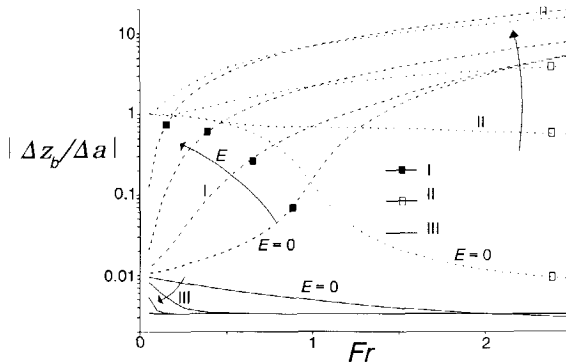
Fig.2.12 Bed-level response.

2.5. Boundary conditions.

2.5.1. Introduction.

The *number* of boundary conditions is determined by the sign of characteristics; one negative and two positive characteristics implies two conditions upstream and one condition downstream. Because characteristics of mobile-bed models are non-zero and do not change sign, the number of conditions at a boundary is constant for all types of flow regime. This is in contrast with fixed-bed models.

The *type* of boundary conditions is determined by the characteristic equations; the boundary conditions substitute the "incoming" characteristic equations. Therefore, one should be able to reconstruct the incoming characteristic equations from the boundary conditions.

In river-engineering, stage-discharge relations are often applied to obtain discharges from records of water levels. In case of flood waves, hysteresis effects should be taken into account (e.g. Jansen *et al.*, 1979). With respect to the use of waterlevel records at higher values of *Fr*, the following is noted. In mountain rivers with high roughness (high values of *E*), flood waves can be approximated as diffusion waves. If the contribution of time changes to the dynamics of the wave can be neglected (quasi-steady flow but not uniform), discharges can be written as

$$Q = Q_s \sqrt{1 - \frac{(1-Fr^2)}{i_b} \frac{\partial a}{\partial x}} \quad ; \quad Q_s = aC\sqrt{ai_b}B \qquad (2.43)$$

The role of the *Fr* number is evident. The hysteresis due to non-uniformity diminishes in critical flow and reverses in supercritical flow. Hence, for supercritical flows, Q is smaller than Q_s at the rising stage, and larger than Q_s at the falling stage of the hydrograph.

2.5.2. Type of boundary conditions.

At the boundaries, additional conditions complete the set of equations together with the *out*going characteristic equations. Hence, conditions prescribed at boundaries must be consistent with the information carried by characteristic equations that leave the domain of computation. This consistency comprises the number and type of boundary conditions.

30

Different combinations are possible as long as the problem is well-posed. In this section, this well-posedness is analysed locally at one boundary, without considering the conditions at the other boundary. According to Hirsch (1990), a problem is well-posed if the full information on the ingoing and outgoing characteristics can be recovered from the imposed condition.

If the problem is well-posed at the boundaries, the boundary conditions can be substituted by equivalent *in*going characteristic equations. In the following analysis, the latter format is the starting point. Objective is to prove the equivalence with the boundary conditions.

Conform Hirsch (1990), a distinction between the imposed variables v^p and the free variables v^n is made. As a result, the set of valid characteristic equations (outgoing information) at the boundary can be written as

$$\left[T_n^n\right] v^n + \left[T_n^p\right] v^p = \Delta t\ S + \left[T_n^n\right]v_0^n + \left[T_n^p\right]v_0^p = S^n \qquad (2.44)$$

The equations resulting from the set of additional boundary conditions can be written as

$$\left[T_p^n\right]v^n + \left[T_p^p\right]v^p = S^p \qquad (2.45)$$

Hence, the solution of the set of equations at the boundary can be written as

$$\begin{bmatrix} T_n^n & T_n^p \\ T_p^n & T_p^p \end{bmatrix} \begin{bmatrix} v^n \\ v^p \end{bmatrix} = \begin{bmatrix} S^n \\ S^p \end{bmatrix} \qquad (2.46)$$

The free variables v_n can be recovered from the internal conditions S^n if

$$v^n = \left[T_n^n\right]^{-1}\left[S^n - T_n^p v^p\right] \quad \rightarrow \quad \det\left| T_n^n \right| \neq 0 \qquad (2.47)$$

At the upstream boundary, a combination of two imposed variables is represented by the *vector* v^p, and the free variable is represented by the *scalar* v^n.

For the three different types of conditions at the upstream boundary, the condition for local consistency (Eq.2.47) can be written as

$$v^n = a \quad \rightarrow \quad \det \left| T_n^n \right| = \frac{\phi_1}{Fr^2} \neq 0$$

$$v^n = u \quad \rightarrow \quad \det \left| T_n^n \right| = \phi_1 \left(1 - \phi_1\right) \neq 0 \tag{2.48}$$

$$v^n = z_b \quad \rightarrow \quad \det \left| T_n^n \right| = \frac{1 - \phi_1}{Fr^2} \neq 0$$

with $\phi_1 = c_l/u$, representing the non-dimensional, upstream-directed celerity.

At the downstream boundary, the imposed variable can be a, u or z_b and is represented by the scalar v^p. The free variables are a combination of two variables represented by the vector $\bar{v}_n$. For the downstream boundary, the combination of two free variables is represented by the *vector* v^n, and the prescribed variable is represented by the *scalar* v^p.

For the three different types of conditions at the downstream boundary, the condition in Eq.2.47 can be written as

$$v^p = a \quad \rightarrow \quad \det \left| T_n^n \right| = \frac{(1 - \phi_3)(1 - \phi_2)(\phi_2 - \phi_3)}{Fr^2} \neq 0$$

$$v^p = u \quad \rightarrow \quad \det \left| T_n^n \right| = \frac{\phi_2 - \phi_3}{Fr^2} \neq 0 \tag{2.49}$$

$$v^p = z_b \quad \rightarrow \quad \det \left| T_n^n \right| = \phi_2 \phi_3 \left(\phi_3 - \phi_2\right) \neq 0$$

with ϕ_2 and ϕ_3 representing the non-dimensional, downstream-directed celerities.

The dimensionless values of determinants that correspond with the different options are constructed in Figure 2.13.
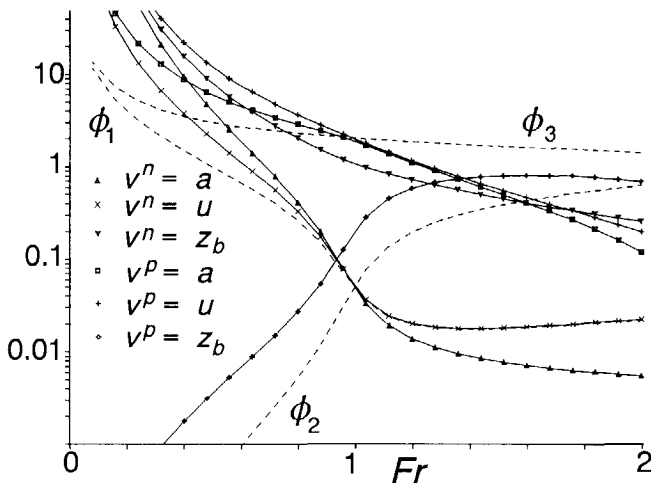
Fig.2.13 Determinants of variable prescription.

With respect to boundary conditions, again three regimes are distinguished; subcritical flow ($Fr < 0.8$), transcritical flow ($0.8 < Fr < 1.2$) and supercritical flow $Fr > 1.2$.

For all regimes and all combinations, the value of the determinant is non-zero. Hence, in principle, due to the mutual coupling of variables, prescription of any variable at either boundary would be possible, as long as the conditions at the up- and downstream boundary are consistent and the problem is well-defined. However, not every combination is a good one. Based on the relative values of the determinants, the performance of the combinations is qualified. If a value that corresponds to a combination of conditions approaches zero relative to other combinations, it can be expected to perform badly.

With respect to downstream boundaries in subcritical flows, prescription of bed levels can be expected to result in inconsistent solutions, whereas prescription of water depth or velocity performs well. For supercritical flows, description of bed level is to be preferred over description of velocity or depth at the downstream boundary. For transcritical flows, values of determinants are of similar order, but prescription of velocity or depth still is to be preferred.

If, with respect to the upstream boundary, values of determinants are compared, depth or bed level (free surface level) as free variables are to be preferred for very small values of Fr. With increasing value of Fr the situation changes in favor of bed level as a free variable and at the cost of depth as a free variable.

33

At transcritical and supercritical flows, prescription of velocity and depth at the upstream boundary are to be preferred in mobile-bed models.

The analysis on local consistency is not sufficient for selecting combinations of conditions at the boundaries up- and downstream of the computation domain. For example, in correspondence with the symmetrical behaviour of solutions at transcritical flows, symmetrical boundary conditions could be expected. However, up- and downstream boundary conditions should be consistent as well; prescription of depths at up- and downstream boundaries can induce multiple steady-state solutions.

Some combinations of up- and downstream boundary conditions and a qualitative indication of applicability have been presented in the table. The remarks concern the general applicability of respectively the option for the upstream and the option for the downstream boundary.

upstream condition	downstream condition		
	a $Fr < 1.2$	u $Fr < 1.2$	z_b $Fr > 1.2$
u, z_b $Fr < 0.8$	$Fr < 0.8$		
a, z_b			
a, u $Fr > 0.8$		$0.8 < Fr < 1.2$	$Fr > 1.2$

Table 2.1. Type of boundary conditions.

Hence, prescription of waterlevels at the downstream boundary can be expected to perform well in both subcritical and supercritical flow regimes. In the first regime this will imply prescription of a or u, mainly, whereas in the latter regime, this boundary condition mainly affects the bed level z_b.

Prescription of discharge and sediment transport at the upstream boundary will enable determination of u and z_b in subcritical flows, whereas these boundary conditions can be used to determine a and u in trans- and supercritical flows.

34

Chapter three.

Concepts for models with sediment mixtures.

3.1. Introduction.

One of the main features of mountain rivers is a graded composition of alluvial sediments. Apart from non-uniform and unsteady hydraulic conditions, this gradation characterizes the river morphology. Size-selective entrainment, transport and deposition results in paved or armoured bed surfaces and longitudinal sorting of grain sizes. One of the effects of size-selective mobility is a bimodal size-frequency distribution that can often be observed (Kellerhals and Bray, 1971).

To account for variable compositions of a river bed, in general, a layer concept conform Hirano (1971, 1972) is used, including layers of transport and storage.

In this chapter, some theoretical aspects with respect to the modelling of river beds with a variable composition are reviewed. Changes in bed level and composition appear to be coupled. Nevertheless, numerical models often apply a non-simultaneous solution sequence. In Section 3.3, the effect of decoupling changes in composition and bed level is analysed.

By analysis of a quasi-steady flow model, Ribberink (1987) detected a mathematical instability of this model in case of erosion of a coarse bed surface that covers finer material. Although Rahuel (1988) did not observe this phenomenon when analysing the celerities, the instability forms a severe limitation at values of Fr larger than 0.8 (Sieben and Sloff, 1994). The mathematical stability is discussed and options for stabilization of the model are summarized (Section 3.4).

To enable a proper selection of layer thickness, dynamic responses for different conditions are analysed in Section 3.5. Different options such as the number of layers, the type of sediment fluxes and the definition of thickness and its relation with physical phenomena will be reviewed. Some remarks with respect to the definition of layer thicknesses are added in Section 3.5.3.

Some analytical and numerical applications to armouring phenomena and longitudinal sorting effects can be found in Chapter Four.

3.2. Mathematical formulation.

3.2.1. Introduction.

With respect to mathematical modelling, it should be noted that alluvial transport of sediment mixtures includes many processes that complicate prediction and subsequently restrict the possibilities for modelling. Some aspects are reviewed.

hiding and exposure.

An accurate prediction of individual particle movements in graded material is out of scope. This would require a correct description of local particle-shear stress and resistive forces by grain-grain contact forces. The resulting movement of coarse fractions is often considered as being random and infrequent (e.g. Einstein, 1972; Nakagawa and Tsujimoto, 1980; Nakagawa 1988; Shuyou *et al.*, 1988; Bunte, 1992).

In this study, micro-scale effects such as dampening of turbulence and subsequent shear stress by larger particles, hiding of smaller particles, irregular grain-grain interactions and funneling of flow by grain patterns are all assumed to be characterized by lumped coefficients. After Einstein (1950), many empirical hiding-correction formulae have been developed, often only applicable to a corresponding transport-rate predictor (e.g. Egiazaroff, 1965; White and Day, 1982; Parker *et al.* 1982; Proffit and Sutherland, 1983; Misri *et al.* 1984; Andrews and Parker, 1987; Diplas, 1987; Wilcock, 1988). A clear review can be found in Sutherland (1991).

bed-form interaction.

In rivers with coarse bed material, small-scale ripple, dune and anti-dune features are generally absent (Hey and Thorne, 1986), due to relatively small particle shear-stresses (Parker *et al.* 1982; Pitlick, 1992). As a result, theoretical and experimental analyses on for example armouring processes are mainly limited to flat bed conditions. However, in case of sufficiently graded material, bed forms at coarsening beds can increase the coarsening or destabilize the bed surface (Klaassen *et al.* 1986; Wilcock and Southard, 1989; Dinehart, 1989; Klaassen, 1990; Chiew, 1991; Dinehart, 1992).

Laronne and Carson (1976) and Brayshaw *et al.* (1983) distinguished different kinds of clustering of fine particles near large ones. This clustering induces

36

local deposition and erosion (Kuhnle and Southard, 1988). Dinehart (1989) measured the production of rapidly migrating gravel dunes.

With respect to sorting at the scale of bars, observations by for example Bhowmik and Demissie (1982), Church and Jones (1982), Wesche *et al.* (1987), Ho (1988), Carling (1990), Whiting and Dietrich (1991) and Diplas (1994) can be mentioned that describe armouring of riffle sections or segregation of coarse particles from fines in the lee areas. These two-dimensional sorting effects can be significant in the stabilization of bars and riffles (Jeaggi and Smart, 1982; Church and Jones, 1982; Parker, 1991c) and in case of river bends (Olesen and Kalkwijk, 1987; Bridge, 1992).

Longitudinal and transversal sorting effects due to gravity, which result in the deposition of coarse material in deeper parts of the bed, are not considered in this study. The contribution to longitudinal sorting can, however, be incorporated by correcting sediment-transport rate predictors for local-slope effects. For transversal sorting, information on the cross-section should be incorporated (e.g. Crosato, 1995).

initiation of particle movement.

In case of sediments with bi-model size-distributions, distinct mobility of fractions (e.g. Drake *et al.* 1988) can result in abrupt changes in transport rates and composition (Klingemann and Emmet, 1982; Church *et al.* 1991). Exceedance of a shear-stress threshold can result into a sudden supply of fine material (Jaeggi and Rickenmann, 1987; Petts *et al.* 1989; Simons and Simons, 1987). Hence, inaccurate prediction of critical shear stress (Richards, 1990) directly result in difficulties in predicting morphological changes.

Nevertheless, much effort is spend to develop transport predictors for mountain-river conditions. The dominant role of shear-stress exceedance over threshold, as applied in sediment transport predictors such as Meyer-Peter and Müller (1948), is confirmed by many observations. At low levels of particle shear, relative differences in mobility are pronounced, whereas this reduces with increasing shear stress (e.g., Çeçen and Bayazit, 1973; Bayazit, 1975; Parker *et al.* 1982; Suzuki and Michiue, 1988; Kuhnle, 1988; Wathen 1995). Since at higher discharges, differences in mobility diminish, annually-averaged transport rates are biased to the bed surface composition (Kuhnle and Willis, 1992).

3.2.2. Introduction of layer concept.

The implementation of variable bed-compositions into models for river morphology requires an accurate description of sediment mixtures. To account for grain-size distributions, size fractions are introduced. A size fraction p_{pi} is defined as the portion of a specific grain size D_i in a reference volume. This reference volume per area river bed can be defined by a reference layer-thickness δ_p (Figure 3.1). The resulting layer concept is introduced by Hirano (1971, 1972) and has been applied and developed widely since. Developments are reflected by Bennet and Nordin (1977), Borah *et al.* (1982a and b), Karim and Holly (1986), Ribberink (1987), Rahuel (1988), Rahuel *et al.* (1989), Armanini and Di Silvio (1989), Di Silvio (1991) and Niekerk *et al.* (1992).

With respect to flow, the mathematical model used in this chapter consists of the mass continuity for water and the momentum equation.

$$\frac{\partial a}{\partial t} + u\frac{\partial a}{\partial x} + a\frac{\partial u}{\partial x} = 0$$

$$\frac{\partial u}{\partial t} + u\frac{\partial u}{\partial x} - g_z\frac{\partial a}{\partial x} - g_z\frac{\partial z_b}{\partial x} = g_x + \frac{g_z u^2}{C^2 a}$$

(3.1)

3.2.3. Definition of a single-layer model.

As described in the introduction, reference storage-layers are defined to account for changes in composition. Apart from storage layers in the bed, transport layers in the flow are distinguished. Vertical fluxes are the mass exchange between storage layers and layers with horizontal, alluvial transport.

For a single reference-layer at the surface of the bed, mass fluxes of sediment and fractions in transport and storage layers are defined as shown in Figure 3.1. It should be noted here that generally the differences between pavement and substratum are subtle and affected by the sampling method (Klingemann and Emmet, 1982; Church *et al.* 1987). The mass flux of a fraction i between substratum and reference layer is defined as

$$\Phi_{oi} = -c_0\,\beta_{oi}\frac{\partial z_b}{\partial t}$$

(3.2)

with $\beta_{oi} = p_{oi}$ in case of erosion and $\beta_{oi} = p_{pi}$ in case of sedimentation.

38
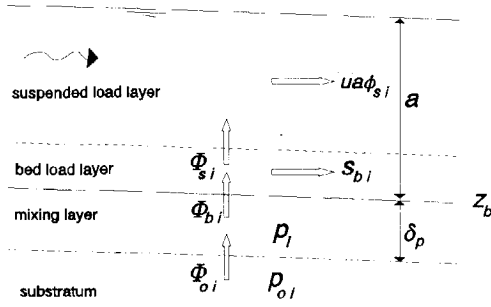
Fig.3.1 Single-layer model.

The mathematical model is constructed by defining size-specific mass balances for sediment in the different layers. Sediment fluxes are as defined in Figure 3.1. Sediment-continuity for a fraction i in the bed-load layer reads

$$f_{ui}\frac{\partial u}{\partial x} + f_{pi}\frac{\partial p_{pi}}{\partial x} + f_{Di}\sum_{j=1}^{N-1}(D_j-D_N)\frac{\partial p_{pj}}{\partial x} + \Phi_{si} - \Phi_{bi} = 0 \qquad (3.3)$$

The introduction of N size fractions requires the formulation of N-1 fraction-specified sediment-mass balances such as Eq.3.3 in combination with

$$\sum_{i=1}^{N} p_{pi} = 1 \qquad (3.4)$$

The coefficients f in Eq.3.3 refer to partial derivatives of a sediment-transport predictor

$$f_{ui} = \frac{\partial s_i}{\partial u} \quad ; \quad f_{pi} = \frac{\partial s_i}{\partial p_{pi}} \quad ; \quad f_{Di} = \frac{\partial s_i}{\partial D_{mp}} \qquad (3.5)$$

Mass continuity in the reference layer with a constant layer thickness is described by

$$\Phi_{bi} + c_0\beta_{oi}\frac{\partial z_b}{\partial t} + c_0\delta_p\frac{\partial p_{pi}}{\partial t} = 0 \qquad (3.6)$$

39

Eqs 3.3 and 3.6, and the mass balance for sediment in suspension can be combined to eliminate Φ_{bi}

$$a\frac{\partial \phi_{si}}{\partial t} + c_0\beta_{oi}\frac{\partial z_b}{\partial t} + c_0\delta_p\frac{\partial p_{pi}}{\partial t} + ua\frac{\partial \phi_{si}}{\partial x} + f_{ui}\frac{\partial u}{\partial x} +$$

$$+ f_{pi}\frac{\partial p_{pi}}{\partial x} + f_{Di}\sum_{j=1}^{N-1}(D_j - D_N)\frac{\partial p_{pj}}{\partial x} = 0$$

(3.7)

3.2.4. Definition of a multiple-layer model.

To account for vertical structures in the bed composition and to improve the mathematical stability, Ribberink (1987) introduced a transition layer between the reference layer at the surface and the sediment in the substratum (Figure 3.2).
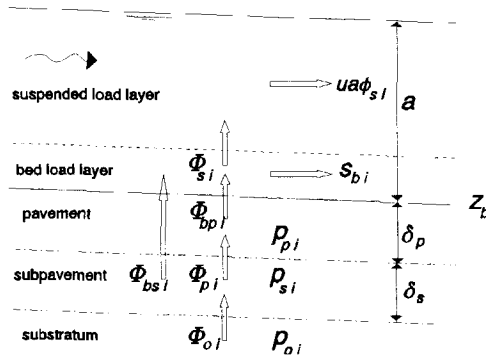
Fig.3.2 Double-layer model.

After Di Silvio (1991), the layers are referred to as pavement and subpavement layer. Then, fluxes can be defined as

$$\Phi_{bpi} = -\kappa\, c_0\beta_{pi}\frac{\partial z_b}{\partial t} \quad ; \quad \Phi_{bsi} = -(1-\kappa)\, c_0\beta_{si}\frac{\partial z_b}{\partial t} \quad ; \quad \Phi_{oi} = c_0\beta_{oi}\frac{\partial z_b}{\partial t}$$

(3.8)

with κ the probability of mass exchange between pavement and bed-load layer, relative to the subpavement. Such a concept accounts for horizontal distributions in composition ("patches", e.g., Paola and Seal, 1995). The cross-sectionally averaged median grain size of the river bed is defined as

$$D_m = \kappa\sum_{i=1}^{N}p_{pi}D_i + (1-\kappa)\sum_{i=1}^{N}p_{si}D_i$$

(3.9)

40

In case of erosion; $\beta_{pi} = p_{si}$, $\beta_{si} = p_{si}$ and $\beta_{oi} = p_{oi}$. In case of sedimentation; $\beta_{pi} = p_{pi}$, $\beta_{si} = p_{Ti}$ and $\beta_{oi} = p_{si}$. The dampening effect of an additional layer on the dynamics of a bed composition is illustrated in Section 3.5.2.

To preserve mass continuity in case of large bed-level fluctuations and to extend the flexibility of the model, a relatively inactive third layer can be distinguished (Figure 3.3).
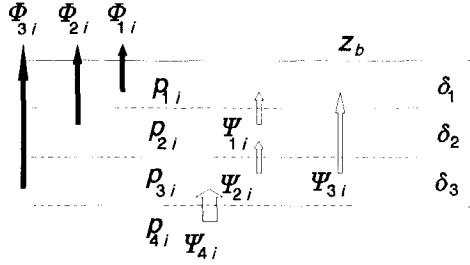
Fig.3.3 Triple-layer model.

Again, a mass balance with corresponding fluxes can be defined for each layer. If a constant layer-thickness is applied, these balances can be written as

$$c_0 \frac{\partial \delta_1 \, p_{1i}}{\partial t} + \Phi_{1i} - \Psi_{1i} - \Psi_{3i} = 0$$

$$c_0 \frac{\partial \delta_2 \, p_{2i}}{\partial t} + \Phi_{2i} + \Psi_{1i} - \Psi_{2i} = 0 \qquad (3.10)$$

$$c_0 \frac{\partial \delta_3 \, p_{3i}}{\partial t} + \Phi_{3i} + \Psi_{2i} + \Psi_{3i} - \Psi_{4i} = 0$$

The mass fluxes between the mutual layers are defined as

$$\Psi_{1i} = -c_0 \, \kappa_1 \left(1 - \kappa_3\right) \beta_{1i} \frac{\partial z_b}{\partial t} \quad ; \quad \Psi_{2i} = -c_0 \left(\kappa_1 \left(1 - \kappa_3\right) + \kappa_2\right) \beta_{2i} \frac{\partial z_b}{\partial t} \quad (3.11)$$

$$\Psi_{3i} = -c_0 \, \kappa_1 \, \kappa_3 \, \beta_{3i} \frac{\partial z_b}{\partial t} \quad ; \quad \Psi_{4i} = -c_0 \, \beta_{4i} \frac{\partial z_b}{\partial t}$$

The composition of mass fluxes equals that of the source layer: in case of

deposition, fluxes are downward and β_{ji} equals the composition of the upper layer. In case of erosion, fluxes are upward and β_{ji} equals the composition of the underlying layer.

Vertical fluxes between bed load and river bed are defined with the help of a probability of exchange. Hence, the exchange with the transport layer is optional, which enables switching off different layers. Mass fluxes between bed load and river bed are defined as

$$\Phi_{1i} = \kappa_1 \, \Phi_{bpi} \quad ; \quad \Phi_{2i} = \kappa_2 \, \Phi_{bpi} \quad ; \quad \Phi_{3i} = \left(1 - \kappa_1 - \kappa_2\right) \Phi_{bpi} \quad (3.12)$$

where the coefficients κ_1, κ_2 and κ_3 are distributions coefficients that determine the probability of mass exchange with the different layers.

3.2.5. Analysis of characteristics.

The analysis of characteristics is carried out for a single-layer model with a sediment mixture composed of two size fractions ($N = 2$). Then, 4 PDE's are obtained. The corresponding four celerities, are roots of

$$\left(\frac{c}{u}\right)^4 - \left(2 + \frac{a}{\delta_p} Y_{h1}\right)\left(\frac{c}{u}\right)^3 + \left(\frac{Fr^2 - 1 - \psi}{Fr} + 2\frac{a}{\delta_p} Y_{h1}\right)\left(\frac{c}{u}\right)^2 +$$

$$+ \frac{\psi}{Fr^2}\left(\frac{c}{u}\right) - \frac{a}{\delta_p}\frac{\left((Fr^2 - 1)Y_{h1} - Y_{h2}\right)}{Fr^2}\left(\frac{c}{u}\right) - \frac{a}{\delta_p}\frac{Y_{h2}}{Fr^2} = 0 \quad (3.13)$$

with

$$\psi = \frac{f_{u1} + f_{u2}}{c_0 \, a} \quad ; \quad Y_{h1} = \frac{-\beta_{o1}X_2 + \beta_{o2}X_1}{c_0 \, ua} \quad ; \quad Y_{h2} = \frac{f_{u2}X_1 - f_{u1}X_2}{c_0^2 ua^2} \quad (3.14)$$

$$X_1 = f_{p1} + f_{D1}\left(D_1 - D_2\right) \quad ; \quad X_2 = -f_{p2} + f_{D2}\left(D_1 - D_2\right)$$

Hence, with respect to mobile-bed models with uniform sediment, additional characteristics are found (e.g., Rahuel, 1988). The additional celerity increases almost linearly with δ_p^{-1}; increasing the layer thickness δ_p implies reducing a celerity. For infinite values of δ_p, celerities equivalent to mobile-bed models with uniform sediment (De Vries, 1965) are found. In Figure 3.4, celerities are constructed for different values of δ_p.

42
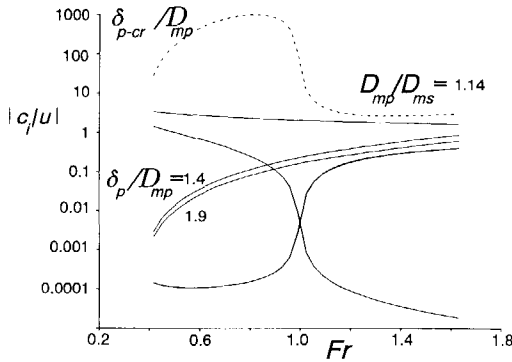
Fig.3.4 Celerities of single-layer model.

3.3. Decoupled solution procedure.

3.3.1. Alternative formulation.

As reported by Ribberink (1987), analysis of characteristics shows that changes in bed level and composition cannot be decoupled. This can be concluded as well when analysing compatibility equations (Sieben, 1994). Nevertheless, to omit application of large algorithms, in general decoupled, or sequential solution procedures are applied; first changes in bed level are computed, then compositions are updated (e.g., Ribberink, 1987; Di Silvio and Peviani, 1989; Evans and Sieben, 1996). This procedure is also applied in the numerical model described in Chapter seven. Therefore, some effects are discussed.

The first step of this procedure resembles that in models with uniform sediment. In this step, the fraction-integrated bed-load mass balance is solved

$$c_0 \frac{\partial z_b}{\partial t} + \sum_{i-1}^{N} f_{ui} \frac{\partial u}{\partial x} + \sum_{i=1}^{N-1} \left[f_{pi} - f_{pN} + \sum_{j=1}^{N} f_{Dj}(D_i - D_N) \right] \frac{\partial p_{pi}}{\partial x} = 0 \quad (3.15)$$

where gradients in p_{pi} are assumed to be constant during one time step. For conditions near the critical shear-stress threshold, this assumption can induce errors and iteration should be applied (e.g. Evans and Sieben, 1996) or time steps should be reduced.

To compute the corresponding changes in composition, Φ_{pi}, the vertical mass-exchange between sediment-transport layers and river bed must be determined.

43

Only if bed levels change, the composition of sediment fluxes between bed and transport layers (bed load and suspended load) can be defined as

$$\beta_i^* = \frac{\Phi_{bi}}{\displaystyle\sum_{i=1}^{N} \Phi_{bi}} = \frac{\dfrac{\partial \phi_i aB}{\partial t} + \dfrac{\partial (s_{bi} + \phi_i ua)B}{\partial x}}{\dfrac{\partial \phi aB}{\partial t} + \dfrac{\partial (s_b + \phi ua)B}{\partial x}} \qquad (3.16)$$

From a numerical point of view, the form of Eq.3.16 is not accurate for low gradients in sediment transport. In case of bed load, this is

$$\beta_i^* = p_{Ti} + s_b \frac{\partial p_{Ti}/\partial x}{\partial s_b/\partial x} \qquad (3.17)$$

with $p_{Ti} = s_{bi}/s_b$. The effect of the second term at the right-hand side of Eq.3.17 can be illustrated as follows.

Consider a mixture with two size fractions. In case of longitudinal coarsening (decreasing fine fraction p_{p1} Figure 3.5) with uniform flow, the total sediment-transport rate will decrease. For values of τ_{*m}/τ_{*cr} close to unity, the *fraction* of fine material in transport will increase in longitudinal direction, which results in $\beta_1^* < p_{T1}$. Due to the low value of s_b, this negative contribution of the second term can become small relative to p_{Ti} (see also Subsection 4.2.2). However, for $\tau_{*m}/\tau_{*cr} \to \infty$, when hiding effects are negligible, the fraction of fine material will decrease as well, which results in $\beta_1^* > p_{T1}$.

longitudinal coarsening   longitudinal fining
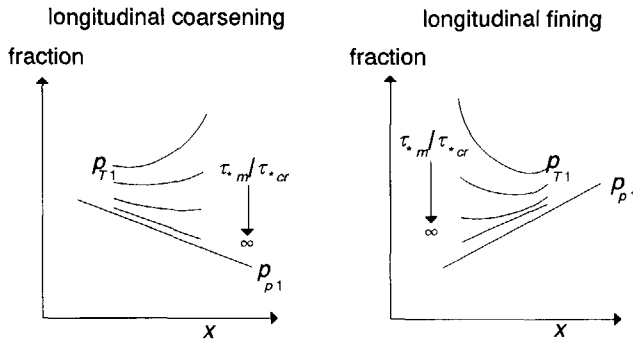
Fig.3.5 Bed-load response to bed composition.

Hence, the downward flux will be coarser than the bed load for $\tau_{*m}/\tau_{*cr} \approx 1$,

and finer in case of $\tau_{*m}/\tau_{*cr} \to \infty$. A similar effect for longitudinal fining can be found. If the second term at the right-hand side in Eq.3.17 is neglected, the error in the rate of changes in composition varies with the level of shear stress.

Now, with the mass balance for the river bed, the total vertical sediment flux can be written as

$$\sum_{i=1}^{N} \Phi_{bi} = - c_0 \frac{\partial z_b}{\partial t} \quad \to \quad \Phi_{bi} = - c_0 \beta_i^* \frac{\partial z_b}{\partial t} \tag{3.18}$$

Note that this formulation is only valid if changes in bed level exist. This implies that as long as gradients in total, fraction-integrated sediment transport rate are zero, no change in bed level and composition is predicted (Eq.3.15), irrespective of *composition* changes in the transported sediment. However, the validity of this formulation can be extended by considering additional fluxes due to short-term fluctuations in bed level (Armanini, 1995).

$$\Phi_{bi} = - c_0 \beta_i^* \overline{\frac{\partial z_b}{\partial t}} - c_0 \left(\beta_i^* \frac{\partial z_b}{\partial t} \right)' \tag{3.19}$$

The effect of this additional flux will be analysed in Subsection 3.4.4. To determine the changes in composition, the vertical flux Φ_{bi} is substituted in the mass balance per fraction i for the reference layer.

$$c_0 \delta_p \frac{\partial p_{pi}}{\partial t} + c_0 \left(\beta_{pi} - \beta_i^* \right) \frac{\partial z_b}{\partial t} = 0 \tag{3.20}$$

In case of a constant β_i^*, Eq.3.20 is a common, ordinary-differential equation (ODE). Then, if N size fractions are considered, a single-layer model with bed load and suspended load would yield a total of $3N+1$ equations, with $N+3$ PDE's and $N-1$ ODE's. Additionally, $N-1$ equations of the type of Eq.3.16 are required to determine β_i^*. The characteristic equation of the corresponding model is

$$\left(\frac{c}{u}\right)^3 - \left(2 - \frac{a}{\delta_p} Y_a\right)\left(\frac{c}{u}\right)^2 + \left[1 - \frac{1+\psi}{Fr^2} - 2\frac{a}{\delta_p} Y_a\right]\left(\frac{c}{u}\right) +$$

$$+ \frac{\psi}{Fr^2} + \left(1 - \frac{1}{Fr^2}\right)\frac{a}{\delta_p} Y_a = 0 \quad \vee \quad c^N = 0 \tag{3.21}$$

45

with

$$\psi = \frac{\sum_{i=1}^{N} f_{ui}}{c_0 \, u \, a} \quad ; \quad Y_a = \frac{\sum_{i=1}^{N-1} \left[f_{pi} - f_{pN} + \sum_{j=1}^{N} f_{Dj}(D_i - D_N) \right] (\beta_{oi} - \beta_i^*)}{c_0 \, u \, a} \tag{3.22}$$

With respect to the number of characteristics, the following is noted. In the complete formulation of a single-layer model as described in Subsection 3.3.4, a total of $2N+2$ PDE's is used, yielding a set of $N+2$ coupled celerities and N decoupled celerities that correspond to changes in suspended fractions.

For the sequential solution of changes in bed level and composition to be equivalent to that of the original model, the information carried along the eliminated N-1 characteristics must now be contained in β_i^*. This implies that for example information on the composition of sediment transport at the upstream boundary should be substituted in Eq.3.16 to determine β_i^*. Some additional remarks on this can be found in Subsection 3.5.5.

With respect to the celerities (Eq.3.21), the direct effect of grain-size distribution can be represented by a single parameter Y_a, that combines effects due to the sediment-transport predictor and the composition of vertical sediment fluxes in and out the reference layer. Some approximative values of Y_a for typical size frequency-distributions have been determined in Appendix B.

3.3.2. Effect of decoupling bed level and composition.

The analysis of the mathematical model with coupled PDE's for bed level and composition is complicated; for N size fractions, $N+2$ solutions result. As described in the previous section, decoupling bed level and composition simplifies the solution of the model. It has been observed that due to this decoupled solution, differences may occur with the original formulation. Here, the effect of the coupling between changes in bed level and composition is considered.

To a certain extent, the effects of decoupling bed level and composition can be studied analytically. Key role in the simplification is the mass exchange between bed and flow; the fraction β_i^* consists of two contributions

$$\beta_i^* = \frac{\partial s_{bi}/\partial x}{\partial s_b/\partial x} = p_{Ti} + s_b \frac{\partial p_{Ti}/\partial x}{\partial s_b/\partial x} \tag{3.23}$$

The second term at the right-hand side represent the coupling between vertical sediment flux and longitudinal gradients. This regards information that is carried along N-1 characteristics in the complete model. In numerical models, both contributions can be determined easily (Chapter 7).

For this analytical study a complete decoupling is performed by assuming β_i^* = p_{Ti}. Hence, the composition of vertical sediment fluxes between flow and bed is assumed to be controlled by the local sediment-transport composition. Such a relation, or transfer function, has also been proposed by Toro-Escobar *et al.* (1996). They fit for flume experiments with deposition conditions

$$\beta_i^* \approx 0.7 \, p_{Ti} + 0.3 \, p_{pi} \tag{3.24}$$

In this section, the complete, original formulation (concept I from Subsection 3.2.3) is compared with the decoupled model that results from assuming β_i^* = p_{Ti}. To simplify the analysis, flow is assumed to be steady. Now, two extremes can be considered; small length-scales with negligible friction (yielding a simple-wave model) and large length-scales (yielding a parabolic model).

For the first case, the steady-state continuity and momentum equation for water can be combined into

$$u \left(1 - \frac{1}{Fr^2} \right) \frac{\partial u}{\partial x} - g_z \frac{\partial z_b}{\partial x} = 0 \tag{3.25}$$

For the second case it can be found

$$- g_z \frac{\partial^2 z_b}{\partial x^2} = 3 \, \frac{g_z u}{C^2 a} \, \frac{\partial u}{\partial x} \tag{3.26}$$

Application of small length-scale conditions to the original model results into a *telegraph* equation

$$\frac{\partial^2 z_b}{\partial t^2} + \frac{u \, \psi}{1 - Fr^2} \left(1 + (1 - Fr^2) \frac{a}{\delta_p} \frac{Y_{h1}}{\psi} \right) \frac{\partial^2 z_b}{\partial x \partial t} + \frac{a}{\delta_p} \frac{u^2 Y_{h2}}{1 - Fr^2} \frac{\partial^2 z_b}{\partial x^2} = 0 \tag{3.27}$$

where the parameters Y_{h1} and Y_{h2} are defined in Eq.3.14.

For the alternative, decoupled formulation, a *simple-wave* equation is found

$$\frac{\partial z_b}{\partial t} + \frac{u}{1-Fr^2}\psi\left(1-(1-Fr^2)\frac{a}{\delta_p}\frac{Y_a}{\psi}\right)\frac{\partial z_b}{\partial x} = f(x) \tag{3.28}$$

where $f(x)$ is an integration constant that represents longitudinal changes in bed composition. If a constant bed composition is considered with an equivalent "uniform sediment", a *simple-wave* model results

$$\frac{\partial z_b}{\partial t} + \frac{u}{1-Fr^2}\psi\frac{\partial z_b}{\partial x} = 0 \tag{3.29}$$

Hence, with respect to simple-wave models for uniform sediment, the propagation rate is reduced.

The propagation rates for both concepts and the equivalent "uniform sediment" model are compared in Figure 3.6. It can be concluded that significant differences in both models are found. Obviously, the second contribution at the right-hand side in Eq.3.23 cannot be neglected for short length-scales. This is in correspondence with the strong coupling of celerities.

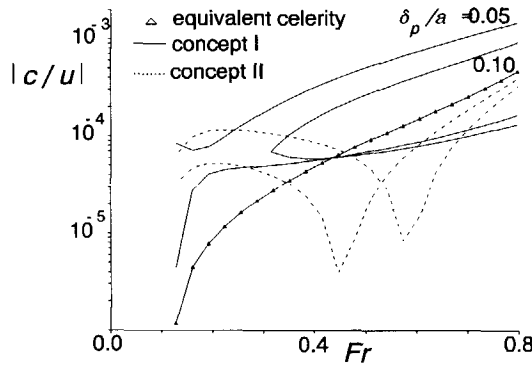**Fig.3.6** Comparison of models for short length-scale.

Application of large length-scale conditions to the Hirano model yields

$$\frac{\partial^2 z_b}{\partial t^2} + u\frac{a}{\delta_p}Y_{h1}\frac{\partial^2 z_b}{\partial x\partial t} - \frac{C^2a^2}{3u}\psi\frac{\partial^3 z_b}{\partial x^2\partial t} - \frac{C^2a^2}{3}\frac{a}{\delta_p}Y_{h2}\frac{\partial^3 z_b}{\partial x^3} = 0 \tag{3.30}$$

For the alternative formulation, the resulting differential equation is

$$\frac{\partial z_b}{\partial t} - u\frac{a}{\delta_p}Y_a\frac{\partial z_b}{\partial x} - \frac{C^2a^2}{3u}\psi\frac{\partial^2 z_b}{\partial x^2} = f(x) \qquad (3.31)$$

where $f(x)$ is again an integration constant that represents longitudinal changes in bed composition, and Y_a is defined in Eq.3.22. For a river bed with constant composition, a parabolic model is found

$$\frac{\partial z_b}{\partial t} - \frac{C^2a^2}{3u}\psi\frac{\partial^2 z_b}{\partial x^2} = 0 \qquad (3.32)$$
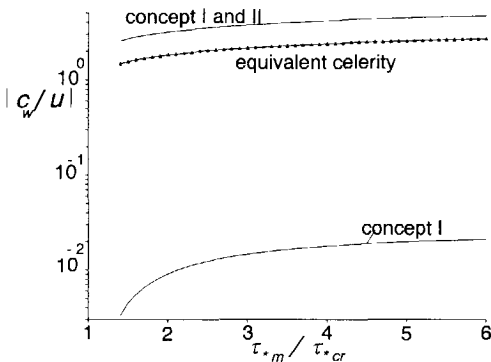
Fig.3.7-a Propagation rates.
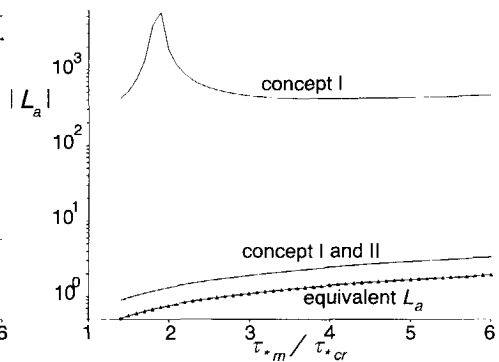
Fig.3.7-b Attenuation lengths.

In Figures 3.7-a and 3.7-b, the propagation rates and attenuation lengths of wave type solutions are constructed. Now, similarity between both concepts exists. The additional wave in the complete formulation that is neglected in the simplified approach, has a low propagation and deformation rate. Considering the large differences in propagation and deformation rates, this slow, stable wave can be decoupled from the fast, diffusive waves.

The presence of the slow wave can be explained when rewriting Eq.3.30.

$$\frac{\partial}{\partial t}\left(\frac{\partial z_b}{\partial t} + \frac{a}{\delta_p}uY_{h1}\frac{\partial z_b}{\partial x}\right) - \psi\frac{C^2a^2}{3u}\frac{\partial}{\partial x^2}\left(\frac{\partial z_b}{\partial t} + \frac{a}{\delta_p}u\frac{Y_{h2}}{\psi}\frac{\partial z_b}{\partial x}\right) = 0 \quad (3.33)$$

If $Y_{h1} \approx Y_{h2}/\psi$ (Figure 3.8), concept I indeed contains a simple wave and parabolic model (compare Eq.3.32).
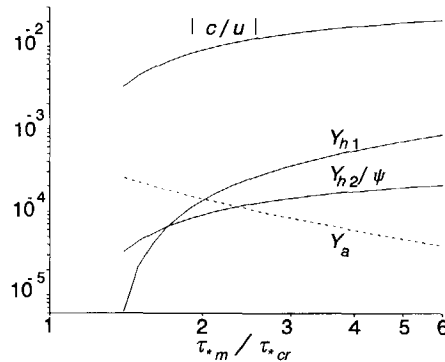
Fig.3.8 model coefficients

Due to decoupling of bed level and composition, the number of solutions is reduced. The assumption of $\beta_i^* = p_{Ti}$ can be considered erroneous in case of small length-scales.

For large length-scales (quasi-uniform flow), the total solution consists of a combination of a slow simple-wave type and a parabolic type solution. The latter part of the solution is not affected by the assumption $\beta_i^* = p_{Ti}$. The slow and relatively stable, downstream-propagating wave is, however, neglected. From Eq.3.33 it can be concluded that only if δ_p/a is large and/or Y_{h1} and Y_{h2} are small (values of τ_{*m}/τ_{*cr} near unity, see Figure 3.7), this parabolic contribution is dominant and the contribution of the simple-wave type solution diminishes.

3.4. Mathematical stability.

3.4.1. Introduction.

As described in Subsection 3.2.5, some celerities that can be related to changes in bed level and composition vary with different values of δ_p; reducing the layer thickness will enlarge the celerity (Figure 3.4). Obviously, limits exist; it does not seem realistic in rivers with alluvial transport that changes in morphological variables propagate faster than changes in hydraulic variables. Increasing the layer thickness will reduce the celerity and in some cases enable larger modelling time steps.

However, another limit concerns large values of δ_p, when celerities intersect. Because then, the number of celerities has reduced to that of uniform-sediment models again, Suzuki (1976) defined the corresponding value for δ_p as a

dynamic layer thickness.

However, if celerities intersect due to large values of δ_p, two cases exist. In case of deposition, celerities coincide and the local contribution of grain-size distribution disappears (Sieben, 1994). In case of erosion of a coarse layer at a finer substratum, complex characteristics result. Then, the mathematical model has an elliptic character and becomes instable (Ribberink, 1987). Figure 3.9 indicate the two transitions for real and complex celerities. It is noted that δ_p/a values larger than 0.5 do not seem realistic in case of significantly varying bed compositions. Hence, only the lower limit for δ_p/a is considered of interest.

The introduction of a second reference layer does not entirely exclude mathematical instability at higher values of Fr (Sieben, 1994).
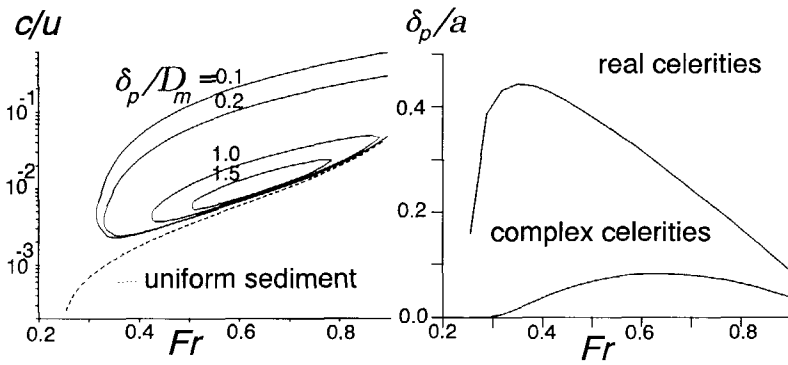
Fig.3.9 range of real celerities

Such a critical value of δ_p has been constructed with a dashed line in Figure 3.4 It is noted that for transcritical and supercritical flows, the critical layer thickness has decreased significantly. In Figure 3.9, this instable behaviour has been illustrated for the quasi-steady model with $N = 2$.

If a fraction i is immobile, then $\Phi_{bi} = 0$ and the sediment-mass balance of the reference layer (Eq.3.6 in Subsection 3.2.3) reduces to an ordinary differential equation. In that case, no elliptic character can be found.

3.4.2. Stabilizing options.

Instabilities can arise for conditions prevailing in mountain rivers (paved bed-surfaces and higher values of Fr). To obtain a more stable model, different

options exist. First, reference is made to Eq.3.21 in Subsection 3.3.1. It is noted that by solution of changes in composition and level with the help of a vertical flux, direct intersection of characteristics can be omitted; the number of coupled characteristics to be solved amounts three. However, because the model solved is equivalent to the conventional model, the problem of instability has not been eliminated. This corresponds with observations of numerical experiments by Evans and Sieben (1996).

One option is to manipulate celerities by limiting layer thicknesses to a critical value (Sieben, 1994; Sieben and Sloff, 1994). However, this can result in rather thin layers at trans- and supercritical flows with, subsequently, small numerical time steps.

A stabilizing effect can also be obtained by adjusting the layer thickness to changing flow conditions. This can be explained as follows. The critical layer-thickness δ_c decreases if the surface layer becomes coarser relative to the underlying material. Due to a higher shear-stress level, the extend of mixing increases in the accelerating flow and relatively fine material from underlying layers is transferred to the coarser surface layer. As a result, the surface will be less coarse and the critical value of the layer thickness will increase. Hence, if for example $\delta_p = \delta_c$ at a certain time level, both values increase and stability in the next time step will be guaranteed if during this step

$$\frac{\partial \delta_p}{\partial t} < \frac{\partial \delta_c}{\partial t} \qquad (3.34)$$

It is noted that this stabilizing effect may not be sufficient in for example supercritical flows, where the increase in δ_c due to a finer composition is very small.

Another option to stabilize the set of PDE's, is to change characteristics by introducing a short adaption of bed-load composition. This option will be described briefly in the next section.

3.4.3. Changes in bed load.

In models for morphology with uniform sediment, bed load is generally assumed to adapt instantaneously to local hydraulic conditions (Subsection 2.2.2). However, in case of mixtures, changes in transport rates due to changes in composition have a larger time scale. Therefore, the effect of adaption of bed-load rate and composition to changes in bed composition are considered.

52

Some concepts to include this adaption are described briefly.

In the following, ϕ_b represents the total sediment concentration in the bed-load layer with thickness δ_b. The mass fraction with size D_i, present in this layer is p_{bi}. The fraction velocity is represented with u_{gi}. Now, a sediment mass flux s_{bi} of fraction i can be defined as

$$s_{bi} = p_{bi}u_{gi} \; \overline{\phi_b\delta_b} = p_{Ti} \; \overline{\phi_b\delta_b u_g} \quad ; \quad \overline{u_g} = \sum_{i=1}^{N} p_{bi}u_{gi} \qquad (3.35)$$

The sediment-mass balance for a fraction i in the bed-load layer is (Figure 3.1)

$$\frac{\partial \phi_b p_{bi}\delta_b}{\partial t} - \Phi_{pi} + \frac{\partial s_{bi}}{\partial x} = 0 \qquad (3.36)$$

Hence, if relaxation effects of bed load are to be included, either fraction velocity u_{gi} or concentration of bed-load mass ϕ_b should be specified. Because additional variables require the introduction of new equations, first some simplified concepts are considered.

One option would be to assume $p_{bi} = p_{pi}$; the composition of the bed load layer equals the composition of the bed surface. Although physical distinction between compositions of a transporting bed-load layer and a storage layer at the bed surface is arbitrary, conceptually, this assumption is not correct. This can be illustrated as follows. If two layers (bed load and bed surface) have equal composition, mass fluxes between the layers must have a similar composition. This implies

$$\Phi_{pi} = P_{pi} \; \Phi_p \quad \rightarrow \quad \phi_b\delta_b\frac{\partial p_{pi}}{\partial t} + \frac{\partial s_{bi}}{\partial x} = p_{pi}\sum_{i=1}^{N} \frac{\partial s_{bi}}{\partial x} \qquad (3.37)$$

Then, with the help of mass balances of reference and bed-load layer it can be found

$$\delta_p\frac{\partial p_{pi}}{\partial t} + \left(\beta_{pi} - p_{pi}\right)\frac{\partial z_b}{\partial t} = 0 \qquad (3.38)$$

Hence, the character of size-selective pickup is neglected; in the resulting model, changes in composition are only due to vertical structures in bed

composition when $\beta_{pi} \neq p_{pi}$. This conclusion is confirmed by numerical experiments.

A second possibility would be to assume

$$\frac{\partial p_{bi}}{\partial t} = \frac{\partial p_{pi}}{\partial t} \qquad (3.39)$$

which implies that time scales of changes in fractions correspond. Substitution into the mass balance of bed-load and reference layer yields

$$p_{bi}\delta_b \frac{\partial \phi_b}{\partial t} + \frac{\partial s_{bi}}{\partial x} + \delta_p c_0 \left(1 + \frac{\phi_b}{c_0}\frac{\delta_b}{\delta_p}\right)\frac{\partial p_{pi}}{\partial t} + c_0 \beta_{pi}\frac{\partial z_b}{\partial t} = 0 \qquad (3.40)$$

If the contribution of changes in ϕ_b is neglected, the resulting model corresponds with the conventional one. Then, the problem of ellipticity is not eliminated. The dampening effect of changes in bed-load composition is accounted for by an effectively larger layer thickness. Because in general $\delta_p \geq \delta_b$ and $c_0 \geq \phi_b$, this effect will be very small.

Therefore, another possibility is considered. If it is defined

$$\Phi_{pi} = \beta_i^* \sum_{i=1}^{N} \Phi_{pi} \qquad (3.41)$$

then, the mass balances of the bed-load and reference layer can be written as

$$\left(\beta_i^* - p_{Ti}\right)c_0 \frac{\partial z_b}{\partial t} + \frac{\partial\left(p_{bi} - p_{Ti}\right)\phi_b\delta_b}{\partial t} + \delta_b\phi_b\left(\frac{\partial p_{Ti}}{\partial t} + \frac{s_b}{\phi_b\delta_b}\frac{\partial p_{Ti}}{\partial x}\right) = 0 \qquad (3.42)$$

It is noted that if $\beta_i^* = p_{Ti}$, as used in Subsection 3.3.2, size-selective pickup will still be included. Then, Eq.3.42 can be reduced to

$$\frac{\partial\left(p_{bi} - p_{Ti}\right)\phi_b\delta_b}{\partial t} + \delta_b\phi_b\left(\frac{\partial p_{Ti}}{\partial t} + \frac{s_b}{\phi_b\delta_b}\frac{\partial p_{Ti}}{\partial x}\right) = 0 \qquad (3.43)$$

To reduce the number of variables, it can further be assumed $p_{bi} = p_{Ti}$; the composition in the bed-load layer equals that of the horizontal bed-load mass flux. The assumption $p_{bi} = p_{Ti}$ implies that $u_{gi} = \bar{u}_g$ (Eq.3.35). Substitution of $p_{bi} = p_{Ti}$ in Eq.3.43, results in

54

$$\frac{\partial p_{bi}}{\partial t} + \frac{s_b}{\phi_b \delta_b} \frac{\partial p_{bi}}{\partial x} = 0 \qquad\qquad (3.44)$$

This yields N-1 equations that describe changes in bed-load composition with a propagation rate $\bar{u}_g$. Hence, in contrast with the total decoupling as described in Subsection 3.3.1 and 3.3.2, the introduction of a "kinematic model" for particles traveling as bed load enables conservation of the total number of celerities and hence, the total number of wave-type solutions.

If $u_{gi} = \bar{u}_g$, differences in particle mobility (and hence transport rates per size fraction) are accounted for by differences in bed-load composition. This assumption of $u_{gi} = \bar{u}_g$; one travel rate for all fractions, corresponds to the concept introduced by Einstein (1950), but is rather hypothetical because consistent, and explicit data on both bed-load concentration and particle velocity are scarce (see Church and Hassan (1992) for a brief review).

Motion-picture observations by Drake *et al.* (1988) of bed-load particles at low-flow conditions seem to correspond with $u_{gi} = \bar{u}_g$. Tracking of tracer grains of a sand-gravel mixture through a flume, showed gravel fractions to have the largest mean travel-velocity (Iseya and Ikeda, 1987), analysis of tagged surface grains indicated a decreasing travel-distance with particle size (Church and Hassan, 1992). Although mechanisms such as bed undulations, grain-grain interactions, inertia and turbulence can be expected to diffuse particle motion and reduce differences in fraction velocity (e.g. Rakoczi, 1991), more observations on the kinematics of bed-load particles are required.

Considering the uncertainties on the validity of the simplification $u_{gi} = \bar{u}_g$, some numerical tests are carried out in Subsection 3.4.4 to analyse the effect on the model.

The resulting mass balance of the reference layer is

$$\left(\beta_{oi} - p_{bi} \right) \frac{\partial z_b}{\partial t} + \delta_p \frac{\partial p_{pi}}{\partial t} = 0 \qquad\qquad (3.45)$$

With this option, the number of *coupled* celerities would reduce to three; intersection of celerities, and subsequent instability of the model is prevented. The total number of celerities, and hence the number of wave type solutions, and the number of upstream boundary conditions is similar to that in the conventional model. Hence, equivalent boundary conditions to both

formulations can be imposed.

3.4.4. Numerical comparison.

Some numerical experiments are added to compare solutions of the stabilized model described in Subsection 3.4.3, relative to the conventional formulation as described in Subsections 3.2.2, 3.2.3 and 3.2.4. These experiments concern the deformation of a disturbance of the bed-level profile.

To account for changes in bed load, a fraction-averaged particle velocity u_g must be introduced. Einstein (1950) suggests $u_g/u_* \approx 11.6$, Van Rijn (1984a) mentions a range of u_g/u_* from 3 to 11 that increases with shear stress. In the following experiments, it is used $u_g/u_* = 7$ (Van Rijn, 1989), to analyse the effect of the formulation. A widely graded mixture is considered. Non-dimensional particle shear-stresses are $\tau_{*1}/\tau_{*cr} = 18.00$, $\tau_{*2}/\tau_{*cr} = 1.80$ and $\tau_{*3}/\tau_{*cr} = 0.18$
($D_1 = 0.0003$ m, $D_2 = 0.003$ m and $D_3 = 0.03$ m). The first and second reference layers are equal ($\delta_1 = \delta_2$).

The original model as described in Subsection 3.2.3 is referred to as concept I, concept II is the stabilized model as described in Subsection 3.4.3. Coarsening occurs at the eroding part of the hump, fining at the deposition part (Figure 3.10 and 3.11).

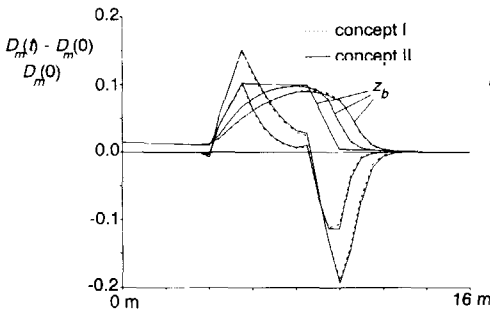**Fig 3.10** $\delta_1/D_3 = 10$; single layer. **Fig. 3.11** $\delta_1/D_3 = 2$; single layer.
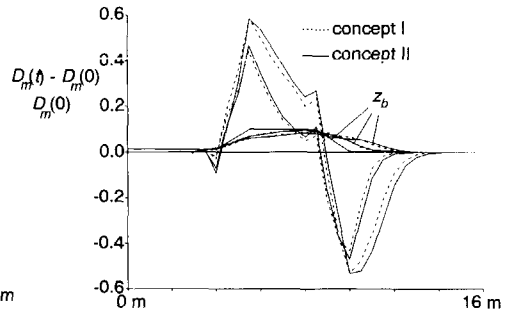
Changes in layer composition are larger for the stabilized concept II. The differences increase for smaller layer thickness. For higher values of Fr, similarity remains but differences between both models increase. Apparently, to obtain equivalent solutions in the conventional and stabilized model,

relatively larger layer thicknesses must be applied in the latter model.
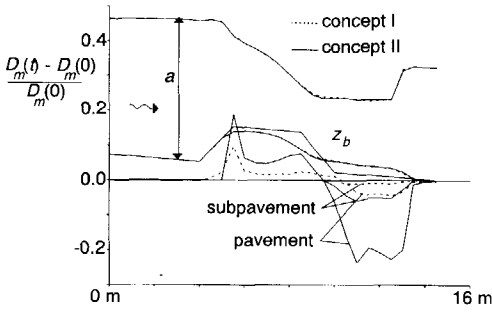
Fig. 3.12 $\delta_1/D_3 = 2$; double layer. **Fig.3.13** $\delta_1/D_3 = 2$; effect of u_g.
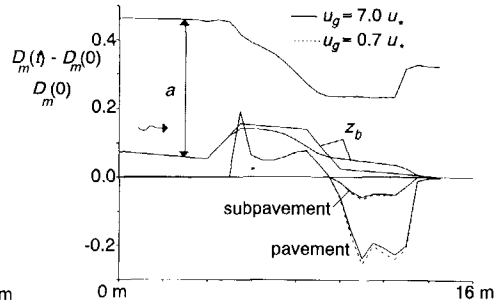
In case of morphological changes due to bed-level disturbances, both models yield comparable solutions. Therefore, some test cases of morphological changes driven by gradients in composition are considered. In the following example, a flat bed of fine sediment ($D_m = 3.7$ mm) with a coarse section ($D_m = 10.0$ mm) at subcritical flow conditions is considered. The gradients in composition induce deposition at the upstream part of the coarse section, and erosion downstream. Fluxes are arranged to represent a single-layer model, $\delta_1 = 3D_3$ ($D_1 = 0.1$ mm, $D_2 = 1$ mm and $D_3 = 10$ mm).
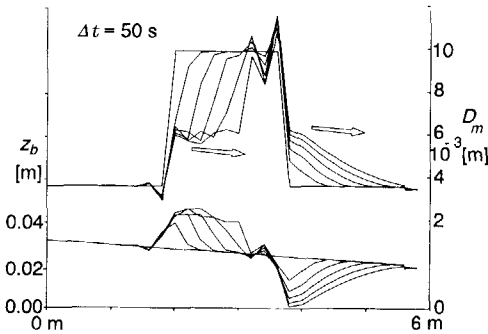
Fig.3.14 Conventional model. **Fig.3.15** Stabilized model.
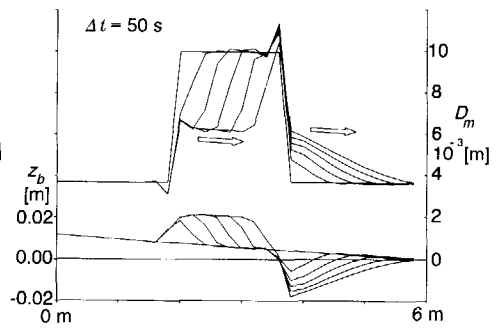
Again, solutions are similar (Figures 3.14 and 3.15). In the stabilized model, wiggles in the solution are reduced.

In case of a similar bed configuration in supercritical flow, responses of the

stabilized model are slower than the conventional model. Again, the conventional model (concept I) shows large wiggles near the transitions. Hence, for these larger values of particle shear-stress, now a relatively smaller layer thickness must be applied in the stabilized model, to obtain results similar the the conventional model.
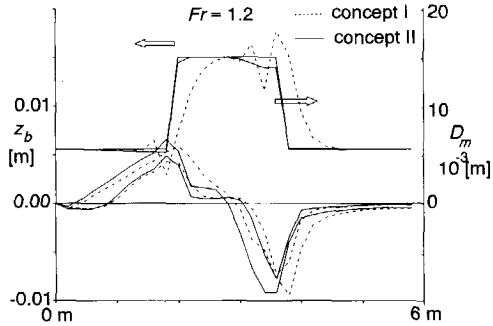
Fig.3.16 Conventional model.

3.5. Definition of reference layers.

3.5.1. Introduction.

As described in the previous sections, a reference volume (or layer) must be introduced to define size fractions. Because fractions should be representative for the entire reference volume, the extend of the layer is limited to a zone of homogeneous composition. Therefore, a reference layer is often defined as the extent of mixing of sediment at the surface of a river bed. The type and subsequently extent of this mixing is related to the *scale of the phenomena of interest*.

However, the physical interpretation of such a layer is not clear. With respect to defining layer thicknesses, representation of physical mixing processes (*causal* orientated) as well as composition changes in the corresponding model (*result* orientated, considering the applied transport predictor) should be taken into account. At present state, discrepancies between both categories can be observed (Belleudy, 1994).

Before considering the definition of a layer thickness in Subsection 3.5.3, the relation with fraction dynamics is considered in Subsection 3.5.2. For armouring processes, different layer thicknesses are reviewed in Subsection 4.2.4.

58

3.5.2. Dynamics of fractions.

The relation between changes in bed level and composition can be written as an ODE (Subsection 3.3.1). In terms of mean grain-sizes, the relation of composition and bed level change is

$$\frac{\partial D_{mp}}{\partial t} = \frac{\left(D_m^* - D_{mo}\right)}{\delta_p} \frac{\partial z_b}{\partial t} \tag{3.46}$$

with D_{mo}, D_{mp} and D_m^*, mean grain sizes of substratum, bed surface and vertical sediment flux.

Due to differences in particle mobility, the mixture in transport is finer than the mixture at the bed surface. Hence, in general, it can be expected for values of τ_{*m}/τ_{*cr} larger than unity, that the composition of the vertical flux is finer than the bed ($D_m^* < D_{mo}$, e.g. Toro-Escobar et $al.$ 1996). Then, coarsening is predicted in case of degradation, fining in case of deposition. This effect can be illustrated by flume observations as reported by Ribberink (1983) (Figure 3.17).

However, it should be considered that at the scale of particle movements, or if $\tau_{*m}/\tau_{*cr} \approx 1$, contributions of particle interaction and gravity to vertical fluxes and horizontal transport can result in $D_m^* > D_{mo}$. An example is the collection of coarse particles at the aggradation front of bed features (e.g. Klaassen et $al.$ 1986).
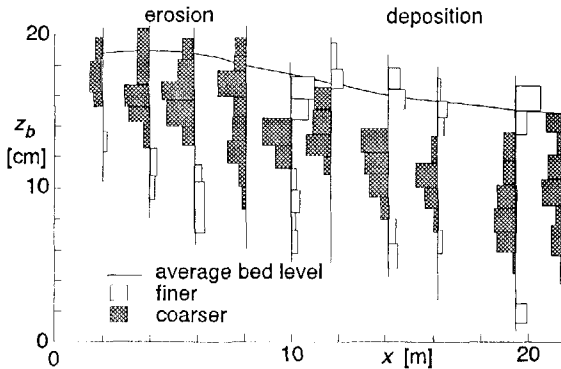

Fig.3.17 Vertical structure of bed composition (Ribberink, 1983).

Another illustrative example with $D_m^* > D_{mo}$ is due to Iseya and Ikeda (1987).

In their experiments with longitudinal sorting in a sand-gravel mixture, the flow regime was supercritical upstream in the flume and subcritical at the reach of deposition. The hydraulic jump that marked the upstream border of the deposition was observed to successively move up- and downward.

Significant longitudinal sorting and corresponding transport fluctuations were observed. Apart from the interaction between sediment transport and local bed configuration, as indicated by Iseya and Ikeda (1987), the fluctuating jump at the upstream boundary of the deposition zone can be a source of fluctuations.

bed state	congested	transitional	smooth	congested
plan view				
longitudinal view				
particle movement	intermittent		usually continuous	intermittent
bed load transport rate			sand	gravel
bed load balance			in out	
	aggrading		degrading	aggrading
bed slope	steep	intermediate	gentle	steep
sedimentary structure of superficial layer	open-work	half matrix-filled	matrix-filled	open-work

Fig.3.18 Interaction level and composition (Iseya and Ikeda, 1987).

With respect to Eq.3.46, observations (Figure 3.18) indicate that at the upstream (erosion) side of the bed-level wave, a fine surface was found, at the downstream (deposition) side, a coarse surface was observed. Iseya and Ikeda (1987) explained this effect by considering the fluctuation in grain roughness and the state of the bed, and its effect on the fraction mobility; at fine beds, gravel is relatively mobile due to exposure, colliding grains subsequently initiate motion of sand.

To analyse the influence of pavement and subpavement layer on fraction response, sediment-mass balances are linearized by prescribing a continuous change in bed level with a rate w_z. A similar exercise can be found in Ribberink (1987). This enables the construction of analytical solutions that give information about response rates and equilibrium conditions. To account for hiding effects, size fractions in the vertical mass flux are defined as $p_{Ti} = f_i\, p_{pi}$ (in case of equal mobility $f_i = 1$). Situations of erosion and sedimentation should be considered separately.

60

In case of erosion, the sediment mass balance of the pavement and subpavement can be written as

$$\frac{\partial p_{pi}}{\partial t} = -\frac{\kappa w_z}{\delta_p} \left(-f_i p_{pi} + p_{si}\right)$$

$$\frac{\partial p_{si}}{\partial t} = -\frac{w_z}{\delta_{sp}} \left(-\kappa p_{si} - (1-\kappa)f_i p_{pi} + p_{oi}\right)$$

(3.47)

In case of two size fractions and constant f_i, combination of both ODE's yields

$$\frac{\partial^2 p_{p1}}{\partial t^2} - \frac{\kappa w_z}{\delta_p}\left(f_1 + \frac{\delta_p}{\delta_s}\right)\frac{\partial p_{p1}}{\partial t} + \frac{f_1 w_z^2 \kappa}{\delta_p \delta_s} p_{p1} = \frac{w_z^2 \kappa}{\delta_s \delta_p} p_{o1}$$

(3.48)

and

$$\frac{\partial^2 p_{sp1}}{\partial t^2} - \frac{\kappa w_z}{\delta_p}\left(f_1 + \frac{\delta_p}{\delta_s}\right)\frac{\partial p_{sp1}}{\partial t} + \frac{f_1 w_z^2 \kappa}{\delta_p \delta_s} p_{sp1} = \frac{w_z^2 \kappa f_1}{\delta_s \delta_p} p_{o1}$$

(3.49)

The equilibrium compositions of the pavement are affected by the mobility correction f_1. Conform observations by Belleudy (1994), the effects of hiding corrections and layer thickness on the solution correspond; for a single-layer model, both can even be combined into one parameter. Apparently, a layer thickness in a model is related to the type of sediment-transport predictor applied.

Due to the definition of the vertical flux composition, the equilibrium composition in the pavement will be $p_{p1} = p_{o1}/f_1$ and $p_{s1} = p_{o1}$. Hence, a decrease in mobility of the fine fraction will result in a finer surface. At higher levels of particle shear-stress, where hiding corrections are less effective, surfaces of eroding beds will be coarser.

The homogeneous part of the solution for pavement and subpavement can be written as $C\, e^{\lambda t}$ with

$$\lambda = \frac{\kappa w_z}{2\delta_p}\left[f_1 + \frac{\delta_p}{\delta_s} \pm \sqrt{\left(f_1 + \frac{\delta_p}{\delta_s}\right)^2 - 4\frac{f\,\delta_p}{\delta_s \kappa}}\right]$$

(3.50)

A representative time scale for fraction changes is

$$T = \frac{\delta_p}{|w_z|}$$ (3.51)

which indicates the period needed to degrade a bed over the layer thickness. This relation of layer thickness and time scale of fraction responses will be used in Subsection 3.5.3, to review different types of layer definitions.

The character of λ (complex or real) indicates the type of solution. If two complex roots are found, a type 1 solution exists, if two real roots are found a type 3 solution results and if both roots coincide, a type 2 solution can be found.
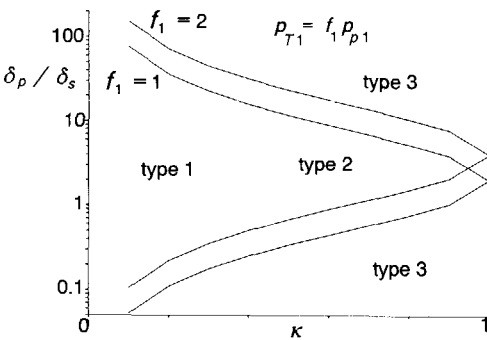
Fig.3.19-a Type of solution.　　　**Fig.3.19-b** Type of solution.
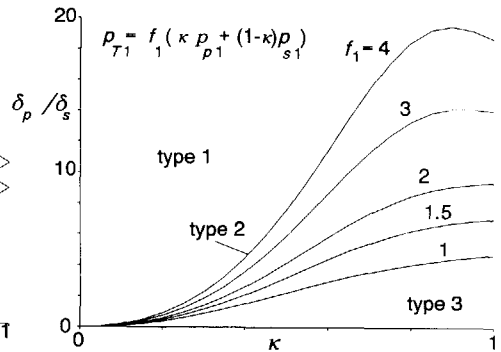
In Figures 3.19-a and b, two definitions of vertical flux composition are compared. Some common values are $\delta_p/\delta_s = 2$, and $\kappa \approx 0.84$ (e.g. Di Silvio, 1991; Ribberink, 1987). Hence, in general, for double-layer models, a type 1 solution is obtained.

For single-layer models ($\delta_s \rightarrow \infty$ and $\kappa = 1$), a type 3 solution is found. Borah *et al.* (1982a) separate functions of the reference layer by defining a thin contact layer at the surface that affects sediment transport, and a mixing layer underneath, to record changes in bed composition. This would yield a type 3 solution. An example of all types is presented in Figure 3.20.

62
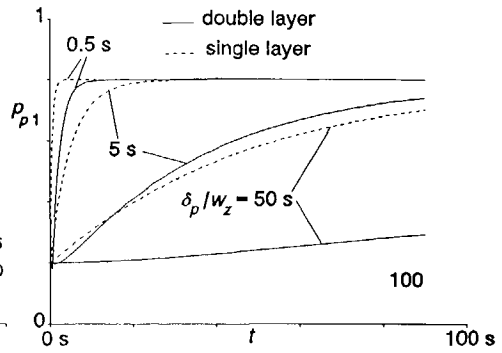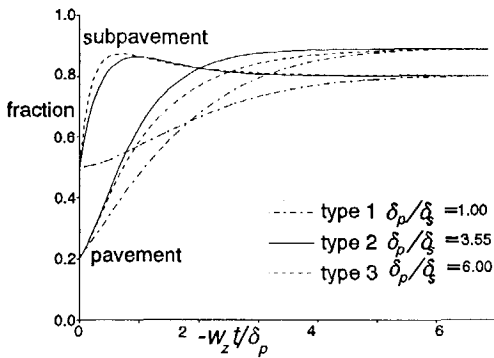
Fig.3.20 Type of fraction-response. **Fig.3.21** Effect of subpavement layer.

The fraction response of a single-layer model will be faster than a double-layer model (Figure 3.21); distinction of a transition layer clearly dampens the response of the pavement.

For illustration, field observations by Gomez (1983) are mentioned. At peak discharges in a small channel, when all particles moved, a thorough mixing resulted in a homogeneous composition of bed and surface. After the peak, when observations started, a coarsening of the bed surface occurred during several minor discharges.
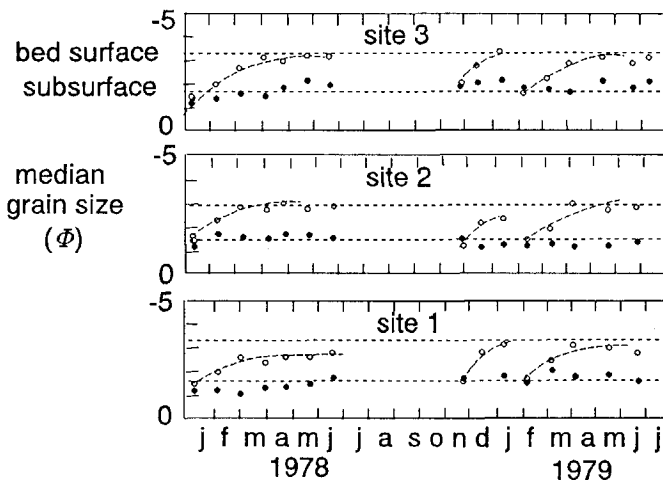
Fig.3.22 River-bed coarsening (Gomez, 1983).

Although the assumption of constant degradation is in conflict with reality,

63

observed changes are comparable with the exponential solutions of the analytical model. In Figure 3.23, all curves representing different sites are combined into one graph.
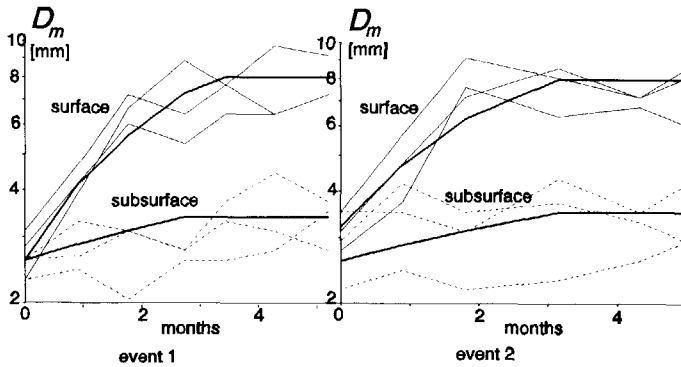
Fig.3.23 Comparison linearized model and observations.

Fat curves represent the linearized model, thin lines represent observations at different locations. Sediment is described with a sand ($D_1 = 2$ mm) and a gravel ($D_2 = 8$ mm) fraction. The response time of the bed composition appears to be two months, but this includes periods of low flow where all fractions are stable. Note that changes in the subpavement are minor (for the thick lines, the ratio of subpavement and pavement thickness is $\delta_s/\delta_p = 5$).

3.5.3. Selection of layer thickness.

Reference, or mixing layers have been coupled to sediment features such as grain-size (e.g., Di Silvio and Peviani, 1991), and combinations of sediment features and hydraulic conditions such as particle shear-stress (Niekerk et al, 1992) or bed-form height (e.g. Ribberink, 1987). Obviously, the application of different concepts should be carried out with care.

The selection of layer thickness with respect to bed-level change determines the response of fractions. Application of a small thickness relative to bed level change (such as the "contact layer" as applied by Borah *et al.*, 1982a) results in "instantaneous" adaption of size fractions at the surface of the river bed. The selection of a relatively large thickness value eliminates the effect of short-term fluctuations. This can be illustrated by applying the linear model as described in Subsection 3.5.2 to alternating sequences of deposition and erosion. The effect of the time-scale ratio of *active* fluctuation and *response* is illustrated in Figure 3.24.

64

If T_{act} approaches T_{resp}, no dampening in response is present, if $T_{act} << T_{resp}$, changes are negligible.
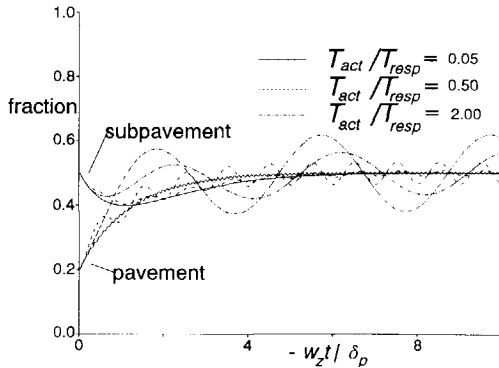
Fig.3.24 Effect of short-term fluctuations.

The effect of additional mass flux in case of bed forms can be illustrated with the case of a degrading bed (Figure 3.25-a). For slow fluctuations (T_{act}/T_{resp} large), compositions range between β_{o1}/f (during erosion) and p_{T1} (during deposition). Not only the period, but also the amplitude affects the adaption period and equilibrium composition of the bed. If $\Delta z_b/\delta_p << 1$, the magnitude of fluctuations in composition disappear; minor fluctuations can be dampened by selecting a larger layer thickness (Figure 3.25-b).
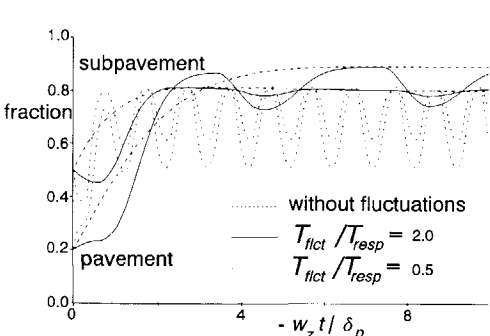
Fig.3.25-a Effect of period. **Fig.3.25-b** Effect of amplitude.

Hence, two extreme situations can be distinguished:

$T_{flct}/T_{resp} = 0$; no change in composition during the "fluctuation"

$T_{flct}/T_{resp} \rightarrow \infty$; instantaneous change in composition, relative to change in bed level during the "fluctuation"

65

Hence, with respect to the selection of a layer thickness, time-scales of morphological changes are of relevance. Now, two extremal conditions are considered; for *large* scales of length, a parabolic model approximates the solution (Subsection 3.3.2). If, for *small* length-scales, changes in composition can be neglected, a simple-wave model results. An indication of corresponding T_{resp} values is added in Table 3.1. Here, L_m and ΔZ_b represent a characteristic length and height of a bed-level disturbance. A representative period T_m is found with $T_m = L_m/u$.

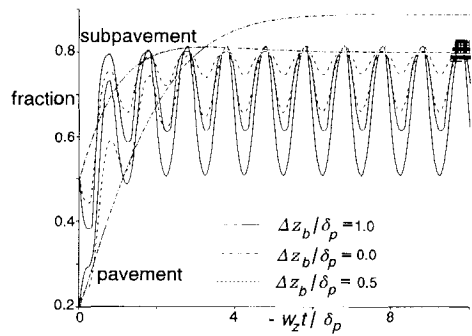| length-scale	model	$\dfrac{T_{resp}}{T_m}$	$\dfrac{\Delta Z_b}{\delta_p}$
small (no friction) ($Fr < 0.8$ or $Fr > 1.2$)	$\dfrac{\partial z_b}{\partial t} + \dfrac{u\psi}{1-Fr^2}\dfrac{\partial z_b}{\partial x} = 0$	$\dfrac{\lvert 1-Fr^2 \rvert}{\psi}$	$O(10^2)$
small (no friction) ($0.8 \leq Fr \leq 1.2$)	$\dfrac{\partial^2 z_b}{\partial t^2} - \dfrac{u^2\psi}{2Fr^2}\dfrac{\partial^2 z_b}{\partial x^2} = 0$	$\dfrac{Fr}{\sqrt{\psi/2}}$	$O(10)$
large; $L_m > 3a/i_b$	$\dfrac{\partial z_b}{\partial t} - \dfrac{C^2 a^2 \psi}{3u}\dfrac{\partial^2 z_b}{\partial x^2} = 0$	$3\,\dfrac{i_b}{a}\dfrac{L_m}{\psi}$	$> 10^2$

Table 3.1 Estimation of response time-scale.

T_{resp} and T_m more or less correspond if approximately $\delta_b/\Delta Z_b \approx 0.1$. To obtain a homogeneous distribution of fractions in the reference layer, an instantaneous mixing with respect to changes in bed level is required. This implies that $T_m/T_{resp} \to \infty$, or $\delta_b/\Delta Z_b \ll 1$ is necessary. Hence, in order to define a layer thickness, relevant changes in bed level must be known. This explains the amount of layer definitions that can be reviewed for different phenomena such as armouring processes or large-scale longitudinal sorting (Laguzzi, 1994).

Another example of the considerations as described above concerns changes in roughness due to changes in surface composition. Local compositions of river beds respond relatively quickly. Observations from flume experiments (Suzuki and Michiue, 1988) and prototype measurements (Foley, 1975; Klingemann and Emmet, 1982; De Jong and Ergenzinger, 1992; Dinehart, 1992) showed significant coarsening during rising stages of floods.

These changes in composition (and subsequent roughness) can be predicted if time scales are of the order of or larger than response time scales;

$$T_{resp} = \frac{\delta_p}{|w_z|} = \frac{\delta_p}{a} \frac{1}{n \phi} \frac{1}{|\partial u/\partial x|} \ll T_{wave} \qquad (3.52)$$

For diffusive flood waves, this criterion can be approximated with

$$\frac{\delta_p}{a} \frac{1}{n \phi} \ll \frac{\Delta u}{c_{wave}} \approx \frac{2}{3} \qquad (3.53)$$

or approximately $\delta_p/a \approx \phi$.

3.5.4. Comparison of layer definitions.

In the previous section it has been concluded that the layer thickness should be selected relative to the time scale of relevant composition changes. Furthermore, the mixing mechanism responsible for transferring composition changes through the reference layer must be "instantaneous" relative to regular changes in bed level and composition. In this subsection, some layer predictors are compared.

In low-land rivers, propagating bed-forms are generally considered to be the main cause of mixing. In that case, the extent of mixing, or layer thickness, is related to bed-form height Δz_b (Ribberink, 1987), which enables predicting δ_p (and δ_s) with existing bed-form predictors. The bed-form period is defined as $T_{bedf} = L_b/c_b$, where L_b is the bed-form length and c_b is the propagation rate, that can be estimated by applying a rigid-lid approach (e.g. Jansen, 1979). For $0 < \theta < 10$ (θ is a transport parameter) the steepness can be approximated roughly with (Van Rijn, 1984b)

$$\frac{\Delta z_b}{L_b} \approx 3 \left(\frac{a}{D_{50}} \right)^{0.3} \qquad (3.54)$$

In case of gravel-bed rivers with large differences in particle mobility, significant changes in composition are accompanied with minor changes in bed level. Then, mixing at the scale of particle movements should be considered. However, individual movements of particles in gravel-bed rivers are rather obscure; apart from wide scatter which reveals the stochastic character, burial depths of approximately $5 \sim 10$ times D_{50} can be observed (Hassan and Church, 1992).

The particle-movement period can be defined as

$$T_{part} = \phi_b \, \frac{L_p \, \delta_b}{s_b} \qquad (3.55)$$

where δ_b is the thickness of the bed-load layer, ϕ_b is the sediment concentration in the bed-load layer and L_p the step or saltation length of a particle. This step length L_p can be defined as $k \, D_{50}$, but experiments (e.g. Fernandez-Luque and Van Beek, 1976; Van Rijn, 1984a; Niño et al., 1994) reveal a wide range of scatter, inherent to the stochastic character of particle motion. The extend of mixing δ_p can be related to δ_b. Van Rijn (1984a) suggests k values that range from 10 to 100, with τ_{*m}/τ_{*cr} values ranging from 1 to 11.

The mixing mechanism must be instantaneous relative to regular changes in composition. This implies that $T_{mix} << T_{resp}$. For layer predictors based on a bed-form scale and particle-motion scale, this condition is considered in Table 3.2. Here, n is from the powerlaw $s_b = mu^n$. Note that the expressions in Table 3.2 are indicative only.

length-scale	mixing-layer definition	
	bed-form height applicable if $\dfrac{L_m}{\Delta Z_b} >>$	particle movement applicable if $\dfrac{L_m}{\Delta Z_b} >>$
small (no friction) ($Fr < 0.8$ or $Fr > 1.2$)	$\dfrac{L_b}{\Delta z_b} \approx 3 \left(\dfrac{a}{D_{50}}\right)^{0.3}$	$k \, \dfrac{\phi_b}{c_0} \dfrac{D_{50}}{a} \dfrac{n}{\lvert 1 - Fr^2 \rvert}$
small (no friction) ($0.8 \leq Fr \leq 1.2$)	no bed forms	$k \, \dfrac{\phi_b}{c_0} \dfrac{D_{50}}{a} \dfrac{n}{Fr} \dfrac{1}{\sqrt{2\psi}}$
large (0-order uniform) $L_m > 3a/i_b$	$\lvert 1 - Fr^2 \rvert \left(\dfrac{a}{D_{50}}\right)^{0.3} \dfrac{a}{i_b L_m}$	$k \, \dfrac{\phi_b}{c_0} \dfrac{D_{50}}{a} n \dfrac{a}{i_b L_m}$

Table 3.2 Applicability of layer definitions.

In general, mixing layers scaled on particle-movement seem to be applicable for "steeper" (larger values of $\Delta Z_b/L_m$) bed-level disturbances. Mixing layers scaled on mechanisms with larger mixing-lengths (bed forms or other periodic fluctuations) are applicable at more uniform disturbances (lower values of $\Delta Z_b/L_m$) and longer length-scales.

3.5.5 Short-term fluctuations.

Because vertical fluxes in case of deposition and erosion are different, short-term fluctuations with alternating erosion and sedimentation affect the bed compositions. When referring to Eq.3.19 in Subsection 3.3.1, the mass fluxes between river bed and flow can be written as

$$\overline{\Phi_{pi}} = -c_0\beta_i^* \frac{\partial z_b}{\partial t} - c_0\beta_i^{*\prime} \frac{\partial z_b^\prime}{\partial t} \tag{3.56}$$

In flume experiments in the bed-form regime, Ribberink (1987) observed subpavements, coarser than the underlying substratum. This could be explained by considering fluxes due to short-term fluctuations in bed level. To account for the net effect of such short-term fluctuations, Ribberink (1987) suggested a gradient-type, diffusive flux. Analogously, Armanini (1995) applies diffusive mass fluxes to explain vertical structures in bed composition.

If an additional flux due to vertical structures in bed composition is introduced, the mass balances of pavement and subpavement read

$$\delta_p \frac{\partial p_{pi}}{\partial t} + \kappa \Phi_{pi} + \kappa\beta_{pi}\frac{\partial z_b}{\partial t} + \kappa \Phi_{pi}^\prime = 0$$

$$\tag{3.57}$$

$$\delta_s\frac{\partial p_{si}}{\partial t} + (1-\kappa) \Phi_{pi} + \left(\beta_{oi}-\kappa\beta_{pi}\right) \frac{\partial z_b}{\partial t} + (1-\kappa) \Phi_{si}^\prime = 0$$

This flux can be of the form

$$\Phi_{pi}^\prime = \epsilon_{pi} \left(p_{pi} - \xi_i p_{Ti}\right) \quad ; \quad \Phi_{si}^\prime = \epsilon_{si} \left(p_{si} - \xi_i p_{Ti}\right) \tag{3.58}$$

with ϵ_{pi} and ϵ_{si} exchange rates ($[\epsilon_{pi}]$ = m/s), often related to sediment transport rates (e.g., Di Silvio, 1991) and ξ_i a coefficient to account for size-preferences in vertical mixing between the transport and storage layer. To indicate the limited stability of Eqs 3.57 and 3.58, the solution for a first-order perturbation is analysed. If a zero-order, equilibrium composition is assumed, and gradients in fraction-integrated transport rates are absent, first-order changes in fraction i can be described as

$$\frac{\partial p_{pi}}{\partial t} = -\kappa \epsilon_{pi} p_{pi} \left(1 - \xi_i \frac{d p_{Ti}}{d p_{pi}}\right) \tag{3.59}$$

Substitution of an exponential solution yields a stable solution of Eq.3.58 if

$$\xi_i \, \frac{d\, p_{Ti}}{d\, p_{pi}} \; < \; 1 \tag{3.60}$$

This concept (Eq.3.57 and 3.58) can be stabilized by stating that diffusive fluxes occur if the actual composition in the transport layer deviates from equilibrium compositions.

Obviously, distinction of additional fluxes affect the type of fraction response. If degradation is considered, combination yields a second-order ODE for fractions in pavement and subpavement. Again, different types of solution (Subsection 3.5.2) can be found.
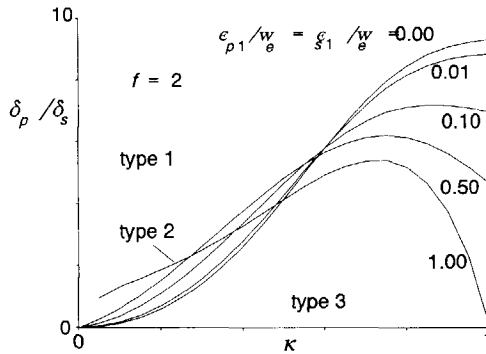
Fig.3.27 Type of solution.

With respect to the definition of the flux due to short-term fluctuations conform Armanini (1995), the following remarks can be made. Additional sediment fluxes are found due to integration of bed-level changes (and subsequent mass fluxes) over a time interval. It should be noted, however, that correlation with slower changes can only be neglected if time-scales of changes are an order of magnitude lower than response scales of composition.

$$\frac{T_{fluct}}{T_{resp}} \; = \; \frac{L_b}{\delta_p} \, \frac{|w_z|}{c_b} \; \ll \; 1 \tag{3.61}$$

where L_b and c_b are the length and propagation rate of the zero-average fluctuations. In case of bed forms, length and height are related ($H_b = \alpha L_b$). Hence, to distinguish an additional flux due to bed forms, either bed levels should be close to equilibrium ($|w_z| \ll c_b$) and/or changes in composition

70

should be very small ($\delta_p >> L_b = H_b/\alpha$).

Mainly, for conditions close to equilibrium, the additional flux in Eq.3.56 becomes of interest. This can be illustrated with the following example. At equilibrium conditions for bed level and composition in a flume, Ribberink (1983) changed the *composition* of input sediment at the upstream boundary of a flume, while keeping the total *volume* of sediment-feed constant. During this experiment where bed forms developed, significant changes in composition and subsequent changes in bed level were induced.

In the conventional model (Section 3.2), transport gradients per size fraction are used explicitly to determine changes in composition; no additional flux is required to simulate the observed changes (Figure 3.28-a). However, in mathematical models such as the stabilized concept (Subsection 3.4.3) without additional fluxes as defined in Eq.3.56, this condition of zero-gradients in sediment transport at the upstream boundary would result in constant bed levels and composition.

The relevance of the additional flux in Eq.3.56 for the stabilized model can be demonstrated numerically as follows. Conditions similar to the transition experiment of Ribberink (1983) are applied. In absence of these fluxes, indeed no changes were observed in the stabilized model, whereas if additional fluxes are included, changes in composition and bed level were initiated (Figure 3.28-b). The additional fluxes are caused by zero-average bed-level fluctuations (bed forms) and differences in actual and equilibrium composition in the transport layer.
Differences in propagation rates in both models can be observed similar to examples in Subsection 3.4.4. The predicted equilibrium conditions in both models are equal.
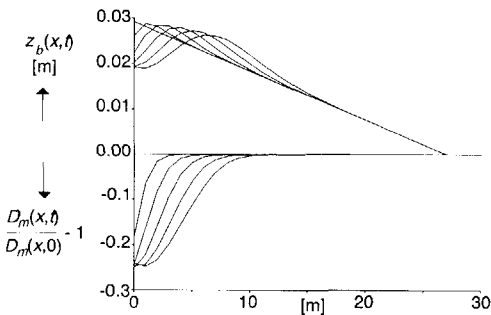
Fig.3.28-a Conventional model.   **Fig.3.28-b** Stabilized model.
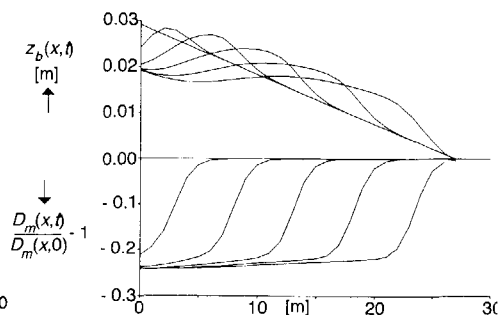
Hence, with respect to the stabilized model (Subsection 3.4.3), the following can be concluded. In case of equilibrium bed levels, information on sediment composition at the upstream boundary is properly transferred with the help of additional fluxes that represent short-term bed-level fluctuations. Due to this flux, the strong coupling between bed-level changes and composition is reduced. An application of a similar experiment can be found in Subsection 4.4.4.

Chapter four.

Some effects of sediment mixtures on morphology.

4.1. Introduction.

As concluded in Chapter three, changes in bed level and composition are coupled. In this chapter, analytical and numerical methods are used to analyse some effects of graded sediment. The analytical models concern armouring processes (Section 4.2) and longitudinal sorting effects (Section 4.3). The numerical model is described in Chapter seven. Numerical solutions are compared with experiments on degradation downstream of dams, the deformation of bed-level disturbances and bed levels in narrowed sections, and the responses to changes in upstream sediment supply. (Section 4.4).

4.2. Streambed armouring.

4.2.1. Introduction.

One of the most distinct morphological features in rivers with graded sediment is the appearance of armoured bed surfaces; a thin layer of stable coarse grains on top of finer material. This can often be considered an equilibrium condition, either static (no motion) or dynamic (bed-load composition equals substratum) (Andrews and Parker, 1987; Jain, 1990).

Armouring processes can significantly affect morphological changes in a river; coarsening of the bed surface results in an increase of critical shear stress (Egiazaroff, 1965), and a subsequent reduction or dampening of bed degradation (Karim and Holly, 1986). An example of low-flow bed stabilization due to armouring was studied in flume experiments by Whittaker and Jaeggi (1982) or Grant and Mizuyama (1991). Here, armoured anti-dunes were considered to be responsible for the typical step-pool systems, that can be found in steeper mountain streams.

Different studies on armouring in flumes have been carried out (e.g., Gessler, 1970; Little and Mayer, 1976 and Chin, 1985). To describe the size-selective stability, entrainment and movement of particles in armouring processes, often concepts based on critical shear-stress have been applied. Theoretical models vary from one-step models, predicting equilibrium compositions and scouring depths, to multiple-step models, describing different stages of coarsening processes (Sutherland, 1987).

With different levels of excess shear-stress, Raudkivi and Ettema (1982) distinguish stages in a coarsening process, that range from no particle movement, overpassing of large particles at high exposure, entrainment of smaller particles and finally motion of all grains. As described by Chin (1985) in the initial phase of the armouring process, the transport of fine material results in bed features propagating downstream. With a reducing availability of finer fractions, the surface of the bed is rearranged: finer particles cluster up- and downstream of stable coarser fractions. This phase of the armouring process is accompanied by a rapid decrease of degradation and sediment transport rate.

Due to particle-interaction, surface coarsening consists of two-dimensional patterns of mobile and immobile particle populations (Drake *et al.* 1988). Then, stabilized parts at the river thalweg can be combined with finer margins near the banks (Klingeman and Emmet, 1982). Shifting of flow patterns, or disintegration of a local, armoured surface can induce transport fluctuations of fine sediment (Jaeggi and Rickenmann, 1987).

To analyse the coarsening process, a situation with zero sediment feed as shown in Figure 4.1 is studied. In this section, mathematical models based on the layer concept as described in Chapter three are used to explain the general pattern of coarsening, without modelling particle movements in detail. The models are derived for the case of armouring, where velocity and depth can be assumed constant. The construction of analytical solutions enables analysing the effect of model parameters and comparing different models. These solutions are constructed and applied in Subsections 4.2.2 and 4.2.3.
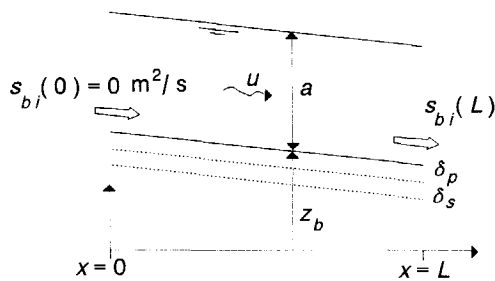

Fig.4.1 Model configuration for armouring.

4.2.2. Analytical models.

First, the concept proposed by Hirano (1972) (Subsection 3.2.2.) is used to construct an analytical solution. The number of fractions amounts 2. The total mass balance for sediment, integrated over a length L is

$$\frac{\partial z_b}{\partial t} + \frac{\partial \sum_{i=1}^{N} \left[s_{bi}(t, L) - s_{bi}(t, 0) \right]}{\partial x} = 0 \qquad (4.1)$$

If the input of sediment at the upstream boundary $(x=0)$ is zero, the time derivative of sediment transport at $x=L$ can be written as

$$\frac{\partial s_b(t)}{\partial t} = - L \frac{\partial^2 z_b}{\partial t^2} \qquad (4.2)$$

The mass balance for a fraction i contains the time gradient in composition

$$\frac{\partial p_{pi}}{\partial t} + \frac{\beta_{pi}}{\delta_p} \frac{\partial z_b}{\partial t} + \frac{s_{bi}(t)}{L \, \delta_p} = 0 \qquad (4.3)$$

Assuming that $s_{bi} = f(u, p_{pi}, D_i, D_m)$, gradients in transport of a fraction are

$$\frac{\partial s_{b1}}{\partial t} = \left(\frac{\partial s_{b1}}{\partial p_{p1}} + (D_1 - D_2) \frac{\partial s_{b1}}{\partial D_m} \right) \frac{\partial p_{p1}}{\partial t} = X_1 \frac{\partial p_{p1}}{\partial t}$$

$$\frac{\partial s_{b2}}{\partial t} = \left(- \frac{\partial s_{b2}}{\partial p_{p2}} + (D_1 - D_2) \frac{\partial s_{b2}}{\partial D_m} \right) \frac{\partial p_{p1}}{\partial t} = X_2 \frac{\partial p_{p1}}{\partial t} \qquad (4.4)$$

This enables writing

$$X_2 \frac{\partial s_{b1}}{\partial t} - X_1 \frac{\partial s_{b2}}{\partial t} = 0 \quad ; \quad X_2 \frac{\partial^2 s_{b1}}{\partial t^2} - X_1 \frac{\partial^2 s_{b2}}{\partial t^2} = 0 \qquad (4.5)$$

Using the mass balances for both fractions, it can be found

$$\frac{\partial^3 z_b}{\partial t^3} + \frac{\left((1-\beta_{p1})\, X_1 - \beta_{p1} X_2\right)}{\delta_p\, L} \frac{\partial^2 z_b}{\partial t^2} = 0 \qquad (4.6)$$

After substitution of the boundary conditions, the solution is

$$z_b(t) = \frac{s_b(0)}{\lambda L}\left(1 - e^{\lambda\, t}\right) \; ; \quad \lambda = -\frac{\beta_{p2} X_1 - \beta_{p1} X_2}{\delta_p\, L} = -\frac{a}{\delta_p}\frac{Y_{h1} u}{L} \quad (4.7)$$

In absence of non-uniform conditions of flow, the degradation process in case of armouring can be characterized as essentially uniform in longitudinal direction (e.g., Ashida and Michiue, 1971). This implies that if sediment fluxes between flow and bed are written as

$$\frac{\Phi_{pi}}{\displaystyle\sum_{i=1}^{N} \Phi_{pi}} = p_{Ti} + s_b \frac{\partial p_{Ti}/\partial x}{\partial s_b/\partial x} \qquad (4.8)$$

the contribution of the second-term at the right-hand side is small (see also Parker and Sutherland, 1990). This enables application of a simplified model (see also Subsection 3.2.5), which will be used in the following.

The number of fractions is N. The derivative of sediment transport is defined as

$$\frac{\partial \displaystyle\sum_{i=1}^{N} s_{bi}(t)}{\partial t} = \sum_{i=1}^{N} \frac{\partial s_{bi}}{\partial u}\frac{\partial u}{\partial t} + \sum_{i=1}^{N}\left[\frac{\partial s_{bi}}{\partial p_{pi}} - \frac{\partial s_{bN}}{\partial p_{pN}} + \sum_{j=1}^{N}\frac{\partial s_{bj}}{\partial D_m}(D_i - D_N)\right]\frac{\partial p_{pi}}{\partial t} \quad (4.9)$$

Now, sediment-mass continuity in pavement and subpavement is described by

$$\delta_p \frac{\partial p_{pi}}{\partial t} + \kappa \left(p_{si} - p_{Ti}\right)\frac{\partial z_b}{\partial t} = 0$$

$$\delta_s \frac{\partial p_{spi}}{\partial t} + \left(p_{oi} - (1-\kappa)p_{Ti} - \kappa \, p_{si}\right)\frac{\partial z_b}{\partial t} = 0$$

(4.10)

After combining Eqs 4.2, 4.9 and 4.10 it can be obtained

$$\frac{\partial^2 z_b}{\partial t^2} + \frac{\kappa X}{L\delta_p}\frac{\partial z_b}{\partial t} = 0$$

(4.11)

with

$$X = \sum_{i-1}^{N} \left[\frac{\partial S_{bi}}{\partial p_{pi}} - \frac{\partial S_{bN}}{\partial p_{pN}} + \sum_{j=1}^{N}\frac{\partial S_{bj}}{\partial D_m}(D_i - D_N)\right]\left(p_{Ti} - p_{spi}\right)$$

(4.12)

After substitution of boundary conditions, a solution for the bed level can be found.

$$z(t) = \frac{s_b(0)}{\lambda \, L}\left(1 - e^{\lambda \, t}\right) \; ; \; \lambda = -\frac{\kappa \, X}{L \, \delta_p} = \kappa \, \frac{a}{\delta_p}\frac{Y \, u}{L}$$

(4.13)

Hence, the general form of solutions (Eqs 4.7 and 4.13) in both concepts correspond. For high values of τ_{*i}/τ_{cr}, the transport-composition!approaches the composition of the bed surface and X approaches zero. Then, degradation rates (and subsequently sediment-transport rates) become constant. A similar result is found if $\delta_p \rightarrow \infty$.

The linearized models (Eqs 4.7 and 4.13) contain information on changes and equilibrium conditions of bed level, sediment transport and surface grain size. Obviously, Eq.4.13 is convenient in case of a large number of size fractions. In the following sections, Eq.4.13 is applied to predict degradation of bed level, decline of sediment transport and coarsening of the bed surface.

4.2.3. Armouring process.

Chin et al. (1994) recorded bed-level changes in conditions as described in Figure 4.1. Except for minor roughness changes due to coarsening, hydraulic

77

conditions were kept constant by correcting the bed level for eroded volumes. Degradation rates were analysed with different mixtures at various levels of shear stress. In the following, analytical solutions are applied to these measurements.

In Section 3.5, it is shown that magnitudes of layer thickness are related to the scale of relevant composition changes. Here, the effect of δ_p on the armouring process is analysed as well.

For the prediction of bed-level changes, Eq.4.13 is used. Sediment transport related values for $s_b(0)$ and X are based on the Meyer-Peter and Müller (1948) formula corrected for horizontal-hiding effects.

$$
s_{bi} = p_{pi}\, k\, \sqrt{g\Delta D_i^3} \left(\tau_{*i} - p \left(\frac{D_i}{D_m} \right)^r \tau_{*cr} \right)^{3/2} \tag{4.14}
$$

From reported erosion rates, the total transport $s_b(0)$ can be used to calibrate Eq.4.14 (Figure 4.2). Note that the transport rate per size fraction is not calibrated, which increases the level of inaccuracy in the results.
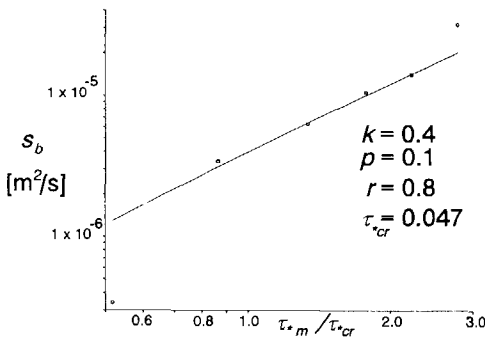
Fig.4.2 Calibration of transport rate.   Fig.4.3 Bed levels (analytical).
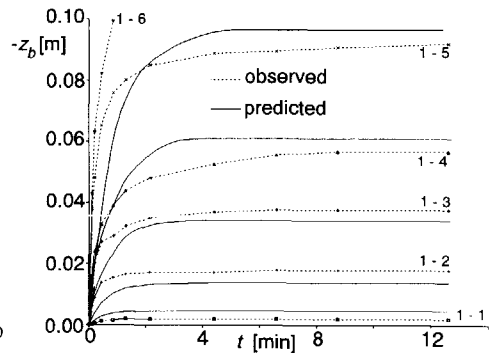
The layer thickness is taken as $\delta_p/D_1 = 0.23$ for all levels of shear stress. Initial erosion rates are underpredicted (Figure 4.3). In experiment 1-6, the equilibrium armour layer is not obtained in the test facility. Some remarks on λ, or, since the sediment transport rate has been calibrated, values of δ_p/D_1 will be added in Section 4.2.4. To analyse the effect of linearization, Eq.4.11 is solved numerically.

78
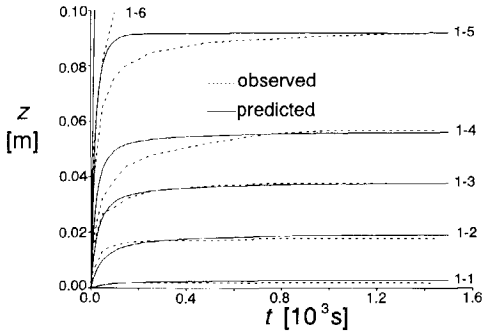
Fig.4.4. Bed levels (numerical). **Fig.4.5** Coarsening (numerical).
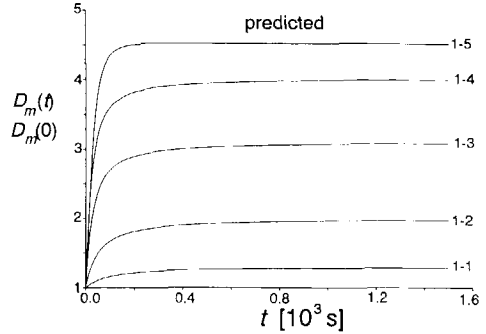
Predicted changes in bed level and mean grain size are presented in Figure 4.4 and 4.5. Changes in mean grain size are larger with increasing shear stress, as will be show in Section 4.2.4. Calibrated values of the layer thickness are shown in Figure 4.6.
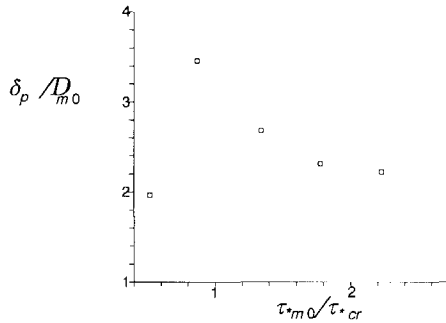
Fig.4.6 Calibrated layer thickness.

It is noted that the trend of decreasing layer thickness with increasing shear-stress can be due to calibration inaccuracies. In the experiments with higher shear stress (1-4 and 1-5), the armouring process is overpredicted.

Due to the fluctuating character of particle motions, the process of armouring is a discontinuous sequence of coarsening steps. As a result, linearization of the entire coarsening process is erroneous. This can be illustrated by analysing the decline in sediment transport rate. The predicted decline in the linearized model is

$$\frac{s_b(t)}{s_b(0)} = e^{\lambda t} \tag{4.15}$$

79

To illustrate the applicability of Eq.4.15, armouring experiments by Little and Mayer (1972) are memorized. Reference can be made to Bettes (1982) and Paris (1991), who also observed an exponential decrease of transport rates in armouring experiments.

In the following, sediment transport rates observed by Tait *et al.* (1992) in armouring experiments with different mixtures are shown. The mixtures in Experiments 2 and 3 are similar, but shear stresses differ. At low particle-shear stresses (Exp.2, Figure 4.7-a), the stochastic fluctuations by individual particle motions dominate. Then, sequences of armouring processes can be recognized with different λ values (increasing adjustment time).
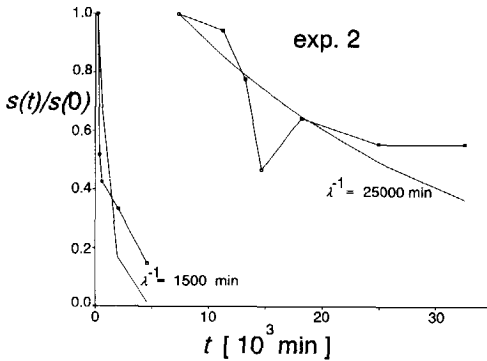

Fig.4.7-a Experiment No.2.   **Fig.4.7-b** Experiment No.3.
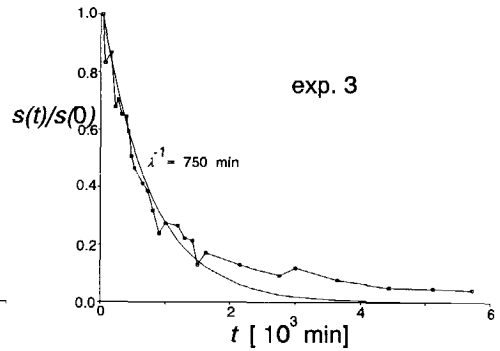
At higher particle-shear stresses (Figure 4.7-b and 4.7-c), the relative contributions of short term fluctuations decrease and a more or less continuous armouring process develops corresponding to the linearized model. The sediment used in experiment 4 consists of coarser grain sizes.
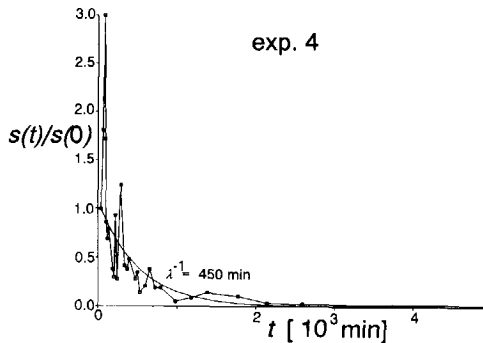
Fig.4.7-c Experiment No.4.

After longer periods, limits of the linearization are encountered.

Apart from degradation rate and transport decline, coarsening of the surface can be considered. With the linearized model, mean grain sizes in the reference layer are predicted as

$$\frac{D_m(t)}{D_m} = 1 - \frac{s(0)}{X}\left(\frac{D_{mT} - D_{ms}}{D_m}\right)(1 - e^{\lambda\, t}) \qquad (4.16)$$

with D_{mT}, D_{mp} and D_{ms} as mean grain diameters of sediment transport, surface layer and subsurface layer.

Garde *et al.* (1977) defined a coarsening parameter

$$F(t) = \frac{D_m(t) - D_m(0)}{D_m(\infty) - D_m(0)} \qquad (4.17)$$

Based on recorded coarsening processes in flumes, a power law function for coarsening rates was fitted. Substitution of the analytical solution (Eq.4.16) yields

$$1 - F(t) = e^{\lambda\, t} = e^{\left(\ln 0.25 \, \frac{t}{t_{0.75}}\right)} \qquad (4.18)$$

The fitted power laws and the analytical solution of the linear model are presented in Figure 4.8. As can be concluded, general trends correspond.
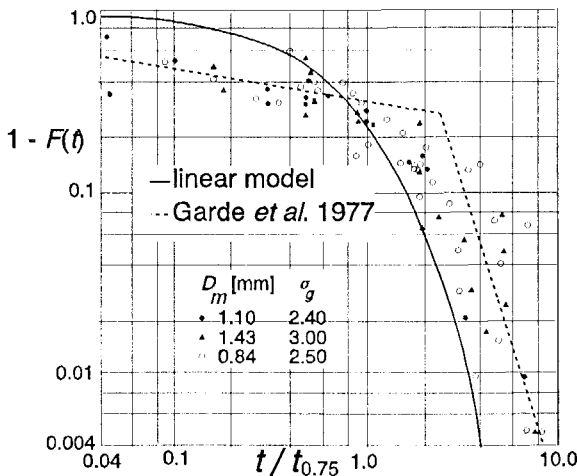
Fig.4.8 Coarsening of bed surface (Garde *et al.* 1977).

81

After a sufficiently long period. The mean grain-size of the armour layer according to the linearized model is

$$\frac{D_m(\infty)}{D_m} = 1 + \frac{s(0)}{X} \left(1 - \frac{D_{mT}}{D_m} \right) \tag{4.19}$$

In Figure 4.9, predicted mean armour-diameters are compared with the D_{50} of the armour layer in the measurements of Chin et al. (1994). Maybe due to poor calibration of the sediment-transport predictor, there is an overestimation of the coarsening.
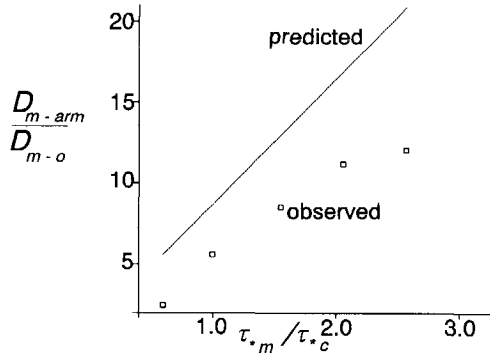
Fig.4.9 Composition of armour-layer.

4.2.4 Reference-layer thickness for armouring conditions.

In layer models as described in Subsection 3.2, the thickness of the predicted armour layer follows from the predefined reference layer thicknesses. Conform concepts introduced by Ashida and Michiue (1971), Borah et al. (1982a and 1982b) state that armour layers have a thickness of D_a, the smallest immobile grain size in the mixture. According to Figure 4.6, a reference layer is of the order of 2 or 3 times D_m. Lamberti and Paris (1992) measured changes in size fraction and derived corresponding values of layer thickness equal to D_{50} of the armour layer. During breakup of the armour layer they calibrated with $\lambda_p = 2$ D_{50}.

It can be concluded from Eq.4.13 that the thickness δ_p of the reference layer determines the rate and equilibrium state of the armouring process. A larger thickness results in slower coarsening and larger erosion depths. This relates (but not equals) the reference layer-thickness to the scouring depth defined as $d_e = -z_b(t \rightarrow \infty)$.

$$\frac{\delta_p}{D_1} = \frac{d_e \, \kappa \, X}{s_b(0) \, D_1} \tag{4.20}$$

Different options for the definition of δ_p exist. Some are calibrated for the Chin *et al.* (1994) experiments, reviewed in Table 4.1 and constructed in Figure 4.10.

option	definition	trend
particle shear-stress (Niekerk *et al.* 1992)	$\dfrac{\delta_p}{D_1} = 5 \cdot 10^{-4} \dfrac{D_m}{D_1} \dfrac{\tau_{*m}}{\tau_{*c}}$	constant
active layer (Borah *et al.*, 1982)	$\delta_p = D_a \left(1 - \sum\limits_{i=1}^{a-1} p_i \right)^{-1}$ (a = smallest stable fraction)	constant
sediment-transport rate	$\dfrac{\delta_p}{D_1} = \sum\limits_{i=1}^{N} s_{bi} \, (u_* D_1)^{-1}$	decreasing
mean grain-size (e.g. Lamberti and Paris, 1992)	$\dfrac{\delta_p}{D_1} = 25 \cdot 10^{-3} \dfrac{D_m}{D_1}$	increasing
grain-size (e.g. Di Silvio, 1991)	$\dfrac{\delta_p}{D_1} = 0.23$	constant

Table 4.1. Layer definitions for armouring processes.

In Figure 4.10, these types of predictors are represented together with values calibrated from the experiments by Chin *et al.* (1994).
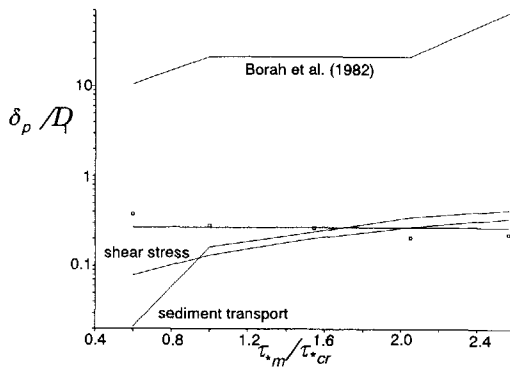
Fig.4.10 Layer predictors.

It is noted that using sediment-transport rates for layer prediction results in zero values for equilibrium conditions, and can therefore be considered not appropriate for armouring processes. Application of Eq.4.20 to measured scouring depths enables deriving values for δ_p/D_1 for different levels of shear stress.

With respect to the predictor of Borah *et al.* (1982), the following can be noted. The scouring depth is assumed to be equal to the volume of mobile material in a predefined active layer. It is noted that in contrast with the linearized model (Eq.4.20), the predicted scouring depth is smaller than this active layer.

$$d_e = D_a \sum_{i=1}^{a-1} p_i \left(1 - \sum_{i=1}^{a-1} p_i\right)^{-1} \tag{4.21}$$

Because this contradicts with observations where all original fractions are found to be present in armour layers, Eq.4.21 yields a conservative prediction (Borah, 1989). However, comparison with observed values (Chin *et al.*, 1994) yields relatively good results (Figure 4.11).
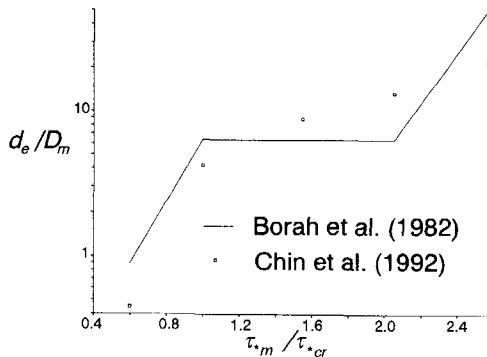
Fig.4.11 Prediction of scour-depth.

84

Critical shear-stresses are computed with empirical formulae (Van Rijn, 1989). The discretization of the size-frequency distribution significantly affects the predictor. Apparently, the predictor suggested by Borah *et al.* (1982a and 1982b), should be used for equilibrium conditions only.

4.3. Longitudinal sorting; abrasion or selective transport.

4.3.1 Introduction.

Another aspect of graded material in river beds is a downstream fining of sediment. The study of this phenomenon started in the 19th century (e.g. Sternberg, 1875; Schoklitsch, 1914), as reviewed by Mikoš (1993). Some recent examples are due to Deigaard (1982) and Seal and Paola (1995). Apart from size-selective entrainment, transport and deposition, fluvial sorting in longitudinal direction can result from abrasion of moving grains (Sinha and Parker, 1996).

Initially, fluvial abrasion was thought to be the main cause of the fining. Sternberg (1875) introduced for the relative weight loss $\Delta W/W$ of a grain travelling a distance Δs

$$\frac{\Delta W}{W} = -\alpha \ \Delta s \qquad (4.22)$$

where α represents the empirical weight-reduction coefficient α ($[\alpha]=[m^{-1}]$). This can be rewritten as

$$\frac{\Delta D}{\Delta s} = -\frac{\alpha}{3} D \qquad (4.23)$$

Fig.4.12 Weight-reduction law (Sternberg, 1875).

Traditionally, the combined effects of selective transport and fluvial abrasion have been lumped into α. As a result, especially in rivers at steeper slopes with

coarse sediment, high and varying values of α were found.

In the last decade, more effort is put into describing size-selective entrainment and transport of particles, which enables integrated modelling of size-selectivity and abrasion ef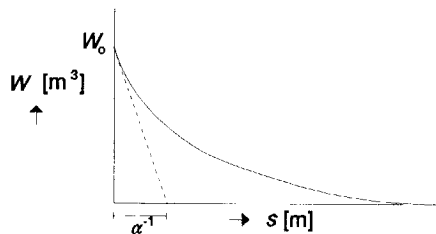fects. Parker (1991a; 1991b) demonstrated numerically the contribution of abrasion to longitudinal sorting effects for hard and soft material (quartzite and limestone). It was concluded that the relevance of fluvial abrasion largely depends on sedimentological properties and the length-scale of the reaches of interest.

As a result, downstream fining can in general be subscribed to longitudinal sorting. For example, Hoey and Ferguson (1994) simulated downstream fining in the Allt Dubhaig, Scotland, by considering size-selective transport.

In the following sections, an attempt is made to generalize this result analytically by including different hydraulic conditions. Therefore, a simple abrasion model is derived in Subsection 4.3.2, and implemented into a model for quasi-steady and -uniform flow (Subsection 4.3.3) to determine a sorting relaxation-length.

4.3.2. Abrasion model.

In general, a mixture is described with a grain-size frequency distribution , represented with discrete fraction values. Hence, the mass, or volume of a fraction i can be described by grain size D_i and fraction p_{pi}. In morphological models, changes in composition (or mass distribution over the grain sizes) are changes in fraction p_{pi}, with a constant "label" D_i.

Abrasion losses in fractions of large grain sizes are assumed to transfer to fractions of smaller grains. Strictly, abrasion is a reduction of a grain mass due to mechanical action. Now, the following hypothesis is used. Abrasion can be interpretated as a grain-mass changing into a reduced grain by production of an abrasion residue. Hence, a fraction i in a mixture has two sources; one based on *production* of residue material (with original size D_j) and a one based on *reduction* of grains (with original size D_h). This can be written with the Sternberg law as

$$ W_i = W_j + W_h \;\; ; \;\; D_j = \frac{3}{\alpha \Delta s} D_i \;\; ; \;\; D_h = \left(1 - \frac{\alpha \Delta s}{3}\right)^{-1} D_i \;\; \textbf{(4.24)} $$

If for $\Delta s \rightarrow 0$, $D_j > D_{max}$, then the contribution of the abrasion residue is zero.

86

Such a model is valid only if grain sizes of production and reduction are within or near the original range of diameters. Abrasion experiments (Mikoš, 1993), indicate, however, the production of an "abrasion" fraction with relatively small grain size. In that case, a separate size fraction i_a for abrasion residue can be considered. The original mixture should be corrected with a weight reduction factor (Mikoš, 1993).

Hence, all fractions with $D_i \leq D_{ia}$ (or according to the definition used $i \leq i_a$) are considered as separate and constant abrasion residue material. To determine the original fractions of the reduced grains, the grain-size distribution F must be introduced.

$$p_{pj} = F\left(D_j/D_m\right) \quad ; \quad p_{ph} = F\left(D_h/D_m\right) \tag{4.25}$$

Then, changes in size fraction with $i > i_a$ are

$$p_{pi}(\alpha s + \alpha \Delta s) = p_{pi}(\alpha s) - \frac{\alpha \Delta s}{3} \frac{D_i}{D_m} F_{Di} \tag{4.26}$$

For $\alpha \Delta s \rightarrow 0$, this yields

$$\frac{dp_{pi}}{ds} = -\frac{\alpha}{3} \frac{D_i}{D_m} \frac{d\ F_i}{d\ D_i/D_m} \tag{4.27}$$

This simple "diffusion" model produces a composition with a reducing range of grain sizes (*not* a constant grain size). A hypothetical example of changing composition is given in Figure 4.13 ($\alpha \Delta x = 0.2$). Due to abrasion, also maximum and minimum grain sizes reduce.
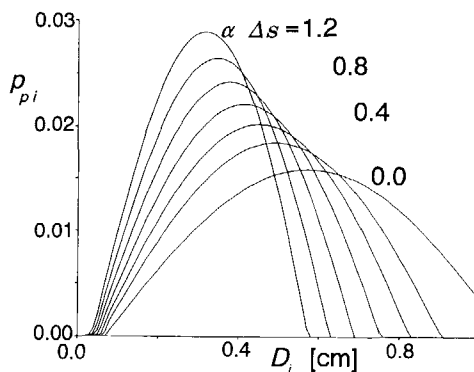
Fig.4.13 Abrasion model.

With respect to the abrasion residue, changes in fraction ($i \leq i_a$) can be written as

$$p_{pi}(\alpha s + \alpha \Delta s) = p_{pi}(\alpha s) + \sum_{D_j = D_{i_a+1}}^{D_N} \alpha_j \Delta s \; F(D_j) \qquad (4.28)$$

For $\alpha \Delta s \to 0$, this yields

$$\frac{\mathrm{d}p_{pi}}{\mathrm{d}s} = \sum_{D_j = D_{i_a+1}}^{D_N} \alpha_j \; F(D_j) \qquad (4.29)$$

The abrasion model as described by Eqs 4.26 and 4.28 is applied to abrasion experiments by Mikoš (1993) (Fig.4.14-b to f). Broken lines represent the changes predicted by the model. The grain-size frequency distributions of the original mixtures are represented in Figure 4.14-a. Grain sizes range from 2 to 128 mm, 10 fractions are distinguished. The abrasion residue is represented by fraction $i = 1$ ($D_1 < 1.0$ mm).

Assuming that fluvial abrasion can be simulated with a tumbling mill, the abrasion of Alpine Rhine sediment (limestone predominantly) was studied. Mean weight-reduction rates (or abrasion residue production rates) observed in the laboratory are of the order of 10^{-2} km^{-1}.
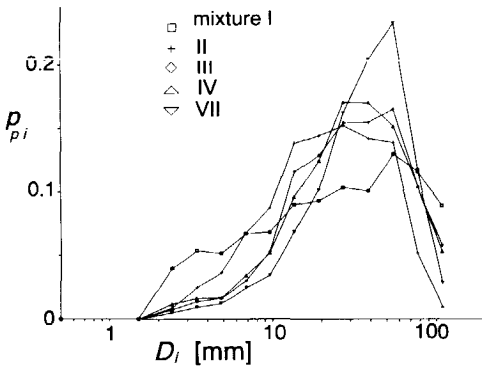
Fig.4.14-a Review of mixtures.   Fig.4.14-b Mixture I.

88
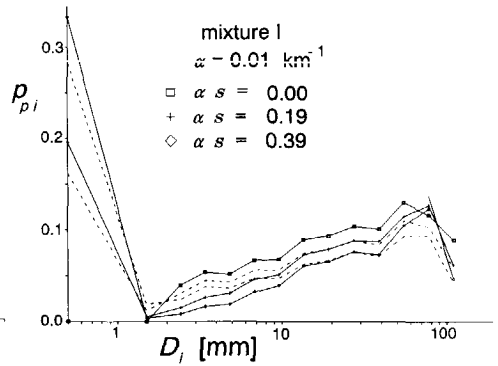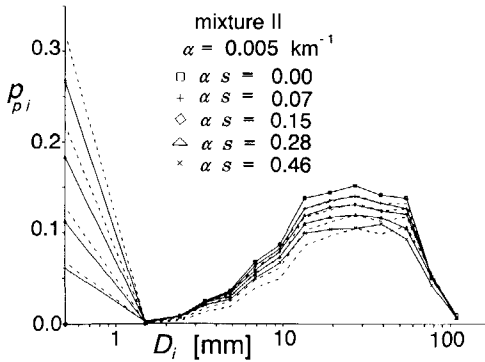
Fig.4.14-c Mixture II.
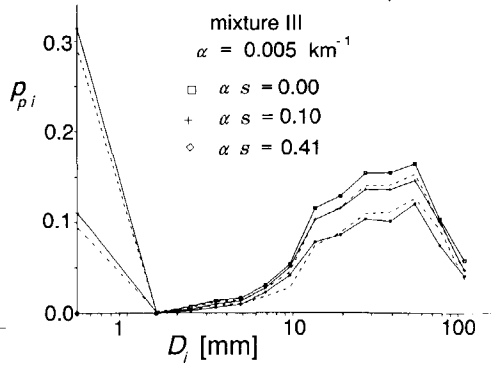
Fig.4.14-d Mixture III.
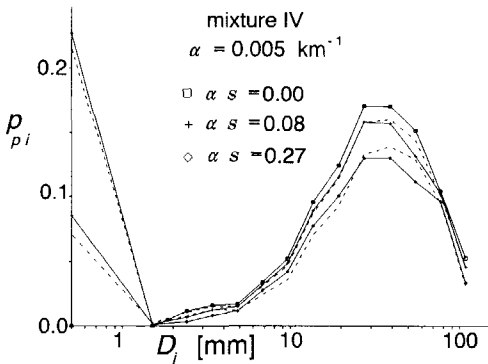
Fig.4.14-e Mixture IV.
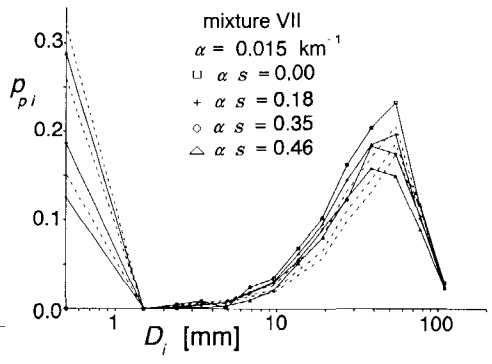
Fig.4.14-f Mixture VII.

Based on the small αs values it can be concluded that the duration of these experiments is relatively short.

4.3.3. Sorting relaxation-length.

Using Sternberg's law, the abrasion rate of a fraction p_{pi} in layer δ_p can be written as

$$A_i = \frac{\Delta p_{pi} \delta_p}{\Delta t} = \left(p_{pi} \; \delta_p \right) \; \alpha_i \; \frac{\Delta s}{\Delta t} \qquad (4.30)$$

89

If the average grain-velocity in a bed load layer is substituted, the abrasion volume of a fraction can be written as

$$\frac{\Delta p_{pi}\delta_p}{\Delta t} = \left(p_{pi}\ \delta_p\right)\alpha_i\ \frac{s_{bi}}{p_{pi}\delta_b} = \alpha_i\ s_{bi}\ \frac{\delta_p}{\delta_b} \qquad (4.31)$$

In the following, it is assumed that abrasion occurs in the bed load layer only ($\delta_p = \delta_b$). Hence, time changes in bed-load composition due to abrasion are considered. Changes in volume of fraction i due to abrasion are defined as

$$\frac{\Delta p_{pi}\delta_b}{\Delta t} = -\frac{p_{pi}^n\delta_b}{\Delta t} + \alpha_f s_{bj} + \left(\frac{p_{ph}^n\delta_b}{\Delta t} - \alpha_h s_{bh}\right) =$$

$$= \left(p_{ph}^n - p_{pi}^n\right)\frac{\delta_b}{\Delta t} + \alpha_f s_{bj} - \alpha_h s_{bh} \qquad (4.32)$$

or, using Eq.4.27

$$\frac{\Delta p_{pi}\delta_b}{\Delta t} = \alpha_h \delta_b \frac{D_i}{D_m}\frac{\Delta s}{\Delta t}\frac{dF}{dD_i/D_m} + \alpha_f s_{bj} - \alpha_h s_{bh} \qquad (4.33)$$

Now, the mass balance for a fraction i in the bed load layer is

$$\frac{\partial p_{pi}\delta_b}{\partial t} + \frac{\partial s_{bi}}{\partial x} + \beta_{Ti}\frac{\partial z_b}{\partial t} - \alpha_h \frac{D_i}{D_m}\frac{dF_i}{dD_i/D_m}\sum_{i=1}^{N}s_{bi} + \left(\alpha_h p_{Th} - \alpha_f p_{Tj}\right)\sum_{i=1}^{N}s_{bi} = 0$$

$$(4.34)$$

Stating that α is constant for different grains, Eq.4.34 can be integrated over all size fractions yielding

$$\sum_{i=1}^{N}\frac{\partial s_{bi}}{\partial x} + \frac{\partial z_b}{\partial t} - \alpha\sum_{i-1}^{N}\frac{D_i}{D_m}\frac{dF_i}{dD_i/D_m}\sum_{i=1}^{N}s_{bi} = 0 \qquad (4.35)$$

Because large-scale changes are considered (basin scale), the momentum equation can be reduced to that of uniform flow. If flow conditions are also assumed to be steady, this yields

$$\frac{\partial z_b}{\partial x} = -\frac{u^2}{C^2 a} \qquad (4.36)$$

90

Differentiation to x and elimination of velocity gradients with Eq.4.36 yields

$$-\frac{C^2 a}{3u}\sum_{i=1}^{N} f_{ui}\frac{\partial^3 z_b}{\partial x^3} + \sum_{i=1}^{N} X_i\frac{\partial^2 p_{pi}}{\partial x^2} + \frac{\partial^2 z_b}{\partial t \partial x} +$$

$$- \alpha \sum_{i=1}^{N} \frac{D_i}{D_m}\frac{dp_{pi}}{dD_i/D_m}\left(-\frac{C^2 a}{3u}\sum_{i=1}^{N} f_{ui}\frac{\partial^2 z_b}{\partial x^2} + \sum_{i=1}^{N} X_i\frac{\partial p_{pi}}{\partial x}\right) + \qquad \textbf{(4.37)}$$

$$- \alpha \sum_{i=1}^{N} s_{bi}\sum_{i=1}^{N} \frac{D_i}{D_m}\frac{d\,\dfrac{\partial p_{pi}}{\partial x}}{dD_i/D_m} = 0$$

Now, an exponential solution for an equilibrium state is defined

$$\begin{bmatrix} z_b \\ p_{pi} \end{bmatrix} = \begin{bmatrix} \Delta z_b \\ p_{pi\,0} - p_{pi\,\infty} \end{bmatrix} e^{\lambda x} + \begin{bmatrix} 0 \\ p_{pi\,\infty} \end{bmatrix} \qquad \textbf{(4.38)}$$

Without abrasion, non-trivial exponential solutions exist if

$$\lambda = 0 \quad \vee \quad \lambda = \frac{3u}{C^2 a}\frac{\displaystyle\sum_{i=1}^{N} X_i\left(p_{pi\,0} - p_{pi\,\infty}\right)}{\Delta z_{b\,0}\displaystyle\sum_{i=1}^{N} f_{ui}} \qquad \textbf{(4.39)}$$

If abrasion is accounted for, the sediment-mass balance is as derived in the previous section.

$$\sum_{i=1}^{N} f_{ui}\frac{\partial u}{\partial x} + \sum_{i=1}^{N} X_i\frac{\partial p_{pi}}{\partial x} + \frac{\partial z_b}{\partial t} - \alpha \sum_{i=1}^{N} \frac{D_i}{D_m}\frac{dF_i}{dD_i/D_m}\sum_{i=1}^{N} s_{bi} = 0 \quad \textbf{(4.40)}$$

Again, the solution Eq.4.38 can be substituted. Now, λ^{-1}, the relaxation length of the exponential bed level and the weight reduction length α^{-1} are compared. However, the contribution of abrasion to λ^{-1} cannot even be distinguished in Figure 4.15, which is constructed with a Meyer-Peter and Müller (1948) transport formula corrected for hiding effects.
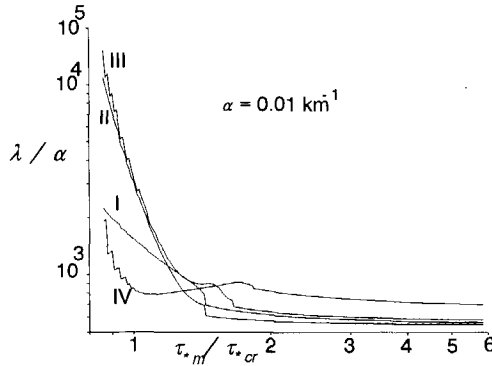
Fig.4.15 Sorting relaxation-length.

The Roman numbers refer to the sediment mixtures described in Appendix B. It can be concluded that the length scale of abrasion is significantly larger than the relaxation length of the bed level. Hence, the contribution of size-selectivity in entrainment, transport and deposition is dominant. This effect decreases with shear stress. Longitudinal sorting can be expected to be most significant (and sensitive to hydraulic conditions) at lower values of shear stress.

4.4. Numerical tests.

4.4.1. Degradation downstream of a dam.

One of the classical experiments on armouring processes is presented by Ashida and Michiue (1971), concerning degradation downstream of a dam. The series of flume experiments included one with a steep slope, where conditions of flow initially are critical ($Fr \approx 1$), and change into subcritical during the degradation. For the numerical simulation, the following parameters are used. The mixture is described with grain sizes $D_1 = 0.0004$ m, $D_2 = 0.0018$ m and $D_3 = 0.0065$ m. The numerical grid is $\Delta x = 1.00$ m and $\Delta t = 0.25$ s. The average bed slope is 0.01, discharge and roughness coefficient are $q = 0.03925$ m^2/s and $C = 30.9$ m$^{1/2}$/s. The single-layer concept in the stabilized model is used with $\delta_p = D_3/2$.
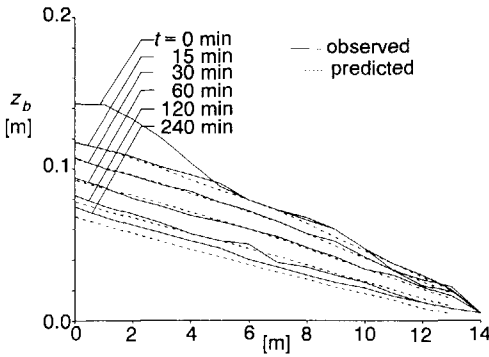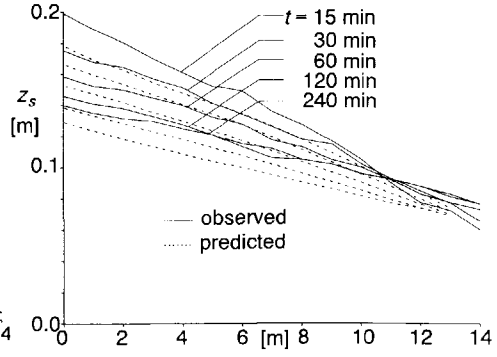
Fig.4.16-a Bed levels.   **Fig.4.16-b** Free-surface levels.
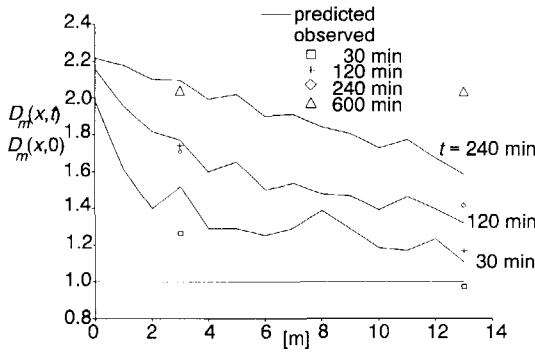
Fig.4.16-c Process of coarsening.

In the Figures 4.16-a and -b, the predicted and observed bed levels z_b and free surface levels z_s during the degradation are compared. In Figure 4.16-c, the predicted and measured coarsening is shown. The degradation process is rather gradual. This can be explained by the absence of significant non-uniformity in flow; the solution approaches the quasi-uniform flow model (Eq.3.33).

4.4.2. Propagation and deformation of a bed-level disturbance.

Detailed observations of changes in bed level and composition in case of sediment mixtures are rare. An early analysis of propagating disturbances in bed level and composition has been carried out by Suzuki (1976). More recently, Suzuki and Michiue (1991) observed the deformation of a triangle-shaped profile (height $\Delta z_b = 0.02$ m, length $L = 2.00$ m). It is noted that the scale of the disturbance is very small and of the order of a dune ($\Delta H_b/a \approx 0.2$, $\Delta H_b/L = 0.01$).

93

The trends observed were a coarsening at the upstream-facing slope of the disturbance, and a fining at the downstream-facing slope. As a result, upstream parts of the hump tend to stabilize due to coarsening (or even armouring), whereas the propagating part of the hump becomes finer. The latter results in a reduction of the disturbance height and an increase in propagation rate. This mechanism corresponds with observations on bedforms of finer material that propagate over coarser beds (e.g. Klaassen, 1990).

For the computation, the following data are used; $q = 0.050$ m^2/s; $i = 2 \cdot 10^{-3}$; $a = 0.108$ m; $C = 31.5$ m$^{1/2}$/s and $\Delta = 1.65$. The mixture is described with the grain sizes $D_1 = 0.73$ mm, $D_2 = 1.88$ mm and $D_3 = 3.10$ mm ($D_m = 1.90$ mm and $\sigma^2 \approx D_3/D_1 = 4.24$). The layer thickness is assumed to be constant in time and space by stating $\delta_1/D_2 = 1.0$. Sediment-transport rates are predicted by

$$ s_i = 5 \, p_{pi} \sqrt{-g_z \Delta D_i^3} \left(\tau_{*i} - 0.047 \left(\frac{D_m}{D_i} \right)^{0.7} \right)^{3/2} \tag{4.41} $$

Observed data are represented in broken lines, continuous lines refer to model predictions.
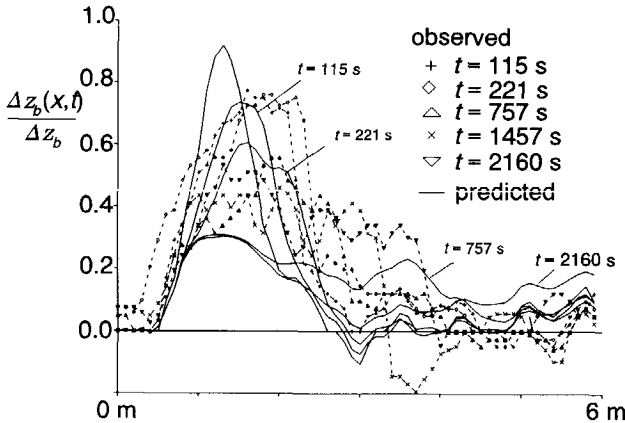
Fig.4.17-a Deformation of hump (stabilized model).
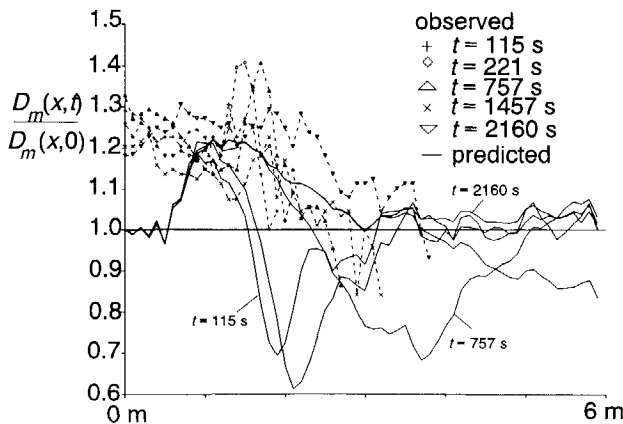
Fig.4.17-b Changes in composition (stabilized model).

First, the formulation as described in Subsection 3.4.3 is applied (Figures 4.17-a and 4.17-b). Comparison indicates discrepancies due to differences in initial and boundary conditions. The propagation of the hump is significantly overestimated. However, considering the small scale (where individual particle movements are dominant), a general correspondence between prediction and observations exist.

The results of the conventional model are shown in figures 4.18-a and 4.18-b.
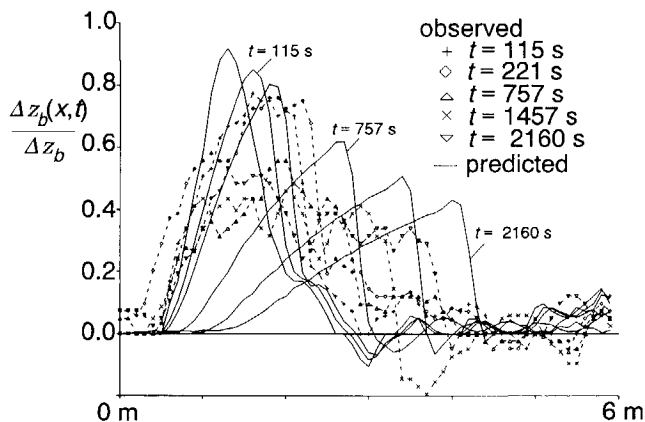
Fig.4.18-a Deformation of hump (conventional model).
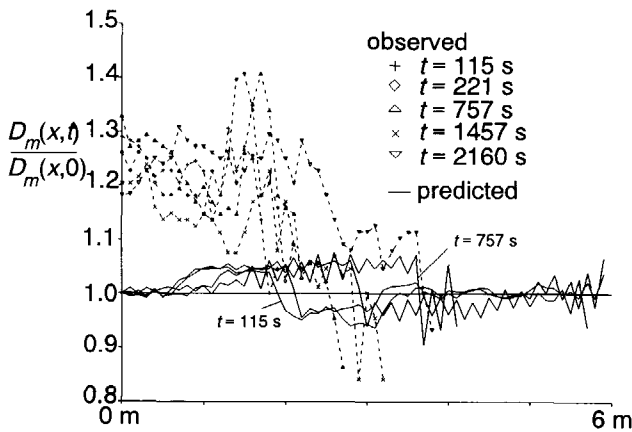
Fig.4.18-b Changes in composition (conventional model).

Now, propagation rates correspond, but coarsening is underestimated. Unstable wiggles in composition develop.

4.4.3. Scouring in a confined section.

Wang *et al.* (1993) (or Wang *et al.* 1994) analysed the effect of sediment composition on scour development in confining flow conditions. Two sediment mixtures, identified as *A* (uniform) and *B* (non-uniform) are compared. The material consists of crushed coal, with a specific weight of 1480 kg/m^3 ($\Delta =$ 0.48). The grain sizes are represented as indicated in Table 4.2.

grain size [m]	mixture A	mixture B
D_1	0.0011	0.0007
D_2	0.0030	0.0030
D_3	0.0048	0.0080

Table 4.2 Composition of mixtures.

Slopes are kept constant on a value of 0.00245. Widths reduce from 0.50 m to 0.20 m. Here, equilibrium conditions with both mixtures for low and high discharge are compared. The values of discharge are $Q = 0.01$ m^3/s (with C = 36.1 m$^{1/2}$/s) and $Q = 0.04$ m^3/s (with $C = 26.6$ m$^{1/2}$/s). It is noted that due to the reduction in width, two-dimensional effects are introduced that are not accounted for in the model.

96

In general, erosion was reduced due to coarsening of the bed surface. However, for both discharges, the effect of gradation on erosion depth was minor, both in the physical and numerical model. In the numerical model, the coarsening in the eroded section was larger in case of the lower discharge (with particle shear stress closer to the threshold of motion).
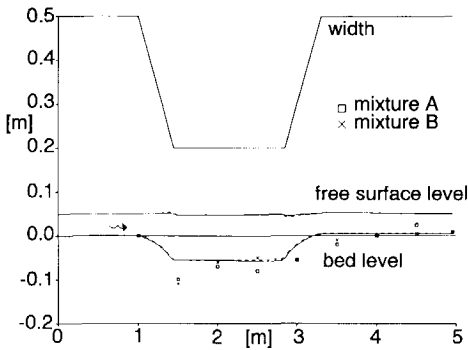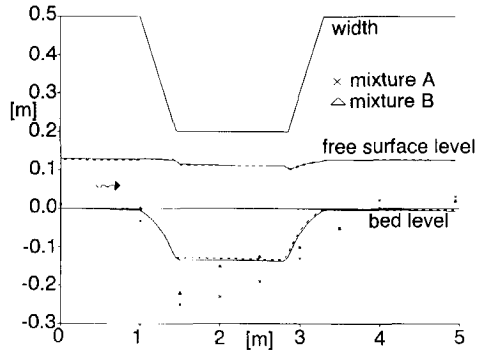
Fig.4.19 $Q = 0.01$ m^3/s.   **Fig.4.20** $Q = 0.04$ m^3/s.

Some additional remarks on these experiments are added in Appendix A.3.

4.4.4. Changes in sediment supply.

To analyse changes in bed level and composition, Ribberink (1983) carried out flume experiments with sediment composed of two fractions; $D_1 = 0.78$ mm and $D_2 = 1.29$ mm. A few of the experiments concern effects of overload and underload of sediment at the upstream boundary. Here, two single-layer models are applied to predict the recorded bed levels in the transition experiments. The conventional model is described in Section 3.2, the stabilized model in Subsection 3.4.3. In contrast with the experiment mentioned in Subsection 3.5.5, the composition of the sediment supply remains constant.

type of experiment	initial state			equilibrium state		
	p_{p1} [-]	p_{T1} [-]	s_b [10^{-6} m^3/s]	p_{p1} [-]	p_{T1} [-]	s_b [10^{-6} m^3/s]
overload	0.17	0.20	2.95	0.20	0.20	4.89
underload	0.20	0.20	4.89	0.18	0.20	1.11

Table 4.3 Transition experiments (Ribberink, 1983).

97

It is noted that with respect to the bed composition p_{p1} in Table 4.3 refers to a size fraction that is averaged over the reference and the bed-load layer. Thicknesses of the reference layer were stated to be constant at 0.0365 m in the overload experiment, and 0.028 m in the underload experiment. First, observed and predicted bed levels in the overload experiment are compared. The resulting aggradation is shown in Figures 4.21 and 4.22.
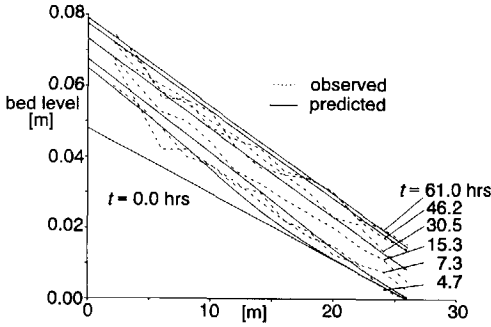
Fig.4.21 Stabilized model. **Fig.4.22** Conventional model.
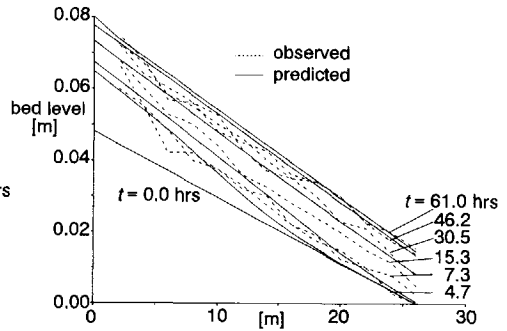
The degradation in the underload experiment is represented in Figures 4.23 and 4.24.
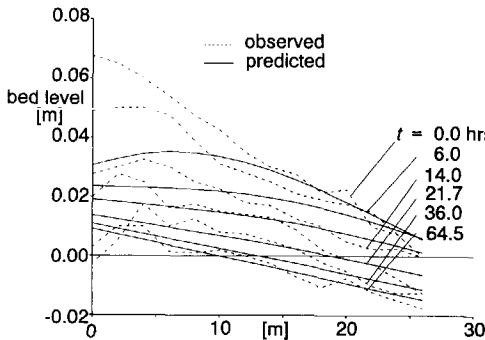
Fig.4.23 Stabilized model. **Fig.4.24** Conventional model.
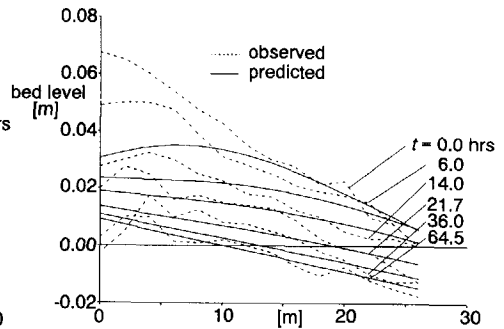
Because bed compositions remain almost constant, negligible differences in both models can be observed. In both experiments changes are forced by gradients in sediment transport. Therefore, significant velocity gradients are absent, which explains the gradual change in bed level that approximates the diffusive solution of the parabolic model.

98

However, differences in both modelling concepts can be observed in case of a changing sediment composition. The following experiment of Ribberink (1987), is also mentioned in Subsection 3.5.5. Here, the *total* sediment feed is constant, but the fine fraction in the supplied sediment decreases linearly from $t = 0$ hrs to $t = 30$ hrs. As a result, the bed becomes coarser and steeper by aggradation.
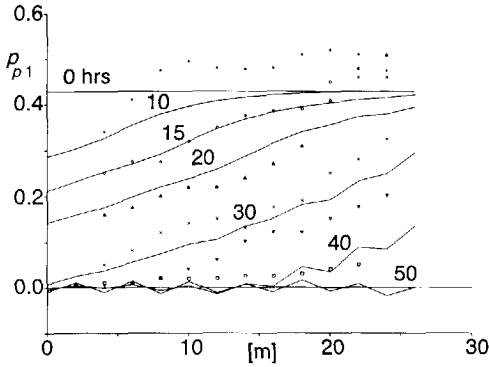
Fig.4.25 Changes in composition (conventional model).
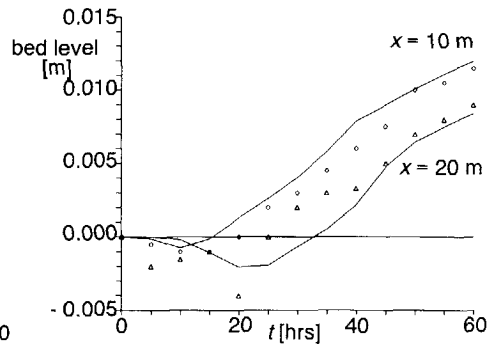
Fig.4.26 Changes in bed-level (conventional model).

The predictions of bed level and composition changes of the conventional model correspond qualitatively with the measurements. For $p_{p1} \rightarrow 0$, wiggles develop, which eventually induce instabilities.
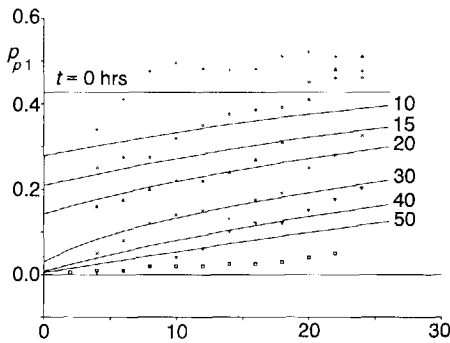
Fig.4.27 Changes in composition (stabilized model).
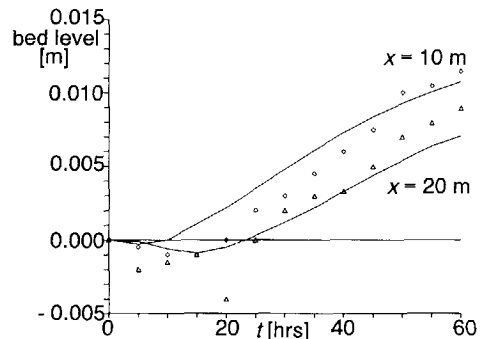
Fig.4.28 Changes in bed-level (stabilized model).

This qualitative correspondence of predictions with measurements can also be observed for the stabilized model. The propagation of composition changes is underestimated. The mutual parameters in both models are equal. The layer

99

thicknesses used in the conventional and stabilized model are 0.02 m and 0.01 m for the pavement and subpavement layers respectively, based on Ribberink (1987). For the stabilized model, a smaller thickness improves the prediction of composition changes.

Chapter five

Numerical concepts for mobile-bed models.

5.1. Introduction.

In mountain rivers, flooding hazards are often determined by single, extreme events. Hence, to indicate future flooding-probabilities for different areas, many extreme-event scenarios must be analysed to construct a representative distribution of flooding probability (Davies, 1989; FRIMAR, 1995).

At transcritical flows and higher levels of bed mobility, changes in bed level, depth and velocity are of comparable order (Chapter two). Hence, the system of PDE's should be solved simultaneously for all variables. Due to relatively fast rates of changes in velocity and depth, this seriously restricts the time step and limits the prediction of long term morphological changes.

To reduce computational efforts, often simplified modelling concepts are applied. As a result, there often is a major gap between prototype rivers and one-dimensional representations in mathematical models (Crosato, 1995). At present (1997), the applicability of simplified modelling concepts have been tested for low-land rivers mainly (e.g. De Vries, 1993). Therefore, assumptions with respect to steadiness or uniformity of flow should be tested for conditions present in mountain rivers (e.g. non-uniform geometry, transcritical flows).

The simplifications that are studied theoretically and numerically in this chapter concern

> neglecting the non-linear interaction between changes in flow and morphology

> use of quasi-steady flow for computation of morphological changes

> use of quasi-steady and quasi-uniform flow for computation of morphological changes

The nonlinear interaction between hydraulics and morphology is analysed in Subsection 5.2.2. The quasi-steady flow model is analysed in Subsection 5.2.3, and the quasi-steady and quasi-uniform flow model is analysed in Subsection 5.2.4.

In Section 5.3., the applicability of the different concepts is tested numerically. The test cases concern the application of a complete dynamic-flow model (I), a decoupled dynamic-flow model (II), a quasi-steady flow model (III), and a quasi-steady and -uniform flow model (IV).

5.2. Theoretical analysis.

5.2.1. Introduction.

If, in hyperbolic models, extreme scale differences occur, some "wave-type" solutions can be approximated with steady or uniform flow-type solutions. This is used when introducing the *quasi-steady flow* assumption (De Vries, 1966; Vreugdenhil and De Vries, 1973), which implies an "instantaneous" adaption of flow variables with respect to "slow" changes in bed level. Now, fast "hydraulic" waves are eliminated, and models can be adjusted to large morphological time steps.

This concept very well suits subcritical flows ($Fr < 0.8$) where the interaction between hydraulics and bed mobility is weak. However, in flows with higher values of Fr, the increasing non-linear interaction becomes more significant, which limits the applicability of decoupled solution techniques.

These concepts have been applied, analysed (Barneveld, 1988) and verified (e.g., Ribberink and Van der Sande, 1985) for different cases with subcritical flow. In this study, some remarks are made with respect to the applicability in sub-, trans- and supercritical flows.

5.2.2. Nonlinear interaction of flow and morphology.

The difference between fixed-bed and mobile-bed models includes the introduction of an additional wave-type solution and the interaction between hydraulics and morphology. If the interaction between flow and morphology is low, the resemblance between fixed-bed and mobile-bed models enables decoupling changes in hydraulics and morphological variables.

In a decoupled, or non-simultaneous solution technique two steps are made; changes in depth and velocity are determined with a fixed bed; changes in bed level (and composition) are determined with the new depth and velocity.

This decoupling implies neglecting:

a). the non-linear feedback of changing morphology on flow

b). the effect of flow-unsteadiness on changes in morphology (see Subsection 5.2.3, and Appendix A.3)

ad a). To a certain extend, the non-linear feedback of changing morphology on flow can be analysed by comparing fixed-bed and mobile-bed models. The effect of bed-level changes on flow is expressed by bed-level gradients in the flow-momentum equation. If this term in the momentum equation is assumed to be constant, the resulting, quasi-fixed bed or quasi-coupled model is

$$\frac{\partial^3 z_b}{\partial t^3} + 2\frac{\partial^3 z_b}{\partial x \partial t^2} + \frac{Fr^2 - 1}{Fr^2}\frac{\partial^3 z_b}{\partial x^2 \partial t} - \frac{\psi}{Fr^2}\frac{\partial^3 z_b}{\partial x^3} + E\left(\frac{\partial^2 z_b}{\partial t^2} + \frac{3}{2}\frac{\partial^2 z_b}{\partial x \partial t}\right) = 0 \quad \textbf{(5.1)}$$

Compared to Eq.2.41, this model yields good approximations if

$$\psi \ll |1 - Fr^2| \qquad \textbf{(5.2)}$$

This explains differences in celerities of fixed-bed and mobile-bed models for the approximate range $0.8 < Fr < 1.2$.

Obviously, for solutions with larger values of E and/or smaller values of ψ, the contribution of the neglected nonlinearity decreases. For *linearized* morphological models, solutions of velocity and depth are not affected if river beds are assumed to be fixed during a time step. This similarity between linearized quasi-fixed bed or quasi-coupled and complete models can be shown as follows. If solutions are substituted into linearized versions of the complete and the quasi-fixed bed or quasi-coupled model, the following conditions for similarity can be found (Sieben, 1996)

$$(1 - \theta_1)(1 - \theta_2)(1 - \theta_3) = -\frac{1}{Fr^2}$$

$$\theta_1 + \theta_2 + \theta_3 = 2 \qquad \textbf{(5.3)}$$

$$\theta_1 \theta_2 \theta_3 = -\frac{\psi}{Fr^2}$$

with $\theta_j = c_j/u$ a non-dimensional celerity. Substitution proves that θ_j equals

roots of the characteristic equation (De Vries, 1966).

$$\theta^3 - 2\,\theta^2 + \left(1 - \frac{(1+\psi)}{Fr^2}\right)\theta + \frac{\psi}{Fr^2} = 0 \qquad (5.4)$$

Hence, similarity is satisfied; solutions of quasi-fixed bed or quasi-coupled models converge to exact solutions for all values of Fr if non-linearity decreases (e.g. Holly and Rahuel, 1990a and 1990b). The three conditions for similarity (Eq.5.3) provide equations to analyse θ_j, additional to Eq.5.4. Some examples are added in Sieben (1996).

Hence, errors due to decoupling reduce with steadiness and uniformity of flow, or if time steps are sufficiently small (e.g. Lyn, 1987; Cui *et al.*, 1996).

5.2.3. Quasi-steady flow.

The quasi-steady flow approach in models for river morphology consists of neglecting time changes in a and u in the mathematical model, and is applicable if the contribution of flow unsteadiness to the solution is negligible. The resulting, linearized model of non-dimensional, first-order derivatives is

$$\frac{3}{2}E\frac{\partial z_b}{\partial t} + \frac{1-Fr^2}{Fr^2}\frac{\partial^2 z_b}{\partial t \partial x} - \frac{\psi}{Fr^2}\frac{\partial^2 z_b}{\partial x^2} = 0 \qquad (5.5)$$

The fast, downstream-propagating wave III is eliminated. The applicability can be analysed by considering harmonic solutions of the simplified and complete model with varying values of E (Barneveld, 1988).
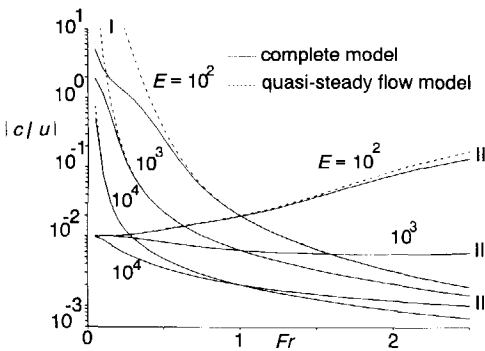
Fig.5.1-a Wave propagation rate.   **Fig.5.1-b** Relative difference.
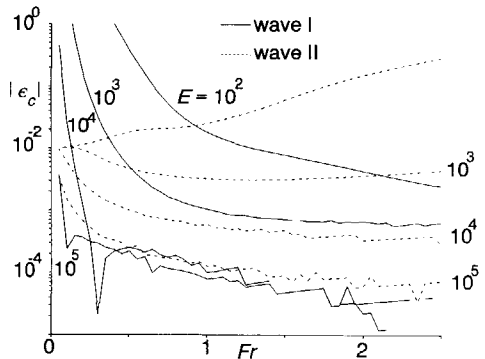
For constant values of $\psi = 10^{-2}$, the absolute values of wave propagation rates in both models are shown in Figure 5.1-a, relative differences are constructed in Figure 5.1-b.

The error in the quasi-steady flow model changes with wave type and flow regime. For subcritical flows, the error is present in upstream-propagating waves I, and for supercritical flows, the largest error can be found in the downstream-propagating wave II. The error, and the wave-type discriminating effect of Fr, decreases with larger values of E. For $E > 10^4$, the relative difference in propagation rate is can be approximated as $\epsilon_c \approx 10\, E^{-1}$.

This enables the construction of a qualitative figure for applicability of the quasi-steady flow assumption. In Figure 5.2, areas of applicability for waves I and II are indicated. For the conditions represented by the double-shaded area, both waves are represented by the quasi-steady flow model. For transcritical flow and $E < 10^3$, errors in the quasi-steady flow model are significant.
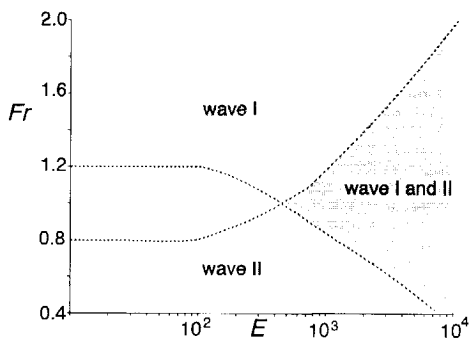
Fig.5.2 Applicability of quasi-steady flow assumption.

5.2.4. Quasi-steady and quasi-uniform flow.

The *quasi-steady flow* assumption (De Vries, 1966) enables deriving models with a mixed hyperbolic / parabolic character (Vreugdenhil and De Vries, 1973), that can be illustrated by means of a *Péclet* number (Vreugdenhil, 1982): quasi-steady models approximate a pure "convection" (or simple-wave) equation for short waves, and a pure "diffusion" equation for long waves.

The latter situation leads to a parabolic model that combines assumptions of quasi-steady and quasi-uniform flow. This model is analysed here, again by comparing propagation rates and attenuation lengths of the simplified and complete model.

For transcritical flows, the complete model develops a symmetrical behaviour of waves I and II. As a result, solutions in the complete and parabolic model show an analogous behaviour. This resemblance can be explained when considering the celerities.
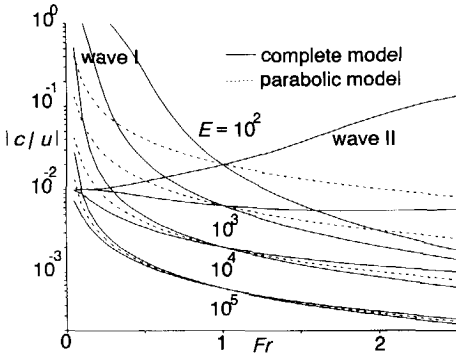
Fig.5.3 Wave propagation-rate.
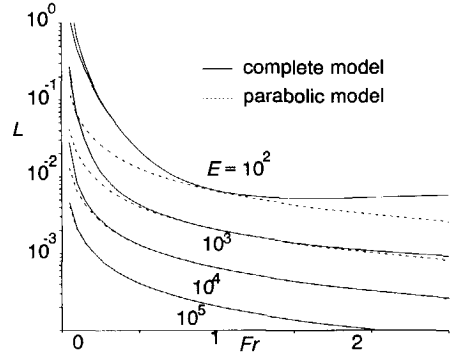
Fig.5.4 Wave attenuation-length.

An exact solution of the similarity conditions in Eq.5.3, and consequently of the characteristic equation Eq.5.4 is

$$Fr = \sqrt{1 + \psi/2} \quad ; \quad \theta_{1,2} = \pm \frac{\sqrt{\psi/2}}{Fr} \quad ; \quad \theta_3 = 2 \qquad (5.6)$$

Because $\theta_1 = -\theta_2$, a symmetric behavour with respect to waves I and II can be expected. If friction is neglected ($E \to 0$), the mathematical model can be reduced to

$$\frac{\partial}{\partial t}\left(\frac{\partial^2 z_b}{\partial t^2} - \frac{\psi}{2Fr^2}\frac{\partial^2 z_b}{\partial x^2} \right) + 2\frac{\partial}{\partial x}\left(\frac{\partial^2 z_b}{\partial t^2} - \frac{\psi}{2Fr^2}\frac{\partial^2 z_b}{\partial x^2} \right) = 0 \qquad (5.7)$$

This diffusive behaviour of waves I and II expands to other values of Fr (sub- and supercritical flows) for $E \to \infty$. Differences in damping are present for low values of E; and diminish for large values of E.

5.3. Numerical analysis.

5.3.1. Introduction.

The verify the theoretical results of Subsections 5.2.3 and 5.2.4, numerical test

106

cases are carried out with three models.

decoupled model with different time steps for hydraulics and morphology
quasi-steady flow model
quasi-steady and quasi-uniform flow model

The tests concern the deformation of a hump (height and length of 0.50 m and 60.00 m) for different conditions of flow (Table 5.1) and sediment (grain size and gradation) are considered. Sediment mixtures were described with three grain sizes. The median grain sizes considered are 0.01 m, 0.05 and 0.25 m. The gradation, defined as $\sigma^2 = D_3/D_1$, includes 2, 5 and 10. For a complete description, reference is made to Evans and Sieben (1996).

i_b	Fr	E		
		$T = 10$ min	$T = 20$ min	$T = 40$ min
0.013	0.7	27	54	109
0.033	1.1	51	101	203
0.055	1.5	71	143	285

Table 5.1 Summary of experiments.

The corresponding parameters of the experiments are shown in Figure 5.8, in combination with representative values of some typical rivers (Sieben, 1996).
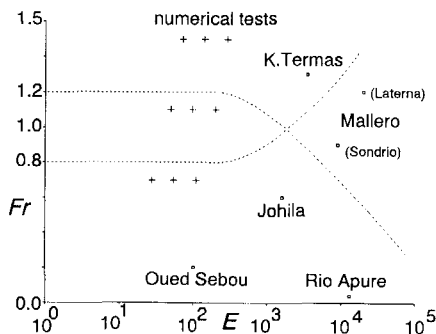
Fig.5.5 Parameters numerical tests.

The Oued Sebou (Morocco) combines a smooth bed with tidal waves at flat slopes. The resulting low values of E indicate the significant dynamic character

107

of flow (Vreugdenhil, 1977). The Rio Apure (Venezuela) represents a typical low-land river with negligible effects of flow unsteadiness (Delft Hydraulics, 1971). The Johila river (India) is an ephemeral river with steep hydrographs and a relatively steep slope of 0.0022 (De Vries, 1994). The Mallero river (Italy) combines steep slopes of the order of 0.02, and short flood waves with rough beds (FRIMAR, 1996). The Kali Termas Lama (Indonesia) has a relatively steep slope, and drains the Kelud Volcano. The supply of fine sediments results in a smooth bed, and subsequent high velocities (Sloff, 1993b).

Due to the relatively high sediment-transport rates, the deformation of the hump in the numerical experiments appeared to be very fast; in the following figures, bed level profiles are compared after a period of 10 min. A constant layer thickness of 0.50 m has been used. Space steps are $\Delta x = 10.00$ m, time steps are $\Delta t = 1.0$ s.

5.3.2. Application of simplified models.

In the next figures, the following solutions are presented:

> I   reference solution ($\Delta t_m = \Delta t_h$)
> II decoupled solution with
> > $\Delta t_m/\Delta t_h = 25$ for $Fr = 0.7$
> > $\Delta t_m/\Delta t_h = 10$ for $Fr = 1.1$
> > $\Delta t_m/\Delta t_h = 6$ for $Fr = 1.5$
> III quasi-steady flow solution
> IV quasi steady and quasi uniform flow solution

The effect of sediment transport rate on the applicability of different simplifications can be considered by changing D_m. The next three figures at the left-hand side represent solutions for $D_m = 0.01$ m, at the right-hand side, $D_m = 0.05$ m. For all figures, gradation is 5 and $T = 20$ min.
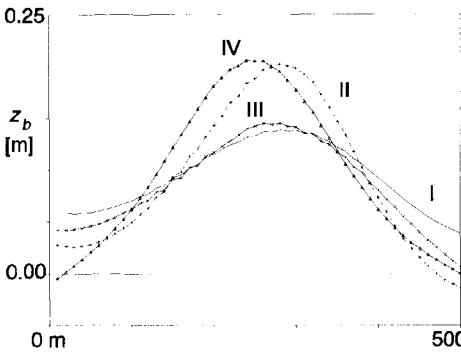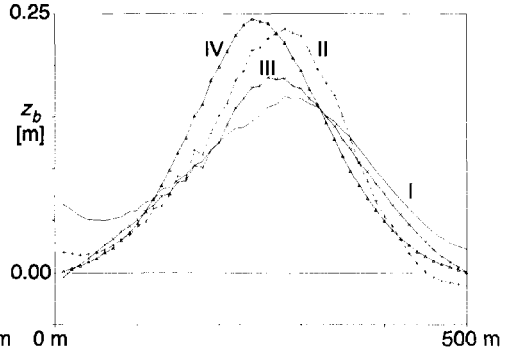
Fig.5.6-a $Fr = 0.7$; $D_m = 0.01$ m.   **Fig.5.6-b** $Fr = 0.7$; $D_m = 0.05$ m.
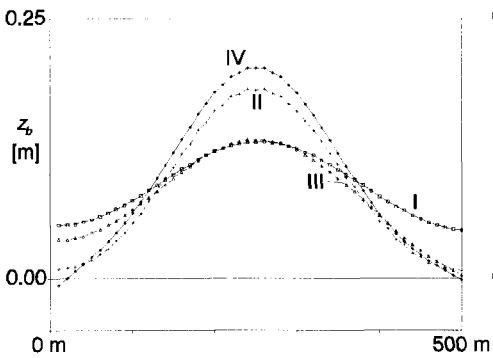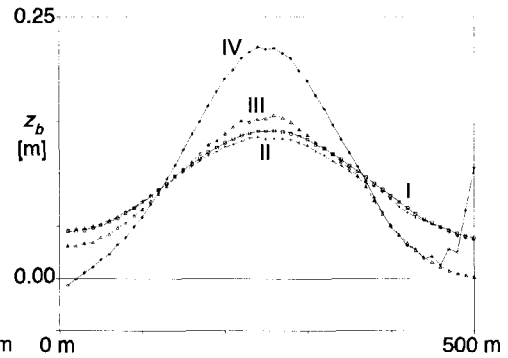
Fig.5.6-c $Fr = 1.1$; $D_m = 0.01$ m.   **Fig.5.6-d** $Fr = 1.1$; $D_m = 0.05$ m.
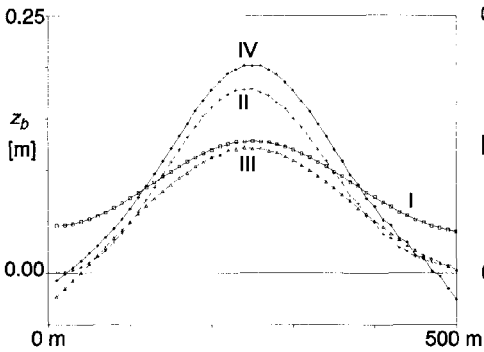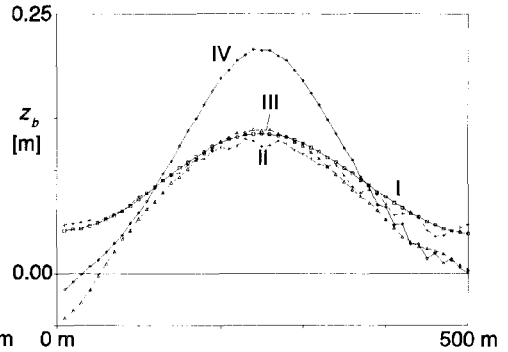
Fig.5.6-e $Fr = 1.5$; $D_m = 0.01$ m.   **Fig.5.6-f** $Fr = 1.5$; $D_m = 0.05$ m.

109

5.3.3. Quasi-steady flow.

The effect of flow unsteadiness on the simplifications is compared explicitly in the following figures. In the three figures at the left-hand side, $T = 20$ min, at the right-hand side, $T = 40$ min. In all figures, the median grain size is $D_m = 0.05$ m and gradation is $\sigma^2 = D_3/D_1 = 5$.
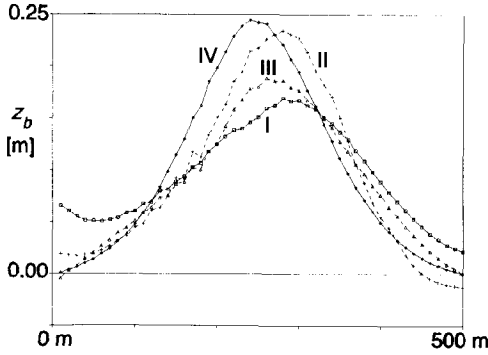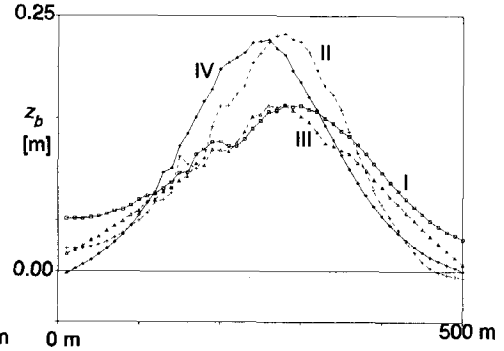
Fig.5.7-a $Fr = 0.7$; $T = 20$ min.   **Fig.5.7-b** $Fr = 0.7$; $T = 40$ min.
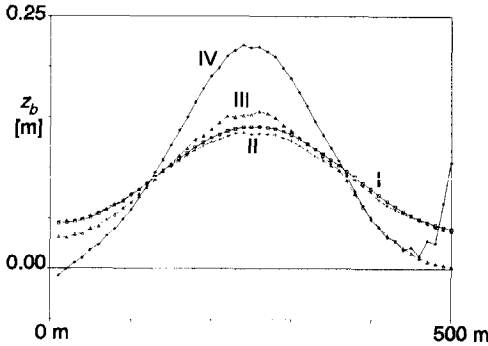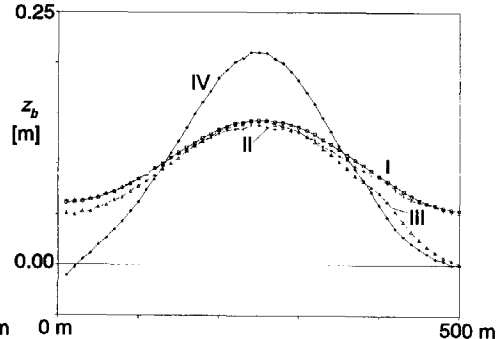
Fig.5.7-c. $Fr = 1.1$; $T = 20$ min.   **Fig.5.7-d** $Fr = 1.1$; $T = 40$ min.

110
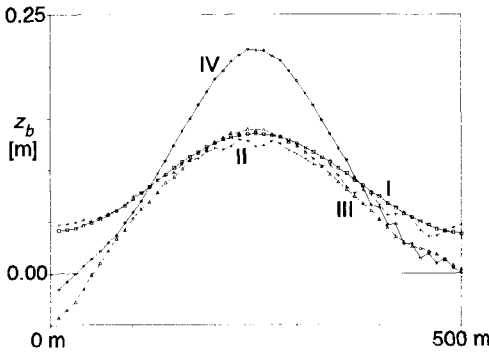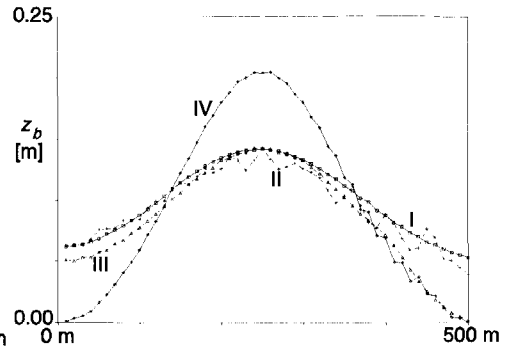
Fig.5.7-e $Fr = 1.5$; $T = 20$ min.   **Fig.5.7-f** Fr - 1.5 ; $T = 40$ min.

As can be expected, the error of the quasi-steady flow approach reduces for waves with longer periods. Considering the relatively small values of E used here, it is noted that the contribution of flow unsteadiness on the solution will be small in steeper rivers with larger values of Fr.

Apart from boundary effects that are present in the different models, the effect of the quasi-steady flow assumption (solution III) is small for downstream propagating waves, and large for upstream propagating waves in subcritical flows. For transcritical and supercritical flows, the contribution of flow-unsteadiness decreases relative to flow-nonuniformity. As a result, the quasi-steady flow approach performs well.

This can be explained by analysing sinusoidal solutions of the dynamic equations; for higher values of Fr (and E), a wave solution indeed approaches a quasi-steady character (Sieben, 1996). Hence, for trans- and supercritical flows, representative values of L (Eq.2.44) should be based on geometrical length-scales rather than characteristic periods of hydrographs. This can have significant consequences with respect to the application of simplified models.

For example, in the Mallero river in Northern Italy, E-values based on flood hydrographs range from 10^3 to 10^4 (Figure 5.5). This implies length-scales of $L = u_0 T \approx 50$ km. If longitudinal profiles of width and bed level (relative to an average slope of 0.068) are considered (Figure 5.8), the ratio of length-scales of flood wave and geometry (L_g) is approximately $\lambda = u_0 T/L_g \approx 5$ to 10. Hence, flow non-uniformity will be caused by geometrical variations mainly.

Consequently, if a geometrical length-scale is considered, corresponding values of $E \approx 10^2$ are found. At values of E of this order, flow unsteadiness can be

expected to affect morphological changes, which implies the use of complete models.
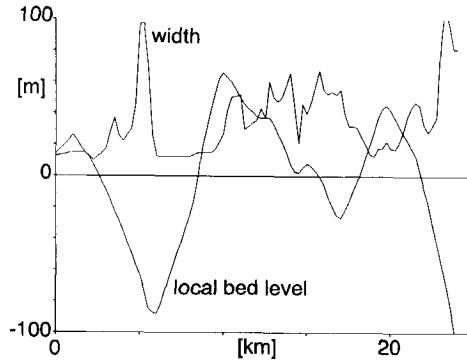
Fig.5.8. Longitudinal geometry of the Mallero river.

Backwater effects in the Mallero river due to width-fluctuations can be neglected in case of larger length-scales L_w only (approximately $L_w > -g_z/C^2 \Lambda_{min} \approx 500$ m, Appendix A.3).

5.3.4. Quasi-uniform flow.

With respect to the reference solution I, the deformation of the hump is underestimated by the quasi-steady and quasi-uniform flow model (solution IV). The underestimation of transport gradients is due to neglection of convective terms. Apparently, the values of E in the numerical tests are too small for this simplification; if a more uniform geometry is considered, the combination of assuming quasi-steady and quasi-uniform flow becomes less erroneous (Evans and Sieben, 1996).

To analyse the effect of flow non-uniformity on the applicability of the quasi-uniform flow assumption, two cases are compared with different space steps. The following three figures at the left-hand side refer to the test cases with $\Delta x = 10$ m, as described in Subsection 5.3.1. The three figures at the right-hand side refer to similar cases, but with $\Delta x = 100$ m. The broken lines represent solutions for simplified models based on quasi-steady and quasi-uniform flow, the continuous lines represent the reference solution.

112
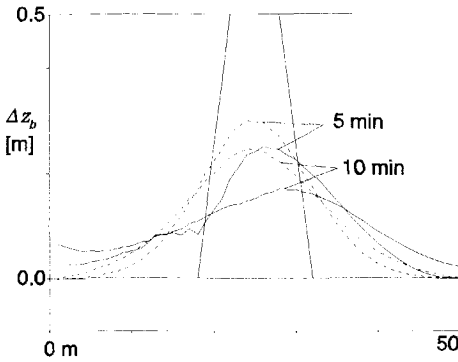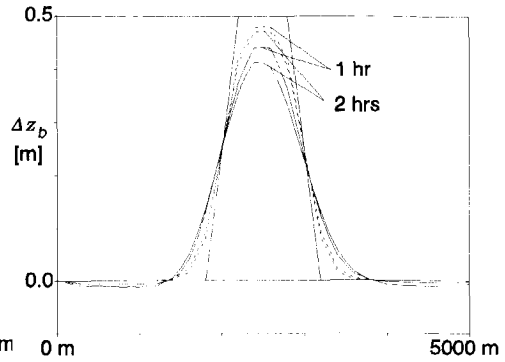
Fig.5.9-a. $Fr = 0.7$; $\Delta x = 10$ m.

Fig.5.9-b. $Fr = 0.7$; $\Delta x = 100$ m.
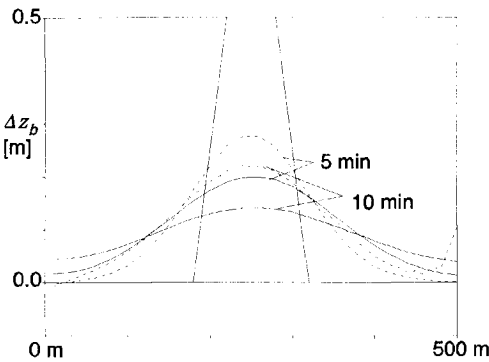
Fig.5.9-c. $Fr = 1.1$; $\Delta x = 10$ m.
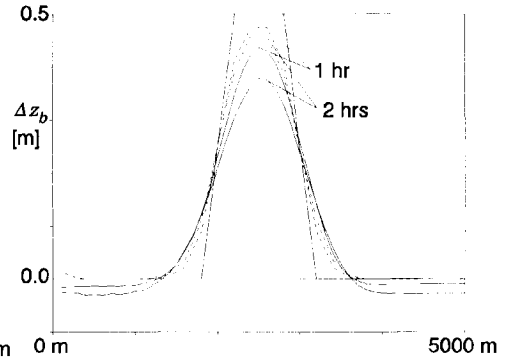
Fig.5.9-d $Fr = 1.1$; $\Delta x = 100$ m.
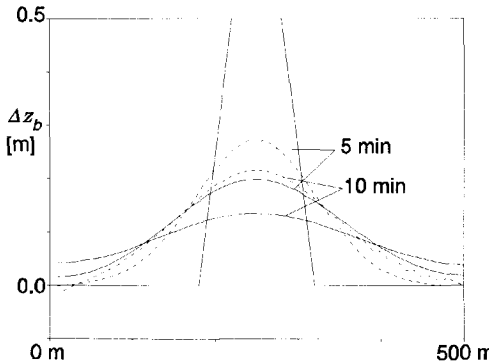
Fig.5.9-e $Fr = 1.5$; $\Delta x = 10$ m.
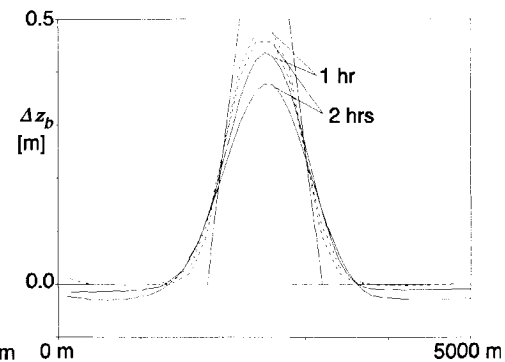
Fig.5.9-f $Fr = 1.5$; $\Delta x = 100$ m.

With reduction of the non-uniformity in geometry and flow, the deformation of the hump in both models correspond, as can be expected. Due to neglecting

113

convective terms, still a difference can be observed in the rate of deformation.

Chapter six

Analysis of discontinuous solutions.

6.1. Introduction.

In upper parts of rivers, features are often dominated by a non-uniform character of slope, width, discharge and sediment transport, sediment size and composition. Due to these non-uniform conditions, various wave-type phenomena are introduced (propagation of hydrographs or aggradation fronts) that can develop into discontinuous profiles. And if this is the case, water and bed levels in a river during a flood can be fundamentally affected.

The occurrence of discontinuous flows in rivers is rare, nevertheless, under special conditions, it has significant physical relevance. Some examples can be given. In lowland reaches of rivers, bores can travel upstream due to tidal effects (e.g. Dronkers, 1964). The propagation of bores upstream a river can have significant implications in terms of navigation, flooding risks and the stability of structures. The breaking of a dam can cause a destructive shock-wave, propagating through downstream river reaches (e.g. Ogink and De Jong, 1989).

Another type of discontinuous river flow can be found at confluences and bifurcations, where mass and momentum fluxes in a river occur. These type of stable discontinuities, which are rather prominent in mountain rivers, will not be reviewed here.

In rivers in mountainous regions, also hydraulic jumps can be observed at transitions in flow regime. If, at transcritical and supercritical flows, the bed material is mobile, bed levels immediately respond; a sudden decrease of velocity due to a hydraulic jump results in an "instantaneous" deposition of sediment.

With respect to morphology, the occurrence of local humps, trenches, distinct regressive-erosion zones and deposition fronts (delta's in lakes or reservoirs, alluvial fans) can be mentioned. Large-scale mass movements can result in discontinuous bed-level profiles. A reported example is the Mallero river in the Italian part of the Alps where large-scale landslides overloaded the conveyance system of the river. The aggradation volume propagated downstream and resulted in flooding (Di Silvio and Peviani, 1989).

115

It should be noted that the term "discontinuity" refers to *double-valued parameters at a single point in a mathematical model*, in an attempt to describe physical phenomena with an extremely short length-scale. Hence, the definition of a discontinuity is relative to a length-scale.

However, discontinuous solutions of a mathematical model are a simplified, mathematical representation of a physical phenomenon. Discontinuous flows as defined above cannot be observed in nature; changes in conditions of state will always have dimensions in time or space. Instead, relatively thin regions with relatively steep gradients in variables can be distinguished. With respect to the larger length scale of the computation domain, these thin regions can be assumed concentrated into a unique location.

In this study, emphasize will be put on effects of discontinuities on continuous states of river hydraulics and morphology, rather than a detailed description of flow within the transition state. Examples of these neglected effects are local energy dissipation by increased turbulence, development of vertical velocity, local changes in mechanisms responsible for sediment-transport.

Hence, although the importance is recognized, a proper and detailed description of additional effects that are present in transition zones is not included. This implies that one set of PDE's is applied for both continuous and discontinuous solutions.

Within a fair range of accuracy with respect to hydrodynamics, this assumption is supported by observations of Basco (1989) and Gharangik and Chaudhry (1991). The latter modelled rapidly varying flow with the shallow-water equations, extended with the Boussinesq term to account for changes in pressure distribution due to vertical velocities. The contribution of vertical velocities to numerical solutions that included hydraulic jumps was found to be negligible.

This small effect on the *numerical* solution does not imply negligible vertical velocities in hydraulic jumps. At strong shocks, bed-pressure measurements by Hager and Bretz (1986) in hydraulic jumps at positive and negative steps show deviations from hydrostatical pressure-distributions.

6.2. Mathematical aspects.

6.2.1. Generalized or non-differentiable solutions.

Mathematical models for flows with mobile beds consist of PDE's based on

116

mass and momentum conservation laws. Discontinuous flows can develop due to the non-linear character of the PDE's that describe the hydrodynamics of river flows and the corresponding morphological changes. If conditions are sufficiently non-uniform, *characteristics from the same family, originating from neighbouring points, intersect.* Information carried by the characteristics collapses into a single point and a discontinuity is formed.

Although differential equations using continuous variables fail at points of discontinuities, the physical concept of mass and momentum conservation still applies. Therefore, at a discontinuity, conservation laws can be defined and applied additional to the mathematical model that is valid in the zones of continuous flow.

Due to this concept of separating continuous and discontinuous flows, additional relations, the *Rankine-Hugionot*, or shock relations can be derived. These relations describe mass and momentum conservation at the discontinuity, and can be considered valid at the zone of discontinuous flow only.

With the Rankine-Hugoniot relations, a solution can be constructed that satisfies the mass and momentum conservation relations in integrated form. Such a *non differentiable* solution is defined as a *generalized* (or weak) solution (Lax, 1954, or Abbot, 1975).

The derivation of the shock relations is illustrated by an example due to Lax (1973). Consider a PDE

$$\frac{\partial u}{\partial t} + \frac{\partial F}{\partial x} = 0 \quad ; \quad F = f(u) \tag{6.1}$$

Now, a solution $u(x,t)$ can be found at each side of a smooth curve $x = y(t)$ (Figure 6.1). An interval $x_l \leq x \leq x_r$ is chosen that includes the curve y.
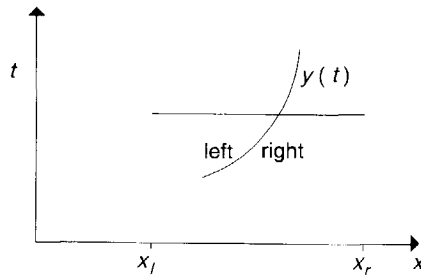
Fig.6.1 Definition of two continuous solutions.

Then, a quantity $I(t)$ is defined as

$$I(t) = \int_{x_l}^{x_r} u(x,t)dx = \int_{x_l}^{y} u(x,t)dx + \int_{y}^{x_r} u(x,t)dx \tag{6.2}$$

Derivation to t yields

$$\frac{dI(t)}{dt} = \int_{x_l}^{y} \frac{\partial u(x,t)}{\partial t}dx + u(x_l,t)\, c + \int_{y}^{x_r} \frac{\partial u(x,t)}{\partial x}dx - u(x_r,t)\, c \; ; \; c = \frac{dy}{dt} \tag{6.3}$$

At either side of the discontinuity, Eq.6.1 is applicable. This results in

$$\frac{dI(t)}{dt} = F(x_l,t) - F_l(y,t) + u(x_l,t)\, c + F_r(y,t) - F(x_r,t) - u(x_r,t)\, c \tag{6.4}$$

where $F_l(y,t)$ and $F_r(y,t)$ represent the fluxes directly left and right of the discontinuity at $y(t)$. The PDE Eq.6.1 in conservative form is

$$\frac{dI(t)}{dt} = F(x_l,t) - F(x_r,t) \tag{6.5}$$

This is satisfied for the interval $x_l \leq x \leq x_r$ if the following *shock relation* is valid

$$F_r(y,t) - F_l(y,t) = c \left[u(x_r,t) - u(x_l,t) \right] \tag{6.6}$$

Analogously, shock relations can be derived for one- and two-dimensional models for flow with mobile beds (Sieben, 1995). The conservation equations for the discontinuity include all fluxes, diffusive and source terms. Because the length of the zone of discontinuous flow is relatively short, in general only fluxes are considered.

6.2.2. Entropy conditions.

Consider a one-dimensional, depth-averaged model for flow with a mobile bed. The system of PDE's consists of a fluid mass and a sediment mass balance and a momentum equations. The number of variables is three; velocity, depth and bed level. At a point of discontinuity, the number of variables is doubled and

118

amounts six. In addition, the rate of the shock is unknown, which totals a number of seven unknown variables.

The Rankine-Hugoniot conditions are again three non-linear equations with the seven variables mentioned. Now, the rate of the discontinuity and two variables can be calculated with the Rankine-Hugionot relations. The remaining four variables must be determined with information carried by incoming characteristics.

In principle, the total number of characteristics that can be calculated in the neighbouring zones of continuous flow equals the number of variables at the shock: 2 x 3. However, because characteristics cannot be calculated through discontinuities; a limited number of characteristics (and consequently characteristic equations) is valid. In order to solve the system, *at least four characteristics should not intersect with the time path of the shock.* This criterion limits the interval of propagation rates and can be visualized in a *x-t* diagram (Figure 6.2).

To generalize this line of reasoning, a system of N variables is considered. A shock is propagating with a rate w. The number of unknowns at the shock is $2N+1$, the number of Rankine-Hugoniot relations is N. This implies that $N+1$ characteristics should arrive at the discontinuity to close the system of equations.
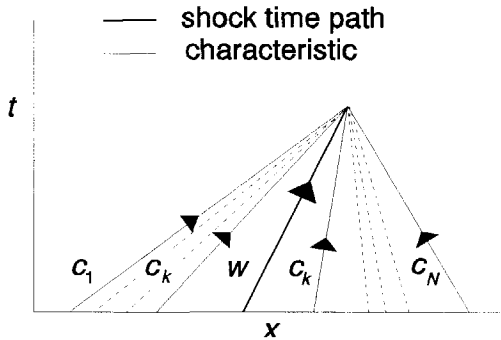
Fig.6.2 Intersection of valid characteristics.

The characteristics are marked with index i, with $i = 1..N$ and $c_i < c_{i+1}$. From the left, (upstream) side of the shock, k characteristics arrive, whereas from the right (downstream) side, $N-k+1$ are valid. This implies that N shock types are possible. Hence, for a one-dimensional model of flow with mobile bed, three shocks can develop.

119

The shock is called a k-type shock if the propagation rate w_k satisfies

$$c_{k - downstr} < w_k < c_{k - upstr} \qquad \textbf{(6.7)}$$

Obviously, the higher the shock type, the more information is transferred from upstream.

In case of convex coefficients for flux terms in the PDE's, satisfying Eq.6.7 implies satisfying the so-called entropy condition as well, that states that over a discontinuity, entropy must increase (e.g., Lax, 1973). Therefore, Eq.6.7 can be called the *entropy condition*. Now, a shock wave is defined as a discontinuity that satisfies the shock relation (Eq.6.6) and the entropy condition (Eq.6.7).

The entropy condition determines the stability of the shock. This can be illustrated as follows. If characteristics c_k up- and downstream of the discontinuity converge, a shock is stable. If characteristics c_k diverge, Eq.6.7 is not satisfied. Then, the discontinuous solution develops into a rarefaction or expansion wave, and the discontinuity will disappear. Although variables will be continuous, derivatives can be discontinuous.

6.2.3. Analysis of shock relations.

To analyse the behaviour of discontinuous solutions, the theory in the previous subsection is applied to a one-dimensional, depth-averaged model with mobile bed. First the corresponding shock relations are analysed. A distinction is made in variables upstream (x^+) and downstream (x^-) of the discontinuity.
Over the discontinuity a conservative flow-mass and -momentum balance and a sediment-mass balance can be defined. The propagation rate of the shock wave is defined as w. Flow-mass balance

$$w\,(a^+ - a^-) = u^+ a^+ - u^- a^- \qquad \textbf{(6.8)}$$

Momentum balance

$$w\,(u^+ a^+ - u^- a^-) = (u^+)^2 a^+ - (u^-)^2 a^- + \frac{g_z}{2}((a^-)^2 - (a^+)^2) + \qquad \textbf{(6.9)}$$

$$+ g_z \frac{a^+ + a^-}{2}\left(z_b^- - z_b^+\right)$$

120

Sediment-mass balance

$$w\left(c^+a^+ + z_b^+ - c^-a^- - z_b^-\right) = u^+c^+a^+ - u^-c^-a^- + s_b^+ - s_b^- \quad \textbf{(6.10)}$$

Suspended load is neglected ($c^+ = 0$, $c^- = 0$). The bed-load transport is predicted with a power-law $s_b = mu^n$, where m and n are coefficients.

Now, differences in variables over the shock are introducing by using

$$a^- = a^+ + \Delta a \quad ; \quad u^- = u^+ + \Delta u \quad ; \quad z_b^- = z_b^+ + \Delta z_b \quad \textbf{(6.11)}$$

In the following, the subscript $+$ is left out for convenience. The result is a non-linear system of 3 equations with 7 unknowns. For simplicity's sake, it is stated that $n = 3$. A general analysis with varying values of n can be found in Appendix E. For $n = 3$, it can be found

$$
\begin{aligned}
&\left[\phi\left(\frac{\Delta a}{a}\right)^2\left(2+\frac{\Delta a}{a}\right) - 2Fr^2(1+\frac{\Delta a}{a})^2\right]\left(\frac{w}{u}\right)^3 + \\[2mm]
&+ \left[3\phi\frac{\Delta a}{a}\left(2+\frac{\Delta a}{a}\right) + 4Fr^2\left(1+\frac{\Delta a}{a}\right)^2\right]\left(\frac{w}{u}\right)^2 + \\[2mm]
&+ \left[\left(2+\frac{\Delta a}{a}\right)\left(\left(1+\frac{\Delta a}{a}\right)^3+3\phi\right) - 2Fr^2\left(1+\frac{\Delta a}{a}\right)^2\right]\left(\frac{w}{u}\right) + \\[2mm]
&- \phi\left(6 + 9\frac{\Delta a}{a} + 5\left(\frac{\Delta a}{a}\right)^2 + \left(\frac{\Delta a}{a}\right)^3\right) = 0
\end{aligned}
\quad \textbf{(6.12)}
$$

For $\Delta a/a \rightarrow 0$, infinitely small disturbances are found that should propagate with the characteristic celerities. Indeed, in that case Eq.6.12 can be reduced to

$$\left(\frac{w}{u}\right)^3 - 2\left(\frac{w}{u}\right)^2 + \left[1 - \frac{1+3\phi}{Fr^2}\right]\left(\frac{w}{u}\right) + \frac{3\phi}{Fr^2} = 0 \quad \textbf{(6.13)}$$

which equals the corresponding equation for celerities (De Vries, 1966).

If a, u, s_b and Δa are prescribed, three solutions for the propagation rate w can be found; if initial conditions in the model as described are discontinuous, three different type of waves can develop.

121

In the following, the Rankine-Hugoniot relations are solved. To analyse the behaviour of the shock, values of w are compared with characteristics up- and downstream. If a positive discontinuity in depth is considered ($\Delta a/a = 0.3$), propagation rates and surrounding characteristics are (Figure 6.3)
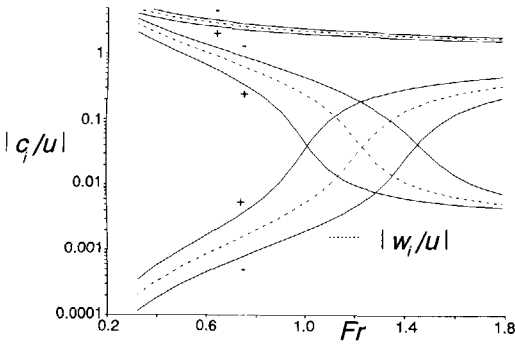
Fig.6.3 Propagation rates for $\Delta a/a = 0.3$.
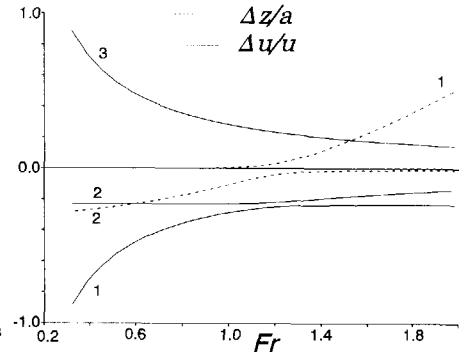
Fig.6.4 Differences for $\Delta a/a = 0.3$.

The characteristics marked with + and - refer to up- and downstream conditions. The differences in variables over a corresponding discontinuity are represented in Figure 6.4.

Now, a decrease in water depth over the shock is substituted in the shock relations ($\Delta a/a = -0.3$). Propagation rates and surrounding characteristics are (Figure 6.5). Differences are presented in Figure 6.6.
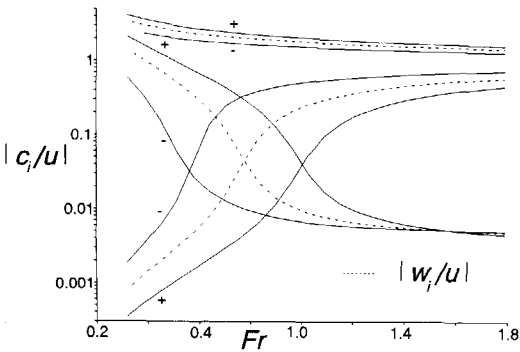
Fig.6.5 Propagation rates for $\Delta a/a = -0.3$.
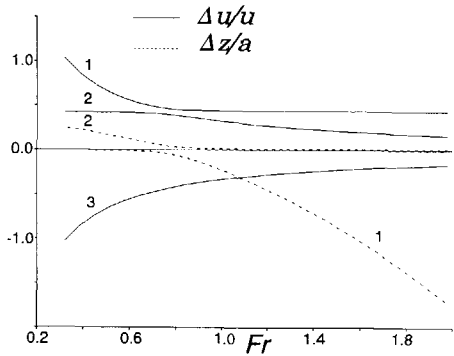
Fig.6.6 Differences for $\Delta a/a = -0.3$.

122

6.3. Behaviour of discontinuous solutions.

With the results from Subsection 6.2.3, the behaviour of discontinuous solutions can be analysed. The analysis can be simplified by the following observation. For $Fr < 0.8$ and $Fr > 1.2$, the deformation of a profile is due to one wave-type solution mainly. This enables the identification of distinct surface and bed level waves, in accordance with the decoupling criteria found in Subsection 5.2.3 Hence, for $Fr < 0.8$ and $Fr > 1.2$, a simplified treatment of discontinuous solutions is possible.

First morphology is considered. Morphological changes are related to type 1 and 2 waves mainly. Type 3 shocks are relatively fast hydraulic phenomena that can be analysed decoupled from morphological effects. For low values of Fr, significant changes in bed level are associated with type 2 shocks only. In supercritical flows at high values of Fr, changes in bed level propagate upstream with type 1 shock predominantly. In the following figures, positive and negative differences in depth are combined.
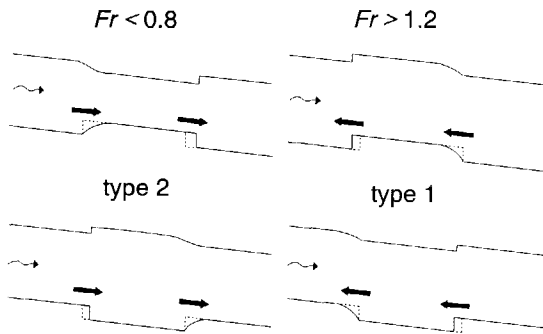
Fig.6.7 Shock and expansion waves in bed level.

In Figure 6.7, a qualitative deformation of a discontinuous bed level (shoal and trench) is presented. At subcritical flow and supercritical flow, the direction of propagation and the location of expansion wave and shock wave reverses.

Despite differences in rheological properties, some interesting similarity consists with discontinuous behaviour of free surface mud flows and debris flows. An extraordinary example of a positive, upstream-propagating shock wave can be found in Takahashi (1991), who reviews the upstream propagation of a stable deposition front (Figure 6.8), due to a flattening of the bed slope. The number of Fr for the incoming debris flow amounts 1.8. This would correspond with a type I shock wave in a supercritical flow regime.
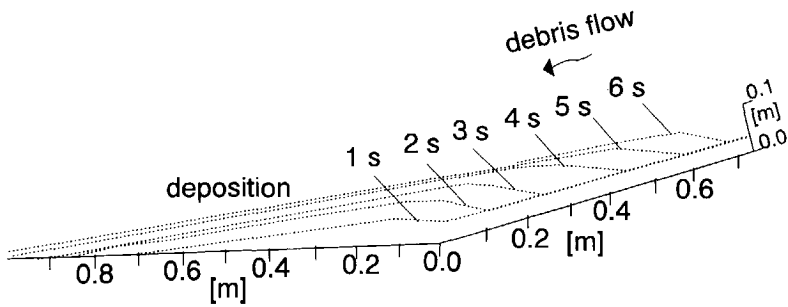
Fig.6.8 Deposition profile of debris flow (Takahasi, 1991).

In flume experiments, Armanini and Scotton (1992) observed two types of impacts of debris flows hitting a check dam; a reflected bore at milder slopes and a vertical, jet-like bulge at steeper slopes. The different phenomena were explained by considering an accelerating (jet) and decelerating (bore) flow (Armanini, 1993), but it is tempting to speculate that the different impacts represent different flow regimes. In subcritical flows, fast type I shock waves propagate upstream, whereas in supercritical flows, upstream propagation rates are much smaller, inducing a large vertical velocity in front of the structure.

If discontinuous surface levels are considered, the following situations can develop if $Fr < 0.8$ or $Fr > 1.2$.
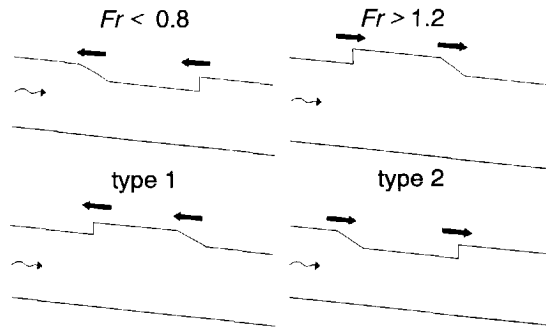
Fig.6.9 Shock and expansion waves in free-surface level.

At transcritical flow (Fr near unity), changes in bed level clearly propagate up- and downstream along both type 1 and 2 shock waves. Then, the deformation of a discontinuity is cannot be assigned to one single wave anymore, but is dominated by two waves.

124

The surface wave profiles are either shock type 1 or 2. The wave type, and direction of propagation is a related to the flow regime, type 1 upstream in subcritical flows, and type 2 downstream in supercritical flows. Another solution can be identified as a type 3 shock, which is always directed downstream.
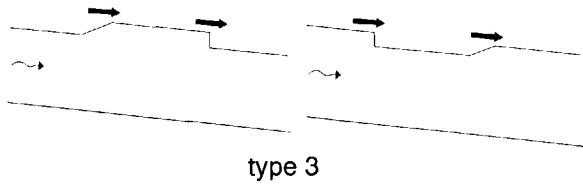
type 3

Fig.6.10 Type 3 shock and expansion waves.

6.4. Numerical aspects.

6.4.1. Introduction.

Because discontinuous conditions in rivers are rare, research on discontinuous solutions in numerical models mainly originate from gas dynamics. For extensive treatments, interested readers are referred to Fletcher (1988a and 1988b), Hirsch (1988 and 1990), LeVeque (1990), Anderson *et al*. (1984). Here, only some aspects on application of the numerical model to discontinuous solutions are discussed.

6.4.2. Review of solution techniques.

For solution of discontinuous solutions in numerical models, two methods are reviewed briefly.

Shock-fitting method.

Mathematically, discontinuities in solutions are defined as instantaneous transitions in two continuous states. This is valid if time or space dimensions of the transition can be assumed negligible with respect to the scale of the continuous states. This concept of separate scales for continuous and discontinuous flows in numerical models is used in *shock-fitting* procedures.

The method concerns the application of two different models; one for changes

at the "instantaneous" scale of the discontinuity (shock relations), and one for changes at the scale of the continuous states (e.g. characteristic equations).

The application of different models (a conventional PDE-model for continuous solutions and shock-relations for local discontinuous solutions) enables an easy description of local effects regarding e.g., energy dissipation or sediment transport.

Merit of shock-fitting methods is the use of a relatively large grid (Δt and Δx), that can be adjusted to the state of continuous flow. This can be explained as follows. The length-scale of a discontinuity in a numerical solution is of the order of the grid size. Therefore, unless the discontinuity is treated in an isolated manner (as it is the case in *shock-fitting* procedures), the grid in the model should correspond with the length scale of the physical transition zone.

However, tracking of (multiple) shocks requires significant additional effort. For mobile-bed models, shock relations are strongly non-linear; the additional iterative solution procedure for the discontinuity will increase significantly the total computation costs.

Shock-capturing method.

In case of *shock-capturing* methods, the mathematically defined discontinuity (double-valued variables at a single location) is interpretated somewhat differently. Based on the work by Lax (1954) (Subsection 6.2.2), discretized equations of mass continuity and momentum conservation are integrated over continuous as well as discontinuous reaches. The solutions obtained are weak solutions.

This omits the use of additional relations and shock tracking. However, some remarks should be made. In contrast with shock fitting methods where different models are applied, descriptions of local effects such as energy dissipation or sediment transport should be valid in discontinuous and continuous flows. In shock-capturing methods, scales in zones of discontinuous and continuous states should be of comparable magnitude. This forces the usage of high-resolution grids for the entire computation domain. An alternative option is introducing additional dissipation terms, to be switched on at zones of extremely large gradients (Subsection 2.6.3).

However, the computation effort for complex flow conditions can expected to be lower for shock capturing methods, relative to models based on a shock-

fitting approach. Therefore, this concept will be applied in the numerical model. Some consequences will be discussed in the next section.

6.4.3. Integration of discontinuous solutions.

Finite-difference equations can be solved if intergrid distributions both along Δt and Δx can be solved (Subsection 7.3.2). The predictor step that uses characteristic equations (Subsection 7.3.3) is applied both to continuous and discontinuous solutions. However, characteristic equations defined along celerities that cross the shock time-path (Subsection 6.2.2) are not valid. Hence, implicitly, invalid information is used. In theory, two options are available to overcome this error.

The first option would be to replace invalid characteristic equations with shock relations (*Rankine-Hugoniot* relations), introduce double-valued variables and shock-propagation rates (e.g. Savic, 1991). In fact, this procedure has been applied by Stoker (1957) to construct analytical solutions for dambreak waves. The implementation of shock-tracking procedures is optional. For models of flows at mobile beds, however, this procedure results in a considerable extension of computational effort.

A second option would be to modify the formulation of the characteristic equations, in order to include higher-order effects. This effect can be illustrated with the following example. If a linear distribution of variables between grids (space and time) is assumed (Figure 6.11)., values of for example depth can be written as

$$a_A = a \quad ; \quad a_B = a + \Delta x \frac{\partial a}{\partial x}$$

$$\text{(6.14)}$$

$$a_C = a + \Delta x \frac{\partial a}{\partial x} + \Delta t \frac{\partial a}{\partial t} + \Delta x \Delta t \frac{\partial^2 a}{\partial x \partial t} \quad ; \quad a_D = a + \Delta t \frac{\partial a}{\partial t}$$
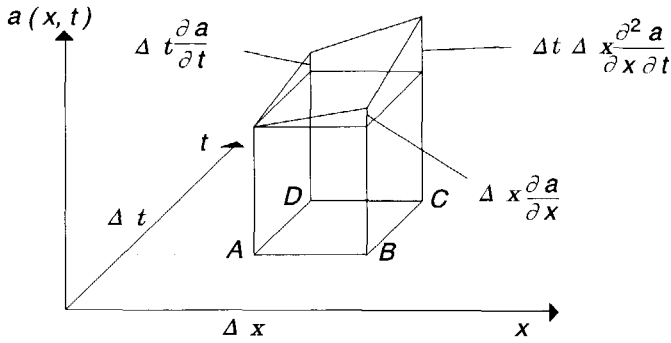
Fig.6.11 Linear intergrid distribution.

The corresponding continuity equation for flow would be

$$\left(1+\frac{\Delta t}{2}\frac{\partial u}{\partial x}\right)\frac{\partial a}{\partial t} + \left(u+\frac{\Delta t}{2}\frac{\partial u}{\partial t}+\Delta x\frac{\partial u}{\partial x}\right)\frac{\partial a}{\partial x} + a\frac{\partial u}{\partial x} =$$

$$= -\frac{\Delta x}{2}\left[1+\frac{\Delta t}{\Delta x}\left(u+\Delta x\frac{\partial u}{\partial x}\right)+\frac{\Delta t^2}{\Delta x}\left(\frac{\partial u}{\partial t}+\Delta x\frac{\partial^2 u}{\partial x\partial t}\right)\right]\frac{\partial^2 a}{\partial x\partial t} + \qquad (6.15)$$

$$-\frac{\Delta t}{2}\left[a+\Delta t\frac{\partial a}{\partial t}+\Delta x\frac{\partial a}{\partial x}\right]\frac{\partial^2 u}{\partial x\partial t}$$

Analogously, a momentum equation and a sediment continuity equation can be derived. For $\Delta t \to 0$ and $\Delta x \to 0$, the conventional set of PDE's would be obtained. However, due to a linear intergrid-distribution, higher-order terms will appear in the difference equation, both in coefficients and as additional source terms. As a result, celerities and characteristic equations that correspond to the difference equations in the numerical model will change in case of significantly non-uniform flow.

Because spatial gradients have finite values, both in reality and in numerical solutions, the contribution of these higher-order terms can be reduced by using smaller values of Δt and Δx. Therefore, if a grid is applied with a sufficiently high resolution, a similar set of characteristic equations can be used for both continuous flows, and flows with steep gradients.

For acceptable time and space steps, this simplification does, however, affect the solution. The information loss on exact front propagation can result in artificial oscillations, if opposite propagating waves meet. A numerical stabilization can be obtained by adding monotonicity procedures (Van Leer,

128

1979; Collella and Woodward, 1984), that eliminate over and undershoots near discontinuities.

The effect of a simple monotonicity procedure is shown in Figure 6.12. If a depth in the corrector is larger or smaller than both neighbouring intergrid-depths from the predictor, it is stated to be equal to the nearest value of depth. Note that the uncertainty in shock-wave position equals at least one grid size.
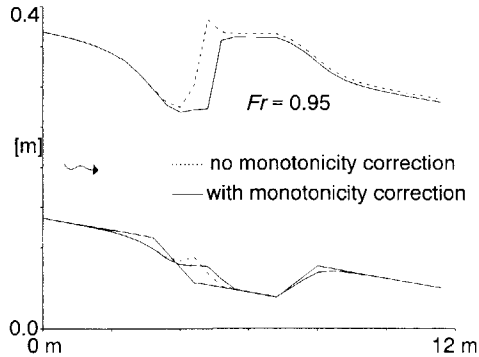
Fig.6.12 Effect of monotonicity correction.

6.4.4. Numerical dissipation.

For continuous flow, the error in the numerical solution will be related to the order of the intergrid distribution, which can be illustrated by approximating a solution with a Taylor series expansion, and substitution into the finite-difference equation (e.g. Vreugdenhil, 1994). For discontinuous flows, with mathematically undetermined gradients, a Taylor series expansion is not convenient. However, the order of the truncation error significantly determines the behaviour of a discontinuous solution.

Truncation errors in first-order accurate finite-difference equations act as artificial viscosity coefficients (*dissipation*) that reduce steep transitions in a discontinuous solution (e.g. Anderson *et al.*, 1984). Truncation errors in second-order accurate finite-difference equations cause a phase shift of wave components in the solution (*dispersion*), which can result in high-frequency parasitic waves near steep gradients (e.g., MacCormack and Baldwin, 1975; Anderson *et al.*, 1984).

The numerical model as applied here is of first-order accuracy (Chapter 7). In general, the contribution of numerical dissipation should be of a higher order than that due to physical dissipation. Only if numerical side-effects are

129

understood, the stabilizing effect can be considered favourable in a limited number of cases (Lax and Wendroff, 1960; Ames, 1977; Abbott, 1979). Neumann and Richtmeyer were the first to introduce an artificial viscosity consisting of quadratic terms of such form and strength, that the shock transition would be a smooth one, extending over a few space intervals (Richtmyer, 1972). The effect of numerical dissipation for different intergrid distribution assumptions is illustrated in Section 7.4.3.

6.5. Numerical solutions.

6.5.1. Introduction.

For subcritical flows ($Fr < 0.8$) and supercritical flows ($Fr > 1.2$), shock waves and expansion waves in hydraulic and morphological variables can be distinguished. As a result, discontinuous initial conditions develop into one dominating shock or expansion wave. In the previous figures, these situations have been analysed.

However, at a point of discontinuity, the number of waves that develop (either of a shock or expansion type) is equal to the number of variables. For transcritical flows ($0.8 < Fr < 1.2$), interaction between hydraulic and morphological variables is significant, which implies that discontinuities in initial conditions develop into multiple shock and expansion waves. To account for multiple waves, the solution must be obtained numerically. Therefore, examples of numerical experiments are added. The numerical model is described in Chapter Seven.

6.5.2. Deformation of humps and trenches.

The discontinuities concern a hump (trench), with heights (depths) equal to $a/5$.
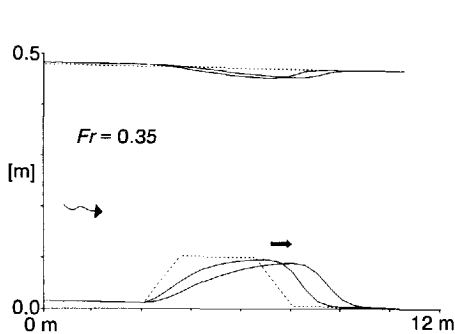
Fig.6.13 Hump ($Fr = 0.35$).
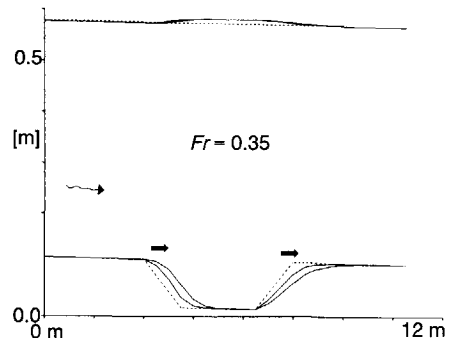
Fig.6.14 Trench ($Fr = 0.35$).

130

For subcritical flows, the discontinuous profile predominantly develops into a shock and expansion wave, in correspondence with the analysis in Section 6.3.

For transcritical flows, discontinuities in bed level clearly develop into multiple waves. From the upstream side of the hump, a slow shock wave (hydraulic jump) propagates in upstream direction and an expansion wave diffuses the hump profile in downstream direction. At the downstream side of the hump, a small shock wave propagates downstream, and an upstream propagating expansion wave diffuses the hump. A corresponding solution is found for the trench. Here, the upstream propagation of the hydraulic jump is hindered by a downstream propagating shock wave of the bed level. This results in a decrease of jump intensity by deposition in the middle of the trench.
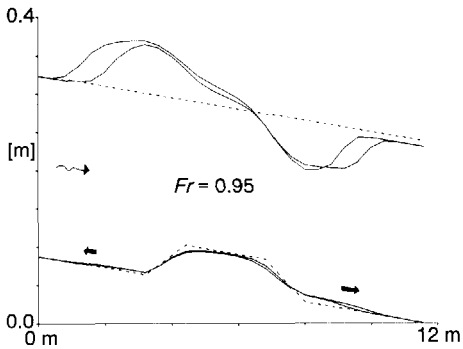
Fig.6.15 Hump ($Fr = 0.95$).
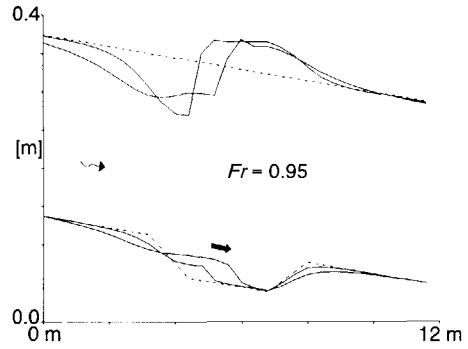
Fig.6.16 Trench ($Fr = 0.95$).

In supercritical flows, again correspondence with the analysis of Section 6.3 is found.
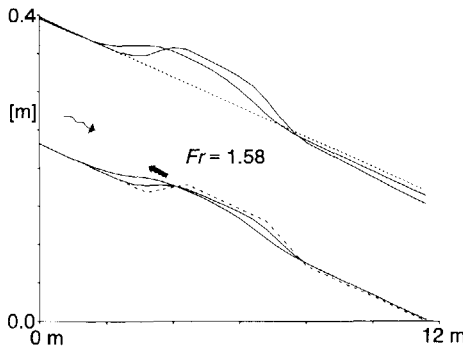
Fig.6.17 Hump ($Fr = 1.58$).
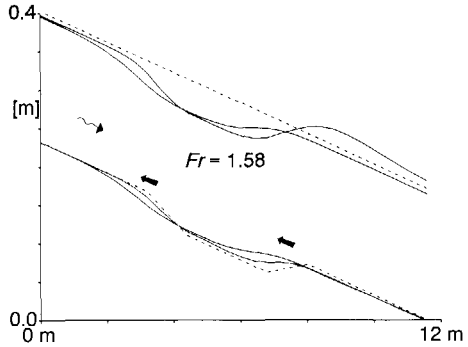
Fig.6.18 Trench ($Fr = 1.58$).

131

6.5.3. Backward-facing step.

Laboratory experiments on the behaviour of discontinuities with respect to morphology either concern discontinuous boundary conditions, or discontinuous initial conditions. With respect to studies on discontinuous boundary conditions, the case of overload at the upstream boundary can be mentioned (e.g. Sony *et al.*, 1980; Cui *et al.*, 1996). Basile (1994) studied the effects of downstream boundaries by analysing sedimentation of sand and gravel due to check dams. An experimental study on the deformation of a backward-facing step in the longitudinal bed level profile has been reported extensively by Brush and Wolman (1960).

One of the recent studies on the deformation of backward-facing steps is due to Lee and Hwang, 1994). However, the conditions in the experiments are rather extreme, with step heights of the order of flow depth. This inevitably induces contributions of vertical velocities to flow and sediment that are not included in the mathematical model. A second phenomenon not included in the model is separation of flow. Hence, changes in flow conditions due to the step in bed level will not be smoothened over a separation length. As a result, the non-uniform behaviour of flow will be overpredicted. Some examples are given.

No.	q [m^2/s]	i_b [-]	C [m$^{1/2}$/s]	Δz_b [m]	a_{down} [m]
1	0.0173	0.002	39	0.08	0.07
2	0.0063	0.002	36	0.10	0.63
3	0.0127	0.002	38	0.08	0.05

Table 6.1. Backward-facing step experiments (Lee and Hwang, 1994)

In Figure 6.19, test No.1 is considered; symbols refer to the experiment, line refer to the numerical model. It is noted that relatively large space steps have been applied ($\Delta x = 0.50$ m $\approx 6 \, \Delta z_b$). In Figure 6.20, the numerical model as described in Chapter seven has been applied to test No.3.

132
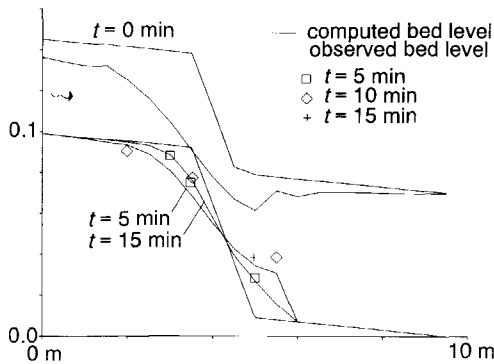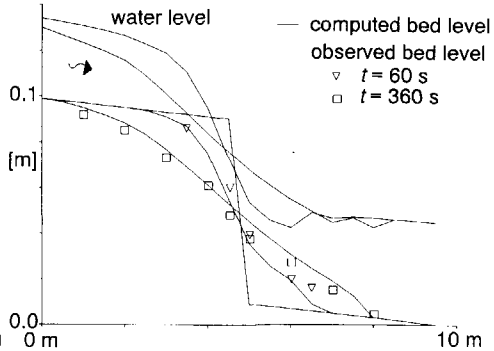
Fig.6.19 Test No.1.　　　　　　　**Fig.6.20** Test No.3.

Sediment transport rates are predicted with the formula proposed by Meyer-Peter and Müller (1948), calibrated for the experiments. Numerical grid: $\Delta t = 0.005$ s, $\Delta x = 0.50$ m. The observed deformation of the step profile demonstrates the contributions of an expansion wave and a shock wave that causes a hydraulic jump. While propagating downstream, the strength of this jump is decreasing.

6.5.4. Discontinuous geometry.

An extension to the previous experiments is the analysis of Okabe *et al.* (1994), which combines non-uniform bed levels and changes in width. The resulting non-uniformity in flow causes changes in flow regime, marked by the presence of hydraulic jumps. Both water and bed levels were recorded and presented. The numerical model described in Chapter seven is used to simulate the morphological changes. Uniform sediments were used ($D_m = 0.00085$ m). Discharge rates were kept constant ($3.5 \cdot 10^{-3}$ m³/s), and downstream waterlevels were fixed. Flume widths are presented in Figure 6.21; widths range from 0.4 to 0.1 m. The length of the flume is 16.0 m, space steps in the model are 0.2 m.
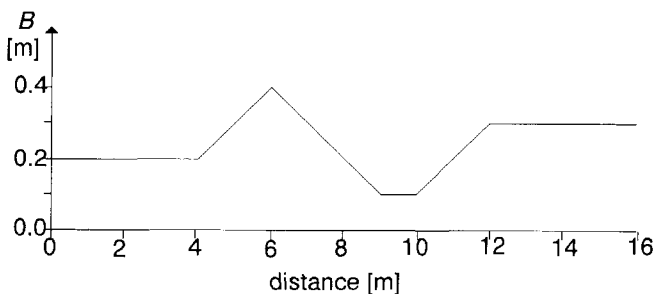
Fig.6.21 Flume width (Okabe *et al.* 1994).

133

In the flume, a non-erodible section is included at 6 m $\leq x \leq$ 7 m. In the numerical simulation, this is accounted for by introducing locally a large, stable grain size. Sediment transport rates are predicted with the help of the Meyer-Peter and Müller (1948) formula. Predictions of the numerical model are compared with the measurements at $t = 15$ min and $t = 60$ min. Except for the propagation rate of the deposition front, results correspond.
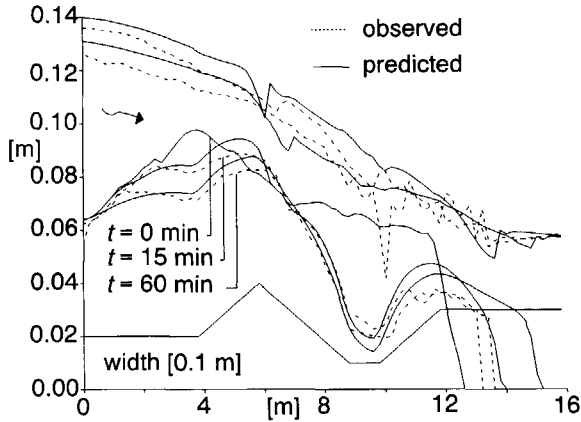
Fig.6.22 Flume experiment with non-uniform geometry.

Chapter seven.

Description of numerical model.

7.1. Introduction.

For solution of a non-linear mathematical model such as described in Chapter two, numerical procedures must be applied. Different techniques are available, based on characteristics methods, finite-difference or finite elements methods. For a general review, reference can be made to numerous authors such as Anderson *et al.* (1984), Fletcher (1988a and 1988b), Hirsch (1988 and 1990), Tan (1992) and Vreugdenhil (1994) among others.

In this chapter a method is selected to solve a set of PDE's for one-dimensional changes in hydraulics and morphology in sub-, trans- and supercritical flows. The objective is to solve numerically a set of PDE's that represents highly non-uniform (or even discontinuous) flows with changing flow regimes. The hyperbolic character of the mathematical model and the type of computations to be performed, determine the selection of the solution method.

One of the merits of finite-elements methods is an accurate description of topography. However, in this study one-dimensional models are considered only, hence, a finite-difference method will be applied.

Although simultaneous solution of all variables brings forward high computation costs, conditions prevailing in mountain rivers (non-uniform flow with different flow regimes, relatively fast morphological changes), reduce the benefits of simplified, non-simultaneous solution procedures (Chapter five).

For the solution procedure, the *Godunov* method (Godunov, 1959) is used in a modified form (e.g. Savic, 1991). The application of this method will be motivated in Section 7.2 by giving a brief review of numerical methods for flows with mixed regimes. In Section 7.3, the structure of the numerical model is described. Some details on interpolation procedures are presented in Section 7.4, the treatment of boundaries are added in Section 7.5.

Applications of the model can be found in Chapters three, four and six.

7.2. Selection of numerical solution method.

7.2.1. Method of characteristics.

In rivers with non-uniform slopes and widths, alternating sub- and supercritical flows can be observed. As described in Chapter two, in the range of subcritical, transcritical and supercritical flow, solutions change significantly. To simulate all these conditions of flow, a high claim is made on the numerical modelling procedures.

A solution of the complete set of characteristic equations (celerities and compatibility equations) represents the highest level of mathematics (and hence the represented physics) to be introduced in numerics. Then, both the *direction* and *type* of information flow through a computation domain is accounted for properly, and the resulting model performs with equal quality in different flows regimes.

For discontinuous flows, the method of characteristics can be used in combination with shock-fitting algorithms (e.g. Terzides and Strelkoff, 1970; Sakkas and Strelkoff, 1973; Katopodes and Strelkoff, 1978). In the shock-fitting method (Subsection 6.4.2), shocks are isolated from the continuous flow domain, and treated by a local-integral approach.

One of the consequences of this exact solution is adjustment of the grid to the type of flow; at multiple discontinuities (which can be expected when including multiple variables), the result will be a complicated grid. The frame changes into an irregular topography with changing densities at variable and unknown locations. The resulting computation costs will be high.

An alternative method is to solve characteristic equations in a fixed grid (e.g., Courant *et al.*, 1952; Lister, 1967; Jolly and Yevjevich, 1974; Yevjevich, 1975; Lai, 1976). Points along a characteristic are interpolated from neighbouring grid points. The advantage of a convenient grid in complicated conditions of flow is reduced by the introduction of errors relative to the method of characteristics, due to the intergrid-interpolation. These errors can be examined by comparing numerical and analytical solutions (Subsection 7.3).

However, when using characteristic equations, a mathematical model in divergent form is used. As described for example by Abbott (1974), this induces errors with respect to mathematical models in conservative form (Subsection 6.4.3). Hence, a numerical model based on PDE's in divergent

136

form alone will not be strictly conservative. Because one of the objectives is modelling of discontinuous flows, a conservative numerical method must be used. Therefore, finite-difference methods are considered.

7.2.2. Finite-difference methods.

Finite-difference methods have been applied widely with numerous types of difference schemes, either explicit or implicit. The merit of the latter class of methods is the application of larger time steps. However, because non-uniform and discontinuous flows will be considered, the applied time steps are limited by accuracy, which reduces the advantage of implicit methods (e.g. Finlayson, 1992).

A review of some numerical methods for hydrodynamic models can be found in Fennema and Chaudhry (1986, 1987, 1990). Two categories can be distinguished: *central-based* schemes (no distinction of up- and downstream influences) and *upwind* schemes that distinguishes the direction of propagating waves through the model.

In transcritical and supercritical flows, changes in celerities and changes in information that is transferred along characteristics (Subsection 2.4.1) are significant. Therefore, the direction of information-transfer through a mathematical model should correspond with the orientation of the difference scheme. Because the type of information that is transferred along a characteristic changes with flow regime, finite-difference methods are often limited to a specified range of *Fr* values.

upwind schemes

Because positive and negative celerities can be found in mobile-bed models, application of pure *upwind* schemes, that consider information from upstream locations only, is not possible. An alternative would be to use alternating difference directions for predictor and corrector steps, as suggested by MacCormack (1969). To obtain a good representation of non-uniform or discontinuous solutions, sequences of difference-direction in this method should be in correspondence with the direction of wave-propagation (e.g., Kutler, 1975; Garcia and Kahawita, 1986; Jiménez and Chaudry, 1988). This can induce difficulties when describing flows with mixed regimes (Garcia-Navarro and Saviron, 1992).

central-based schemes

In that respect, *central-based* difference schemes do seem more appropriate, since contributions from both up- and downstream locations are accounted for. However, these schemes do not explicitly account for changes in characteristic equations that can be observed in transcritical flow (Subsection 2.4.1). In non-uniform or discontinuous solutions, central-based schemes will generally be more dissipative (LeVeque, 1990).

Since both types of differencing have disadvantages that can affect the numerical solution, other techniques should be considered.

flux-splitting methods

For models of flows with fixed-beds, a change of sign in celerity at critical flow can be observed. In that case, a very valuable and effective extension to the "common" finite-difference schemes is to relate the direction of difference to the sign of the characteristics (*flux-splitting* methods, e.g. Steger, 1978; Moretti, 1979, Gabutti, 1983). However, because no change in sign of celerity consists in mobile-bed models, this method cannot be applied.

flux-difference methods

An alternative technique classified as *flux-difference* splitting methods concerns the use of both celerities and compatibility equations in the difference algorithm. An example is the *Godunov* method (Godunov, 1959), where the solution of characteristic equations in a predictor step enables proper determination of mass and momentum fluxes in the conservative corrector step.

Because this method takes into account changes in the type of information that is transferred along a celerity, it can be applied to mobile-bed models with mixed flow regimes. It is noted that for mobile-bed models, the elegance of the method is paid for with computation costs.

The *Godunov* method as applied in this study is described in Section 7.3.

138

7.3. Application of the *Godunov* method.

7.3.1. Introduction.

Probably due to computation costs and the analogy between gasdynamics and fixed-bed hydraulics, the application of the *Godunov* method has been restricted to fixed-bed models only (e.g. Botev, 1991; Savic and Holly, 1991; Savic, 1991; Alcrudo and Garcia-Navarro, 1993).

For application to discontinuous phenomena in gas dynamics, Godunov (1959) suggested to transform the time-integration problem of fluxes at cell boundaries to a spatial-integration problem with the help of the theory of characteristics. This implies that changes in *time* are determined from *spatial* gradients by solving the compatibility equations.

The use of spatial gradients requires knowledge on intergrid distributions. In the method proposed by Godunov (1959) a piecewise uniform distribution of variables over an interval Δx around a grid point was assumed. This results in a sequence of small discontinuous states, with a Riemann problem to be solved at the cell boundary. The resulting numerical scheme is of first-order accuracy (Richtmyer and Morton, 1967) and has dissipative properties (Colella *et al.*, 1983; Savic, 1991).

The implementation of the Riemann problem in the *Godunov* method yields a relatively high accuracy but complicates the algorithm. In the original *Godunov* scheme, the solution of the compatibility equations (or Riemann variants) was exact, using an iteration procedure. The speed up the algorithm, approximate Riemann solvers have been developed since (e.g., Roe, 1981; Vila, 1986 and 1987; Glaister, 1988).

The mathematical model in conservative and divergent form, that is used to describe sub-, trans- and supercritical flows with mobile bed and sediment mixtures has been described in Chapter two. The conservative form is used in the corrector step. The corresponding difference equations are given in Appendix B. The divergent form (or characteristic equations) is solved in the predictor step.

7.3.2. Structure of the model.

The method consists of a predictor and corrector step, as will be described briefly.

139

A system of PDE's in conservative form can be represented as

$$\frac{\partial U}{\partial t} + \frac{\partial F}{\partial x} - S = 0 \qquad (7.1)$$

To obtain a difference equation, Eq.7.1 must be integrated over a time interval Δt and a space step Δx. This yields

$$\int_{t}^{t+\Delta t} \int_{x}^{x+\Delta x} \left[\frac{\partial U}{\partial t} + \frac{\partial F}{\partial x} - S \right] dxdt = 0 \qquad (7.2)$$

For convenience, it is used (Figure 7.1)

$$t = t^n \quad ; \quad t + \Delta t = t^{n+1} \quad ; \quad x = x_{j-1/2} \quad ; \quad x + \Delta x = x_{j+1/2} \qquad (7.3)$$

Eq.7.2 can be rewritten as

$$\int_{x}^{x+\Delta x} \left[U^{n+1} - U^n \right] dx + \int_{t}^{t+\Delta t} \left[F_{j+1/2} - F_{j-1/2} \right] dt - \int_{t}^{t+\Delta t} \int_{x}^{x+\Delta x} S \, dxdt = 0 \qquad (7.4)$$

Now, time-averaged values of fluxes F, space-averaged values of storage terms U and time- and space-averaged values of source S must be introduced. This, however, requires information on the intergrid distribution. Hence, to determine the time-averaged values of F, intergrid variables P^* are used at a new time level $t = t^n + \Delta t/2$ (Figure 7.1).
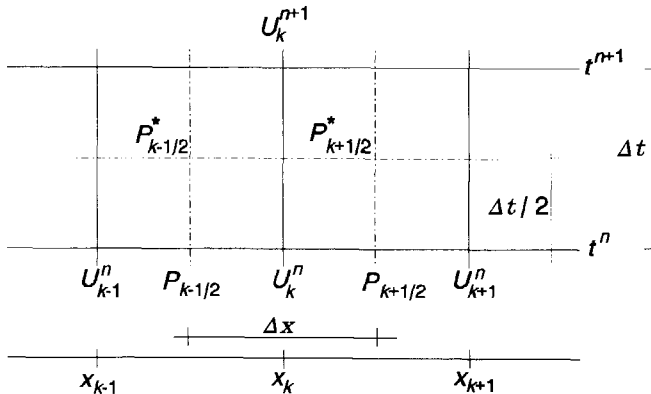
Fig.7.1 Grid points for predictor and corrector.

For a good determination of these intergrid variables $P^*_{k-1/2}$ and $P^*_{k+1/2}$ at $x_{k-1/2}$ and $x_{k+1/2}$, a predictor step is applied. This predictor step is described in the following subsection. Now, with the help of these predictor variables, time-integrated fluxes can be approximated. It is assumed that the flux at $t = t^n + \Delta t/2$ represents the time-averaged flux for the interval Δt (Fryxell *et al.*, 1986; Vila, 1987; Savic, 1991).

$$\int_t^{t+\Delta t} \left[F_{k+1/2} - F_{k-1/2}\right] \, dt = \Delta t \left(F^*_{k+1/2} - F^*_{k-1/2}\right) \qquad (7.5)$$

Solution of the subsequent difference equation (Appendix B) completes the corrector step.

7.3.3. Predictor step.

The predictor step consists of solving the characteristic equations with a fixed grid. Originally, Godunov (1959) assumed a constant, piecewise distribution in a zone around a grid point. Then, by solving a Riemann problem for each zone, changes in variables (and subsequent fluxes) at the zone-boundary can be determined. This can be illustrated as follows.

As described in Section 2.3., the linearized mathematical model can be transformed into characteristic equations represented as

$$\frac{\partial W_i}{\partial t} + c_i \frac{\partial W_i}{\partial x} = O_i \qquad (7.6)$$

where W_i are equivalent Riemann invariants defined for celerity c_i. In discretized form, this results in

$$W^*_{i\,k+1/2} = W^n_{i\,k+1/2} - \Delta t \, c_i \, \frac{\Delta W_i^+}{\Delta x} + \Delta t \, O_i \quad \text{if} \quad c_i < 0$$

$$\hspace{10cm} (7.7)$$

$$W^*_{i\,k+1/2} = W^n_{i\,k+1/2} - \Delta t \, c_i \, \frac{\Delta W_i}{\Delta x} + \Delta t \, O_i \quad \text{if} \quad c_i > 0$$

Hence, with gradients in W_i along x at $t = t^n$, changes in W_i at $x = x_{k+1/2}$ along t can be determined. To obtain the spatial gradients in W_i, intergrid-distribution functions must be assumed (Section 7.4). For the solution of W_i, compatibility equations in difference form must be used. Since these are formulated in

implicit form, the solution can be obtained iteratively with a Newton-Raphson procedure (e.g. Press *et al.*, 1992).

7.4. Interpolation procedure.

7.4.1. Introduction.

Because the characteristic equations are applied to a fixed grid, this requires the assumption of an intergrid distribution for $P(\sigma)$ at time level $t = t^n$ (Figure 7.2). Different options are analysed for $P(\sigma)$, where σ represents the Courant-Friedrichs-Lewis stability number defined as $\sigma_i = c_i \Delta t / \Delta x$.
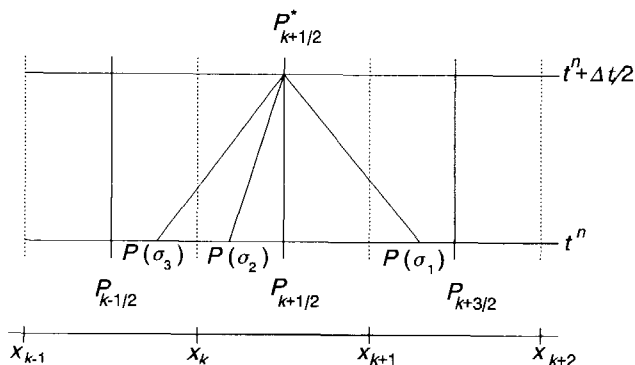
Fig.7.2 Solution of characteristic equations.

With respect to the *Godunov* method, the interpolation procedure has become more and more sophisticated. A review of this development can be found in Savic (1991). Godunov (1959) used a piecewise constant distribution, yielding a first-order difference scheme. Van Leer (1979) introduced a linear interpolation yielding a second-order accurate difference scheme, and Woodward and Colella (1984) used a piecewise-parabolic interpolation which yielded a third-order accurate difference scheme in case of continuous solutions. Obviously, solution algorithms expand with increasing accuracy.

The type of interpolation affects the solution differently at varying flow regimes; in a *linearized* set of characteristic equations, contributions of first and second-order gradients to solutions were found to vary with Fr (Sieben, 1996). The effect of the order of interpolation on accuracy can be illustrated as follows. For continuous flows, the variable P can be written with a Taylor series expansion.

$$P(\sigma) = P_k + \frac{(1-\sigma)}{2}\Delta x \frac{\partial P}{\partial x} + \frac{(1-\sigma)^2}{4}\frac{\Delta x^2}{2}\frac{\partial^2 P}{\partial x^2} + \frac{(1-\sigma)^3}{8}\frac{\Delta x^3}{6}\frac{\partial^3 P}{\partial x^3} \quad (7.8)$$

For $\sigma \approx 1.0$, assuming a constant distribution would be sufficient. However, in mobile-bed models, multiple σ values occur with a wide range of magnitude. With large differences in σ, large differences in accuracy are introduced.

If, for linear interpolations, the gradient in P can be approximated as

$$\frac{\partial P}{\partial x} = \frac{P_{k+1} - P_{k-1}}{2\Delta x} + \frac{\Delta x^2}{3}\frac{\partial^3 P}{\partial x^3} + .. \quad (7.9)$$

Substitution into Eq.7.8 yields

$$P(\sigma) - P_k + \frac{(1-\sigma)}{4}\left(P_{k+1} - P_{k-1}\right) + \frac{(1-\sigma)^2}{4}\frac{\Delta x^2}{2}\frac{\partial^2 P}{\partial x^2} + .. \quad (7.10)$$

However, in case of non-uniform or discontinuous solutions, artificial averaging (or flux limiting) should be applied to this "central-based differencing". An alternative is to distinguish different distributions of variables in up- and downstream zones. If gradients are approximated as

$$\frac{\partial P}{\partial x} - \frac{P_k - P_{k-1}}{\Delta x} + \frac{\Delta x}{2}\frac{\partial^2 P}{\partial x^2} - \frac{\Delta x}{6}\frac{\partial^3 P}{\partial x^3} + .. \quad (7.11)$$

then, the interpolated value of P is

$$P(\sigma) = \frac{(1+\sigma)}{2}P_k + \frac{(1-\sigma)}{2}P_{k-1} + \frac{(\sigma^2-1)}{4}\frac{\Delta x^2}{2}\frac{\partial^2 P}{\partial x^2} + .. \quad (7.12)$$

For the different options ("central averaging" Eq.7.10 and "up- and downstream separation" Eq.7.12), second-order terms appear with different signs and order.

However, the order of approximation of the intergrid distribution alone, is not representative for the total accuracy of the method (predictor and corrector). Therefore, another analysis must be performed. The alternatives for variable distribution for $x_k \leq x \leq x_{k+1}$ studied in this report are illustrated in the following figures.

Fig.7.3-a Uniform-separate.
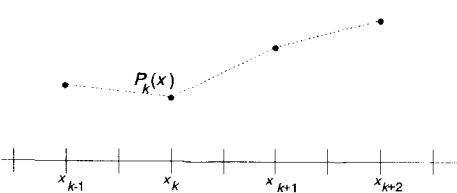
Fig.7.3-b Linear-central.
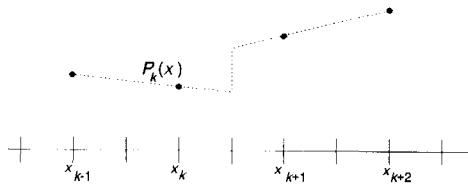
Fig.7.3-c Linear-separate.
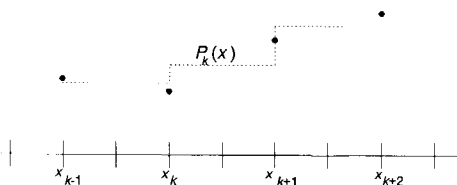
Fig.7.3-d Uniform-central.

7.4.2. Von Neumann analysis.

To analyse the stability and accuracy of different intergrid interpolation-functions in the *Godunov* method, exact and numerical solutions should be compared. For this purpose, a simplified model is used to indicate the effect of different interpolations. It is noted that discrepancies exist between the simple model analysed here, and the mobile-bed model.

Consider an advective transport process of a quantity c in a medium with uniform velocity u. The corresponding PDE for the continuity can be written as

$$\frac{\partial c}{\partial t} + u \frac{\partial c}{\partial x} = 0 \tag{7.13}$$

With the proper initial conditions, this model can be solved analytically. With the Von Neumann analysis, this analytical solution can be compared with the solution of a finite-difference model (Vreugdenhil, 1989). This gives information on stability and diffusion of the numerical scheme. The solution of a finite-difference model is given as

$$c(t=t^{n+1}, x=x_k) = \rho \, c_0 \, e^{i \, n\beta\Delta t} \, e^{i \, k\alpha\Delta x} = \rho \, c(t=t^n, x=x_k) \tag{7.14}$$

144

The multiplification factor is a complex number that introduces growth or decline of amplitudes (stability) and differences in propagation rate (diffusion). For different interpolation procedures, stability and diffusion can be compared; different intergrid distributions are used to solve c_r^* (at $x=x_{k+1/2}$ and $t=t^n+\Delta t/2$) and c_l^* (at $x=x_{k-1/2}$ and $t=t^n+\Delta t/2$) from the characteristic equations.

In the corrector step, changes in c are found with

$$c_k^{n+1} = c_k^n - \sigma\left(c_r^* - c_l^*\right) \quad ; \quad \sigma = \frac{u\Delta t}{\Delta x} \tag{7.15}$$

Method I: uniform-separate.

The first option is to assume a constant distribution conform the original Godunov (1959). This yields an upwind-based difference scheme for the predictor step. The predicted variables c_r^* and c_l^* are defined as

$$c_r^* = c_k^n \quad ; \quad c_l^* = c_{k-1}^n \tag{7.16}$$

Hence, the multiplification factor is

$$\rho = 1-\sigma[1-\cos(\alpha\Delta x)] - i\sigma\sin(\alpha\Delta x) \tag{7.17}$$

Method II: uniform-central.

An alternative option is a central-based difference scheme

$$c_r^* = \frac{c_{k+1}^n + c_k^n}{2} \quad ; \quad c_l^* = \frac{c_k^n + c_{k-1}^n}{2} \tag{7.18}$$

Then, ρ is

$$\rho = 1 - i\sigma\sin(\alpha\Delta x) \tag{7.19}$$

Because the amplitude of ρ is larger than unity, this method is instable.

Method III: linear-separate.

The second class of interpolation methods result when a linear distribution is

assumed, as suggested by Van Leer (1979). This yields for the predictor step

$$c_r^* = \frac{\left(3c_k^n - c_{k-1}^n\right)}{2} + \frac{\sigma}{2}\left(c_{k-1}^n - c_k^n\right) \quad ; \quad c_l^* = \frac{\left(3c_{k-1}^n - c_{k-2}^n\right)}{2} + \frac{\sigma}{2}\left(c_{k-2}^n - c_{k-1}^n\right) \tag{7.20}$$

After application of the corrector step, ρ can be found

$$\rho = 1 - \frac{\sigma(3-\sigma)}{2} - \sigma\left[(\sigma-2)\cos(\alpha\,\Delta x) - \frac{(\sigma-1)}{2}\cos(2\alpha\,\Delta x)\right] +$$

$$+ i\sigma\left[(\sigma-2)\sin(\alpha\,\Delta x) - \frac{(\sigma-1)}{2}\sin(2\alpha\,\Delta x)\right] \tag{7.21}$$

Method IV: linear-central.

An alternative formulation is obtained when applying a central-based interpolation.

$$c_r^* = c_{k+1}^n \frac{(1-\sigma)}{2} + c_k^n \frac{(1+\sigma)}{2} \tag{7.22}$$

The corresponding amplification factor is

$$\rho = 1 - \sigma^2[1 - \cos(\alpha\,\Delta x)] - \sigma i\sin(\alpha\,\Delta x) \tag{7.23}$$

From the amplitude of ρ it can be concluded that this interpolation form yields instable results.

A third class of interpolation procedures results when a second-order or parabolic distribution is applied (Colella and Woodward, 1984). For continuous flows, this raises the order of accuracy. However, for short waves (such as discontinuous solutions) monotonicity algorithms to avoid artificial over- and undershoots must be introduced that reduce again the order of accuracy of this method. Therefore, this relatively complicated interpolation procedure is not considered here.

An indication of accuracy can be given by comparing propagation rates in numerical and analytical solutions. The ratio of propagation rates for methods I and III are presented in Figure 7.4, the amplification factor is shown in Figure 7.5.

146

The accuracy of linear interpolation (method III) and the uniform distribution (method I) are comparable, with a slightly better performance for the linear distribution. To enable a proper selection, some numerical tests of both methods are added in Subsection 7.4.3.
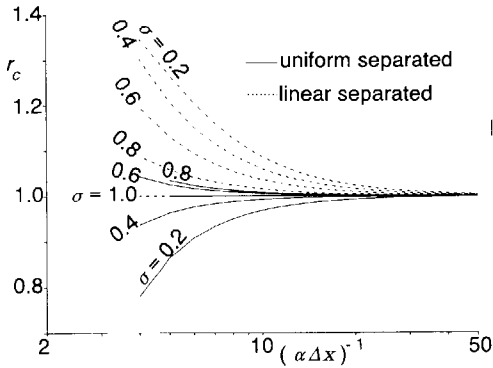
Fig.7.4 Ratio of propagation rates.   **Fig.7.5** Amplification factor.
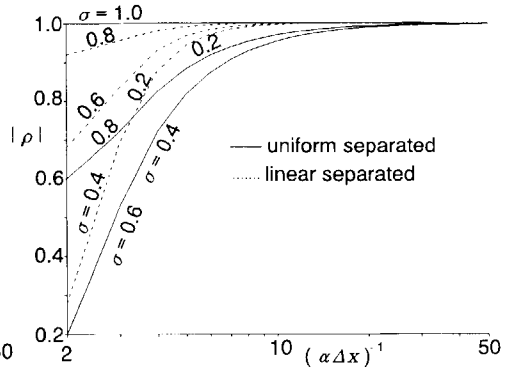
7.4.3. Discontinuous solutions at fixed beds.

As can be concluded from the Von Neumann analysis in the previous section, the effect of different interpolations is most significant at waves with short lengths. Therefore, discontinuous solutions for different intergrid-distributions are compared. In the following examples, referred to as Case I and Case II, friction and slope effects are neglected, which implies that no *physical* dissipation is present. Analytical solutions, if present, are added with broken lines.

The propagation rate w of the shock can be found with

$$w = u_1 \pm \sqrt{-g_z \frac{a_2}{a_1} \frac{(a_1 + a_2)}{2}} \qquad (7.24)$$

where the subscripts 1 and 2 refer to the states, up- and downstream of the shock (e.g. Chow, 1959).

Case I. positive surge

Due to an increase in discharge from 1 m³/s to 2 m³/s, a downstream-

147

propagating shock develops. Depths changes from 0.91 m to 1.31 m. The space step is $\Delta x = 0.20$ m, which can be considered relatively large. Now, three interpolation functions are tested to obtain P.

method I: uniform-separate.

The first is a piecewise constant distribution.

$$c < 0 \quad \rightarrow \quad P(\sigma) = U_{k+1} \quad ; \quad c > 0 \quad \rightarrow \quad P(\sigma) = U_k \quad ; \quad \sigma = \frac{c\Delta t}{\Delta x} \quad (7.25)$$

method II: linear-central

The second option is a linear distribution, with gradients determined by a "central-based" approximation

$$c < 0 \quad \rightarrow \quad P(\sigma) = U_{k+1} - \frac{\sigma}{2} \left(U_{k+2} - U_k\right)$$

$$(7.26)$$

$$c > 0 \quad \rightarrow \quad P(\sigma) = U_k - \frac{\sigma}{2} \left(U_{k+1} - U_{k-1}\right)$$

method III: linear-separate

The third option is again a linear distribution, with a complete separation of upstream and downstream parts of the domain of dependance.

$$c < 0 \quad \rightarrow \quad P(\sigma) = U_{k+1} - \sigma \left(U_{k+2} - U_{k+1}\right)$$

$$(7.27)$$

$$c > 0 \quad \rightarrow \quad P(\sigma) = U_k - \sigma \left(U_k - U_{k-1}\right)$$
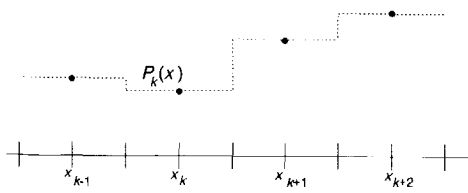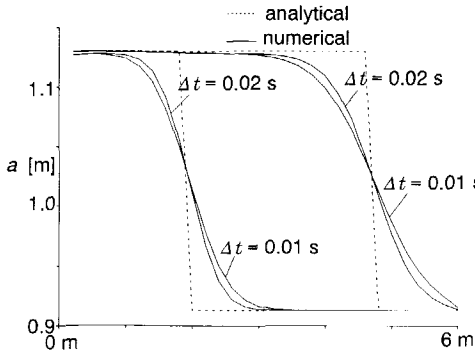
Fig.7.6-a Uniform-separate.
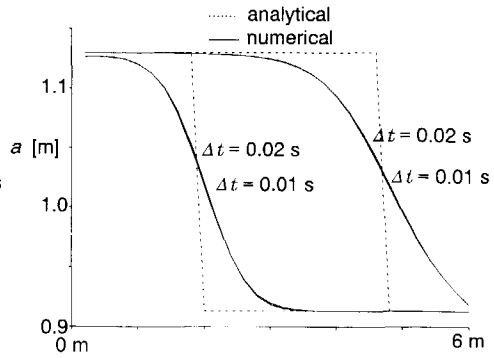
Fig.7.6-b Linear-central.
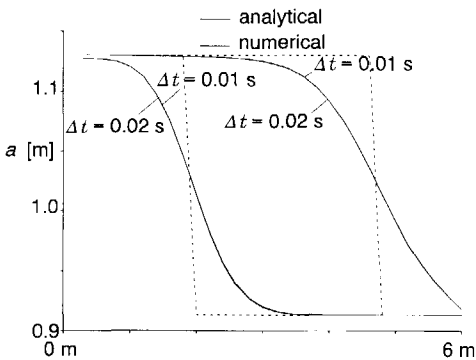
Fig.7.6-c Linear-separate.
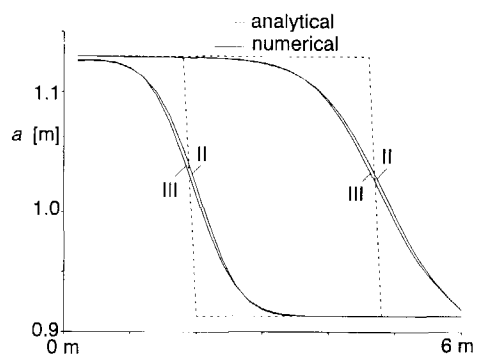
Fig.7.6-d Central and separate.

From these figures, some conclusions can be drawn. If a piecewise-uniform distribution (option I) is used, the numerical diffusion is more or less constant for varying Δt. Hence with an increasing number of time steps, the total diffusion increases.

If a linear distribution is assumed, the numerical diffusion will reduce almost linearly for smaller times steps. As a result, the solution after N time steps of Δt resembles the solution after $2N$ time steps of $\Delta t/2$. Hence, applying a linear distribution improves the performance.

Case III dambreak wave

A combination of a positive shock wave and a negative expansion wave occurs in the similarity solutions for dam-break waves. Analytical solutions concerning linearized models are due to Ritter (1892) or Stoker (1957). These solutions

149

refer to an initial state with zero velocity. Because this condition is not implemented in the numerical model, a proper comparison with analytical solutions is not possible.

Again, the different interpolation methods are compared. In the initial situation, a discharge of 1 m³/s flows through two zones with depths of 1.91 m and 0.91 m. The space step is 0.20 m for all examples. The shock-wave part of the solution, with the corresponding depth and velocity are conform Eq.7.24.
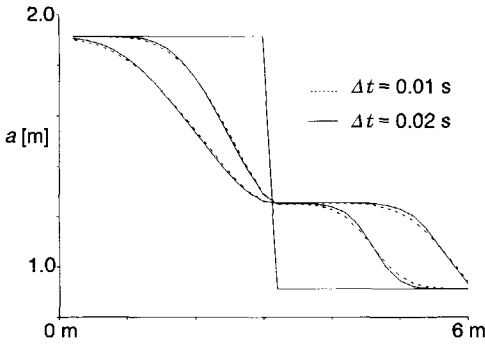
Fig.7.7-a Uniform-separate.
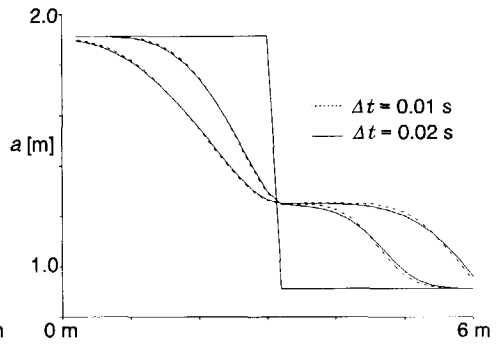
Fig.7.7-b Linear-central.
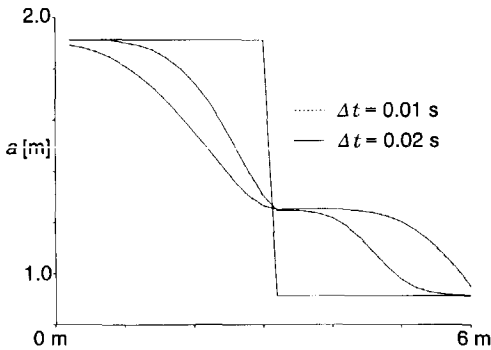
Fig.7.7-c Linear-separate.
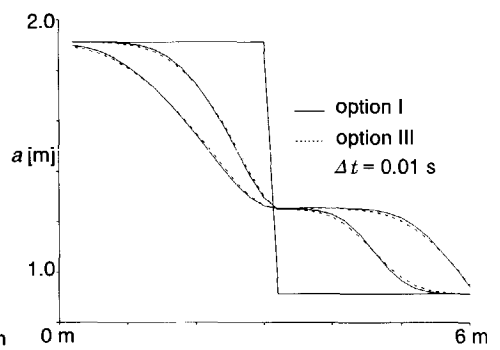
Fig.7.7-d Linear and uniform.

Again, the sensitivity to Δt is minimal in method III. Because the total diffusion is constant for varying Δt in case of interpolation according to method III, this will be selected for application.

7.4.4. Discontinuous solutions at mobile beds.

An important aspect with respect to interpolation procedures, concerns the difference between models for fixed and mobile beds. The effect of morphology on flow acts via the bed pressure that is introduced as a boundary condition when the three-dimensional PDE's are integrated over the depth.

In characteristic equations of fixed-bed models, this term acts as a source similar to friction, which is usually integrated over up- *and* downstream parts of the domain of dependance. In characteristics equations of mobile-bed models, this term is interpreted as a flux, that should be integrated based on either up- *or* downstream parts of the domain of dependance. The latter requires an explicit separation of up- and downstream bed levels, with possibly a discontinuous distribution of variables over the domain of dependance. The former implies a continuous distribution over the entire domain of dependance.

If a river bed with stable parts is considered, both fixed- and mobile-bed conditions occur. Then, one of the celerities can become zero, and the bed level is undetermined. This induces instable numerical solution procedures. Therefore, if a bed level is (locally) stable, intergrid distributions of bed level are assumed to be continuous and linear over the domain of dependance.

The stable interpolation options I (uniform distribution) and III (linear distribution) are compared for a mobile-bed case and different values of Fr.
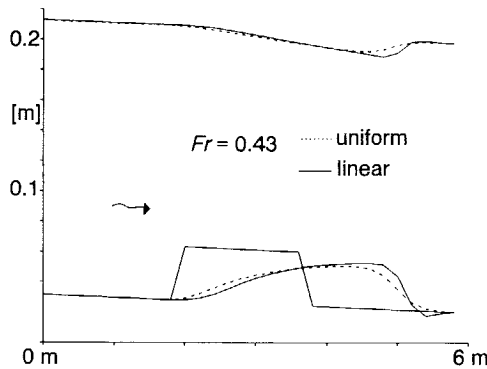
Fig.7.8 Subcritical flow.
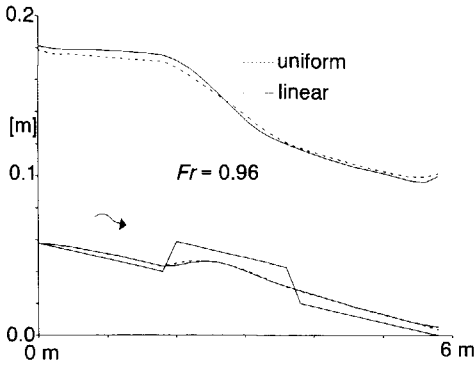
Fig.3.9 Transcritical flow.   **Fig.7.10** Supercritical flow.
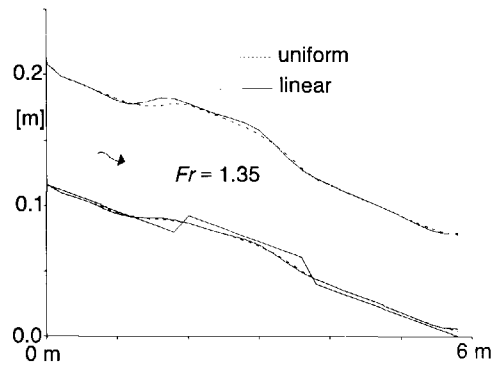
At all flow regimes, the difference between both distributions becomes effective at discontinuous flows. Then, the uniform distribution introduces significant diffusion. In case of a strong shock wave, the linear distribution appears to stabilize the discontinuous solution by suppressing secondary, parasitic waves. This can be observed in Figure 7.11, where the deformation of a trench in transcritical flow is represented.
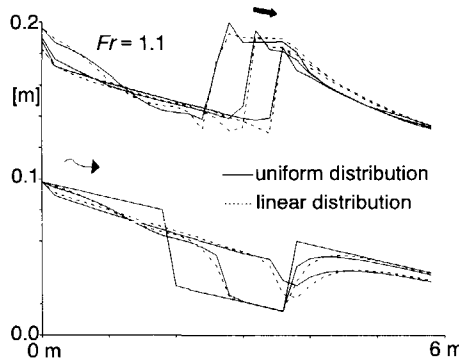
Fig.7.11 Transcritical flow.

7.5. Boundary conditions.

7.5.1. Introduction.

The solution of the system of PDE's is carried out in two steps (Section 4.5). For both steps, additional information at the boundaries of the computation domain is required in the form of boundary conditions. These conditions can be of a Dirichlet or Neumann type, and must be formulated with the variables used

152

in the model.

For the predictor step, where primitive variables are used, this information should concern values of a, u, z_b etc. In general, however, conservative quantities such as discharge and sediment transport are used. The transformation of conservative quantities to primitive variables is often enabled with linearization procedures.

In the corrector step, fluxes are used at cell boundaries. At the boundaries, the problem is to determine variables P^*, outside the computation domain (Figure 7.12). Hence, to enable the use of a double grid (one for the predictor and one for the corrector), fictitious points with variables U_{ub} and U_{db} are introduced (Figure 7.12). This enables solution of characteristic equations at the boundaries, and subsequent determination of P^* and the time-averaged fluxes for the corrector step.
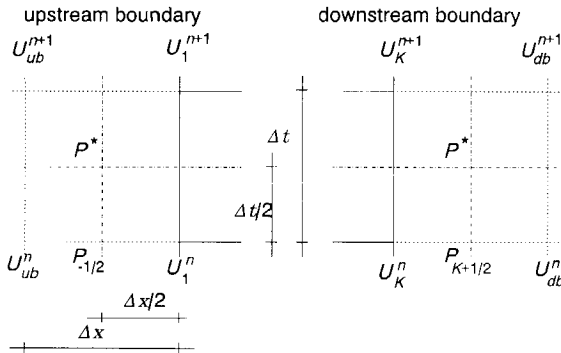
Fig.7.12 Fictitious points at boundaries.

The required boundary conditions can be prescribed at the additional grid points. The information originating from these points is transferred by characteristic equations into the computation domain.

In Subsection 7.5.2, the numerical procedure is described to perform the predictor and corrector step at the boundaries of the computation domain.

7.5.2. Characteristics-extrapolation method.

The introduction of fictitious points enables the determination of time-averaged mass and momentum fluxes, as described in the previous section. In this section, the procedure applied to solve U_{ub} and U_{db} is described.

153

At the upstream boundary, the characteristic equation that corresponds with the upstream-directed characteristic ($c_1 < 0$) is used to determine variables U^*_1 at an intergrid point (Figure 7.13).

In difference form, this characteristic equation can be written as

$$T_1^T \left(U_1^* - U_1^{n-1} \right) = \Delta t \, S_1 \tag{7.28}$$

with T a vector containing the coefficients and S the source term of the compatibility equations. The boundary conditions are described with U_{ub}.
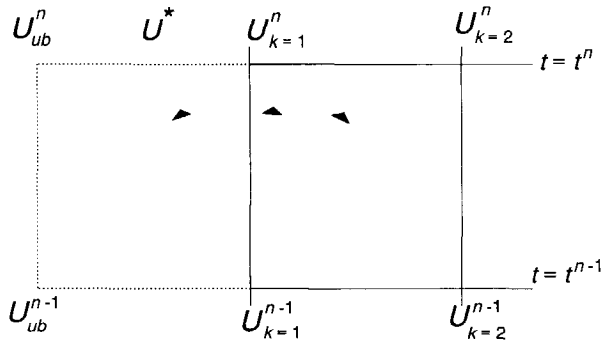
Fig.7.13 Extrapolation at upstream boundary.

The variables U^*_1 and U_{ub} can be related to other variables at t^n by extrapolation techniques. Therefore, the method can be called a *characteristic-extrapolation technique* (Hirsch, 1990). With a Taylor-polynomial approach, gradients in variables at the boundary can be approximated as

$$\frac{\partial U}{\partial x}\bigg|_{k-1} = \frac{U_{k=2}^n - U_{ub}^n}{2\Delta x} \tag{7.29}$$

Linear interpolation yields for the intergrid point

$$U_1^* = U_{k=1}^n + c_1 \Delta t \, \frac{\partial U}{\partial x}\bigg|_{k-1} = U_{k=1}^n + \frac{c_1 \Delta t}{2\Delta x} \left(U_{k=2}^n - U_{ub}^n \right) \tag{7.30}$$

This linearization can cause instable conditions if steep waves propagate through the boundaries. In that case, a uniform distribution for the intergrid point will be more robust.

After elimination of U^*_1 at the intergrid point, the variables U_{ub} at the fictitious boundary can be written explicitly as

$$-\frac{c_1 \Delta t}{2 \Delta x} T_1^T U_{ub}^n = \Delta t \, S - T_1^T \left(U_{k-1}^n - U_{k=1}^{n-1} \right) - \frac{c_1 \Delta t}{2 \Delta x} T_1^T U_{k=2}^n \quad (7.31)$$

Now, one equation is formulated for the upstream boundary. In case of suspended load with N fractions, $2N+1$ complementary boundary conditions must be supplied.

A similar procedure can be carried out for the downstream boundary. With suspended load consisting of N fractions, $2N+1$ outgoing characteristic equations exist, and only one boundary condition must be supplied. Solution of the $2N+1$ characteristic equations yields the variables U_j^*.

$$T_j^T \left(U_j^* - U_K^n \right) = \Delta t \, S_j \quad (7.32)$$

with $j = 2,\ldots,2N+1$. In Figure 7.14, only two outgoing characteristic equations are indicated $(N=1)$.
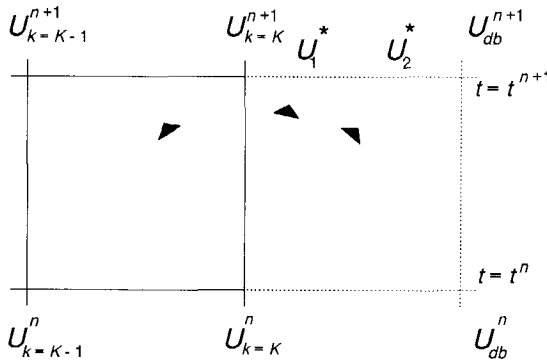
Fig.7.14 Extrapolation at downstream boundary.

With the help of extrapolation, the intergrid points can be related to the variables at the neighbouring grid points.

$$U_j^* = U_{k=K}^{n+1} + \frac{c_j \Delta t}{2 \Delta x} \left(U_{db}^{n+1} - U_{k=K-1}^{n+1} \right) \quad (7.33)$$

Substitution in the characteristic equations yields

$$\frac{c_j \Delta t}{2\Delta x} T_1^T U_{db}^n = \Delta t \ S - T_j^T \left(U_{k=K}^{n+1} - U_{k=K}^n \right) + \frac{c_j \Delta t}{2\Delta x} T_j^T U_{k=K-1}^{n+1} \quad \textbf{(7.34)}$$

Chapter eight

Summary and conclusions.

8.1. Distinction of flow regimes.

Based on the behaviour of the celerities, three different types of flow regime can be distinguished for one-dimensional models with mobile bed. The categories mentioned can also be distinguished in analytical solutions of the mathematical model in linearized form, and in numerical solutions.

subcritical flow:
> For Fr numbers smaller than 0.8 approximately, bed disturbances propagate along one, downstream directed celerity mainly.

supercritical flow:
> For Fr numbers larger than 1.2 approximately (supercritical flow), bed disturbances again propagate along one celerity mainly, but now in upstream direction.

transcritical flow:
> In the transition regime of approximately $0.8 < Fr < 1.2$ (transcritical flow), bed disturbances propagate both in up- and downstream directions, along celerities with comparable magnitude. The latter results in solutions with a diffusive behaviour.

The general correspondence with downstream-propagating dunes in subcritical flows, upstream-propagating antidunes in supercritical flows and a washout of bed forms in transitional regimes is noted.

It is noted that the rather straightforward distinction of categories refers to one-dimensional models. The characteristic equations of a two-dimensional, depth-averaged model have been studied briefly. For values of Fr, larger than approximately 0.6, a significant part of the characteristic surfaces becomes sensitive to the mobility of the bed. This indicates a strong coupling between changes in flow and morphology. In critical and supercritical flow, bicharacteristics related to bed-level changes can be found, that are directed in both upstream *and* downstream directions. Apparently, at these flow regimes, transversal morphological changes, which are strongly coupled to changes in flow, can contribute to changes in longitudinal directions.

This effect is omitted in one-dimensional models, which indicates that solutions of one-dimensional and two-dimensional morphological models can deviate at supercritical flows, in case of conditions with distinct effects of two-dimensionality. This discrepancy of one- and two-dimensional models can be recommended for further research. As a start, an harmonic analysis of a two-dimensional model in linearized form is suggested.

8.2. Boundary conditions.

In mobile-bed models, celerities have non-zero values for all values of Fr. This implies that in contrast with fixed-bed models, the number of conditions at upstream and at downstream boundaries is constant for all regimes of flow. The number of conditions for different models are indicated in the table.

boundary	bed composition (with N size fractions)			
	constant		variable	
	total load	suspended + bed load	total load	suspended + bed load
downstream	1	1	1	1
upstream	2	3	$N+1$	$2N+1$

Table 8.1. number of boundary conditions

The selection of the type of boundary conditions is determined by the prototype boundary conditions and limited by conditions of global and local consistency. The first requires consistent conditions at up- and downstream boundaries, the second refers to consistency of boundary conditions and neighbouring grid points. An indication of the latter can be made by analysing the characteristic equations that transfer in- and outgoing information. Based on this analysis, Table 2.1 has been composed.

downstream boundary

In general, prescription of depth of flow, directly or indirectly via a stage-discharge curve, can be expected to perform well for subcritical flows. Prescription of bed level is appropriate in supercritical flows, and to a certain extend in transcritical flows. Hence, a combination of both, prescription of free surface level, can expected to be consistent at all flow regimes.

158

At the upstream boundary, discharge and sediment transport should be specified in any case. Sediment transport (either a single quantity for total load of bed material, or distincted values for suspended and bed load), includes both composition and rate. However, with respect to model variables, (depth, velocity and bed level) some options consist. For subcritical flow regimes, prescription of bed level and velocity is appropriate. For transcritical and supercritical flows, the depth of flow and velocity should be combined.

8.3. Sediment mixtures.

Via differences in particle mobility, the gradation of grain sizes affects the solution of mathematical models. For example, for problems with short length-scales, morphological models with uniform sediment approach a simple-wave model, models with mixtures approach a telegraph model. For problems with large length-scales, a parabolic model is found for uniform-sediment models, whereas for sediment mixtures, a mixed parabolic / simple wave type model results.

The scale of the contribution of sediment mixtures in mathematical models for river morphology is determined by different variables, which can be combined into two, indicative parameters.

$$Y_a = \frac{\sum_{i=1}^{N}\left[f_{pi}-f_{pN}+\sum_{j=1}^{N}f_{Dj}(D_i-D_N)\right](\beta_{pi}-\beta_i^*)}{ua} \wedge \frac{a}{\delta_p} \tag{8.1}$$

grain-size frequency distribution

The parameter Y_a includes effects of the

    a) difference in grain-size frequency distribution of vertical fluxes, into and out of the reference layer at the surface of the river bed

    b) sensitivity of sediment-transport rate predictors to the composition of the reference-layer

Note that the variable β_i^* includes effects of longitudinal gradients in sediment

transport composition. The magnitude of Y_a, and subsequently the contribution of sediment gradation, decreases with increasing shear-stress level. In case of symmetric hiding corrections, the effect of gradation in normal size-frequency distributions is smaller than in case of bi-modal size-frequency distributions.

thickness of reference layer

The parameter a/δ_p is the ratio between depth of flow and the thickness of the reference layer that represents changes in composition of the river bed. For small values of this ratio, size-frequency distributions will have a minor effect on morphological changes.

The definition of a homogeneous distribution of size fractions over the reference layer implies that the period of "mixing" should be "instantaneous" relative to the regular morphological changes. This limits the applicability of layer predictors to $\delta_p/\Delta z_b << 1$, where Δz_b is the amplitude of a representative bed level change.

No general, physically based concept for the definition of the reference layer thickness exist; the magnitude of a reference layer is related to a representative length-scale L_m and amplitude Δz_b of a problem. In general, small layer thicknesses scaled with particle travel-distance are also applicable for conditions with higher values of $\Delta z_b/L_m$, whereas layer thicknesses scaled with bed-form height are only applicable for conditions with lower values of $\Delta z_b/L_m$.

With the help of a linearized model, it can be found that compositions can be considered adapted for time scales larger than $4 \mid \delta_p/w_z \mid$. In case of quasi-steady flow models, larger thicknesses, with subsequent slower changes enable using larger modelling time steps. On the other hand, if, for example, changes in composition, and subsequently roughness, during a diffusive flood wave are taken into account, values of δ_p/a smaller than or of the order of $\phi = s_b/ua$ have to be used.

8.4. Mathematical instability.

In case of erosion of a river bed with a coarse surface at a finer substratum, this coupled behaviour can cause a mathematical instability for both single- and double-layer models (Ribberink, 1987). This problem of instability is due to the elliptic character of the set of PDE's, and increases at higher values of Fr.

Stabilizing measures either concern the prevention of the conditions that allow ellipticity or elimination of the cause of ellipticity. The first category includes

- reduction of layer thickness

- reduction of vertical gradients in bed composition by definition of

  - a transitional, intermediate storage layer (Ribberink, 1987)
  - additional, diffusive sediment fluxes between transport and storage layer
  - a variable thickness of the storage layer

In this report, an alternative formulation is tested and compared with the conventional model. In this alternative concept, the composition of fluxes between bed-load layer and river bed is controlled by the composition in the bed-load layer. This enables elimination of complex celerities, which stabilizes the model. An additional variable used in the model is the velocity of grain fractions in the bed-load layer. Solutions of the conventional and stabilized model are equivalent, but quantitative differences exist. These differences concern propagation rates of changes in bed-level and composition, and are a function of particle shear-stress.

8.5. Surface coarsening.

An analytical model is derived for describing coarsening surfaces in case of a zero supply of sediment upstream. This model is based on the assumption of constant and uniform flow conditions. The solution enables prediction of time scales and equilibrium conditions. The applicability of this analytical model is restricted by the linearizations and the assumption of uniform flow.

Application to armouring experiments in flumes confirm general trends of bed-level degradation, surface coarsening and decline of transport. Fitting of solutions to experimental observations indicates that layer thicknesses in case of armouring are of the order of the largest grain size.

8.6. Simplified models.

For lowland rivers, simplified concepts for one-dimensional mathematical models of river morphology have been tested and applied extensively. Software packages for manipulations with symbolic algebra (e.g., Wolfram, 1991), and the development of computational capacity enables extension of classic analyses

to study morphological models in the highly non-linear domain of mountain river conditions.

The main aspects that are analysed in this study concern the applicability of quasi-steady and quasi-uniform flow models and the non-linear interaction between flow and morphology.

interaction of flow and morphology.

Morphological models include a mobile boundary, and a subsequent interaction between flow and river bed. The contribution of this interaction is not constant, which can be illustrated by comparing celerities of fixed-bed and mobile-bed models. The interaction appears to be negligible for

$$|1 - Fr^2| \gg \psi \qquad (8.2)$$

Because changes in flow during a time step in linearized fixed-bed and linearized mobile-bed models are equivalent, the interaction between flow and morphology is nonlinear. Hence, quasi-coupled models converge to the exact solution for decreasing non-linearity. Especially if Eq.8.2 is not satisfied, this claim significantly reduces the modelling time step.

level of unsteadiness or non-uniformity of flow.

If Eq.8.2 is satisfied, changes in flow and morphology can be determined in a decoupled manner irrespective of its wave length or period. However, this condition may be too strict when solutions with a larger length scale or time scale, and hence a lower nonlinearity are involved.

Hence, to simplify a morphological model for a mountain river, both length scale and time scale of the problem should be considered. These time- and length-scales result from initial or boundary conditions and can be expressed with the parameter E, defined as

$$E = 2 \frac{|g_z|}{C^2} \frac{L}{a} \qquad (8.3)$$

where L is a representative length-scale, that can be based on hydrograph periods or geometrical features. Obviously, quasi-steady, or quasi-uniform flow assumptions are appropriate for increasing values of E.

162

With respect to the definition of a representative length scale the following is noted. To indicate the presence of flow-dynamic effects in a river, the length of the hydrograph should be related to the river length, in order to estimate whether dynamic effects of flow are relevant. Relatively short hydrograph periods that can be observed in small and steep catchment areas, can induce rather steady discharges with negligible effects of flow dynamics if the draining river is short.

The contribution of flow-unsteadiness to the morphological model tends to decrease with respect to flow-non-uniformity, with increasing values of Fr. This implies that for transcritical and supercritical flows, time and length scales of the solution are controlled by geometrical features mainly.

Based on the analysis of the linearized model, the following indications can be made. Numerical tests correspond with the theoretical results.

quasi-steady flow

For quasi-steady flow models, the error decreases with increasing value of E, decreasing value of ψ, and changes with Fr and wave type. For $E > 10^3$, the quasi-steady flow model can be applied for all values of Fr. For lower values of E and transcritical flows, the quasi-steady flow model cannot be applied. For $E < 10^3$ and subcritical flow, the error is made in upstream-propagating waves. For $E < 10^3$ and supercritical flow, the error is made in wave-type solutions propagating downstream.

The merit of the quasi-steady flow assumption is the elimination of fast, hydraulic wave-type solutions. This yields a significant reduction in computation costs for subcritical flows. However, for transcritical and supercritical flows, rapid changes in morphology can be observed. The resulting small modelling time steps again reduce the benefit of quasi-steady flow modelling.

Additionally, the computation of backwater curves in reaches with different flow regimes may require application of relatively slow relaxation techniques, based on sets of PDE's that partially include flow dynamics. Therefore, it can be concluded that quasi-steady flow models can be applied in transcritical flow regimes, but the benefit with respect to the complete model is very small.

quasi-steady and quasi-uniform flow

The combination of quasi-steady and quasi-uniform flow assumptions yields a

simple model with low computation costs. Again, the performance of this simplified model varies significantly with Fr and E. For a small range of Fr values near unity, this model is applicable for $E > 10^3$. However, for subcritical and supercritical flows, E values should be larger than 10^5.

The performance of the quasi-uniform flow model in transcritical flows can be explained by "diffusive behaviour" of solutions in this regime. As a result, solutions of this simplified model correspond qualitatively with solutions of the complete model. However, for values of E that are too small, morphological changes are underestimated.

8.7. Discontinuous flows.

The response of flow to changes in width or bed level at higher values of Fr can be significant; most often sudden geometrical variations can be detected in short transitions of free surface level. Corresponding changes in shear stress can induce changes in sediment transport and subsequently in bed level. With respect to discontinuous flows at fixed beds, an impressive line of developments in history can be distinguished, whereas the effects of the mobility of the bed at these conditions are considered only recently.

For analysis of discontinuous solutions, shock relations and entropy conditions must be used. With respect to the latter it is concluded that the occurrence of for example hydraulic jumps at mobile beds in mathematical models are physically realistic if conditions of entropy-increase are satisfied. This implies that the time-path of the jump is limited by celerities. Because these celerities have non-zero values, a hydraulic jump cannot be steady at a mobile bed, without transversal exchange of mass and momentum at the boundaries.

A discontinuity in variables is stable (shock wave) if celerities neighbouring the time path of the discontinuity converge. Similarly, a discontinuity is unstable (expansion wave) if celerities neighbouring the time path of the discontinuity diverge. Because the propagation rate of a discontinuity is related to celerities, the behaviour of discontinuous solutions can also be classified with the three flow regimes that are distinguished; subcritical, transcritical and supercritical flows.

For all flow regimes, fast, downstream propagating discontinuities in flow variables can be distinguished that can be associated with wave III type solutions. Although morphological changes can be the cause (e.g., sudden narrowing or raise of a river section due to a land slide overload), the

164

discontinuities can be considered decoupled from the morphological variables.

For the remaining types of discontinuities (type I directed upstream and II directed downstream), distinction of "hydraulic" and "morphological" shock waves is possible in subcritical or supercritical flows only. With respect to the first category, the classic analyses of rapidly varying flow can be mentioned (e.g. Chow, 1959). With respect to the morphological discontinuities, illustrations of deformating humps and trenches have been given.

For transcritical flows, which can also develop for discontinuities of sufficient intensity, such a distinction is not possible. As a result, analyses can only be carried out numerically. In correspondence with the relevant celerities, wave types I and II have become equally import; shock waves and expansion waves can travel in up- and downstream direction. The resulting deformation tends to be symmetrical in the direction of flow, which corresponds with a diffusion-dominated solution.

The contribution of the different shock and expansion waves to the deformation of bed levels correspond with experimental observations of for example deposition fronts and backward-facing steps. However, detailed prediction of both water and bed levels near intense shocks still appears to be rather difficult.

8.8. Application of the *Godunov* method.

Due to different mathematical structures, as reflected by differences in celerities, the behaviour of fixed-bed and mobile-bed models is fundamentally different. These differences are very pronounced in transcritical flow. In fixed-bed models, the domain of dependance changes from partially up- and downstream at subcritical flows to entirely upstream in supercritical flows. In mobile-bed models, this domain of dependance is located up- and downstream for all flow regimes. However, the type of information that originates from the different parts of this domain changes significantly.

As a result, the applicability of numerical solution methods for fixed-bed and mobile-bed models differ as well. An explicit, numerical model has been developed based on a concept proposed by Godunov (1959). The model fully accounts for the structure of the mathematical model as represented by the characteristic equations. This method can also be applied to two-dimensional models.

Due to consequent separation of information originating from up- and downstream zones, numerical diffusion has been reduced as much as possible. However, because fixed grid points are used, intergrid distributions have to be assumed. The order of this distribution controls the accuracy of the numerical solution. Here a linear distribution is used which results in a second-order accuracy of continuous solutions.

It is noted that the separation of up- and downstream information changes in case of sections with a non-uniform fixed-bed. Then, linearization of intergrid bed levels over up- and downstream parts of the domain of dependance stabilizes the solution.

To represent discontinuous solutions, no additional flux-limiter device has been applied. At large discontinuities that develop due to the encounter of "conflicting" information carried by up- and downstream waves, this can lead to artificial fluctuations. An example is the development of a hydraulic jump in a deforming trench (Chapter six). These numerical effects can be suppressed by reducing the numerical grid.

Boundaries of the computation domain are treated with characteristic extrapolation technique, which results in non-reflective boundaries. The extrapolation can cause local instabilities in case of extremely non-uniform conditions at the boundary. The performance of the different types of boundary conditions is conform the theoretical analysis in Chapter two.

In the model, three grain-size fractions are distinguished, and bed-material load is divided into bed load and suspended load. Obviously, in case of mixtures with a wide range in diameter (coarse in the mainstream, fine in the flood plains), different modes of transport can occur. However, in case of large morphological activity during extreme events, the relevance of the distinction between bed load and suspended load is not clear. The total number of variables is 12 and includes flow depth and velocity, the concentration of sediment fractions in suspension and the composition of three storage layers in the river bed. The large number of variables and the rather complicated numerical algorithm cause relatively high computation costs.

Throughout the report, different applications can be found of the numerical model. No case study of a morphological event in a mountain river is included. Instead, some isolated morphological phenomena such as bed-level deformation and changes in composition in laboratory conditions can be described to a certain level of accuracy.

166

8.9. Recommendations.

The conditions posed by hydraulic and morphological features of mountain rivers put high claims on mathematical and numerical modelling approaches. Based on the analyses in this study, that focus on some details only, some remarks with respect to modelling can be made.

mountain rivers

Rivers in mountainous regions include rough, unsteady streams at steeper sections as well as tranquil flow at wider sections in flatter regions. Therefore, in general, the qualification "mountain river" can be considered to be topographical only, without indication of hydraulics and morphology. In the following, a limited definition is used; alluvial mountain rivers are specified as rivers with steep hydrographs, where different flow regimes can develop, with mobile beds and graded sediment.

coupled models

Evidently, a restricted availability and quality of input data, either measured or predicted, controls the accuracy-level of any model output. However, this aspect is not addressed here. To construct mathematical and numerical tools for support of engineering in mountain rivers, the distinct interaction between hydraulics and morphology must be accounted for. Because benefits of decoupled models based on the quasi-steady flow assumption are small, coupled models, with a simultaneous solution of both hydraulic and morphological changes are to be preferred.

discontinuous flows

At larger values of *Froude*, non-uniform conditions of flow can easily develop into stable shock waves. These can significantly affect morphological changes in the river in cases of hydraulic structures or natural dam formation. Hence, numerical models should include shock-fitting algorithms or have shock-capturing properties. If accurate representation of such discontinuous solutions has to be ensured, no benefits of implicit methods over explicit methods exist. For the cases considered in this study, the modified-*Godunov* method performed well.

simplified models

If, at the length-scale of interest, non-uniformity in flow conditions is negligible, values of *Froude* are near unity and lower accuracy levels are permitted, application of simplified models based on quasi-uniform flow assumptions enable a significant lowering of computation costs.

sediment mixtures

Distinction of size fractions is indispensable for modelling of mountain rivers where grain sizes of the alluvial material range from cobbles to silt. Considering the large speed of morphological processes, the reference layer for the river-bed surface must be small, of the order of a representative grain size. To prevent mathematical instabilities in cases of erosion with coarse surface layers, stabilization is recommended for conditions of mountain rivers. In this respect, an improvement was obtained with the options described in this report.

The number of size fractions varies with the level of particle shear stress. For applications with high levels of particle-shear stress, 3 size fractions provided sufficient accuracy in this study. For accurate prediction of morphological changes at lower values of particle-shear stress (e.g. degradation downstream structures or flushing of trout-breeding reaches) a larger number of size fractions may be required.

List of main symbols.

symbol	definition	units
a	depth	[m]
B	width	[m]
c	celerity	[m/s]
c_0	volumetric sediment fraction in the river bed	[-]
C	Chézy roughness parameter	[m$^{1/2}$/s]
d_e	scour depth	[m]
D_i	particle diameter of sediment in the fraction i	[m]
D_{mp}	mean diameter of pavement, defined as $D_m = \sum p_{pi} D_i$ with $i = 1$ to N	[m]
E	flow unsteadiness or non-uniformity parameter defined as $E = -2g_z/C^2\, uT/a$	[-]
f_{ui}	derivative of transport formula of fraction i to velocity	[m^2/m]
f_{pi}	derivative of transport formula of fraction i to fraction p_{1i}	[m^3/ms]
f_{Di}	derivative of transport formula of fraction i to mean grain size D_m	[m^2/ms]
Fr	Froude number, defined as $Fr = u/\sqrt{-g_z a}$	[-]
H_b	height of bed form	[m]
i_b	bed slope	[-]
L_A	adaption length of equilibrium concentration profile in z-direction	[m]
L_b	length of bed form	[m]
L_g	representative geometrical length-scale	[m]
L_w	representative length of width variation	[m]
T	representative period for hydrograph	[s]
T_A	adaption period of equilibrium concentration profile in z-direction	[s]
T_{act}	period of bed-level fluctuation	[s]
T_{resp}	response period of composition changes	[s]
g	gravitation constant	[m/s^2]
g_j	component of gravitation constant in j-direction	[m/s^2]
N	total number of fractions in the sediment mixture	[-]
p_{bi}	fraction i in the bed load layer	[-]
p_{ei}	equilibrium concentration of fraction i in suspension	[-]
p_{si}	actual concentration of fraction i in suspension	[-]
p_{Ti}	fraction i in the transported sediment	[-]
q	discharge per meter width in x-direction defined as $q = ua$	[m^2/s]
Q	discharge	[m^3/s]
s_{bx}, s_{by}	component in x- or y-direction of bed-material load	[m^2/s]
s_{bi}	horizontal mass flux of size fraction i in the bed-load	[m^2/s]

169

t	time coordinate	[s]
u	velocity component in x-direction	[m/s]
u_{gi}	velocity of grains with D_i in the bed load layer	[m/s]
$\bar{u}_g$	fraction-averaged velocity of grains in the bed load layer	[m/s]
u_*	shear velocity defined as $u_* = u\sqrt{-g_z}\,/\,C$	[m/s]
v	velocity component in y-direction	[m/s]
w	shock wave propagation rate	[m/s]
w_z	degradation or aggradation rate	[m/s]
x	space coordinate	[m]
z_b	bed level	[m]
Δz_b	representative height of bed-level fluctuation	[m]
Z_b	reference level	[m]
α	weight-reduction coefficient for abrasion of grains	[m^{-1}]
β_u	coefficient for the transversal distribution of $u^2 a$	[-]
β_i^*	fraction i in the vertical sediment flux between flow and river bed	[-]
δ_b	bed-load layer thickness	[m]
δ_c	critical reference-layer thickness	[m]
Δ	relative sediment density defined as $\Delta = \rho/\rho_s - 1$	[-]
Δt	time step	[s]
Δx	space step	[m]
θ	orientation of bicharacteristic ray	
ξ_i	particle shear-stress correction-coefficient for horizontal-hiding effects at fraction i	[-]
θ	dimensionless celerity defined as $\theta = c/u$	[-]
τ	direction of bicharacteristic ray	
τ_{bj}	component of bed shear-stress in j-direction	[kg/ms^2]
τ_{*i}	particle shear-stress defined as $\tau_{*i} = u^2\,/\,\Delta C^2 D_i$	[-]
τ_{*cr}	critical particle shear-stress describing initiation of motion	[-]
ϕ	volumetric bed-material load concentration defined as $\phi = s_b/q$	[-]
ϕ_s	volumetric sediment concentration in the suspended load layer	[-]
ϕ_{si}	volumetric sediment concentration of size fraction i in the suspended load layer	[-]
ϕ_b	volumetric sediment concentration in the bed-load layer	[-]
Φ_s	volumetric flux of sediment between the river bed and the water-sediment mixture	[m^3/m^{2}s]
Φ_w	volumetric flux of water between the river bed and the water-sediment mixture	[m^3/m^{2}s]
ψ	bed mobility parameter defined as $\psi = \sum f_{ui}/c_0 a$	[-]
ρ	density of water	[kg/m^3]
ρ_s	density of sediment	[kg/m^3]

170

Single-layer model.

p_{pi} — size fraction i in the reference layer — [-]

p_{oi} — size fraction i in the substratum — [-]

β_{oi} — size fraction i of flux Φ_{oi} at level $z = z_b - \delta_p$ — [-]

δ_b — thickness of the bed-load layer — [m]

δ_p — thickness of the mixing layer — [m]

Φ_{si} — vertical sediment flux of fraction i at level $z = z_b + \delta_b$
between the suspended load and bed-load layer — [m^3/m^{2}s]

Φ_{bi} — vertical sediment flux of fraction i at level $z = z_b$
between the reference and bed-load layer — [m^3/m^{2}s]

Φ_{oi} — vertical sediment flux of fraction i at level $z = z_b - \delta_p$
between the substratum and the reference layer — [m^3/m^{2}s]

Double-layer model

p_{pi} — size fraction i in the pavement layer — [-]

p_{spi} — size fraction i in the subpavement layer — [-]

p_{oi} — size fraction i in the substratum — [-]

β_{pi} — size fraction i of flux Φ_{pi} at level $z = z_b - \delta_p$ — [-]

β_{oi} — size fraction i of flux Φ_{oi} at level $z = z_b - \delta_p - \delta_{sp}$ — [-]

δ_p — thickness of the pavement layer — [m]

δ_s — thickness of the subpavement layer — [m]

κ — probability of exposure of the pavement layer — [-]

ϵ_p — sediment exchange rate for bed-load layer and pavement — [m/s]

ϵ_s — sediment exchange rate for bed-load layer and subpavement — [m/s]

Φ_{si} — vertical sediment flux of fraction i at level $z = z_b + \delta_b$
between the suspended load and bed-load layer — [m^3/m^{2}s]

Φ_{bpi} — vertical sediment flux of fraction i at level $z = z_b$
between the pavement layer and bed-load layer — [m^3/m^{2}s]

Φ_{bsi} — vertical sediment flux of fraction i at level $z = z_b - \delta_p$
between the subpavement layer and bed-load layer — [m^3/m^{2}s]

Φ_{pi} — vertical sediment flux of fraction i at level $z = z_b - \delta_p$
between the pavement layer and subpavement layer — [m^3/m^{2}s]

Φ_{oi} — vertical sediment flux of fraction i at level $z = z_b - \delta_p - \delta_s$
between the substratum and subpavement layer — [m^3/m^{2}s]

171

triple-layer model

p_{ji}	size fraction i in layer j	[-]
p_{4i}	size fraction i in the substratum	[-]
β_{ji}	size fraction i of flux Ψ_{ji} at level $z = z_b - \sum \delta_l$ with $l = 1$ to j	[-]
δ_j	thickness of layer j	[m]
κ_1	probability of mass exchange between bed load and layer $j = 1$	[-]
κ_2	probability of mass exchange between bed load and layer $j = 2$	[-]
$1-\kappa_1-\kappa_2$	probability mass exchange between bed load and layer $j = 3$	[-]
Φ_{si}	vertical sediment flux of fraction i at level $z = z_b + \delta_b$ between the suspended load and bed-load layer	[m^3/m^{2}s]
Φ_{bpi}	vertical sediment flux of fraction i at level $z = z_b$ between the pavement layer and bed-load layer	[m^3/m^{2}s]
Φ_{bsi}	vertical sediment flux of fraction i at level $z = z_b - \delta_p$ between the subpavement layer and bed-load layer	[m^3/m^{2}s]
Φ_{pi}	vertical sediment flux of fraction i at level $z = z_b - \delta_p$ between the pavement layer and subpavement layer	[m^3/m^{2}s]
Φ_{oi}	vertical sediment flux of fraction i at level $z = z_b - \delta_p - \delta_s$ between the substratum and subpavement layer	[m^3/m^{2}s]

References.

Abbot, M.B. (1974),
> Continuous flows, discontinuous flows and numerical analysis, Journal of Hydraulic Research, Vol. 12, No. 4, pp. 417-467.

Abbot, M.B. (1975),
> Weak solutions of the equations of open channel flow, pp. 283-311, in K. Mahmood and V. Yevjevich (Eds) *Unsteady flows in open channels*, Volume I, Water Resources Publications, Fort Collins, Colorado.

Abbott, M.B. (1979),
> *Computational Hydraulics. Elements of the theory of free surface flows*, Pitman, London.

Alcrudo, F. and P. Garcia-Navarro (1993); A high-resolution Godunov-type scheme in finite volumes for the 2-d shallow-water equations, Int. J. Num. Meth. Fluids., Vol.16, pp.489-505.

Ames, W.F. (1977),
> *Numerical methods for partial differential equations*, Second Edition, Academic Press, New York.

Anderson, D.A., J.C. Tannehill and R.H. Pletcher (1984),
> *Computational fluid mechanics and heat transfer*, McGraw-Hill Book Company.

Andrews, E.D. and G.Parker (1987),
> Formation of a coarse surface layer as the response to gravel mobility, in *Sediment transport in gravel-bed rivers*, C.R. Thorne, J.C. Bathurst and R.D. Hey (Eds), John Wiley and Sons, pp.269-300.

Armanini, A. and G. Di Silvio (1988),
> A one-dimensional model for the transport of a sediment mixture in non-equilibrium conditions, J. of Hydr. Res., Vol.26, No.3, p.275-292.

Armanini, A. and G. Di Silvio (1989),
> On the coexistance of the bedload and suspended sediment transport for a uniform grainsize material, Int. symp. sediment transport modeling, Proc. ASCE, J.of Hydr.Div., p.581-587.

Armanini, A.; F. Dellagiacoma and L. Ferrari (1989),
> From the check dam to the development of functional check dams, Int. workshop on fluvial hydraulic of mountainous regions, A. Armanini and G. Di Silvio (Eds), pp. B331-B344.

Armanini, A. (1991),
> Longitudinal sorting in unsteady flow, Proc. of the 24th Congr. of the IAHR, Madrid, pp.A461-A470.

Armanini, A. and P. Scotton (1992),
> Experimental analysis on dynamic impact of a debris flow on structure,

6th Interpraevent 1992, Bern, Vol.6.

Armanini, A. (1993),
On the dynamic impact of debris flows, International workshop in debris flow, Kagoshira, Japan.

Armanini, A. (1995),
Non-uniform sediment transport: dynamics of the active layer, J. of Hydr. Res., Vol.33, No.5, pp.611-622.

Ashida and Michiue (1971),
An investigation of river bed degradation downstream of a dam, 14th Congr. of the IAHR, Paris, paper C30, pp. 247-264.

Barneveld, H.J. (1988),
Numerieke methoden voor morfologische berekeningen tijdens kortdurende hoogwatergolven, M.Sc-thesis (in Dutch), Delft Univ. of Techn., 137 p.

Basco, D.R. (1989),
Limitations of the Saint Venant equations in dam-break analysis, Journal of Hydraulic Engineering, Vol. 115, No. 7, pp. 689-695.

Basile, P.A. (1994),
Modellazione dei meccanismi di intercettazione e rilascio di sedimenti da parte delle briglie permeabili, Ph.D. thesis, University of Padua, 121 pp.

Bathurst, J.C. (1978),
Flow resistance of large-scale roughness, Journal of the Hydr. Div. Vol.104, No.HY12, p.1587-1603.

Bathurst, J.C., R.-M. Li and D.B. Simons (1981),
Resistance equation for large-scale roughness, Journal of the Hydr.Div. Vol.107, No.HY12, p.1593-1613.

Bayazit, M. (1975),
Simulation of armor coat formation and destruction, proc. of the 16th congress, IAHR, Vol.2, Subject B, pp.73-80.

Belleudy, Ph. (1994),
Last 10 years' LHF experience in developing river sediment simulation software, Proc. of the Intnl. Symp. East-West, Noth-South encounter on the state of the art in River Eng. Methods and Design Philosophies, Vol.I, pp.143-152.

Bennet, J. and C.F. Nordin (1977),
Simulation of sediment transport and armouring, Hydrological sciences bulletin, 22, Vol.4, pp.555-569.

Berlamont, J. (1976);
Roll waves in inclined rectangular open channels, Proc. of the Symp. on unsteady flow in open channels, BHRA, Newcastle upon Tyne, England, pp. A2-A13.

Berlamont, J. and N. Vanderstappen (1981),
     Unstable turbulent flow in open channels, J. of the Hydr. Div., ASCE,
     Vol.107, No.4, pp.427-449.
Bettes, R. (1982),
     Degradation of river beds and associated changes in the composition of
     the sediments, in *Mechanics of sediment transport*, B.M. Sumer and A.
     Müller (Eds), Proceedings of Euromech 156, Istanbul, Balkema
     Rotterdam, pp.237-242.
Bezzola, G.R.; P.Kuster and S. Pellandini (1990),
     The Reuss river flood of 1987 - Hydraulic model tests and reconstruction
     concepts, pp.317-326, International conference on river flood hydraulics,
     W.R. White (Ed.), John Wiley and Sons, Chichester.
Bhallamudi, S.M. and M.H. Chaudhry (1991),
     Numerical modeling of aggradation and degradation in alluvial channels,
     J. of Hydr. Eng., ASCE, Vol. 117, No. 9, pp. 1145-1164.
Bhallamudi, S.M. and M.H. Chaudhry (1992),
     Computation of flows in open-channel transitions, J. of Hydr. Res.,
     IAHR, Vol. 30, No.1, pp. 77-93.
Bhowmik, N.G. and M. Demissie (1982),
     Bed material sorting in pools and riffles, J. of the Hydr. Div., ASCE,
     Vol.108, No.10, pp.1227-1231.
Borah, D.K., C.V. Alonso and S.N. Prasad (1982a),
     Routing graded sediments in streams, formulations, J. of the Hydr. Div.,
     ASCE, VOl.108, No.12, p.1486-1503.
Borah, D.K., C.V. Alonso and S.N. Prasad (1982b);
     Routing graded sediments in streams, applications, J. of the Hydr. Div.,
     ASCE, VOl.108, No.12, p.1504-1517.
Borah, D.K. (1989),
     Scour-depth prediction under armouring conditions, J. of Hydr. Eng.,
     ASCE, Vol.115, No.10, p.1421-1425.
Botev, I.B. (1991),
     One-dimensional numerical modeling of dam-break wave propagation in
     mild sloping natural streams, J. of Hydroscience and Hydr. Eng., Vol.9,
     No.1, pp.27-42.
Brayshaw, A.C; L.E. Frostick and I. Reid (1983),
     The hydrodynamics of particle clusters and sediment entrainment in
     coarse alluvial channels, Sedimentology, Vol.30, pp.137-143.
Bren, L.J. and A.K. Turner (1978),
     Wave propagation in steep rough mountain streams, J. of the Hydr. Div.,
     ASCE, Vol.104, No.5, pp.745-745.

Bridge, J.S. (1992),
   A revised model for water flow, sediment transport, bed topography and grain size sorting in natural river bends, Water Res.Res., Vol.28, No.4, pp.999-1013.
Bradley, J.B. and S.C. McCutcheon (1985),
   The effects of high sediment concentration on transport processes and flow phenomena, pp.219-226, Proc. of the int. symp. on erosion, debris flow and disaster prevention, The erosion control engineering society, Tsukuba, Japan.
Brush, L.M. Jr. and M.G. Wolman (1960),
   Knickpoint behaviour in noncohesive material: a laboratory study, Bulletin of the Geological Society of America, Vol. 71, pp. 59-74.
Bunte, K. (1992),
   Particle number grain-size composition of bedload in a mountain stream, in *Dynamics of gravel-bed rivers*, P. Billi, R.D. Hey, C.R. Thorne and P. Tacconi (Eds), John Wiley and Sons, New York, pp.55-72.
Burton, A. and J.C. Bathurst (1994),
   Modelling shallow land slide erosion and sediment yield at the basin scale, Intern. workshop on floods and inundations related to large earth movements, Trent, Italy, B7.
Carling, P.A. (1990),
   Particles over-passing on depth-limited gravel bars, Sedimentology, Vol.37, pp.347-355.
Çeçen, K. and M. Bayazit (1973),
   Critical shear stress of armored beds, proc. of the 15th congress, IAHR, Vol.1, Subject A, pp.493-500.
Chanson, H. (1992),
   Drag reduction in self-aerated flows. Analogy with dilute polymer solutions and sediment laden flows, Research Report No.CE141, Dep. of Civil Eng., Univ. of Queensland, 23 p.
Changnon Jr, S.A. (1986),
   A future flood research agenda for the United States, pp.17-25, in *Flood hydrology*, V.P. Singh (Ed.), Proc. of the int. symp. on flood frequency and risk analyses, 14-17 May 1986, Louisiana State Univ. D. Reidell Publ. Comp.
Chiew, Y.M. (1991),
   Bed features in nonuniform sediments, J. of Hydr. Eng., ASCE, Vol.117, No.1, pp.116-120.
Chin, C.O. (1985),
   Stream bed armouring, School of Eng. Rep.No.403, University of Auckland, New Zealand, 253 p..

Chin, C.O., B.W. Melville and A.J. Raudkivi (1994),
Streambed armouring, J. of Hydr. Eng., ASCE, Vol.120, No.8, pp. 899-918.

Chow, V.T. (1959),
Open-channel hydraulics, McGraw-Hill Int. Editions, Civ. Eng. Series, New York, 680 p.

Church, M. and D. Jones (1982),
Channel bars in gravel bed rivers, in *Gravel bed rivers*, R.D. Hey, J.C. Bathurst and C.R Thorne (Eds), John Wiley and Sons, pp.291-338.

Church, M.; D.M. McClean abd J.F. Wolcott (1987),
River bed gravels: sampling and analysis, pp.43-88 in *Sediment transport in gravel-bed rivers*, C.R. Thorne, J.C. Bathurst and R.D. Hey (Eds), John Wiley and Sons, New York.

Church, M.; J.F. Wolcott and W.K. Fletcher (1991),
A test of equal mobility in fluvial sediment transport: behavior of the sand fraction, Water Res. Res., Vol.27, No.11, pp.2941-2951.

Church, M. and M.A. Hassan (1992),
Size and distance of travel of unconstrained clasts on a streambed, Water Res. Res., Vol.28, No.1, pp.299-303.

Cojean, R. (1994),
Role of water as triggering factor for landslides and debris flow, Intern. workshop on floods and inundations related to large earth movements, Trent, Italy, A13.

Colella, P., P. Concus and J. Sethian (1983),
Some numerical methods for discontinuous flows in porous media, pp. 161-186, in R. Ewing (Ed.) *The mathematics of reservoir simulation*, SIAM, Philadelphia.

Colella, P. and P.R. Woodward (1984),
The piecewise parabolic method for gas-dynamical simulations, Journal of Computational Physics, Vol. 54, pp. 174-201.

Correia, L.R.P., B.K. Krishnappan and W.H.Graf (1992),
Fully coupled unsteady mobile boundary flow model, Journal of Hydr. Eng. ASCE, Vol.118, No.3, pp.476-494.

Courant, R. and D. Hilbert (1962),
Methods of mathematical physics, Vol.II, Partial differential equations, Interscience publishers, New York, 830 pp..

Courant, R. E. Isaacson and M. Reeves (1952),
On the solution of nonlinear hyperbolic differential equations by finite differences, Comm. on pure and applied mathematics, Vol.5, pp.243-55.

Crosato, A. (1995),
One-dimensional modelling of morphological processes of mountain

streams and piedmont rivers, in FRIMAR Technical Progress Report, June 1994 - May 1995, ISMES S.p.A., Bergamo Italy.

Cui, Y., G. Parker and C. Paolo (1996),
Numerical simulation of aggradation and downstream fining, J. of Hydr. Res., IAHR, Vol.34, No.2, pp.185-204.

Cunge, J.A. (1975),
Rapidly varying flow in power and pumping canals, pp. 539-586, in K. Mahmood and V. Yevjevich (Eds) *Unsteady flows in open channels*, Volume I, Water Resources Publications, Fort Collins, Colorado.

Daubert, A. and O. Graffe (1967),
Quelques aspects des écoulements presque horizontaux a deux dimensions en plan et non permanents application aux estuaires, La Houille Blanche No.8, p.847-860.

Davies, T.R.H. (1989),
Fluvial hazards in mountain valleys, Int. workshop on fluvial hydraulic of mountainous regions, A. Armanini and G. Di Silvio (Eds), pp. B105-B118.

Deigaard, R. (1982),
Longitudinal sorting of grain sizes in alluvial rivers, in *Mechanics of sediment transport*, B.M. Sumer and A. Müller (Eds), Proceedings of Euromech 156, Istanbul, Balkema Rotterdam, pp.231-236.

Delft Hydraulics (1971),
Regularizacion del Rio Apure en la proximidad de San Fernando, Republica de Venezuela, Ministerio de Obras Publicas, Report No.515.

Diplas, P. (1987),
Bed load transport in gravel-bed streams, J. of Hydr. Eng., ASCE, Vol.113, No.3, pp.277 292.

Diplas, P. (1994),
Modelling of fine and coarse sediment interaction over alternate bars, Journal of Hydrology 159, pp.335-351.

Dinehart, R.L. (1989),
Dune migration in a steep, coarse-bedded stream, Water Resources Research, Vol.25, No.5, pp.911-923.

Dinehart, R.L. (1992),
Evolution of coarse gravel bed forms: field measurements at flood stage, Water Resources Research, Vol.28, No.10, pp.2667-2689.

Dracos, T.A. and B. Glenne (1967),
Stability criteria for open-channel flow, J. of the Hydr. Div., Vol.93, No.6, pp.97-101.

Drake, T.G., K.L. Shreve, W.E. Dietrich, P.J. Whiting and L.B. Leopold (1988),

Bedload transport of fine gravel observed by motion picture, J. of Fluid Mechanics, Vol.192, pp.193-218.

Dronkers, J.J. (1964),
Tidal computations in rivers and coastal waters., North Holland Publishing Co., Amsterdam, the Netherlands.

Escoffier, F.F. and M.B. Boyd (1962),
Stability aspects of flow in open channels, J. of the Hydr. Div., ASCE, Vol.88, No.6, pp. 145-166.

Egashira S. and K. Ashida (1989),
Flow resistance and sediment transportation in streams with step-pool bed morphology, Int. Workshop on Fluv. Hydr. of Mountain regions, Trent, p.A31-A44.

Egiazaroff, I.V. (1965),
Calculation of nonuniform sediment concentrations, J. of the Hydr. Div., ASCE, Vol.91, No.4, pp.225-248.

Einstein, H.A. (1950),
The bed-load function for sediment transportation in open channel flows, Technical Bulletin No.1026, also Appendix B in "Sedimentation Symposium to honor Professor H.A. Einstein", H.W. Shen (Editor).

Einstein, H.A. (1972),
Bed load transport as a probability problem, Appendix C in Sedimentation, H.W. Shen (Editor).

Engelund, F. and E. Hansen (1967),
A monograph on sediment transport in alluvial streams, Teknisk Forlag, Copenhagen.

Evans, P. and A. Sieben (1996),
One-dimensional morphological models for mountain areas: numerical testing, Delft Hydraulics, Report No. Q1327/Q1951, 35 p.

Fennema, R.J. and M.H. Chaudhry (1986),
Explicit numerical schemes for unsteady free-surface flows with shocks, Water Resources Research, Vol. 22, No. 13, pp. 1923-1930.

Fennema, R.J. and M.H. Chaudhry (1987),
Simulation of one-dimensional dam-break flows, Journal of Hydraulic Research, Vol.25, No.1, pp.41-51.

Fennema, R.J. and M.H. Chaudhry (1990),
Explicit methods for 2-D transient free-surface flows, Journal of Hydraulic Engineering, Vol. 116, No. 8, pp. 1013-1034.

Fernandez-Luque, R. and R. Van Beek (1976),
Erosion and transport of bed sediment, J. of Hydr. Res, IAHR, Vol.14, No.2, pp.127-144.

Finlayson, B.A. (1992),
> *Numerical methods for problems with moving fronts*, Ravenna Park Publ. Inc., Seattle USA, 605 p.

Fletcher, C.A.J. (1988a),
> *Computational Techniques for Fluid Dynamics. 1. Fundamentals and general techniques.*, Springer Berlin.

Fletcher, C.A.J. (1988b),
> *Computational Techniques for Fluid Dynamics. 1. Specific techniques for different flow categories.*, Springer Berlin.

Foley, M.G. (1975),
> Scour and fill in ephemeral streams, California Institute of Technology, Report No.KH-R-33, Pasadena, California.

FRIMAR (1995),
> Flooding Risks in Mountain Areas, Progress Report June 1994 - May 1995, Delft Hydraulics (coordinator).

Fryxell, B.A., P.R. Woodward, P. Colella and K.-H. Winkler (1986),
> An implicit-explicit hybrid method for lagrangian hydrodynamics, J. of Comp. Physics, No.63. pp. 283-310.

Fuentes, R. and J. Aguirre-Pe (1991),
> Resistance in composite, macro rough flow, 24th IAHR Congr. Madrid, p. A243-A252.

Furbish, D.J. (1987),
> Conditions for geometric similarity of coarse stream-bed roughness, Mathematical Geology, Vol.19, No.4, p.291-307.

Furbish, D.J. (1993),
> Flow structure in a bouldery mountain stream with complex bed topography, Water Res. Res. Vol.29. No.7, pp.2249-2263.

Gabutti, B. (1983),
> On two upwind finite-difference schems for hyperbolic equations in non-conservative form, Computers and Fluids, Vol. 11, No. 3, pp. 207-230.

Galappatti, R. (1983),
> A depth-integrated model for suspended sediment transport, Comm. on Hydr. and Geot. Eng., Rep. No.83-7.

Galapatti, R. and C.B. Vreugdenhil (1985),
> A depth-integrated model for suspended sediment transport, Journal of Hydr. Res., Vol.23, No.4, p.259-375.

Galay, V. (1987),
> Erosion and sedimentation in the Nepal Himalaya, an assessment of river processes, Icimod Kathmandu, Kefford Press, Singapore.

Garcia, R. and R.A. Kahawita (1986),
> Numerical solution of the St. Venant equations with the McCormack

finite difference scheme, Int. Journal for numerical methods in fluids, Vol. 6, pp. 259-274.

Garcia-Navarro, P. and S.M. Saviron (1992),
McCormack's method for the numerical simulation of one-dimensional discontinuous unsteady open channel flow, J. of Hydr. Res., IAHR, Vol. 30, No. 1, pp. 95-105.

Garde, R.J., K.A. Ali and S. Diette (1977),
Armoring process in degrading streams, J. of the Hydr. Div. ASCE, Vol.103, No.9, pp.1091-1095.

Gessler, J. (1970),
Self-stabilizing tendencies of alluvial channels, J. of the Waterways and Harbors Division, ASCE, Vol.96, No.2, pp. 235-247.

Gharangik, A.M. and M.F. Chaudhry (1991),
Numerical simulation of hydraulic jump, J. of Hydr. Eng., ASCE, Vol.117, No.9, pp.1191-1211.

Ghilardi, P. and G. Menduni (1989),
Numerical analysis of hillslope-channel interaction in first order basins, Int. workshop on fluvial hydraulic of mountainous regions, A. Armanini and G. Di Silvio (Eds), pp. B279-B292.

Glaister, P. (1988),
Approximate Riemann solutions of the shallow water equations, J. of Hydr. Res., IAHR, Vol. 26, No. 3, pp. 293-306.

Glimm, J. (1965),
Solutions in the large for nonlinear hyperbolic systems of equations, Communications on Pure and Applied Mathematics, Vol. 18, pp. 697-715.

Godunov, S.K. (1959),
A difference scheme for numerical computation of discontinuous solution of hydrodynamic equations, Matematiceskij Sbornik, Vol.47, pp. 271-306, (in Russian), Translated US Joint Publ. Res. Service, JPRS 7226 (1969).

Gomez, B. (1983),
Temporal variations in the particle size distribution of surficial bed material: The effect of progressive bed armouring, Geografiska Annaler, 65-A, pp.183-192.

Grant, G.E. and T. Mizuyama (1991),
Origin of step-pool sequences in high gradient streams: a flume experiment, Japan-US workshop on snow avalanche, landslide, debris flow prediction and control, pp.523-532.

Grijsen, J.G. and H.J.M. Ogink (1973),
Mathematical models for surface and open-channel flow, DHL Res.

Report S134-II.

Grijsen, J.G. and C.B. Vreugdenhil (1976),
  Numerical representation of flood waves in rivers, Delft Hydraulics Laboratory publ. No.165.

Hager, W.H. and J.-J. Droux (1986),
  Diffusive flood waves in large rivers, pp.81-95, in *Flood hydrology*, V.P. Singh (Ed.), Proc. of the int. symp. on flood frequency and risk analyses, 14-17 May 1986, Louisiana State Univ. D. Reidell Publ. Comp.

Hager, W.H. and N.V. Bretz (1986),
  Hydraulic jumps at positive and negative steps, J. of Hydr. Res., IAHR, Vol.4, No.4, pp.237-253.

Harten, A.; P.D. Lax and B. van Leer (1983),
  On upstream differencing and Godunov-type schemes for hyperbolic conservation laws, SIAM Rev., 25, pp. 35-62.

Hassan, M.A. and M. Church (1992),
  The movement of individual grains on the streambed, pp.159-176 in *Dynamics of gravel-bed rivers*, P. Billi, R.D. Hey, C.R. Thorne and P. Tacconi (Eds), John Wiley and Sons, New York.

Henderson, F.M. (1963),
  Flood waves in prismatic channels, Journal of the Hydr. Div., ASCE, Vol.89, No.HY4, p.39-67.

Hey, R.D. (1979),
  Flow resistance in gravel-bed rivers, Journal of the Hydr. Div., ASCE, Vol.105, No.HY4, p.365-379.

Hey, R.D. and C.R. Thorne (1986),
  Stable channels with mobile gravel beds, Journal of Hydr. Eng., ASCE, Vol.112, No.8, p.761-689.

Hey, R.D. (1988),
  Bar form resistance in gravel-bed rivers, Journal of Hydr. Eng., ASCE, Vol.114, No.12, p.1498-1508.

Hirano, M. (1971),
  River bed degradation with armoring, Trans. of JSCE, Vol.3, Part 2, pp.194-195.

Hirano, M. (1972),
  Studies on variation and equilibrium state of a river bed composed of non-uniform material, Trans. of JSCE, Vol.4.

Hirano. M.; T. Moriyama and K. Kawahara (1994),
  Prediction of occurrence of debris flow by use of neural network, Intern. workshop on floods and inundations related to large earth movements, Trent, Italy, C1.

Hirsch, C. (1988),
> *Numerical Computation of Internal and External Flows, Vol.1: Fundamentals of numerical discretization.*, John Wiley and Sons.

Hirsch, C. (1990),
> *Numerical Computation of Internal and External Flows, Vol.2: Computational methods for inviscid and viscous flows.*, John Wiley and Sons.

Ho, C.W. (1988),
> A study on the staircase profile and armouring effects of river bed for torrential streams in Taiwan, Int. conf. on river regime, W.R. White (Ed.), Hydr.Res. Ltd, Wallingford UK, pp.241-250.

Hoey, T.B. and R. Ferguson (1994),
> Numerical simulation of downstream fining by selective transport in gravel bed rivers: model development and illustration, Water Res. Res., Vol.30, No.7, pp. 2251-2260.

Holly, Jr F.M. and J.-L. Rahuel (1990a),
> New numerical/physical framework for mobile bed modelling, Part 1: Numerical and physical principles, Journ. of Hydr. Res. IAHR, Vol.28. No.4.

Holly, Jr F.M. and J.-L. Rahuel (1990b),
> New numerical/physical framework for mobile bed modelling, Part 2: Test applications, Journ. of Hydr. Res. IAHR, Vol.28. No.4.

Iseya, F. and H. Ikeda (1987),
> Pulsations in bedload transport rates induced by a longitudinal sediment sorting: a flume study using sand and gravel mixtures, Geografiska Annaler, Vol.69 A, pp.15-27.

Ishihara, T., Y. Iwagaki and Y. Iwasa (1960),
> discussion of "Roll waves and slug flows in inclined open channels", by Mayer (1959), J. of the Hydr. Div., Vol.86, No.2, pp. 45-60.

Iwamoto, M. (1985),
> Effects of check dams on a torrent, pp.407-412, Proc. of the int. symp. on erosion, debris flow and disaster prevention, The erosion control engineering society, Tsukuba, Japan.

Jansen, P. Ph., L. van Bendegom, J. van den Berg, M. de Vries and A. Zanen (1979)
> *Principles of River Engineering*, Delftse Uitgevers Mij., 509 p.

Jain, S.C. (1990),
> Armor or pavement, J. of Hydr. Eng., Vol.116, No.3, pp.436-440.

Jarret, R.D. (1984),
> Hydraulics of high gradient streams, J. of Hydr. Eng., ASCE, Vol. 110, No.11, pp.1519-1539.

Jarret, R.D. (1987),
    Errors in slope-area computations of peak discharges in mountain streams, J, of Hydrology, Vol.96, pp.53-67.
Jarret, R.D. (1990),
    Hydrologic and hydraulic research in mountain rivers, Water Resources Bulletin, Vol.26, No.3, pp.419-429.
Jeaggi, M.N.R. (1983),
    Alternierende Kiesbänke, Mitt. der Vers.Anst. für W.bau, Hydrol. and Glazi., Nr. 62, Eidgen. Techn. Hoch. Zürich.
Jeaggi, M.N.R. and G.M. Smart (1982),
    discussion of "Channel bars in gravel bed rivers", p.325 in *Gravel bed rivers*, R.D. Hey, J.C. Bathurst and C.R. Thorne (Eds), John Wiley and Sons.
Jeaggi, M.N.R. and D. Rickenmann (1987),
    Applications of sediment transport formulae in mountain streams, Proc. of the 22nd IAHR Congr., W.R. White (Ed.), Lausanne, pp. A98-A103.
Jiménez, O.F. and M.H. Chaudhry (1988),
    Computation of supercritical free-surface flows, J. of Hydr. Eng., ASCE, Vol. 114, No. 4, pp. 377-395.
Jolly, J.P. and V. Yevjevich (1974)
    Simulation accuracies of gradually varied flow., J. of the Hydr. Div., ASCE, Vol. 100, No. HY7, pp. 1011-1030.
Jong, de C. and P. Ergenzinger (1992),
    Unsteady flow, bed load transport and bed roughness responses in steep mountain torrents, 5th Int. Symp. on River Sed., Karlsruhe, Vol.1, p.185-192.
Karim, M.F. and F.M. Holly (1986),
    Armoring and sorting in alluvial rivers, J. of Hydr. Eng., ASCE, Vol.112, No.8, pp.705-715.
Katopodes, N. and T. Strelkoff (1978),
    Computing two-dimensional dam-break flood waves, J. of Hydr. Div., ASCE, Vol. 104, No. 9, pp. 1269-1288.
Kellerhals, R. (1970),
    Runoff routing through steep natural channels, J. of Hydr. Div., ASCE, Vol.96, No.HY11, p.2201-2217.
Kellerhals, R. and D.I. Bray (1971),
    Sampling procedures for coarse fluvial sediments, J. of Hydr. Div., ASCE, Vol.97, No.8, pp.1165-1180.
Kellerhals, R. (1988),
    Prozesse in den Bachgerinnen, in Folgen der Waldschäden auf die Gebirgswässer in der Schweiz, V.A.W., ETH Zürich, pp.70-77.

Klaassen, G.J.; H.J.M. Ogink and L.C. van Rijn (1986),
    DHL-research on bed forms, resistance to flow and seidment transport,
    Proc. of the 3rd Intl. Symp. of river sedimentation, Vol.III, S.Y. Wang,
    H.W.Shen and L.Z.Ding (Eds), Mississippi, pp.58-82.
Klaassen, G.J. (1990),
    Sediment transport of armoured rivers during floods, Report No.Q790,
    Delft Hydraulics.
Klingemann, P.C. and W.W. Emmet (1982),
    Gravel bedload transport processes, in *Gravel bed rivers*, R.D. Hey, J.C.
    Bathurst and C.R. Thorne (Eds), John Wiley and Sons, pp.141-180.
Kranenburg, C. (1990),
    On the stability of gradually varied flow in wide open channels, J. of
    Hydr. Res., IAHR, Vol.28, No.5, pp.621-628.
Kuhnle, R.A. and J.B. Southard (1988),
    Bed load transport fluctuations in a gravel bed laboratory channel, Water
    Resources Research, Vol.24, No.2, pp.247-260.
Kuhnle, R.A. (1989),
    Bed-surface size changes in gravel-bed channels, J. of Hydr. Eng.,
    ASCE, Vol.115, No.6, pp.731-743.
Kutler, P. (1975),
    Computation of three-dimensional, inviscid supersonic flows, pp. 287-
    374, Progress in numerical fluid dynamics, Lecture Notes in Physics,
    No. 4, Springer Verlag, New York.
Laguzzi, M. (1994),
    Modelling of sediment mixtures, Delft Hydraulics, Report Q1660, The
    Netherlands.
Lai, C. (1976),
    Some computational aspects of one- and two-dimensional unsteady flow
    simulation by the method of characteristics, Proceedings of the
    International Symposium on Unsteady Flows in Open Channels, BHRA
    Fluid Engineering, Newcastle-upon-Tyne, pp. D1-1 - D1-12.
Lai, C. (1986),
    Numerical modelling of unsteady open-channel flow, Advances in
    Hydrosciences, Vol.14, p.161-333.
Lamberti, A. and E. Paris (1992),
    Analysis of armouring process through laboratory experiments, pp. 227-
    250 in *Dynamics of gravel-bed rivers*, P. Billi, R.D. Hey, C.R. Thorne
    and P. Tacconi (Eds), John Wiley and Sons, New York.
Laronne, J.B. and M.A. Carson (1976),
    Interrelationships between bed morphology and bed-material transport for
    a small, gravel-bed channel, Sedimentology, Vol.30, pp.67-86.

Lax, P.D. (1954),
 Weak solutions of non-linear hyperbolic equations and their numerical applications, Commmunications on Pure and Applied Mathematics, Vol.7, pp. 159-193.

Lax, P.D. and B. Wendroff (1960),
 Systems of conservation laws, Commmunications on Pure and Applied Mathematics, Vol.13, pp. 217-237.

Lax, P.D. (1973),
 Hyperbolic systems of conservation laws and the mathematical theory of shock waves, 48 p., Regional Conference Series in Applied Mathematics, Society for Industrial and Applied Mathematics, Philadelphia.

Lee, H.-Y. and S.-T. Hwang (1994),
 Migration of backward-facing step, J. of Hydr. Res., IAHR, Vol. 120, No. 6, pp. 693-705.

Leer van, B. (1979),
 Towards the ultimate conservative difference scheme. V. A second order sequel to Godunov's method, Journal of Computational Physics, Vol. 32, pp. 101-136.

LeVeque, R.J. (1990),
 Numerical methods for conservation laws, Lectures in Mathematics, ETH Zürich, Birkhäuser, Basel, 214 p.

Li, S.-G., L.Venkataraman and D. McLaughlin (1992),
 Stochastic theory for irregular stream modelling, Part I: Flow resistance, Journ. of Hydr. Eng., Vol.118, No.8, p.1079-1090.

Lin, P.N. and H.W. Shen (1984),
 Two-D flow with sediment by the characteristic method, Journ. of Hydr. Eng. ASCE, Vol.110, No.5, p.615-626.

Lister, M. (1967),
 The numerical solution of hyperbolic partial differential equations by the method of characteristics, pp. 165-179, in *Mathematical methods for digital computers*, A. Ralston and H.S. Wilf (Eds), John Wiley and Sons, New York, 293 p.

Little, W.C. and P.G. Mayer (1976),
 Stability of channel beds by armouring, J. of the Hydr. Div., ASCE, Vol.102, pp. 1647-1660.

Lyn, D.A. (1987),
 Unsteady sediment-transport modelling, J. of Hydr.Eng., ASCE, Vol.113, No.1.

MacCormack, R.W. (1969),
 The effect of viscosity in hypervelocity impact cratering, AIAA Paper 69-354, Cincinnati, Ohio.

MacCormack R.W. and B.S. Baldwin (1975),
   A numerical method for solving the time-dependent compressible Navier-
   Stokes equations with application to shock-boundary layer interactions,
   AIAA Paper 75-1, Pasadena, California.
Mayer, P.G. (1959),
   Roll waves and slug flows in inclined open channels, J. of the Hydr.
   Div., Vol.85, No.6, pp. 99-141.
Meyer-Peter, E. and R. Müller (1948),
   Formulas for bed load transport, Proc. 2nd Congress of the IAHR,
   Stockholm, Sweden, p.39-64.
Mikoš, M. (1993),
   Fluvial abrasion of gravel sediments, Mitteilungen 123, VAW Zürich,
   322 p..
Misri, R.L.; R.J. Garde and K.G. Ranga Raju (1984),
   Bed load transport of coarse non-uniform sediment, J. of Hydr. Eng.,
   ASCE, Vol.110, No.3, pp.312-328.
Moretti, G. (1979),
   The λ-scheme, Computers and Fluids, Vol. 7, pp. 191-295
Naef, F.R.; W.Haeberli and M.N.R. Jaeggi (1988),
   Morphological changes in the Swiss Alps resulting from the 1987 summer
   storms, Hydrology of disasters, Proc. of the W.M.O. Technical Conf.,
   O. Starosolszky and O.M. Melder (Eds), Geneva.
Nakagawa, H. and T. Tsujimoto (1980),
   Sand bed instability due to bed load motion, J. of the Hydr. Div., ASCE,
   Vol.106, No.12, pp.2029-2051.
Nakagawa, H. (1988),
   Stochastic approach to sediment transport problem, J. of Hydroscience
   and Hydr. Eng., Vol.6, No.2, pp.55-74.
Niekerk, A. van, K. Vogel, R.L. Slingerland and J.S. Bridge (1992),
   Routing of heterogeneous sediments over movable bed: model
   development, J. of Hydr. Eng., ASCE, Vol.118, No.2, pp. 246-262.
Niño, Y.; M. García and L. Ayala (1994),
   Gravel saltation 1. Experiments, Water Res. Res., Vol.30, No.6,
   pp.1907-1914.
Ogink, H.J.M. and R.J. De Jong (1989),
   Tous Dam failure, Analysis of studies on the Tous dam failure and
   flooding of the Júcar plain on 20th October 1982, Delft Hydraulics,
   Report No. Q940, The Netherlands.
Okabe, T. (1992),
   Improved model for bed-level changes in mountain rivers, pp.139-146,
   in Erosion, debris flows and environment in mountain regions, proc. of

the Chengdu symp., IAHS Publ. No.209.

Okabe, T., Y. Anase and H. Yamashita (1994),
Numerical model for unsteady sediment transport in mountain torrents, Proc. of the Int. Symp. East-West, Noth-South encounter on the state of the art in River Eng. Methods and Design Philosophies, Vol.I, pp.191-200.

Okunishi, K. and H. Suwa (1985),
Hydrological approach to debris flow, pp.243-247, Proc. of the int. symp. on erosion, debris flow and disaster prevention, The erosion control engineering society, Tsukuba, Japan.

Olesen, K.W. and J.P. Kalkwijk (1987),
Mathematical modelling of grain sorting in river bends, Proc. of the 12th congress, IAHR, Fluvial Hydraulics, pp.142-147.

Paola, C. and R. Seal (1995),
Grain size patchiness as a cause of selective deposition and downstream fining, Water Res. Res., Vol.31, No.5, pp.1395-1407.

Paris, E. (1991),
Time-space bed load evolution in static armour formation, Grain Sorting Seminar, Ascona Switzerland, pp.193-206.

Parker, G. and A.W. Peterson (1980),
Bar resistance of gravel-bed streams, Journal of the Hydr. Div., ASCE, Vol.106, No.HY10, p.1559-1575.

Parker, G. P.C. Klingeman and D.G. McLean (1982),
Bedload and size distribution in paved gravel bed streams, J. of the Hydr. Div., ASCE, Vol.108, No.4, pp.544-571.

Parker, G. and A.J. Sutherland (1990),
Fluvial armor, J. of Hydr. Res., IAHR, Vol.28, No.5, pp. 529-544.

Parker, G. (1991a),
Selective sorting and abrasion of river gravel.II Theory, J. of Hydr. Eng, ASCE, Vol.117, No.2, pp. 113-149.

Parker, G. (1991b),
Selective sorting and abrasion of river gravel. II Formulations, J. of Hydr. Eng, ASCE, Vol.117, No.2, pp. 150-171.

Parker, G. (1991c),
Some random notes on grain sorting, Grain Sorting Seminar, Ascona Switzerland, pp.19-76.

Petts, G.E.; M.C. Thoms, K. Brittan and B. Atkin (1989),
A freeze coring technique applied to the pollution by fine sediments in gravel-bed rivers, The science of the total environment, Vol.84, pp.259-272.

Peviani, M.; L. Crepaldi, G. Porta S. Rafaelli and A. Galletti (1995),
Knowledge and research in the field of sediment production, Technical Progress Report June 1994-May 1995, FRIMAR.

Pitlick, J.C. (1992),
Flow resistance under conditions of intense gravel transport, Water Resources Research, Vol.28, No.3, pp.891-903.

Ponce, V.M. and D.B. Simons (1977),
Shallow wave propagation in open channel flow, Journal of the Hydr. Div. Vol.103, No.HY12, p.1461-1476.

Ponce, V.M., R.-M. Li and D.B. Simons (1978),
Applicability of kinematic and diffusion models, Journal of the Hydr. Div. Vol.104, ASCE, No.HY3, p.353-360.

Press, W.H., S.A. Teukolsky and W.T. Vetterling (1992)
Numerical recipes in Fortran: the art of scientific computing, Second Ed., Cambridge Univ. Press.

Proffitt, G.T. and A.J. Sutherland (1983),
Transport of non-uniform sediments, J. of Hydr. Res., IAHR, Vol.21, No.1, pp.33-43.

Rahuel, J.L. (1988),
Modelisation de l'evolution du lit des rivieres alluvionaires a granulometrie etendue, These, l'Ecole Nationale Supérieure d'Hydraulique et de Mécanique de Grenoble.

Rahuel, J.L., F.M. Holly, J.P.Chollet, P.J. Belleudy and G. Yang, (1989),
Modeling of riverbed evolution for bedload sediment mixtures, J. of Hydr. Eng., ASCE, Vol.115, No.11, pp. 1521-1542.

Rakoczi, L. (1991),
Field tracer investigations of grain sorting in gravel bed rivers, Grain Sorting Seminar, Ascona Switzerland, p.77-92.

Raudkivi, A.J. and R. Ettema (1982),
Stability of armour layers in rivers, J. of the Hydr. Div., ASCE, Vol.108, No.9, pp. 1047-1057.

Raudkivi, A.J. (1990),
Loose boundary hydraulics, 3rd Edition, Pergamon Press, 538 pp..

Renard, K.G. and E.M. Laurson (1975),
Dynamic behavior model of ephemeral stream, J. of the Hydr. Div., ASCE, Vol.101, No.5, pp.511-528.

Ribberink, J.S. (1983),
Experiments with non-uniform sediment in case of bed-load transport, Report No.83-2, Comm. on Geot. and Hdyr. Eng., Delft Univ. of Techn.

Ribberink, J.S. and J.T.M. van der Sande (1985),
  Aggradation in rivers due to overloading - analytical approaches, Journal of Hydraulic Research, Vol.23, No.3, pp.273-283.

Ribberink, J.S. (1987),
  Mathematical modelling of one-dimensional morphological changes in rivers with non-uniform sediment, Ph.D. thesis, 200 p., Report No.87-2, Comm. on Geot. and Hdyr. Eng., Delft Univ. of Techn.

Richards, K. (1990),
  Fluvial geomorphology: initial motion of bed material in gravel bed rivers, Progress in physical geography, Vol.14, No.3, pp.395-415.

Richtmyer, R.D. and K.W. Morton (1967)
  Difference methods for initial-value problems, Second Edition, Interscience Publishers, New York.

Richtmyer, R.D. (1972),
  Methods for (generally unsteady) flows with shocks: a brief survey, pp. 72-81, in H. Cabannes and R. Temam (Eds), Proceedings of the Third International Conference on Numerical Methods in Fluid Mechanics, Vol. 1, General Lectures. Fundamental Numerical Techniques, Lecture Notes in Physics, Springer Verlag.

Rickenmann, D. (1991),
  Hyperconcentrated flow and sediment transport on steep slopes, J. of Hydr. Eng., Vol.117, No.11, pp1419-1439.

Rijn, L.C. van (1984a),
  Sediment transport, Part I: bed load transport, J. of Hydr. Eng., ASCE, Vol.110, No.10, pp.1431-1456.

Rijn, L.C. van (1984b),
  Sediment transport, Part III: bed forms and alluvial roughness, J. of Hydr. Eng., ASCE, Vol.110, No.10, pp.1733-1754.

Rijn, L.C. van (1989),
  Handbook sediment transport by currents and waves, Report H 461, Delft Hydraulics.

Ritter, A. (1892),
  Die Fortpflanzung der Wasserwellen, Zeitschrift des Vereines Deutscher Ingenieure, Vol.26, No.33, pp.947-954.

Roe, P.L. (1981),
  Approximate Riemann solvers, parameters vectors, and difference schemes, Journal of Computational Physics, Vol. 43, pp. 357-372.

Rosso, M.; M. Schiara and J. Berlamont (1989),
  Flow stability and friction factor in rough channels, J. of Hydr. Eng., ASCE, Vol.116, No.9, pp.1109-1118.

Ryan, S.E. and G.E. Grant (1991),
　　Downstream effects of timber harvesting on channel morphology in Elk river basin, Oregon, J. of Env. Quality, Vol.20, No.1, pp.60-72.

Sakkas, J.G. and T. Strelkoff (1973),
　　Dam-break flow in a prismatic dry channel, J. of Hydr. Div., ASCE, pp. 2195-2216.

Savic, L. and F.M. Holly (1991),
　　Modified Godunov method for dambreak flows, 24th IAHR Congr. Madrid, p. A203-A210.

Savic, L. (1991),
　　Computation of open-channel discontinuous flows using the modified Godunov method, (Ph.D thesis), University of Iowa, 337 p..

Schälchli, U. (1995),
　　Basic equations for siltation of river beds, J. of Hydr. Eng., ASCE, Vol.121, No.3, pp.274-287.

Schöberl, F. (1994),
　　Floods and inundation problems in mountain streams - Examples from Austria, Intern. workshop on floods and inundations related to large earth movements, Trent, Italy, B6.

Schoklitsch, A. (1914),
　　Über Schleppkraft und Geschiebebewegung, Verlag von Wilhelm Engelmann, Leipzig und Berlin, 66p..

Seal, R. and C. Paola (1995),
　　Observations on downstream fining on the North Fork Toutle River near Mount St. Helens, Washington, Water Res. Res., Vol.31, No.5, pp. 1409-1419.

Seminara, G. (1989),
　　River bars and non linear dynamics, Int. workshop on fluvial hydraulic of mountainous regions, A. Armanini and G. Di Silvio (Eds), pp. A119-A144.

Shuyou, C.; F. Duo and Z. Chuanyi (1988),
　　Stochastic characteristics of cobble-gravel bed load transport, Proc. of the 1988 Nat. Conf. on Hydr. Eng., ASCE, S.R. Abt and J. Gessler (Eds), Colorado, pp.322-327.

Sieben, A. (1993),
　　Hydraulics and morphology of mountain rivers: a literature survey, Comm. on Hydr. and Geot. Eng., Report No.93-3, 143 pp.

Sieben, A. (1994),
　　Notes on the mathematical modelling of alluvial mountain rivers, Comm. on Hydr. and Geot. Eng., Report No.94-3, 158 pp..

Sieben, A. and C.J. Sloff (1994),
    Analysis of a 2-DH mathematical model for mountain rivers with graded sediment, Intern. workshop on floods and inundations related to large earth movements, Trent, Italy, A3.
Sieben, A. (1995),
    A study on one-dimensional and discontinuous river flows with mobile beds, Comm. on Hydr. and Geot. Eng., Report No.95-3, 62 pp..
Sieben, A. (1996),
    One-dimensional models for mountain-river morphology, Comm. on Hydr. and Geot. Eng., Rep. No.96-2, 104 p.
Silvio, Di G. and M. Peviani (1989),
    Modelling short- and long-term evolutiuon of mountain rivers; an application to the torrent Mallero (Italy), A. Armanini and G. Di Silvio (Eds), Fluvial Hydraulics of Mountain Regions, pp.293-315.
Silvio, Di G. and M. Peviani (1991),
    Long-term equilibirum profile of mountain rivers,IAHR 24th Congress. Madrid.
Silvio, Di G. (1991),
    Sediment exchange between stream and bottom, a four layer model, Grain Sorting Seminar, Ascona Switzerland, p. 163-191.
Simons, D.B. and E.V. Richardson (1960),
    Resistance to flow in alluvial channels, J. of the Hydr. Div., ASCE, Vol.86, No.5, pp.73-99.
Simons, D.B. and E.V. Richardson (1961),
    Forms of bed roughness in alluvial channels, J. of the Hydr. Div., ASCE, Vol.87, No.3, pp. 87 105.
Simons, D.B. and R.K. Simons (1987),
    Differences between gravel- and sand-bed rivers, pp.3-16 in *Sediment transport in gravel-bed rivers*, C.R. Thorne, J.C. Bathurst and R.D. Hey (Eds), John Wiley and Sons, New York.
Sinha, S.K. and G. Parker (1996),
    Causes of concavity in longitudinal profiles of rivers, Water Res. Res., Vol.32, No.5. pp. 1417-1428.
Sloff, C.J. (1992),
    The methods of characteristics applied to analyse 2DH hydraulic models, Report No.92-4, Communications on Hydraulic and Geotechnical Engineering, Report No.92-4, Delft University of Technology.
Sloff, C.J. (1993a),
    Analysis on basic equations for sediment-laden flows, Comm. on Hydr. and Geot. Eng., Rep. No.93-8, 54 p.

Sloff, C.J. (1993b),

   Study on modelling the morphology of torrents on volcano slopes, Journal of Hydr. Res. IAHR, Vol.31, No.3, pp.333-345.

Smart, G.M. amd M.N.R. Jaeggi (1983),

   Sediment transport on steep slopes, Mitteilungen der Versuchsanstalt für Wasserbau, Hydrologie und Glaziologie, Nr.64, Eidgenössischen Technischen Hochschule Zürich.

Sorensen, R.M. (1985),

   Stepped spillway hydraulic model investigation, J. of Hydr. Eng., ASCE, Vol.111, No.12, p.1461-1472.

Steger, J.L. (1978),

   Coefficient matrices for implicit finite-difference solution of the inviscid fluid conservation law equations, Comput. Methods Appl. Mech. Eng., Vol.13, pp.175-188.

Sternberg, H. (1875),

   Untersuchungen über Längen- und Querprofil geschicbeführender Flüsse, Zeitschrift für Bauwesen, Vol.25, pp.483-506.

Stoker (1957),

   Water waves Interscience Publishers, New York, 563 p.

Strelkoff, T. (1969),

   One-dimensional equations of open-channel flow, J. of the Hydr. Div., ASCE, Vol. 95, No. 3, pp. 861-876.

Sutherland, A.J. (1987),

   Static armour layers by selective erosion, pp.243-268, in *Sediment transport in gravel-bed rivers*, C.R. Thorne, J.C. Bathurst and R.D. Hey (Eds), John Wiley and Sons.

Sutherland, A.J. (1991),

   Hiding functions to predict self armouring, Grain Sorting Seminar, Ascona Switzerland, p. 273-298.

Suzuki, K. (1976),

   On the propagation of a disturbance in the bed composition of an open channel, Delft Univ. of Techn., Dept. of Civil Eng., lab. of Fluid Mechanics, Report R. 1976 /09/ L, 41 pp.

Suzuki, K. and M. Michiue (1988),

   Change of river regime and graded-sediment discharge during flood, in Int. conf. on river regime, W.R. White (Ed.), Hydr.Res. Ltd, Wallingford UK, pp. 231-240.

Suzuki, K. and M. Michiue (1991),

   Propagation and deformation of a low mound formed on a river bed and sorting of bed surface sand mixture, Proc. of the 24th IAHR Congress, Madrid, pp.295-301.

Swanson, F.J.; R.L. Graham and G.E. Grant (1985),
Some effects of slope movements on river channels, pp.273-278, Proc. of the int. symp. on erosion, debris flow and disaster prevention, The erosion control engineering society, Tsukuba, Japan.

Tait, S.J., B.B. Willets and J.K. Maizels (1992),
Laboratory observations of bed armouring and changes in bedload composition, in *Dynamics of gravel-bed rivers*, P. Billi, R.D. Hey, C.R. Thorne and P. Tacconi (Eds), John Wiley and Sons, New York, pp. 205-225.

Takahashi, T. (1991),
Debris Flow, IAHR Monograph Series, Balkema Rotterdam, 165 pp..

Takahashi, T. and H. Nakagawa (1994),
Natural dam formation and the disaster - A possible explanation of one extreme event, Intern. workshop on floods and inundations related to large earth movements, Trent, Italy, A8.

Tan Weyan (1992),
Shallow water hydrodynamics, Mathematical theory and numerical solution for a two-dimensional system of shallow water equations, Nanjing Research Institute of Hydrology and Water Resources, Elsevier Oceanograph Series, 55, Water Power & Press, Beijing.

Taylor Jr, R.H. and J.F. Kennedy (1960),
discussion of "Roll waves and slug flows in inclined open channels", by Mayer (1959), J. of the Hydr. Div., ASCE, Vol.86, No.1, pp. 115-122.

Taylor Jr, R.H. and N.H. Brooks (1961),
discussion of "Resistance to flow in alluvial channels", by D.B. Simons and E.V. Richardson, J. of the Hydr. Div., ASCE, Vol.87, No.1, pp.246-256.

Terzidis, G. and T. Strelkoff (1970),
Computation of open channel surges and shocks, Journal of the Hydraulics Division, Vol. 96, No. 12, pp. 2581-2610.

Toro-Escobar, C.M., G. Parker and C. Paola (1996),
Transfer function for the deposition of poorly sorted gravel in response to streambed aggradation, J. of Hydr. Res., IAHR, Vol.34, No.1, pp.35-54.

Trieste, D.J. (1992),
Evaluation of supercritical/subcritical flow in high gradient channel, J. of Hydr. Eng., Vol.118, No.8, pp.1107-1118.

Tung, Y.-K. (1996),
Uncertainty analysis in water resources engineering, pp.29-46, in *Stochastic Hydraulics*, K. S. Tickle, I.C. Goulter, C. Xu, S.A. Wasimi and F. Bouchart (Eds), Balkema Rotterdam.

Turner, A.K. and R.L. Schuster (1996),
   Landslides: investigation and mitigation, special report 247, Transportation Research Board, National Research Council, 675 p..

Vila, J.P. (1986),
   Simplified Godunov schemes for 2x2 systems of conservation laws, SIAM, Journal of numerical analysis, Vol. 23, No. 6, pp. 1173-1192.

Vila, J.P. (1987),
   Schemas numeriques en hydraulique des ecoulements avec discontinuities, Proc. XII Congress IAHR, Lausanne.

Vreugdenhil, C.B. (1972),
   Mathematical methods for flood waves, Delft Hydraulics Laboratory Res. Rep. 89-IV.

Vreugdenhil, C.B. and M. de Vries (1973),
   Analytical approaches to non-steady bedload transport, Delft Hydraulics Laboratory Res. Rep. S78-IV.

Vreugdenhil, C.B. (1977),
   Use of computers for hydraulic engineering problems, Delft Hydraulics Laboratory Publ. No.185.

Vreugdenhil, C.B. (1982),
   Numerical effects in models for river morphology, pp.91-108 in *Engineering applications of Computational Hydraulics*
   Volume I, M.B. Abbot and J.A. Cunge (Eds), Pitman London, 262 p..

Vreugdenhil, C.B. (1989),
   Computational hydraulics. An introduction., Springer-Verlag Berlin, 184 p.

Vreugdenhil, C.B. (1994),
   Numerical methods for shallow-water flow, Water Science and Techn. Library Vol.13, Kluwer Academic Publishers Dordrecht, 262 p..

Vriend, H.J. de (1987),
   Analysis of horizontally two-dimensional morphological evolutions in shallow water, J. of Geophysical Res., Vol.92, No.C4, pp. 3877-3893.

Vries, M. de (1965),
   Considerations about non-steady bed-load transport in open channels, Proceedings IAHR, Leningrad, pp.3.81-3.8.8

Vries de, M. (1966),
   Applications of luminophores in sandtransport-studies, Doct. Diss., 86 p, (also Delft Hydraulics Laboratory Publ. No.39).

Vries de, M. (1973),
   Application of physical and mathematical models for river problems, Delft Hydraulics Laboratory Publ. No.112.

Vries, M. de (1993),

> Use of models for river problems, Studies and reports in hydrology 51,
> UNESCO, 85 pp..

Vries de, M. (1994),

> Rivieren, (*in Dutch*), Lecture Notes f8, Delft Univ. of Techn., Fac. of
> Civil Eng., 214 p..

Wahl, K.L. and J.E. Miller (1996),

> The occurrence of critical and supercritical velocities in natural channels,
> pp.561-568, in *Stochastic Hydraulics*, K. S. Tickle, I.C. Goulter, C. Xu,
> S.A. Wasimi and F. Bouchart (Eds), Balkema Rotterdam.

Wang, Z., W. Kron, X. Lu and E.J. Plate (1993),

> Flume experiments on sediment transport, erosion and siltation of a
> channel bed in unsteady and non-uniform flow conditions, in
> Contributions to non-stationary sediment transport, W. Kron (Ed.),
> No.42, Institut für Hydrologie und Wasserwirtschaft Universität
> Karlsruhe, pp.B1-B82.

Wang, Z.; W. Kron and E.J. Plate (1994),

> An experimental study of bed deformation in unsteady and non-uniform
> flows, Int. J. of Sediment Research, Vol.9, pp.206-215.

Wesche, T.A., V.R. Hasfurther, W.A. Hubert and Q.D. Skinner (1987),

> Assessment of flushing flow recommendations in a steep, rough,
> regulated tributary, in *Regulated streams: advances in ecology*, J.F. Graig
> and J.B. Kemper (Eds), Plenum Press, New York, pp.59-69.

White, R.W. and T.J. Day (1982),

> Transport of graded gravel bed material, in *Gravel bed rivers*, R.D. Hey,
> J.C. Bathurst and C.R Thorne (Eds), John Wiley and Sons, pp.181-213.

Whitham, G.B. (1974),

> *Linear and non-linear waves*, New York, John Wiley and Sons.

Whiting, P.J. and W.E. Dietrich (1991),

> Convective accelerations and boundary shear stress over a channel bar,
> Water Res. Res., Vol.27, No.5, pp. 783-796.

Whittaker, J.G. and M.N.R. Jeaggi (1982),

> Origin of step-pool systems in mountain streams, J. of the Hydr. Div.,
> Vol.108, o.6, pp. 758-773.

Whittaker, J.G. (1985),

> Local scour in mountain rivers in flood, pp.353-363, in the 2nd Int. conf.
> on the hydraulics of floods and and flood control, BHRA, Cambridge,
> England.

Whittaker, J.G.; U. Schälchli and M.N.R. Jaeggi (1985),

> Design problems with torrent check dams in Switzerland, pp.387-394,
> Proc. of the int. symp. on erosion, debris flow and disaster prevention,

The erosion control engineering society, Tsukuba, Japan.

Wilcock, P.R. and J.B. Southard (1989),
Bed load transport of mixed size sediment: fractional transport rates, bed forms and the development of a coarse bed surface layer, Water Resources Research, Vol.25, No.7, pp.1629-1641.

Wilcock, P.R. (1988),
Methods for estimating the critical shear stress of individual fractions in mixed-size sediment, Water Resources Research, Vol.24, No.7, pp.1127-1135.

Willi, H.P. (1989),
Review of mountain river training procedures in Switzerland, Int. workshop on fluvial hydraulic of mountainous regions, A. Armanini and G. Di Silvio (Eds), pp. B317-B330.

Wolfram, S. (1991),
Mathematica, a system for doing mathematics by computer, Second Edition, Addison-Wesley Publishing Company, Redwood City, California, 961 pp.

Woodward, P. and P. Colella (1984),
Review article. The numerical simulation of two-dimensional fluid flow with strong shocks, J. of Computational Physics, Vol. 14, pp. 159-179.

Yevjevich, V. (1975),
Storm-drain networks, Chapter 16 in *Unsteady flow in open channels*, Vol.II, K. Mahmood and V. Yevjevich (Eds), Water Res. Publ. Fort Collins, USA, pp.693-704.

Zimmerman, M. (1990),
Debris flows 1987 in Switzerland, Hydrology of mountainous regions II Artificial reservoirs; water and slopes, IAHS Publ. No.194.

Appendix A

Some effects of a non-uniform geometry.

A.1. Introduction.

As reviewed by Crosato (1995), hydraulics and morphology in rivers with non-uniform width, slope and roughness patterns are often determined by processes with two- or even three characteristic dimensions. Only if contributions of these vertically and transversely oriented phenomena can be considered constant, cross-sectional integration of a river is an efficient approximation. Here, some concepts are discussed to incorporate multi-dimensional, *hydraulic* effects into a one-dimensional model with a fixed bed.

Geometrical non-uniformities (width variations, alternate bars etc), generate secondary flow phenomena that induce transversal fluxes of momentum by velocity and depth profiles and subsequent local energy losses by turbulent dissipation. In general, complex flow patterns will induce two effects in one-dimensional models: energy dissipation and hydraulic dispersion in wave-type solutions (e.g. Jansen *et al.*, 1979). Reference is made to observations by Kellerhals (1970), which showed dispersion of wave fronts due to non-uniformities in geometries.

For high values of Fr, flow patterns as a response to two-dimensional geometrical perturbations can be expected to change with Fr (Furbish, 1993). Then, unless proper correction is applied, accurate prediction of contributions of 2DH-flow patterns to solutions of one-dimensional models is limited.

A.2. Local energy losses.

A significant part of research on hydraulics in non-uniform geometry has been devoted to description of local energy dissipation. Based on *spatial density* (Chow, 1959) and *relative height* of irregularities (e.g. Bathurst *et al.* 1981), different hypotheses have been suggested to describe effects of geometry on flow. These concepts vary from *lumped* friction-loss coefficients (e.g. Bathurst, 1978) or separate contributions of *reach* friction loss and *point* form loss (e.g. Parker and Peterson, 1980; Jaeggi, 1983; Hey, 1988; Egashira and Ashida, 1989) to *sectional* equivalent roughness stripes (e.g. Fuentes and Aguirre-Pe, 1991) or different kinds of roughness *statistics* (Furbish, 1987; De Jong and Ergenzinger, 1992; Li *et al.* 1992).

To illustrate the contribution of geometrical non-uniformity to energy dissipation, a uniform-flow resistance predictor (Hey, 1979) is compared in Figure A.1 with measurements in pool-riffle sequences by Hey and Thorne (1986).
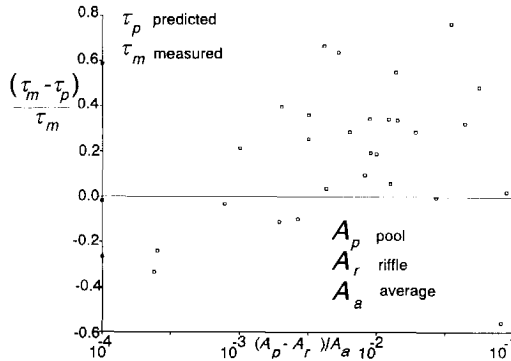

Fig.A.1 Geometry-induced friction losses (Hey and Thorne, 1986).

To illustrate the effect of dissipation due to shock-wave induced turbulence, an additional dissipation term has been added to the numerical model as described in Chapter seven. This additional dissipation in expanding flow is defined as

$$k \, \frac{\Delta a}{\Delta x} \, \Delta u^2 \qquad\qquad (A.1)$$

The intensity of the transition is included by stating that no dissipation is present if $\Delta a < \alpha \Delta x$, with α of the order of 10^{-1}. Hence, to simulate discontinuous flows, the resolution of the numerical grid should correspond with physical length-scales. Numerical examples of expansion losses in different flow regimes are given in the following figures, representing water- and bed levels in sub- and transcritical flow.
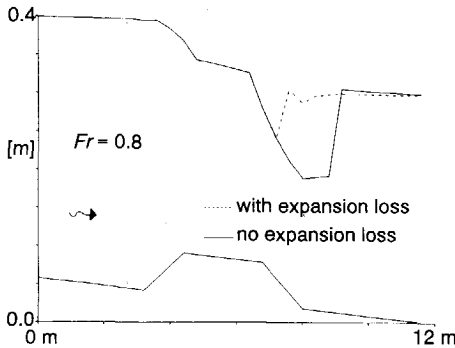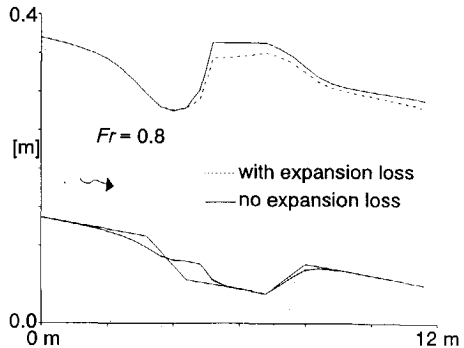

Fig.A.2 Fixed bed.

Fig.A.3 Mobile bed.

200

Hence, the intensity of the jump, and subsequently the location of the jump is affected by lowering sequent depths. In the following figures, the effect of expansion losses for fixed and mobile beds are compared. Expansion losses as defined by Eq.A.1 are not included in the experiments concerning discontinuous flow in Chapter six.

A.3. Effect of width-variations.

Effects of geometry in one-dimensional models appear in width, bed level, and possibly, transversal distributions of velocity and depth. To illustrate the morphological response to width-variations, a harmonic solution of the linearized set of PDE's is performed. Because widths are assumed fixed, the effects of width variation on flow and morphology can be described with source terms.

The system of PDE's can be written as

$$\frac{\partial aB}{\partial t} + \frac{\partial auB}{\partial x} = 0$$

$$\frac{\partial uaB}{\partial t} + \frac{\partial u^2 aB}{\partial x} - g_z aB \frac{\partial a}{\partial x} - g_z aB \frac{\partial z_b}{\partial x} = g_x aB + \frac{g_z u^2 B}{C^2} \quad \text{(A.2)}$$

$$\frac{\partial z_b B}{\partial t} + \frac{\partial sB}{\partial x} = 0$$

The solution is assumed to be composed of steady, uniform zero-order terms and a first-order perturbation. Variables are made dimensionless (Eq.2.40), and the dimensional width B is scaled with the length W.

The set of PDE's can be combined into (see Eq. 2.41)

$$\frac{\partial^3 z_b}{\partial t^3} + 2 \frac{\partial^3 z_b}{\partial t^2 \partial x} + \left(\frac{Fr^2 - 1 - \psi}{Fr^2} \right) \frac{\partial^2 z_b}{\partial t \partial x^2} - \frac{\psi}{Fr^2} \frac{\partial^3 z_b}{\partial x^3} + E_T \left[\frac{\partial^2 z_b}{\partial x^2} + \frac{3}{2} \frac{\partial^2 z_b}{\partial t \partial x} \right] =$$

$$= -\frac{W}{B} \left[\frac{\psi}{Fr^2} + \phi \left(1 - \frac{1}{Fr^2} \right) \right] \frac{d^3 B}{dx^3} + \frac{E_T}{2} \frac{W}{B} (\psi - 3\phi) \frac{d^2 B}{dx^2}$$

(A.3)

where hyphens are left out for convenience. The concentration ϕ is defined as

$\phi = s_b/ua$. Hence, for a steady, first-order width-excitation, the following ODE must be solved.

$$- \frac{\psi}{Fr^2} \frac{\partial^3 z_b}{\partial x^3} + E_T \frac{\partial^2 z_b}{\partial x^2} = -\frac{W}{B} \left[\psi + \phi \left(1 - \frac{1}{Fr^2} \right) \right] \frac{d^3 B}{dx^3} + \frac{E_T}{2} \frac{W}{B} (\psi - 3\phi) \frac{d^2 B}{dx^2}$$

(A.4)

The width-excitation can be defined as

$$B = \Delta B \, e^{i\lambda x} \quad : \quad \lambda = \frac{uT}{L_w} \tag{A.5}$$

where L_w is the wave-length of the perturbation. The dimensional amplitude Δz_b of the bed-level response to a dimensional perturbation ΔB is

$$\frac{\Delta z_b}{a} \frac{B}{\Delta B} = \frac{i\Lambda \left[\dfrac{2\phi(1 - Fr^2) + \psi(\psi - 2 - 3\phi)}{2Fr^2} \right] + \Lambda^2 \dfrac{(\psi - 3\phi)}{2} + \dfrac{\psi}{Fr^4}(\psi + \phi(Fr^2 - 1))}{\Lambda^2 + \left(\dfrac{\psi}{Fr^2} \right)^2} \tag{A.6}$$

with Λ a dimensionless flow-adaptation length defined as

$$\Lambda = \frac{E_T}{\lambda} = \frac{-g_z}{C^2} \frac{L_w}{a_0} \tag{A.7}$$

In case of flow adaption to secondary-flow effects, a more or less corresponding parameter results (e.g. Struiksma *et al.* 1985).

The amplitude and phase shift of this response are constructed in the following figures, where the sediment-transport rate is predicted with $s = m\,u^5$.
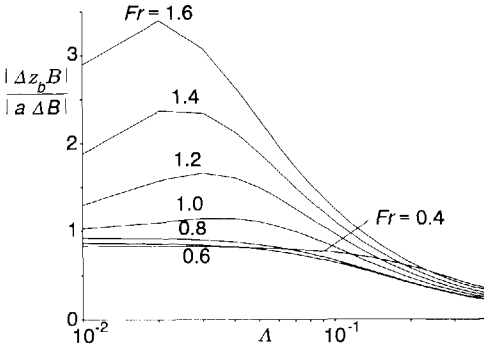

Fig.A.4 Amplitude.　　　　　　　　**Fig.A.5** Phase shift.
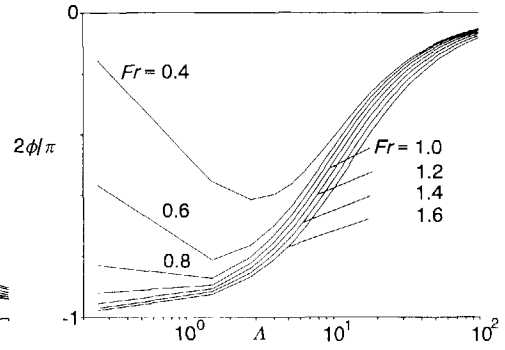
For $\Lambda < 0.1$, bed level responses are sensitive to Fr, for values of $Fr > 0.6$. Then, width-variations with short wave-lengths ($L_w/a < -C^2/g_z$) induce bed-level responses of the order of $a\Delta B/B$. The magnitude of the response is of the order

$$\frac{\Delta z_b}{a}\frac{B}{\Delta B} = 1 + \frac{\phi}{\psi}(Fr^2-1) \qquad\qquad \textbf{(A.8)}$$

For $\Lambda = 0$ or $\Lambda \rightarrow \infty$, the phase shift in bed-level response approaches zero; for $\Lambda > 10^2$, "instantaneous" adaption of flow to local geometry can be assumed. For values of $\Lambda \approx 1$, the phase shift is at maximum and of the order $-\pi/2$ for critical and supercritical flows. For $\Lambda \rightarrow \infty$, the magnitude of response is of the order

$$\frac{\Delta z_b}{a}\frac{B}{\Delta B} = \frac{\phi}{2}\left(\frac{\psi}{\phi}-3\right) \qquad\qquad \textbf{(A.9)}$$

To illustrate the effect of flow unsteadiness and non-uniformity, reference is made to experiments of Wang *et al.* (1993). These experiments include the scouring of a bed in a narrowed flume section, in steady and unsteady flows. The conditions of the experiments are shown in Figure A.6. The large values of λ indicate that the narrowed section can be considered short with respect to the length-scale of the wave.
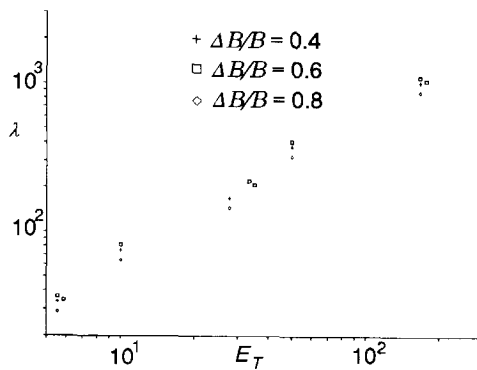
Fig.A.6 Experimental conditions (Wang *et al.*, 1993).

Because values of $\Delta B/B$ were 0.2, 0.4 and 0.6, Eq.A.8, which is valid for relatively small, first-order deviations, is not valid. In addition, vortex-induced erosion effects were observed that increased the erosion rates.

In Figure A.7, maximum erosion depths in case of constant discharge are shown. Values of Fr in the experiments were of the order of 0.6. In correspondence with Figure A.7, the effect of varying Λ is not significant. As also concluded in Subsection 4.4.3, secondary flows (eddy structures) increase the local erosion.

In Figure A.8, the maximum erosion depth during the hydrograph is shown; for infinitely long waves ($E_T \to \infty$), an equilibrium scour depth can be expected. The lines in Figure A.8 connect experiments with similar peak and base flow discharges but different periods. Because the length scale of the narrowed section is short relative to the length-scale of the wave (Figure A.6), obviously, for values of $E_T < 10^2$, wave-unsteadiness affects the morphology.
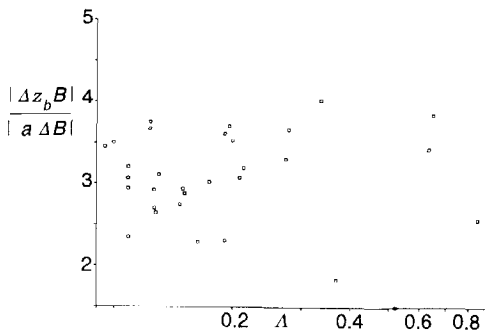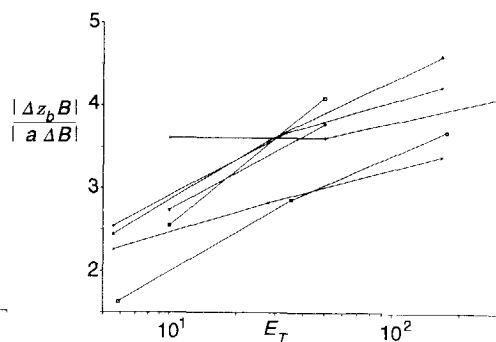

Fig.A.7 Equilibrium scour.

Fig.A.8 Scour during flood wave.

Appendix B

Effects of grain-size distribution.

The effect of grain-size distribution of sediment on morphological changes is related to the shape of the size-frequency distribution and the level of bed shear-stress relative to the threshold value for particle motion. The effects of a sediment mixture in morphological models additional to uniform sediment can be combined in the following two parameters (Eqs 3.21 and 3.22 in Subsection 3.3.1)

$$
Y_a = \frac{\sum_{i-1}^{N} \left[f_{pi} - f_{pN} + \sum_{j=1}^{N} f_{Dj}(D_i - D_N) \right] (\beta_{pi} - p_{Ti})}{ua} \ \wedge \ \frac{a}{\delta_p} \tag{B.1}
$$

The ratio a/δ_p is related to the scale of the phenomena considered and will vary for different types of morphological computations (Section 3.5). Therefore, only Y_a will be considered here. To analyse Y_a, a predictor of transport rate per size fraction i is used, based on the formula proposed by Meyer-Peter and Müller (1948).

$$
s_i = f\left(u, p_{pi}, D_i, D_{mp}, C\right) \ ; \ D_{mp} = \sum_{i-1}^{N} p_{pi}D_i \tag{B.2}
$$

The partial-derivatives of this rate are referred to as

$$
f_{ui} = \frac{\partial s_i}{\partial u} \ ; \ f_{pi} = \frac{\partial s_i}{\partial p_{pi}} \ ; \ f_{Di} = \frac{\partial s_i}{\partial D_{mp}} \tag{B.3}
$$

The general form will be

$$
s_i = p_{pi} \, k \, \sqrt{-\Delta g_z D_i^3} \left[\frac{\mu u^2}{-\Delta g_z C^2 D_i} - p \left(\frac{D_i}{D_{mp}} \right)^{-r} \tau_{*cr} \right]^n \tag{B.4}
$$

For this analysis, it is used $\Delta = 1.65$; $\mu = 1$; $p = 1$; $r = 0.8$; $\tau_{*cr} = 0.047$, $n = 1.5$.

The definition of symbols is as follows.

s_i	transport rate of fraction i
p_{pi}	fraction i in river bed
C	Chézy roughness coefficient
D_i	grain size of fraction i
D_m	mean grain size
k	total transport-rate coefficient
Δ	relative density difference between water and sediment
μ	ribbel-factor correction for bed shear-stress
p	critical shear-stress coefficient
r	hiding-correction coefficient
τ_{*cr}	critical shear-stress

Furthermore, to analyse the effect of different sediment compositions, grain-size frequency distributions are assumed. To obtain a bi-modal mixture, two simple, triangle-shaped distributions are combined. These distributions can be characterized with a peak-frequency grain-size D_{pA} or D_{pB} and a maximum and minimum grain size D_{max} and D_{min}. Both will be mixed with a volumetric fraction α of mixture A and $(1-\alpha)$ of mixture B. The compositions of the hypothetical mixtures considered are presented in Figure B.1.
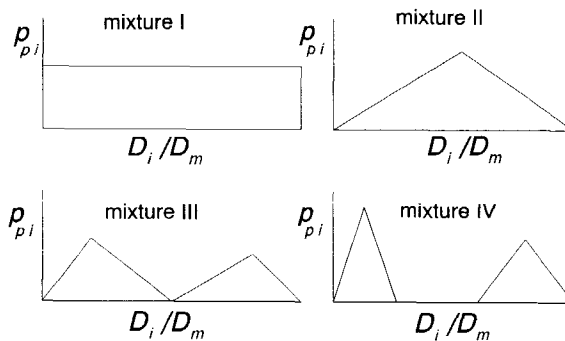

Fig.B.1 Sediment mixtures.

In Figures B.2,3,4 and 5 the composition of sediment transport, as predicted by Eq.B.4 is constructed for the different sediment mixtures. The cumulative size-frequency distributions of the original mixture are represented in broken lines. The relative volume in transport of fraction i is p_{Ti}.
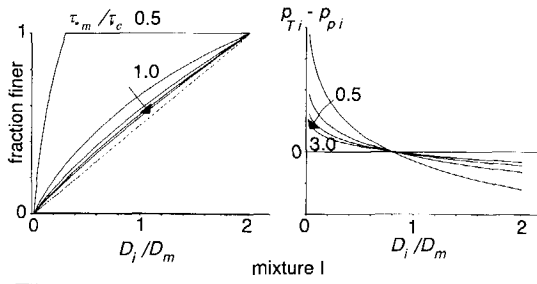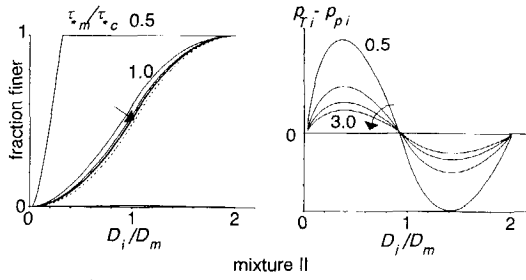
Fig.B.2 Transport composition mixture I.

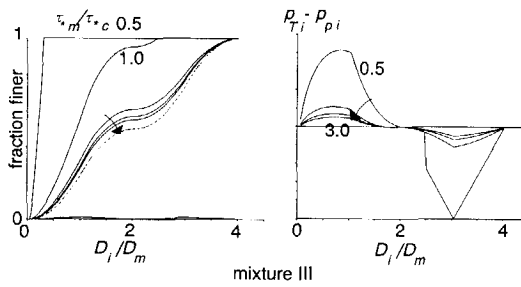**Fig.B.3** Transport composition mixture II.

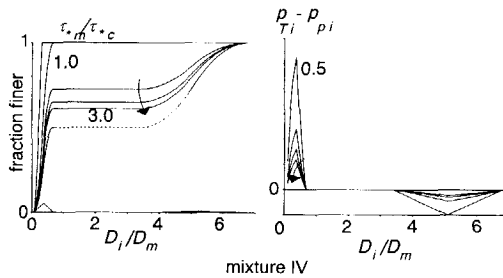**Fig.B.4** Transport composition mixture III.

Fig.B.5 Transport composition mixture IV.

Regardless of the distribution curve, the composition of sediment transport is finer than the river bed. This difference decreases with increasing shear stress. The composition of sediment transport, however, will be strongly related to the river bed size-frequency distribution. Analogously, derivatives of sediment transport rates to size-fraction, velocity and mean grain-size can be determined for the mixtures.
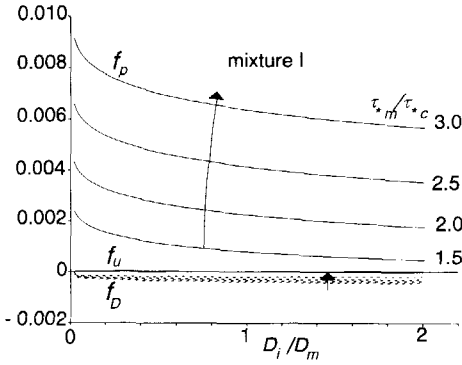

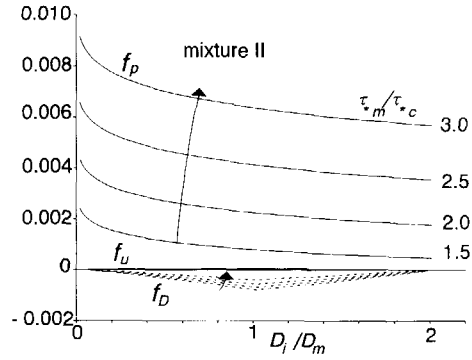**Fig.B.6** Transport derivatives mixture I.
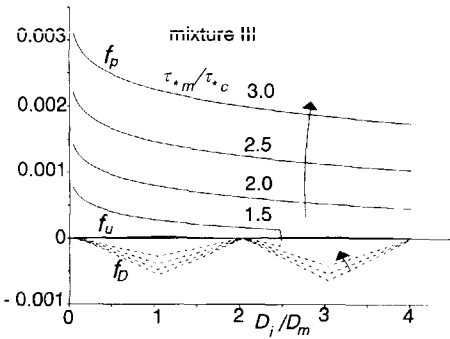

Fig.B.7 Transport derivatives mixture II.

Fig.B.8 Transport derivatives mixture III.
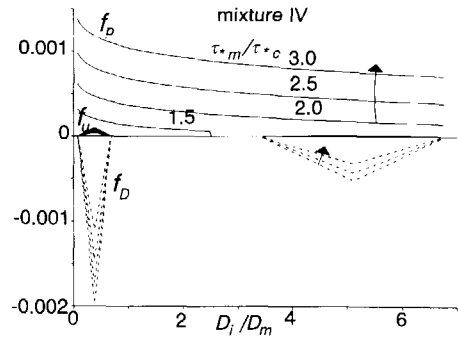

Fig.B.9 Transport derivatives mixture IV.

To construct values of Y_a, values of β_i^* must be substituted. Note that variable β_i^* includes effects of longitudinal gradients in sediment transport composition (Eq.3.16 and 3.17). In Subsection 3.3.2, necessarily a simplification is introduced by assuming $\beta_i^* = p_{Ti}$.

This implies neglecting the contribution of longitudinal gradients in sediment-transport composition. This approximation is only valid for uniform distribution of composition, or for low values of sediment transport. With this assumption, Y_a can be constructed for the different mixtures, and for different levels of shear stress.
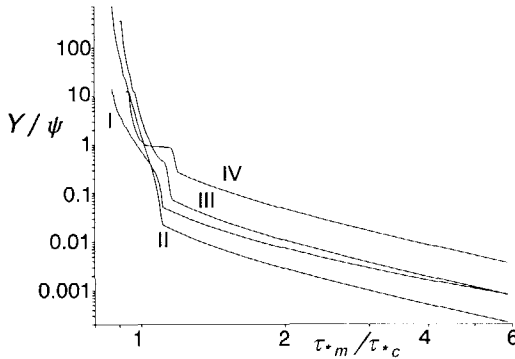

Fig.B.10 Effect of size-frequency distribution.

If symmetric hiding functions are applied, the effect of different grain-sizes is minimal for a mixture with a normal-distribution. For strongly bimodal mixtures, the effect can be significant. For values of $\tau_{*m}/\tau_{*c} > 5$, the effect of size-selective entrainment, deposition and transport diminishes.

209

Appendix C

Difference equations.

C.1 Corrector.

In the corrector step, the set of PDE's as described in Subsections 2.2.1 and 2.2.2 are solved in difference form. Time-integrated fluxes are specified with a superscript *, and are determined with the predictor step at cell boundaries ($x = x_{k-1/2}$ and $x = x_{k+1/2}$).
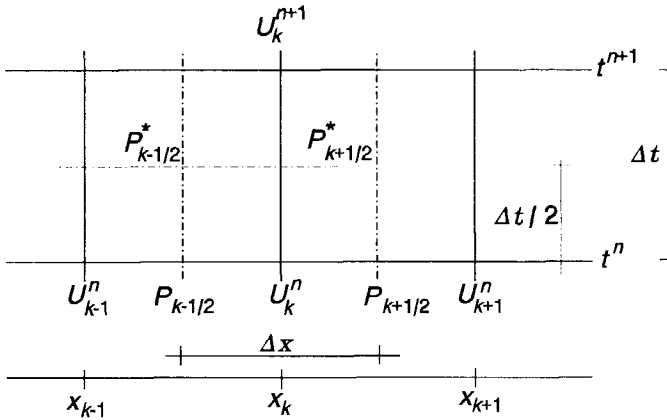
Fig.C.1 Grid points for predictor and corrector.

The depth at $t = t^{n+1}$ is solved from the flow-mass balance

$$a_k^{n+1}\left(c_0 - \frac{1}{2}\left(\phi_{k-1/2}^* + \phi_{k+1/2}^*\right)\right)W_k - a_k^n\left(c_0 - \phi_k^n\right)W_k +$$

$$+ \frac{\Delta t}{\Delta x}\left(u_{k+1/2}^* a_{k+1/2}^*\left(c_0 - \phi_{k+1/2}^*\right) + s_{b_{k+1/2}}^*\right)W_{k+1/2} + \tag{C.1}$$

$$- \frac{\Delta t}{\Delta x}\left(u_{k-1/2}^* a_{k-1/2}^*\left(c_0 - \phi_{k-1/2}^*\right) + s_{b_{k-1/2}}^*\right)W_{k-1/2} = 0$$

The new bed level is determined with the sediment-mass balance

$$\left(z_{b_k}^{n+1}-z_{b_k}^{n}\right)c_0 W_k + \frac{\Delta t}{\Delta x}\left(u_{k+1/2}^{*}a_{k+1/2}^{*}\phi_{k+1/2}^{*}+s_{b_{k+1/2}}^{*}\right)W_{k+1/2} +$$

$$- \frac{\Delta t}{\Delta x}\left(u_{k-1/2}^{*}a_{k-1/2}^{*}\phi_{k-1/2}^{*}+s_{b_{k-1/2}}^{n}\right)W_{k-1/2} = 0$$

(C.2)

Now, the velocity at $t=t^{n+1}$ can be solved with the momentum equation

$$u_k^{n+1}a_k^{n+1}\left(1+\frac{\Delta}{2}\left(\phi_{k-1/2}^{*}+\phi_{k+1/2}^{*}\right)\right)W_k - u_k^n a_k^n\left(1+\Delta\phi_k^n\right)W_k +$$

$$+ \frac{\Delta t}{\Delta x}\left[u_{k+1/2}^{*}{}^2 a_{k+1/2}^{*}\left(1+\Delta\phi_{k+1/2}^{*}\right)W_{k+1/2} - u_{k-1/2}^{*}{}^2 a_{k-1/2}^{*}\left(1+\Delta\phi_{k-1/2}^{*}\right)W_{k-1/2}\right] -$$

$$+ \frac{g_z W_k}{2}\left[a_{k+1/2}^{*}{}^2\left(1+\Delta\phi_{k+1/2}^{*}\right)-a_{k-1/2}^{*}{}^2\left(1+\Delta\phi_{k-1/2}^{*}\right)\right] -$$

(C.3)

$$+ \frac{\Delta t}{\Delta x}\frac{g_z W_k}{2}\left[a_{k-1/2}^{*}\left(1+\Delta\phi_{k-1/2}^{*}\right)+\frac{\left(a_k^{n+1}+a_k^n\right)}{2}\left(1+\frac{\Delta}{2}\left(\phi_{k-1/2}^{*}+\phi_{k+1/2}^{*}\right)\right)\right]\left(\frac{\left(z_{b_k}^{n+1}+z_{b_k}^n\right)}{2}-z_{k-1/2}^{*}\right) +$$

$$+ \frac{\Delta t}{\Delta x}\frac{g_z W_k}{2}\left[a_{k+1/2}^{*}\left(1+\Delta\phi_{k+1/2}^{*}\right)+\frac{\left(a_k^{n+1}+a_k^n\right)}{2}\left(1+\frac{\Delta}{2}\left(\phi_{k-1/2}^{*}+\phi_{k+1/2}^{*}\right)\right)\right]\left(z_{k+1/2}^{*}-\frac{\left(z_{b_k}^{n+1}+z_{b_k}^n\right)}{2}\right) +$$

$$- \frac{\Delta t W_k}{2}\left[\left(g_x a_{k-1/2}^{*}+u_{k-1/2}^{*}{}^2\frac{g_z}{C^2}\right)\left(1+\Delta\phi_{k-1/2}^{*}\right)+\left(g_x a_{k+1/2}^{*}+u_{k+1/2}^{*}{}^2\frac{g_z}{C^2}\right)\left(1+\Delta\phi_{k+1/2}^{*}\right)\right] + LD = 0$$

where *LD* represents a local dissipation term to account for expansion losses. This term is defined as

$$LD = W_k k \frac{\left(a_{k+1}^n - a_{k-1}^n\right)}{2\Delta x}\left(u_{k+1/2}^{*}-u_{k-1/2}^{*}\right)^2$$

(C.4)

and is only included if

$$a_{k+1}^n - a_{k-1}^n \geq 2\gamma\Delta x$$

(C.5)

with $\gamma \approx 0.1$, and $k \approx 0.01$.

Changes in fractions in suspended load are determined with the first-order approximation of the 2-DV model (Eq.2.14 in Subsection 2.2.3).

$$\phi_{i_k}^{n+1} - \phi_{i_k}^{n} + \frac{\Delta t}{\Delta x} \frac{L_{Ai_k}^{n}}{T_{Ai_k}^{n}} \left[\phi_{i_{k+1/2}}^{*} u_{k+1/2}^{*} a_{k+1/2}^{*} - \phi_{i_{k-1/2}}^{*} u_{k-1/2}^{*} a_{k-1/2}^{*} \right] = \frac{\Delta t}{T_{Ai}} \left(\phi_{ei_k}^{n} - \phi_{i_k}^{n} \right)$$

$$(C.6)$$

To determine changes in river-bed composition, first the vertical flux is determined from the bed-load mass balance

$$\Phi_{pi} = \frac{\Delta t}{\Delta x W_k} \left[\left(\phi_{i_{k+1/2}}^{*} u_{k+1/2}^{*} a_{k+1/2}^{*} + s_{bi_{k+1/2}}^{*} \right) W_{k+1/2} - \left(\phi_{i_{k-1/2}}^{*} u_{k-1/2}^{*} a_{k-1/2}^{*} + s_{bi_{k}\ 1/2}^{*} \right) W_{k-1/2} \right] +$$

$$+ \phi_{i_k}^{n+1} a_k^{n+1} - \phi_{i_k}^{n} a_k^{n}$$

Now, changes in composition of the different storage layers can be determined (Eqs 3.10 and 3.11 in Subsection 3.2.4).

$$\delta_1 \left(p_{1i_k}^{n+1} - p_{1i_k}^{n} \right) + \kappa_1 \Delta t \Phi_{pi} + \kappa_1 \left[(1-\kappa_3)\beta_{1i} + \kappa_3 \beta_{3i} \right] \left(z_{b_k}^{n+1} - z_{b_k}^{n} \right) = 0$$

$$\delta_2 \left(p_{2i_k}^{n+1} - p_{2i_k}^{n} \right) + \kappa_2 \Delta t \Phi_{pi} + \left[(\kappa_2 + \kappa_1(1-\kappa_3))\beta_{2i} + \kappa_1(1-\kappa_3)\beta_{1i} \right] \left(z_{b_k}^{n+1} - z_{b_k}^{n} \right) = 0$$

$$(C.8)$$

$$\delta_3 \left(p_{3i_k}^{n+1} - p_{3i_k}^{n} \right) + \left(1 \ \kappa_1 - \kappa_2 \right) \Delta t \Phi_{pi} + \left[\beta_{4i} - (\kappa_2 + \kappa_1(1-\kappa_3))\beta_{2i} - \kappa_1 \kappa_3 \beta_{3i} \right] \left(z_{b_k}^{n+1} - z_{b_k}^{n} \right) = 0$$

C.2 Predictor.

In the predictor step, this mathematical model in divergent form is used. This implies that the continuity equations for fluid and sediment are written as

$$\frac{\partial a}{\partial t} + u \frac{\partial a}{\partial x} + a \frac{\partial u}{\partial x} + \frac{\partial z_b}{\partial t} + \frac{\partial s_b}{\partial x} = - \frac{(ua + s_b)}{B} \frac{\partial B}{\partial x} \qquad (C.9)$$

and

$$\sum_{i=1}^{N} \psi_i a \frac{\partial u}{\partial x} + \frac{a}{1-\phi} \frac{\partial \phi}{\partial t} + \frac{ua}{1-\phi} \frac{\partial \phi}{\partial x} + \frac{c_0 - \phi}{1-\phi} \frac{\partial z_b}{\partial t} + \sum_{i=1}^{N} X_i \frac{\partial p_{pi}}{\partial x} = 0 \qquad (C.10)$$

213

The fluid-momentum equation in divergent form is

$$\frac{\partial u}{\partial t} + u(1-\psi)\frac{\partial u}{\partial x} - g_z\frac{\partial a}{\partial x} - u\sum_{i=1}^{N}\frac{X_i}{a}\frac{\partial p_{pi}}{\partial x} +$$

$$\alpha u\frac{\partial \phi}{\partial t} + \alpha\left(u^2 a - \frac{g_z a}{2}\right)\frac{\partial \phi}{\partial x} - g_z\frac{\partial z_b}{\partial x} - \frac{u}{a}\frac{\partial z_b}{\partial t} = \qquad \text{(C.11)}$$

$$= g_x - \frac{\tau_b}{\rho(1+\Delta\phi)a} + \frac{us_b}{aB}\frac{\partial B}{\partial x}$$

with $\alpha = \Delta/(1+\Delta\phi)$. As described in Chapter one, characteristic equations can be constructed for every celerity c_l.

$$n_1\frac{da}{dt} + n_2\frac{du}{dt} + \left(n_1 - \frac{u}{a}n_2 + (c_0-\phi)n_3\right)\frac{dz_b}{dt} + \sum_{i=1}^{N}(n_{i+3}T_{Ai} + \alpha u n_2 + a n_3)\frac{d\phi_i}{dt} = O_l$$

$$\text{(C.12)}$$

To reduce the number of characteristic equations to 3 coupled and N decoupled ones, changes in composition are solved separately (Subsection 3.3.1). The multiplification coefficients n_i read

$$n_1 = g_z c\prod_{i=1}^{N}P_i \quad ; \quad n_2 = c(u-c)\prod_{i=1}^{N}P_i$$

$$\text{(C.13)}$$

$$n_3 = u\frac{(c(c-u)+g_z a)}{a(\phi-c_0)}\prod_{i=1}^{N}P_i \quad ; \quad n_l - \left(a(c-u)n_3 + \alpha\left(uc + \frac{g_z a}{2}(1+2Fr^2)\right)n_2\right)\frac{1}{P_i}$$

with $l = 4$ to $N+3$ and

$$P_i = L_{Ai} - T_{Ai}c \qquad \text{(C.14)}$$

The celerities c are roots of

$$\left(\frac{c}{u}\right)^3 - \left(2+\psi\frac{1-c_0}{c_0-\phi}\right)\left(\frac{c}{u}\right)^2 + \left(-\frac{1+\psi}{Fr^2}+1+\psi\frac{1-c_0}{c_0-\phi}\right)\left(\frac{c}{u}\right) + \frac{\psi}{Fr^2}\frac{1-\phi}{c_0-\phi} = 0$$

$$\text{(C.15)}$$

$$\vee \quad c = \frac{L_{Ai}}{T_{Ai}}$$

Appendix D

Steep-slope correction

In the mathematical model as described in Chapter two, the longitudinal direction of flow is assumed to be orientated along a constant reference slope. As described in Subsection 2.2.2, this induces errors in case of a river with distinct changes in longitudinal slope. To analyse the contribution of such errors, the following analysis is carried out. Here, flow is assumed to be parallel to a *varying* reference level Z_b. For convenience, the depth a is defined perpendicular to the direction of flow conform Subsection 2.2.2, and a^* is defined in a constant, vertical direction. Local variations in bed level around Z_b are accounted for by distinction of z_b.
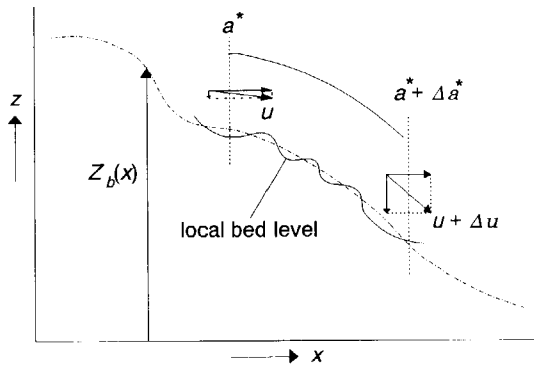

Fig.D.1 Definition of non-uniform reference level.

The velocity is assumed to be parallel to the spatial derivative of Z_b, with

$$\tan(\alpha) = - \frac{\partial Z_b}{\partial x} \tag{D.1}$$

This induces velocity components in x- and z-directions. The difference equation for the mass balance is

$$\frac{\Delta a^*}{\Delta t} + \frac{\cos\left(\alpha + \Delta x \frac{\partial \alpha}{\partial x}\right)\left(u + \Delta x \frac{\partial u}{\partial x}\right)\left(a^* + \Delta x \frac{\partial a^*}{\partial x}\right) - \cos(\alpha)ua^*}{\Delta x} = 0 \tag{D.2}$$

For $\Delta t \rightarrow 0$ and $\Delta x \rightarrow 0$, the corresponding difference equation is obtained.

$$\frac{\partial a^*}{\partial t} + \cos(\alpha)\left(a^*\frac{\partial u}{\partial x} + u\frac{\partial a^*}{\partial x}\right) - ua^*\sin(\alpha)\frac{\partial \alpha}{\partial x} = 0 \qquad \textbf{(D.3)}$$

Similarly, the difference equation for x-directed momentum is

$$\frac{\cos\left(\alpha + \Delta t\frac{\partial \alpha}{\partial t}\right)\left(u + \Delta t\frac{\partial u}{\partial t}\right)\left(a^* + \Delta t\frac{\partial a^*}{\partial t}\right) - \cos(\alpha)ua^*}{\Delta t} +$$

$$+ \frac{\cos\left(\alpha + \Delta x\frac{\partial \alpha}{\partial x}\right)\left(u + \Delta x\frac{\partial u}{\partial x}\right)^2\left(a^* + \Delta x\frac{\partial a^*}{\partial x}\right) - \cos(\alpha)u^2a^*}{\Delta x} + \qquad \textbf{(D.4)}$$

$$+ \frac{g}{2}\frac{\left(a^* + \Delta x\frac{\partial a^*}{\partial x}\right)^2 - (a^*)^2}{\Delta x} + \frac{p_{bed}}{\rho}\left[\frac{\partial z_b}{\partial x} - \tan(\alpha)\right] + \cos(\alpha)\frac{\tau_b}{\rho} = 0$$

Again, the differential equation is obtained for $\Delta t \rightarrow 0$ and $\Delta x \rightarrow 0$

$$-ua^*\sin(\alpha)\frac{\partial \alpha}{\partial t} + \cos(\alpha)\left(a^*\frac{\partial u}{\partial t} + u\frac{\partial a^*}{\partial t}\right) +$$

$$- u^2a^*\sin(\alpha)\frac{\partial \alpha}{\partial x} + \cos(\alpha)\left(2ua^*\frac{\partial u}{\partial x} + u^2\frac{\partial a^*}{\partial x}\right) + \qquad \textbf{(D.5)}$$

$$+ ga^*\frac{\partial a^*}{\partial x} + \frac{p_{bed}}{\rho}\left[\frac{\partial z_b}{\partial x} - \tan(\alpha)\right] + \cos(\alpha)\frac{\tau_b}{\rho} = 0$$

216

The difference equation for z-directed momentum is

$$- \frac{\sin\left(\alpha + \Delta t \frac{\partial \alpha}{\partial t}\right)\left(u + \Delta t \frac{\partial u}{\partial t}\right)\left(a^* + \Delta t \frac{\partial a^*}{\partial t}\right) - \sin(\alpha)ua^*}{\Delta t} +$$

$$- \frac{\sin\left(\alpha + \Delta x \frac{\partial \alpha}{\partial x}\right)\left(u + \Delta x \frac{\partial u}{\partial x}\right)^2\left(a^* + \Delta x \frac{\partial a^*}{\partial x}\right) - \sin(\alpha)u^2 a^*}{\Delta x} + \qquad \textbf{(D.6)}$$

$$+ ga^* - \frac{p_{bed}}{\rho} - \sin(\alpha)\frac{\tau_b}{\rho} = 0$$

with the corresponding differential equation

$$- ua^* \cos(\alpha)\frac{\partial \alpha}{\partial t} - \sin(\alpha)\left(u\frac{\partial a^*}{\partial t} + a^*\frac{\partial u}{\partial t}\right) +$$

$$- u^2 a^* \cos(\alpha)\frac{\partial \alpha}{\partial x} - \sin(\alpha)\left(2ua^*\frac{\partial u}{\partial x} + u^2\frac{\partial a^*}{\partial x}\right) + \qquad \textbf{(D.7)}$$

$$+ ga^* - \frac{p_{bed}}{\rho} - \sin(\alpha)\frac{\tau_b}{\rho} = 0$$

Combination of Eqs D.5 and D.7 yields for the equation of x-directed momentum

$$\frac{\partial ua^*}{\partial t} + \frac{\partial u^2 a^*}{\partial x} + \cos(\alpha)ga^*\frac{\partial\left(a^* + Z_b\right)}{\partial x} + \cos(\alpha)\frac{p_{bed}}{\rho}\frac{\partial z_b}{\partial x} + \frac{\tau_b}{\rho} = 0 \qquad \textbf{(D.8)}$$

The bed pressure p_{bed} on the *local* bed-level can be determined from Eq.D.7, or approximated with the hydrostatic part of the pressure. For gradients in reference level smaller than 0.1, the correction of momentum transfer is negligible. The additional terms appear to be of second-order.

To be consistent with the definitions used in Subsection 2.2.2, a transformation can be performed from a^* into a with $a = a^* \cos(\alpha)$. Substitution into D.3 yields

$$a \tan(\alpha) \frac{\partial \alpha}{\partial t} + \frac{\partial a}{\partial t} + \cos(\alpha) \frac{\partial ua}{\partial x} = 0 \qquad \textbf{(D.9)}$$

The momentum balance can be written as

$$au \tan(\alpha) \left(\frac{\partial \alpha}{\partial t} + u \frac{\partial \alpha}{\partial x} \right) + \frac{\partial au}{\partial t} + \frac{\partial u^2 a}{\partial x} + ga \frac{\partial a}{\partial x} + ga^2 \tan(\alpha) \frac{\partial \alpha}{\partial x} +$$

$$+ \cos(\alpha) \left(\frac{\tau_b}{\rho} + ga \frac{\partial Z_b}{\partial x} \right) + \cos^2(\alpha) \frac{p_{bed}}{\rho} \frac{\partial z_b}{\partial x} = 0 \qquad \textbf{(D.10)}$$

To indicate the small contribution of these corrections, local bed-level gradients of the Mallero (Northern Italy) are shown (FRIMAR, 1995). Hence, in this case, corrections for a non-uniform reference slope would be negligible.
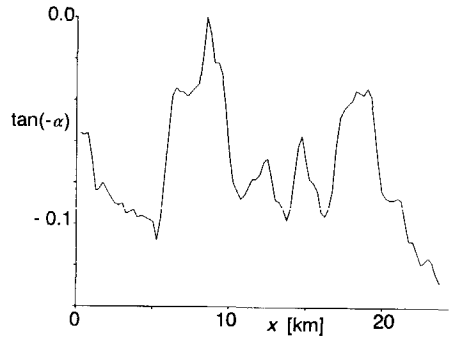

Fig.D.2 Gradients in reference level.

Appendix E

Analysis of generalized shock relations.

In Subsection 6.2.3, shock relations are analysed with a limiting assumption of $n = 3$ in the sediment transport predictor $s_b = mu^n$. Here, an analogous analysis is added for different types of sediment transport predictors.

In case of a one-dimensional model of flow with hydrostatic pressure distribution, bed-material load and a mobile bed, three shock relations can be derived.

$$
w \begin{bmatrix} \Delta a \\ u\Delta a + (a+\Delta a)\Delta u \\ \Delta z_b \end{bmatrix} = \begin{bmatrix} u\Delta a + (a+\Delta a)\Delta u \\ \Delta u(2u+\Delta u)(a+\Delta a) + u^2\Delta a + g\left(a+\dfrac{\Delta a}{2}\right)(\Delta a+\Delta z_b) \\ \Delta s_b \end{bmatrix}
$$

$$\text{(E.1)}$$

where Δ denotes the difference in a variable over a discontinuity, and w the propagation rate of this discontinuity. These shock relations can be combined to obtain

$$
\xi^3 - 2\,\xi^2 + \left(\frac{2Fr^2 - 2 - 3\gamma - \gamma^2}{2\,Fr^2}\right)\xi - \frac{\Delta s_b}{u\Delta a}\frac{2 + 3\gamma + \gamma^2}{2\,Fr^2} = 0 \quad \text{(E.2)}
$$

where $\xi = w/u$, and $\gamma = \Delta a/a$. Because differences in s_b are related to variables up- and downstream of the discontinuity, Eq.E.2 is an implicit equation which is solved with a Picard-iteration method.

Now, two sediment predictors are applied, one equal to the formula proposed by Meyer-Peter and Müller (1948), and one equal to the formula proposed by Engelund and Hansen (1967). In the following, Eq.E.2 is solved for $\gamma = 0.3$ and $\gamma = -0.3$, and for both sediment-transport predictors.

The three solutions are identified as in Chapter five as I (upstream-directed), II and III (downstream-directed) with increasing value of the propagation rate. In the following figures, c_i/u represents a dimensionless celerity.

Curriculum vitae.

Arjan Sieben werd in 1968 geboren in Klazinaveen, en doorliep het VWO aan de reformatorische scholengemeenschap "De Driestar" te Gouda. In 1992 werd een studie in de afstudeerrichting Waterbouwkunde aan de Faculteit der Civiele Techniek van de Technische Universiteit te Delft met lof afgesloten. Het afstudeerproject onder begeleiding van Prof.ir R. Brouwer werd gecombineerd met een stage in Jordanië. Dit project omvatte het ontwerp van een reservoir in de Jordaan vallei en een analyse van de economische haalbaarheid.

In 1992 volgde een aanstelling als Assistent in Opleiding aan de Faculteit der Civiele Techniek in Delft, op het onderwerp "Bergrivieren". Dit onderzoek werd gedeeltelijk gefinancierd door het Waterloopkundig Laboratorium. Het vond plaats onder begeleiding van Prof.dr ir M. de Vries. Tijdens deze aanstelling kon worden deelgenomen aan het Europese FRIMAR project (Flooding Risks in Mountain Areas). Dit maakte samenwerking en kennisuitwisseling met diverse Europese universiteiten en instituten mogelijk. Daarnaast werden contacten gelegd met de Duits-Chinese onderzoeksgroep GESINUS (GErman-SINo Unsteady Sediment transport), welke in 1995 resulteerde in deelname aan een vergadering in Potsdam.

224